

ROBUST MACHINE LEARNING BY TRANSFORMING AND AUGMENTING
IMPERFECT TRAINING DATA

by

Elliot Creager

A thesis submitted in conformity with the requirements
for the degree of Doctor of Philosophy

Department of Computer Science
University of Toronto

Elliot Creager

Doctor of Philosophy

Department of Computer Science

University of Toronto

2023

Abstract

Machine Learning (ML) is an expressive framework for turning data into computer programs. Across many problem domains—both in industry and policy settings—the types of computer programs needed for accurate prediction or optimal control are difficult to write by hand. On the other hand, collecting instances of desired system behavior may be relatively more feasible. This makes ML broadly appealing, but also induces data sensitivities that often manifest as unexpected failure modes during deployment. In this sense, the training data available tend to be imperfect for the task at hand. This thesis explores several data sensitivities of modern machine learning and how to address them. We begin by discussing how to prevent ML from codifying prior human discrimination measured in the training data, where we take a fair representation learning approach. We then discuss the problem of learning from data containing spurious features, which provide predictive fidelity during training but are unreliable upon deployment. Here we observe that insofar as standard training methods tend to learn such features, this propensity can be leveraged to search for partitions of training data that expose this inconsistency, ultimately promoting learning algorithms invariant to spurious features. Finally, we turn our attention to reinforcement learning from data with insufficient coverage over all possible states and actions. To address the coverage issue, we discuss how causal priors can be used to model the single-step dynamics of the setting where data are collected. This enables a new type of data augmentation where observed trajectories are stitched together to produce new but plausible counterfactual trajectories.

This manuscript is dedicated to the memory of William B. Hooper.

Acknowledgements

The research described in this thesis was conducted in the city now known as Toronto, Canada. The Mohawk name for this place, “Tkaronto”, indicates a meeting point between the trees and the water. The land, water, and air that make up the surrounding region are governed by the Dish with One Spoon Wampum; throughout the generations, they have been cared for by many Indigenous peoples, who in turn have been subjected to material and cultural dispossession through a (still ongoing) project of colonization. This is a human tragedy, and also an intellectual tragedy. For example, Leanne Betasamosake Simpson argues that, by failing to engage with Indigenous ontologies that emphasize relationality, Western Scholars often unwittingly use concepts like “abstraction” (the bread and butter of Computer Science) towards extractive ends [Simpson, 2017]. I have seen this pattern emerge frequently in research on technical approaches to mitigate harms in socio-technical systems, which typically exhibit nuanced and context-specific complexities. In the Academy and beyond, much remains to be done when it comes to engaging with Indigenous (and other non-Western) ways of producing and preserving knowledge. These efforts can be understood as a small part of the broader movement towards reconciliation.

On a personal level, I am grateful to this land, and the animal and plant life it supports, for providing a continual source of inspiration throughout my studies here.

Writing about gratitude is difficult for me because the readily available language tends to evoke an outstanding debt or obligation. But these sentiments fail to capture my experience of collaborative research during grad school. When I look back on things now and think of the many people who have helped me complete my studies, it does not suggest some unpaid debt of gratitude for this lesson or that favor. However, I can say that these relationships, experiences, and memories have left a deep imprint on the person that I am today. With humility and deep appreciation, I wish to acknowledge a few people who have left their mark on this thesis and its author.

My supervisor Rich Zemel has been enormously supportive of my research over these past six years, and has managed to do so with care, consistency, and a certain inscrutable deftness. Rich, you established our working relationship on a firm foundation of mutual respect, and always encouraged me to be curious and critical throughout my doctoral work. I will try my best to do the same for my students. Toni Pitassi, you are the paragon of modest brilliance. Thank you for showing me the value of clearly articulating technical assumptions at the outset of a project, which I know see can lead to important insights in the research later on. David Duvenaud, thank you for rounding out my thesis committee with a generous and convivial spirit. You encouraged me to interpret my research against the backdrop of a bigger picture, and showed me the value in drawing connections to other fields.

Thank you to my many mentors throughout the years. David Wingate and Noah Stein, you took a chance on me as a young researcher, and showed me the critical importance of patience and persistence in research. Philippe Depalle, you taught me how to craft a research artifact, and showed me the small pleasures of discussing Fourier analysis over afternoon espressos. Kevin Swersky, you made me feel welcome in a new research lab that was both impressive and intimidating. I am amazed by your ability to bring a smile to every meeting, even when the work approaches drudgery. Sheila McIlraith, more than anyone, you have taught me how to teach. Thank you also for modeling the importance of compassion in building a research community, and for reminding me that impactful

work need not adhere to the trends of the day. Thank you to my guitar teacher Adam Solomon, whose music was a true source of joy for me during weary times, reminding me that all of us are simultaneously teachers and students.

Will Grathwohl, I am glad we could convince each other to take a leap of faith and move to Toronto for grad school. Your ambition and scientific rigor are impressive, but I most appreciate your eagerness to feed a dozen people or more at the drop of a hat. David Madras, I have learned so much from you: how to do the translation work that illuminates commonalities between disciplines, how to stay cool under deadline pressure, and how to find joy in creative pursuits outside of work. Jörn Jacobsen, you echoed this last lesson, and it was a treat to explore the culture of Toronto with you during your brief stay here. At a time when I needed more guidance than I realized, your reminder, that life is slow, was well received. Jesse Bettencourt, you endeared yourself to me starting from our very first semester. As a teacher, your commitment to your students' success and well-being is admirable. Your brilliance, wit, and kindness follow you outside the classroom and wherever you choose to go. Your camaraderie is a treasure to me.

Thank you to the students who I have had the honor of mentoring, especially Robert Adragna, Frederik Traüble, Dilys Dickson, Aisha Alaagib, Arjun Mani, Parand Alizadeh Alamdari, and Benjamin Eyre. These were formative experiences for me; any guidance I may have offered you has already been reciprocated, and I look forward to following your work in the future. Thank you to my wonderful lab mates Renjie Liao, Mengye Ren, Jake Snell, James Lucas, Jackson Wang, Kamyar Ghasemipour, and Eleni Triantafillou. All of you helped keep spirits high in the lab, even when training the most unwieldy neural nets. Thank you to Silviu Pitis and Animesh Garg for patiently explaining the fundamental algorithms of reinforcement learning to me time and again. Thank you Shems Saleh, Yasmin McDowell, Mattie Tesfaldet and Taylor Killian for making Vector Institute a welcoming place for me to work. Thank you to Ria Kalluri, Willie Agnew, Natalia Bilenko, Manuel Sabin, Agata Foryciarz, Micah Carroll, Susanne Kite, Sayash Kapoor, Blaine Harper, and everyone else who has helped me to understand the limits of approaching research from single institutional or disciplinary perspective.

To Tram Ngheim, Khashayar Mohammadi, and all of my close friends in Toronto and beyond, thank you for grounding me during those eight hours of each day not claimed by work or rest. To my partner Claudia Edwards, the depth of your love and support over the years goes beyond a simple summary. Needless to say, thank you, and I reciprocate. Let us continue forward, helping one another along in the strange process of making dreams come true. To my cats, Emu and Roti, thank you for keeping me warm when the work felt alienating or isolating.

Thank you to my family now and always for your endless love and support.

Contents

1	Introduction	1
1.1	Turning Data Into Computer Programs	1
1.2	Data Imperfections	1
1.3	Outline	3
1.4	Topics Covered in This Manuscript	4
1.4.1	Robustness	4
1.4.2	Domain Generalization	4
1.4.3	Algorithmic Fairness	5
1.4.4	Causal Inference	7
1.4.5	Reinforcement Learning	7
2	Representation Learning Approaches to Algorithmic Fairness	9
2.1	The Role of Data Representations in Fair Machine Learning	9
2.2	Encouraging Statistical Parity in Learned Representations with Adversarial Training	10
2.2.1	Background: Fair Classification	10
2.2.2	Background: Adversarial Learning	11
2.2.3	Learning Adversarially Fair and Transferable Representations	11
2.2.4	Experiments	15
2.3	Flexible Fairness: Disentanglement Priors for Subgroup-fair Prediction	20
2.3.1	Background: Variational Autoencoders	20
2.3.2	Flexibly Fair VAE	22
2.3.3	Experiments	25
2.4	Related Work	28
2.5	Discussion	30
3	Leveraging Shortcut Learning to Learn Robust Features	32
3.1	Towards Out-of-distribution Generalization	32
3.1.1	The Role of Side Information in Learning Robust Features	32
3.2	Environment Inference for Invariant Learning	33
3.2.1	Background: Invariant Learning	33
3.2.2	Invariance Without Environment Labels	35
3.3	Experiments	37
3.3.1	Datasets	38
3.3.2	Results	39

3.3.3	Influence of the Reference Model	40
3.4	Related Work	41
3.5	Discussion	43
4	Data Augmentation for Robust Reinforcement Learning	45
4.1	Contemporary RL Often Lacks Data Coverage	45
4.2	The Role of Data Augmentation in RL	46
4.3	Amplifying the Experience Buffer Using Causal Priors	47
4.3.1	Why is Data Augmentation a Useful Heuristic in RL?	47
4.3.2	An Opportunity to Augment: Local Independence of Objects	47
4.3.3	Background: Factored MDPs	48
4.3.4	Local Causal Models (LCMs)	50
4.3.5	A Generic Recipe for Counterfactual Data Augmentation	51
4.3.6	Experiments	54
4.4	Extending the Experience Buffer Using Dynamics Models that Generalize OOD	55
4.4.1	CoDA as an Implicit Generative Model	55
4.4.2	Motivating Model-based CoDA	55
4.4.3	Object-centric Models of Transition Dynamics	56
4.4.4	Model-based CoDA Using Neural Networks	58
4.4.5	Generating the Parent Distribution	58
4.4.6	The Choice of Dynamics Model and RL Algorithm	60
4.4.7	Experiments	61
4.5	Related Work	64
4.6	Discussion	64
5	Conclusion	66
5.1	Summary: All Data are Imperfect Data	66
5.2	What is Next?	67
5.2.1	Some Contradictions Within Contemporary Machine Learning	67
5.2.2	Open Research Questions	70
A	Notes for Chapter 2	72
A.1	Notes on Section 2.2 (LAFTR)	72
A.1.1	Bounding Equalized Odds	72
A.1.2	Experimental Details	73
A.2	Notes on Section 2.3 (FFVAE)	74
A.2.1	Experimental Details	75
A.2.2	Mutual Information Gap	76
B	Notes for Chapter 3	78
B.1	Environment Inference Psuedocode	78
B.2	Proofs	78
B.2.1	Proof of Proposition 1	78
B.2.2	Analysis of the Binning Heuristic	79
B.3	Dataset Details	80

B.4	Experimental Details	81
B.5	Additional Empirical Results	83
B.5.1	ColorMNIST	83
C	Notes for Chapter 4	85
C.1	Proof of Proposition 1	85
C.2	Additional Experiment Details	85
C.2.1	Batch RL	86
C.2.2	Goal-conditioned RL	88
C.3	Proof of Theorem 1	90
C.4	Implementation Details	91
C.4.1	Causal Transition Structure and Parent Set Definitions	91
C.4.2	Parent Distribution	92
C.4.3	Dynamics Models	92
C.4.4	Training Data for the RL Algorithm	94
C.4.5	Reinforcement Learning Algorithms	94
C.5	Experimental Details	94
C.5.1	2D Navigation	94
C.5.2	HookSweep2	96
C.6	MoCoDA sampling pseudocode	98

List of Tables

2.1	Results from Figure 2.3 broken out by task. Δ_{EO} for each of the 10 transfer tasks is shown, which entails identifying a primary condition code that refers to a particular medical condition. Most fair on each task is bolded. All model names are abbreviated from Figure 2.3; “TarUnf” is a baseline, unfair predictor learned directly from the target data without a fairness objective.	19
2.2	Transfer fairness, other metrics. Models are as defined in Figure 2.3. MMD is calculated with a Gaussian RBF kernel ($\sigma = 1$). AdvAcc is the accuracy of a separate MLP trained on the representations to predict the sensitive attribute; due to data imbalance an adversary predicting 0 on each case obtains accuracy of approximately 0.74. . . .	19
3.1	Accuracy (%) on CMNIST, a digit classification task where color is a spurious feature correlated with the label during training but anti-correlated at test time. EIIL exceeds test-time performance of IRM <i>without</i> knowledge of pre-specified environment labels, by instead finding worst-case environments using aggregated data and a reference classifier.	39
3.2	Accuracy (%) on the Waterbirds dataset. EIIL strongly outperforms ERM on worst-group performance, approaching the performance of the GroupDRO algorithm proposed by Sagawa et al. [2020a], which requires oracle access to group labels. In this experiment we feed environments inferred by EIIL into a GroupDRO learner.	40
3.3	EIIL improves worst-group accuracy in the CivilComments-WILDS toxicity prediction task, without access to group labels.	40
4.1	Batch RL (10 seeds): Mean success (\pm standard error, estimated using 1000 bootstrap resamples) on Pong environment. CoDA with learned masking function more than doubles the effective data size, resulting in a 3x performance boost at smaller data sizes. Note that a 1a:5c Real:CoDA ratio performs slightly worse than a 1a:3c ratio due to distributional shift (Remark 4.3.3).	54
4.2	2D Navigation Dynamics Modeling Results: Mean squared error \pm std. dev. over 5 seeds, scaled by $1e2$ for clarity (best model boldfaced). The locally factored model experienced less performance degradation out-of-distribution, and performed better on all distributions, except for the empirical distribution (EMP) itself.	62

4.3	2D Navigation Offline RL Results: Average steps to completion \pm std. dev. over 5 seeds for various RL algorithms (best distribution in each row boldfaced), where average steps was computed over the last 50 training epochs. Training on MOCODA and MOCODA-U improved performance in all cases. Interestingly, even using RAND improves performance, indicating the importance of training on out-of-distribution data. Note that this is an offline RL task, and so SAC (an algorithm designed for online RL) is not expected to perform well.	62
4.4	HookSweep2 Offline RL Results: Average success percentage (\pm std. dev. over 3 seeds), where the average was computed over the last 50 training epochs. SAC and CQL (omitted) were unsuccessful with all datasets. We see that MOCODA was necessary for learning, and that results improve drastically with MOCODA-P, which re-balances MOCODA toward a uniform distribution in the box coordinates (see Figure 4.8). Additionally, we show results from an ablation, which generates the MoCoDA datasets using a fully connected dynamics model. While this still achieves some success, it demonstrates that using a locally-factored model is important for OOD generalization. In this case the more OOD MoCoDA-P distribution does not help, suggesting that the fully connected model is failing to produce useful OOD transitions.	63
B.1	Additional baselines for the CMNIST experiment reported in Table 3.1. The mean and standard deviation of accuracy across ten runs ($\theta_y = 0.25$) are reported. See text for description of the baseline methods.	83

List of Figures

2.1	Model for learning adversarially fair representations. The variables are data X , latent representations Z , sensitive attributes A , and labels Y . The encoder f maps X (and possibly A - not shown) to Z , the decoder k reconstructs X from (Z, A) , the classifier g predicts Y from Z , and the adversary h predicts A from Z (and possibly Y - not shown).	12
2.2	Accuracy-fairness tradeoffs for various fairness metrics (Δ_{DP} , Δ_{EO} , Δ_{EOpp}), and LAFTR adversarial objectives (L_{Adv}^{DP} , L_{Adv}^{EO} , L_{Adv}^{EOpp}) on fair classification of the Adult dataset. Upper-left corner (high accuracy, low Δ) is preferable. Figure 2.2a also compares to a cross-entropy adversarial objective [Edwards and Storkey, 2016], denoted DP-CE. Curves are generated by sweeping a range of fairness coefficients γ , taking the median across 7 runs per γ , and computing the Pareto front. In each plot, the bolded line is the one we expect to perform the best. Magenta square is a baseline MLP with no fairness constraints. see Algorithm 1 and Appendix A.1.2.	16
2.3	Fair transfer learning on Health dataset. Displaying average across 10 transfer tasks of relative difference in error and Δ_{EO} unfairness (the lower the better for both metrics), as compared to a baseline unfair model learned directly from the data. -0.10 means a 10% decrease. Transfer-Unf and -Fair are MLP's with and without fairness restrictions respectively, Transfer-Y-Adv is an adversarial model with access to the classifier output rather than the underlying representations, and LAFTR is our model trained with the adversarial equalized odds objective.	18
2.4	Data flow at train time (2.4a) and test time (2.4b) for our model, Flexibly Fair VAE (FFVAE).	22
2.5	Fairness-accuracy tradeoff curves, DSpritesUnfair dataset. We sweep a range of hyperparameters for each model and report Pareto fronts. Optimal point is the top left hand corner — this represents perfect accuracy and fairness. MLP is a baseline classifier trained directly on the input data. For each model, encoder outputs are modified to remove information about a . $y = X$ Position for each plot.	25
2.6	Black and pink dashed lines respectively show FFVAE disentanglement audit (the higher the better) and predictiveness audit (the lower the better) as a function of α . These audits use A_i =Shape (see text for details). The blue line is a reference value—the log loss of a classifier that predicts A_i from the other 5 DSprites factors of variation (FoV) alone, ignoring the image—representing the amount of information about A_i inherent in the data.	26

2.7	Celeb-A subgroup fair classification results. Sensitive attributes: Chubby (C), Eyeglasses (E), and Male (M). $y = \text{HeavyMakeup}$	27
3.2	CMNIST with varying label noise θ_y . Under high label noise ($\theta_y > .2$), where the spurious feature color correlates to label <i>more</i> than shape on the train data, EIIL matches or exceeds the test performance of IRM <i>without relying on hand-crafted environments</i> . Under medium label noise ($.1 < \theta_y < .2$), EIIL is worse than IRM but better than ERM, the logical approach if environments are not available. Under low label noise ($\theta_y < .1$), where color is <i>less</i> predictive than shape at train time, ERM performs well and EIIL fails. The vertical dashed black line indicates the default setting of $\theta_y = 0.25$, which we report in Table 3.1.	41
4.1	<i>Four instances of CoDA; orange nodes are relabeled, noise variables omitted for clarity.</i> First: Goal relabeling [Kaelbling, 1993], including HER [Andrychowicz et al., 2017], augments transitions with counterfactual goals. Second: Visual feature augmentation [Andrychowicz et al., 2020, Laskin et al., 2020] uses domain knowledge to change visual features S_t^V (such as textures, lighting, and camera positions) that the designer knows do not impact the physical state S_{t+1}^P . Third: Dyna [Sutton, 1991], including MBPO [Janner et al., 2019], augments real states with new actions and resamples the next state using a learned dynamics model. Fourth (ours): Given two transitions that share local causal structures, we propose to swap connected components to form new transitions.	47
4.2	Counterfactual Data Augmentation (CoDA). Given 3 factual samples, knowledge of the local causal structure lets us mix and match factored subprocesses to form counterfactual samples. The first proposal is rejected because one of its factual sources (the blue ball) is not locally factored. The third proposal is rejected because it is not itself factored. The second proposal is accepted, and can be used as additional training data for a reinforcement learning agent.	48
4.3	A two-armed robot (left) might be modeled as an MDP whose state and action spaces decompose into left and right subspaces: $\mathcal{S} = \mathcal{S}^L \oplus \mathcal{S}^R$, $\mathcal{A} = \mathcal{A}^L \oplus \mathcal{A}^R$. Because the arms can touch, the global causal model (center left) between time steps is fully connected, even though left-to-right and right-to-left connections (dashed red edges) are rarely active. By restricting our attention to the subspace of states in which left and right dynamics are independent we get a local causal model (center right) with two components that can be considered separately for training and inference.	50
4.4	Standard online RL (3 seeds): CoDA with the ground truth mask always performs the best, validating our basic idea. CoDA with a pre-trained model also offers a significant early boost in sample efficiency and maintains its lead over the base TD3 agent throughout training. Using the same model to generate data directly (a la Dyna [Sutton, 1991]) performs poorly, suggesting significant model bias.	54
4.5	Goal-conditioned RL (5 seeds): In <code>FetchPush</code> and the challenging <code>Slide2</code> environment, a HER agent whose dataset has been enlarged with CoDA approximately doubles the sample efficiency of the base HER agent.	55

4.6	Training an RL Agent with MoCoDA: We use the empirical dataset to train parent distribution model, $P_\theta(s, a)$ and locally factored dynamics model $P_\phi(s' s, a)$, both informed by the local structure. The dynamics model is applied to the parent distribution to produce augmented dataset $P_\theta P_\phi$. The augmented & empirical datasets are labeled with the target task reward, $r(s, a)$ and fed into the RL algorithm as training data.	59
4.7	2D Navigation Visualization. (Best viewed with 2x zoom) Blue arrows represent transition samples as a vector from (x_t, y_t) to (x_{t+1}, y_{t+1}) . Shaded red areas mark the edges of the initial states of empirical trajectories and the center of the square. We see that 5-step rollouts (DYNA) do not fill in the center (needed for optimal policy), and fail to constrain actions to those that the model generalizes well on. For MOCODA, we see the effect of compounding dataset imbalance discussed in Subsection 4.4.5, which is resolved by MOCODA-U.	62
4.8	HookSweep2 Visualization: Stylized visualization of the distributions EMP (left), MOCODA (center), and MOCODA-P (right). Each figure can be understood as a top down view of the table, where a point is plotted if the two blocks are close together on the table. The distribution EMP does not overlap with the green goal areas on the left and right, and so the agent is unable to learn. In the MOCODA distribution, the agent gets some success examples. In the MOCODA-P distribution, state-actions are reweighted so that the joint distribution of the two block positions is approximately uniform, leading to more evenly distributed coverage of the table.	63
A.1	Mutual Information Gap (MIG) for various (α, γ) settings of the FFVAE. In Fig. A.1a, each line is a different value of $\gamma \in [10, 20, 30, 40, 50, 70, 100]$, with brighter colors indicating larger values of γ . In Fig. A.1b, each line is a different value of $\alpha \in [300, 400, 1000]$, with brighter colors indicating larger values of α . Models trained on DspritesUnfair, MIG calculated on Dsprites. Higher MIG is better. Black dashed line indicates mean (with outliers excluded). $\alpha = 0$ is equivalent to the FactorVAE.	76
A.2	Mutual Information Gap (MIG) for various (α, γ) settings of the FFVAE. In Fig. A.2a, each line is a different value of $\alpha \in [0, 50, 100, 150, 200]$, with brighter colors indicating larger values of α . In Fig. A.2b, all combinations with $\alpha, \gamma > 0$ are shown. Models trained on DspritesUnfair, MIG calculated on Dsprites. Higher MIG is better. Black dashed line indicates mean (outliers excluded). $\alpha = 0$ is equivalent to the FactorVAE.	77
C.1	The Slide2 environment.	89
C.2	Causal graph for local mask	92
C.3	Hypothetical 2D illustration of the GMM-based parent set sampler. It is assumed that there are two non-overlapping parent sets $\{x\}$ and $\{y\}$, but that x and y exhibit dependence in the empirical data. We fit a GMM to each marginal $P(x)$ and $P(y)$ and sample from them independently to get $Q(x, y)$, which has the same marginal distributions (so that the components in a locally factored dynamics model will generalize), but eliminates the spurious dependence in the empirical data.	93
C.4	Left/Middle: Random samples of the two types of trajectories the agent has access to. Right: Random sample of transitions from this empirical dataset.	95

Chapter 1

Introduction

“The purpose of a system is what it does.”

Stafford Beer [Beer, 2002]

1.1 Turning Data Into Computer Programs

Writing computer programs can be tedious. Writing computer programs that work well can be difficult. Machine Learning (ML) provides an attractive approach to writing computer programs that centers the role of data. For the purposes of ML, a good dataset is one that measures desired system behavior across the many contexts where the system will be deployed and expected to work reliably. This thesis addresses the unfortunate reality that the available training data are, in this sense, typically never “good” enough.

To be sure: just like standard programming, ML also involves writing a lot of computer programs. But *these* programs—called learning algorithms—have a distinct role. Say we have an ML “task”, that is, an open-ended problem such as detecting objects within a visual scene or translating text from one language to another. Rather than directly implementing a solution, the learning algorithm consumes training data to produce a “model” capable (hopefully) of tackling the task at hand.

ML has garnered much interest recently, resulting in its deepening integration into the social fabric. A major catalyst of commercial and academic research on ML was the successful application of deep learning to challenging benchmark tasks, especially in the domain of Computer Vision [Krizhevsky et al., 2012, Rajpurkar et al., 2017]. The connectionist paradigm of using simple learning algorithms to train very “deep” neural networks (i.e. models containing many free “parameters” to be tuned during the learning process) proved to be incredibly effective in practice, typically out-performing more bespoke learning algorithms that relied on hand-specified features or probabilistic assumptions. The subsequent successful application of novel neural network architectures to tasks in Natural Language Processing [Devlin et al., 2018, Radford et al., 2019, Vaswani et al., 2017] added to the fervor around deep learning as a kind of panacea for high-quality predictive models.

1.2 Data Imperfections

The sheer pace of recent advancements in deep learning is staggering. And yet the models that deep learning produces can be surprisingly brittle in practice, often failing in unexpected or problematic

ways upon deployment [Buolamwini and Gebru, 2018b, Geirhos et al., 2020a]. In a sense, when any learning algorithm produces a model, it encapsulates certain statistical understandings about past observations. Intuitively, this model is dataset-dependent, so a failure to acquire adequate training data (in terms of quantity, quality, or both) could have dire consequences, especially considering that people across the globe already interact with ML models as a matter of daily routine.

Deep learning has now moved into the forefront of many application areas, such as online content moderation and recommendation, automotive driver-assistance systems, and machine translation, just to name a few. This trend reveals several curious tensions around data dependency in modern machine learning, which will be the focus of our attention in this manuscript. Before we catalog these issues more completely, let us consider just one such tension: the *underspecification* problem. ML tasks often require predictions to be made using high-dimensional inputs such as images or text sequences. In such cases, while the learning algorithm produces just one model during training, it turns out that there are many possible models capable of achieving the same degree of predictive performance. However, upon deployment, especially if the statistics of the deployment differ from what was seeing during training, these models could behave very differently [D’Amour et al., 2020, Fisher et al., 2019]. So we say that the prediction problem itself, when instantiated with a specific training dataset, is “underspecified”. To make matters worse, making the network deeper exacerbates this issue [Sagawa et al., 2020c]. But the heuristic of making the network deeper and deeper is precisely what lead to improvements in predictive performance on benchmark tasks used by the research community, thus catalyzing the (contemporary) success of deep learning in the first place!

What can we make of this apparent contradiction? Is it the case that as learning algorithms get “deeper”, the resulting models become more shallow? There is evidence to suggest that when it comes to aggregate performance, this tends not to be the case [Bartlett et al., 2020, Kaplan et al., 2020]. However, this thesis takes the position that aggregate measures of performance are poor indicators of the *actual* reliability of ML methods. In this regard, we can take inspiration from the cyberneticist position that “the purpose of a system is what it does.” [Beer, 2002]. ML models will be deployed in real-world scenarios, possibly involving direct interaction with human subjects, or indirect influence on the well-being of human subjects through automated decisions. Thus, unexpected model failures can cause real, material harm to people, in spite of any better intentions during the design and training of the ML model. Accordingly, ML researchers have a responsibility to address these failure modes and work towards ensuring equitable outcomes of emerging ML technologies.

There are many possible avenues for reducing the risk of such real-world harms, most notably in policy, regulation, investigative journalism, and community organizing. To be certain, effort along all of these fronts is needed: ensuring that ML works reliably is not merely a technical concern. Many of the most important questions are simultaneously technical *and* non-technical in nature, such as formulating prediction tasks (and articulating whether certain tasks should *not* be solved [Barocas et al., 2020, Hamidi et al., 2018]), and determining which variables to measure as inputs and targets for prediction [Obermeyer et al., 2019]. However, in this thesis, we narrow our focus and take a more technical approach to characterizing and mitigating failure modes of ML systems. In particular, we focus on the sensitivity of learning algorithms to their training data. We use the term “data imperfections” to describe insufficiencies in the training data that cause unexpected failure modes in ML learning models.

Many types of (possibility overlapping) data imperfections exist in practical settings. When data

are collected about human subjects, historically marginalized groups are often underrepresented (or overrepresented in association with negative outcomes), raising concerns that the model may produce unfair outcomes [Blodgett and O’Connor, 2017, Buolamwini and Gebru, 2018a, Hutchinson et al., 2020, Tomasev et al., 2021]. Other data imperfections can involve more subtle aspects of how inputs and targets are measured. For example, the presence during training of “spurious features”, such as imperceptible pixel-level patterns in high dimensional images, can lead to brittle models upon deployment [Beery et al., 2018a, DeGrave et al., 2021, Geirhos et al., 2020a]. In this thesis, the term “data imperfections” is used rather loosely. Rather than providing a precise diagnosis about a specific dataset, it motivates a particular approach to designing learning algorithms, which starts by recognizing that the available training data cannot fully capture intended system behavior.

1.3 Outline

Throughout this manuscript, we will explore three variations on the common theme of training data imperfection. Each of the three central Chapters discusses to a unique way that available training data can be insufficient for the task at hand, and presents learning algorithms aimed at mitigating these insufficiencies. In particular, we cover the following types of data imperfection:

- **(Chapter 2) The training data encodes prior human discrimination.** For ethical and/or legal reasons we seek a prediction model that avoids compounding these social biases, which we will do by incorporating demographic information in the learning process. In particular, we follow the approach of *Fair Representation Learning* in order to mitigate algorithmic discrimination, and propose novel learning algorithms that promote structure in the learned representations conducive to this goal. This Chapter contains work previously published in two conference papers. The first is “Learning Adversarially Fair and Transferable Representations” [Madras et al., 2018], which was co-authored with David Madras, Toniann Pitassi, and Richard Zemel. The second is “Flexibly Fair Representation Learning by Disentanglement.” [Creager et al., 2019], which was co-authored with David Madras, Jörn-Henrik Jacobsen, Marissa Weis, Kevin Swersky, Toniann Pitassi, and Richard Zemel.
- **(Chapter 3) The training data entails an *underspecified* prediction problem.** There are many predictive functions achieving good predictive accuracy given the available data. Some such solutions may rely on *spurious* features that are unreliable in deployment settings. Where available, metadata indicating the “environment” where each training example was collected can be incorporated as side information into the learning process to mitigate this issue. In order to address the more challenging but realistic setting where this side information is not directly available, we introduce a framework of *Environment Inference* that searches for useful side information (environment labels) directly in the training data. This Chapter was adapted from the conference paper “Environment Inference for Invariant Learning” [Creager et al., 2021], which was co-authored by Jörn-Henrik Jacobsen and Richard Zemel.
- **(Chapter 4) The training data does not have sufficient support to solve the task at hand.** We shift our focus away from prediction and towards sequential decision making. In this context, dynamic programming approaches such as Q-learning provably converge to optimal policies, but only with sufficient coverage over state-action space. Many practical RL settings are data-constrained, and so these strict assumptions around coverage do not hold.

We present data augmentation techniques that rely on prior knowledge over the interaction between objects to improve support of the training data, which can be used a pre-processing step to improve sample efficiency and out-of-distribution robustness of reinforcement learning (RL) agents. This Chapter contains work previously published in two conference papers. The first is “MoCoDA: Model-based Counterfactual Data Augmentation” [Pitis et al., 2022], which was co-authored with Silviu Pitis, Ajay Mandlekar, and Animesh Garg.

We then conclude in Chapter 5 by reflecting on the state of contemporary machine learning research and suggesting some fruitful directions for long-term future work.

This thesis comprises my own original research conducted at the University of Toronto. Yet the ideas described herein were profoundly shaped, through a process of collaboration and cooperation, by the co-authors mentioned above. Special commendation is due to Silviu Pitis for his leadership of the projects described in Chapter 4, and David Madras for co-leading the LAFTR project described in Chapter 2.2.

1.4 Topics Covered in This Manuscript

1.4.1 Robustness

Our goal then is clear: we wish to derive new learning algorithms capable of producing reliable models in spite of training data imperfections. In this thesis we will tend to describe such models as “robust”, a term we use loosely to evoke sturdiness upon deployment in novel contexts. Because the statistical properties of deployment data often differ (perhaps subtly) from training data, some explicit notion of out-of-distribution (OOD) generalization is often required for a model to be considered robust. However, within the fields of ML and statistics, “robust” learning has several other (related) meanings. Adversarial robustness [Madry et al., 2019] seeks to address known sensitivities of deep neural classifiers to small perturbations in the input space, such as imperceptible additive pixel noise for high-dimensional images [Goodfellow et al., 2015b]. Robust statistics [Rousseeuw, 1991] is concerned with deriving inference methods capable of handling outliers or deviations from the assumed parametric form of the data distribution. Robust optimization formulates mathematical programs where the resulting solution can tolerate measurement noise in the observed variables [Ben-Tal et al., 2009a]. In a similar vein, Distributionally Robust Optimization seeks to minimize expected risk over a family of related distributions [Duchi et al., 2021], and has been applied to training deep neural networks [Sagawa et al., 2020b]. In causal inference (see below for an overview), “doubly robust” estimators are a popular way to use both parametric methods (learned regressors) and non-parametric models (importance weights) to estimate interventional quantities from observational data. The estimator is called *doubly* robust in the sense that it remains unbiased (in the statistical sense) even if *either* of these two components is biased (although this claim is nullified when both components contain bias).

Robustness serves as a unifying theme throughout the manuscript, and is discussed in each Chapter. However, the precise design goal—what it means for the learning algorithm to produce a robust model—varies Chapter by Chapter according to the contexts described therein.

1.4.2 Domain Generalization

Learning models capable of OOD generalization is an exceedingly ambitious goal. It is unrealistic to ensure the model will behave as expected in a deployment context whose properties are entirely

unknown during training. Domain Generalization (DG) is an attempt to make OOD-robust learning more tractable via a more structured training process [Blanchard et al., 2011, Muandet et al., 2013]. In DG, data are collected from a variety of “domains”, and the learning algorithms is given access to auxiliary labels indicating the domain origin of each training example. The training domains are distinct from the deployment setting; otherwise no OOD generalization would be required. Hopefully the statistical variation across training domains is representative of the *type* of distribution shift expected during evaluation. In this case, the domain labels can provide clues as to which features are unreliable (not predictive in all domains) and thus not worthy of including in the final model. Domain Adaptation is a related problem setting allows for the model to be updated upon deployment using unlabeled input examples [Patel et al., 2015].

DG is the central focus of Chapter 3. In Chapter 4, we discuss the MoCoDA algorithm and how it can be used for task *transfer* in offline Reinforcement Learning, where data from a source task is used to learn a policy on a target task. Transfer learning is also highlighted in Chapter 2. Both of these settings are indeed related to the goal of OOD generalization. However, unlike most DG settings, they assume some degree of information about the target distribution (a target task reward function in the former case, and limited labeled target data in the latter).

1.4.3 Algorithmic Fairness

It is also useful to think about robustness not directly in statistical terms, but instead in terms of whether the model adheres to social and legal norms. This conceptual framing is especially useful for addressing a more insidious type of data imperfection where ML models predict based on immutable characteristics of individuals (or their proxies) such as demographic group membership. This is a tricky technical issue because we live in a stratified society where social status often provides a very strong predictive signal. So this is not simply a matter of solving the underspecification problem; we may have to compromise on aggregate accuracy in order to find a model that does not rely on demographic information. Algorithmic fairness, which seeks various technical mitigations to these issues—is the focus of Chapter 2, and also receives a cursory discussion in Chapter 3.

Concerns of Automated Discrimination The use of algorithms to automate high-stakes decision making raises a serious concern of automated discrimination against vulnerable populations [Barocas and Selbst, 2016a]. This concern is especially relevant for machine learning systems, as historical disadvantages at the population level are often reflected in data used for training [Goel et al., 2021, Mayson, 2019]. Research on characterizing automated discrimination in ML systems has been greatly influenced by legal precedent in US case law, where concepts such as “disparate treatment” and “disparate impact” were introduced to justify rulings on Title VII disputes [Barocas and Selbst, 2016a]. ML systems may also produce predictions that reproduce social inequities even if they do not meet the strict requirement of discrimination in the legal sense; examples include unequal allocation of resources between demographic groups, or replication of harmful stereotypes [Barocas et al., 2017]. Thus, we find a variety of potentially problematic ML system behaviors, which have subsequently informed proposals for how ML systems can be made “fair” in various ways (discussed briefly below). Interestingly, a post-hoc analysis of these fairness definitions suggests that each is underpinned with a distinct set of normative assumptions about when it is acceptable (or not) to treat people differently [Binns, 2018].

Addressing algorithmic discrimination requires a nuanced look at the data collection process

since, since models may produce “unfair” predictions even if they do not directly train on explicit instances of human discrimination. For example, demographic subpopulations may be under-sampled in the training data, which can produce dramatic performance disparities across groups [Buolamwini and Gebru, 2018a]. It is also important to note that algorithmic systems can have malignant social effects even if they do not directly use machine learning; examples include harmful stereotyping in web search [Noble, 2018] and matching algorithms that uphold the status quo in homeless services [Eubanks, 2018]. While the potential for automated discrimination in ML systems remains a serious concern, algorithmic systems sometimes enable a higher degree of scrutiny than human decision makers¹, suggesting that detecting discrimination (and subsequent legal recourse) could be more tractable with some algorithmic systems [Kleinberg et al., 2018].

Definitions of “Fairness” As suggested earlier, there are many non-technical means (community organizing, policymaking, etc.) by which algorithmic discrimination can be effectively addressed. These efforts can be complemented by the pursuit of (statistically) “fair” machine learning models, since some forms of algorithmic discrimination manifest as performance disparities in data-driven prediction. Accordingly, the ML community has proposed many formal definitions of “fairness”² in order to characterize and address disparities in data-driven prediction. Broadly speaking, these definitions fall under the categories of *Group Fairness* and *Individual Fairness*. Group fairness criterion can be understood as statistical independence conditions expressed via the target labels $Y \in \mathcal{Y}$, sensitive attribute labels $A \in \mathcal{A}$, and the predictions—either hard predictions $\hat{Y} \in \mathcal{Y}$ or soft scores $R \in \mathbb{R}$ (e.g., $R = p(\hat{Y} = 1|X)$) where $\hat{Y} = f(X)$ or $R = f(X)$ are the model outputs. Analyses are typically carried out in the setting of binary target labels and sensitive attributes, i.e., $\mathcal{Y} = \mathcal{A} = \{0, 1\}$. *Demographic Parity*³ (DP) requires $\hat{Y} \perp A$ [Calders and Verwer, 2010, Dwork et al., 2012, Kamishima et al., 2011]. Hardt et al. [2016b] note that this requirement may be overly conservative from an accuracy perspective when the base rates of the target label differ between groups ($p(Y|A = 0) \neq p(Y|A = 1)$), and propose *Equalized Odds* (EOdds) as an alternative, requiring $\hat{Y} \perp A|Y$. One-sided Equalized Odds— $\hat{Y} \perp A|Y = 1$ or $\hat{Y} \perp A|Y = 0$ —is called Equal Opportunity (EOpp), and is sometimes more precisely referred to as Equalized False Positive Rates for the $Y = 1$ case and Equalized False Negative Rates for the $Y = 0$ case.

Another category of important group fairness criteria relate to classifier *calibration*, which describes models that output scores consistent with the true label probability: $p(Y|A = a, R = r) = r \forall \{a, r\}$. Calibration was shown to be incompatible with certain parity-based fairness criteria in two influential and concurrent works Chouldechova [2017], Kleinberg et al. [2016].

Dwork et al. [2012] proposed the canonical notion of individual fairness, whereby the classifier must “treat similar individuals similarly”. Formally, this entails specifying a similarity metric $d(X, X')$ for pairs of individuals, then enforcing a Lipschitz smoothness constraint on the classifier output $f(X)$ and $f(X')$ w.r.t. this metric $\forall X, X'$. While intuitive and flexible⁴, this definition shunts the difficulty of defining “fairness” onto the difficulty of defining the metric d , and can thus be difficult to implement in practice.

¹Crucially, this relies on a transparent training process and interpretable model predictions, which are not found in every ML system.

²Interestingly, the standardized testing industry independently discovered many of these notions in the 1960s and 1970s [Hutchinson and Mitchell, 2019].

³Also called *statistical parity*.

⁴Given a sensitive attribute labels, this framework can also be made to express demographic parity.

Fair Classification Given a group fairness criteria and a classification task, learning a fair classifier can be naturally formulated as a constrained or regularized optimization problem. Calders and Verwer [2010] describe how to modify naive Bayes with to achieve DP. Kamishima et al. [2011] describe a more general DP regularization approach suitable for classifiers that output a probability score $R = f(X)$ with $R = p(\hat{Y} = Y|X)$. Hardt et al. [2016b] describe a post-hoc method for converting a naive classifier into a EOdds or EOpp classifier.

Fair Representation Learning The goal of representation learning is broader than that of classification: it seeks a *general purpose* representation of the data that admits efficient and accurate classification for a *variety* of downstream tasks [Bengio et al., 2013a]. The list of admissible representation learning methodologies is also broad, encompassing unsupervised learning with autoencoders and variational autoencoders [Kingma and Welling, 2014, Vincent et al., 2008], to fine-tuning the neural activations of a deep discriminative net [Huh et al., 2016].

In the context of fair machine learning, group fairness constraints can be incorporated into representation learning algorithms to learn an encoding of the data that is invariant to the sensitive attributes. If such an encoding is learned, it serves as a fairness bottleneck that guarantees any downstream predictions computed from the representation alone will satisfy the desired fairness criteria.

1.4.4 Causal Inference

Causal inference is an attempt to reason about fictitious data in a principled way. While machine learning provides many expressive tools for modeling correlational patterns in data—from which accurate predictors can be derived—there are many compelling inference questions (typically concerning causes and effects) that cannot be directly answered using correlation patterns in the data. For example, in order to improve patient health outcomes, we may wish to know: “given the patient health outcomes observed in a clinical setting, how effective was a particular treatment in the patient population?” This requires reasoning about events that did not happen, because in practical settings the treatment was not administered in a uniform or random way. Rather, each patient received an individualized treatment. As it turns out, estimating treatment efficacy from standard conditional probabilities can point us in the wrong direction if there were confounding factors in the data causing some patient subpopulations to take the treatment at higher rates.

Fortunately there are methods for answering such questions by directly using real-world data, although they typically rely on strong (and often untestable) assumptions about the problem setting. There are several influential frameworks for causal inference, most notably the causal graphical models of Pearl and colleagues [Pearl, 2009a] and the potential outcomes framework of Rubin and colleagues [Rubin, 2005]. Chapter 4 makes use of causal graphs to encode domain knowledge about sequential decision-making problems.

1.4.5 Reinforcement Learning

Reinforcement Learning (RL) provides a data-driven approach to sequential decision making, suitable for producing models that must be deployed in a dynamically-changing setting. An RL model, called “policies”, is a mapping from observed state of the setting to an appropriate action. Crucially, the learning algorithm receives a scalar reward signal every time an action is taken at a given state. The overall goal is to learn a policy that maximizes long-term reward, there are algorithms that

provably converge to an optimal policy under certain assumptions, such as a coverage requirement that all states and actions be visited with some frequency. One of the main appeals of RL is its broad applicability, as the learning algorithm can learn an effective policy even without a detailed model of the physical domain (or other dynamics) where the policy is learning. On the other hand, in settings where dynamics *are* known, methods from planning or control theory may yield a solution more efficiently than RL

While there are many RL algorithms of theoretical and practical interest, two general approaches are worth mentioning: The first approach is value iteration (e.g. Q-learning), where intermediate *value functions*, which encapsulate how much reward a policy can accrue starting from a given state, are estimated using dynamic programming. Chapter 4 addresses the coverage assumption of value iteration algorithms head-on, introducing causal graphical priors as a way to assist learning when coverage is lacking. Policy gradient methods provide an alternate approach (not discussed in thesis) where the policy function is optimized directly using unbiased estimates of the long-term rewards. Notably, neural networks have been applied in each of these general approaches as function approximators for the key mathematical objects—value functions, and policies, respectively—to derive useful policies in challenging settings [Maddison et al., 2014].

Chapter 2

Representation Learning Approaches to Algorithmic Fairness

2.1 The Role of Data Representations in Fair Machine Learning

Is it possible for ML to produce models that provide a social utility without replicating inequities in the social context where data was collected? That is our focus in this chapter, where we discuss algorithmic fairness in the context of classification problems [Calders and Verwer, 2010, Hardt et al., 2016b, Kamiran and Calders, 2009, Kamishima et al., 2011, Pedreshi et al., 2008], and ask *how the data should be formatted* so that prior human discrimination is not directly automated in the learning process [Barocas and Selbst, 2016b, Dwork et al., 2011, Obermeyer et al., 2019]. We attempt to address this issue by playing to one of ML’s strengths: its ability to synthesize a wide variety of data formats automatically by training neural networks on top of the raw data. The idea is to formulate the learning problem in terms of both predictive accuracy and a coarse-grained notion of statistical fairness across known demographic groups during training.

Crucially, we emphasize that the model’s internal *representation* of the data—or example, the internal activations within a deep neural network [Bengio et al., 2013b]— should be fair in this sense. This is attractive because the learned representation provides a mapping (from the original data space to a new vector space with group fairness properties) that can be reused in new settings [Louizos et al., 2016b, Zemel et al., 2013]. We hope that this mapping will serve as a fairness bottleneck, enabling the use of a single large dataset to train a variety of ML models, each with a distinct prediction task. It also opens up the possibility of interaction between entities (firms, research groups, or other data-owning collectives) to solve machine learning problems cooperatively. Typically, these types of collaborations would entail some sort of data asymmetry: despite all parties sharing an interest in solving the task, only one party owns and maintains the data. Fair representation learning enables the data owner to automatically format their data in a way that is suitable for training machine learning models, while also encouraging fairness in these downstream models.

2.2 Encouraging Statistical Parity in Learned Representations with Adversarial Training

There are two implicit steps involved in every prediction task: acquiring data in a suitable form, and specifying an algorithm that learns to predict well given the data. In practice these two responsibilities are often assumed by distinct parties. For example, in online advertising the so-called *prediction vendor* profits by selling its predictions (e.g., person X is likely to be interested in product Y) to an advertiser, while the *data owner* profits by selling a predicatively useful dataset to the prediction vendor Dwork et al. [2012].

Because the prediction vendor seeks to maximize predictive accuracy, it may (intentionally or otherwise) bias the predictions to unfairly favor certain groups or individuals. The use of machine learning in this context is especially concerning because of its reliance on historical datasets that may include patterns of previous discrimination or other societal bias. Thus there has been a flurry of recent work from the machine learning community focused on defining and quantifying these biases and proposing new prediction systems that mitigate their impact.

Meanwhile, the data owner also faces a decision that critically affects the predictions: what is the correct *representation* of the data? Often, this choice of representation is made at the level of data collection: feature selection and measurement. If we want to maximize the prediction vendor’s utility, then the right choice is to simply collect and provide the prediction vendor with as much data as possible. However, assuring that prediction vendors learn only *fair* predictors complicates the data owner’s choice of representation, which must yield predictors that are never unfair but nevertheless have relatively high utility.

In this Section, we frame the data owner’s choice as a representation learning problem with an adversary criticizing potentially unfair solutions. Our contributions are as follows: We connect common group fairness metrics (demographic parity, equalize odds, and equal opportunity) to adversarial learning by providing appropriate adversarial objective functions for each metric that upper bounds the unfairness of arbitrary downstream classifiers in the limit of adversarial training; we distinguish our algorithm from previous approaches to adversarial fairness and discuss its suitability to fair classification due to the novel choice of adversarial objective and emphasis on representation as the focus of adversarial criticism; we validate experimentally that classifiers trained naively (without fairness constraints) from representations learned by our algorithm achieve their respective fairness desiderata; furthermore, we show empirically that these representations achieve *fair transfer* — they admit fair predictors on unseen tasks, even when those predictors are not explicitly specified to be fair.

2.2.1 Background: Fair Classification

In fair classification we have some data $X \in \mathbb{R}^n$, labels $Y \in \{0, 1\}$, and sensitive attributes $A \in \{0, 1\}$. The predictor outputs a prediction $\hat{Y} \in \{0, 1\}$. We seek to learn to predict outcomes that are accurate with respect to Y but fair with respect to A ; that is, the predictions are accurate but not biased in favor of one group or the other.

There are many possible criteria for group fairness in this context. One is *demographic parity*, which ensures that the positive outcome is given to the two groups at the same rate, i.e. $\Pr(\hat{Y} = 1|A = 0) = \Pr(\hat{Y} = 1|A = 1)$. However, the usefulness of demographic parity can be limited if the *base*

rates of the two groups differ, i.e. if $\Pr(Y = 1|A = 0) \neq \Pr(Y = 1|A = 1)$. In this case, we can pose an alternate criterion by conditioning the metric on the ground truth Y , yielding *equalized odds* and *equal opportunity* [Hardt et al., 2016b]; the former requires equal false positive and false negative rates between the groups while the latter requires only one of these equalities. Equal opportunity is intended to match errors in the “advantaged” outcome across groups; whereas Hardt et al. [2016b] chose $Y = 1$ as the advantaged outcome, the choice is domain specific and we here use $Y = 0$ instead without loss of generality. Formally, this is $\Pr(\hat{Y} \neq Y|A = 0, Y = y) = \Pr(\hat{Y} \neq Y|A = 1, Y = y) \forall y \in \{0, 1\}$ (or just $y = 0$ for equal opportunity).

Satisfying these constraints is known to conflict with learning well-calibrated classifiers [Chouldechova, 2017, Kleinberg et al., 2016, Pleiss et al., 2017]. It is common to instead optimize a relaxed objective [Kamishima et al., 2012], whose hyperparameter values negotiate a tradeoff between maximizing utility (usually classification accuracy) and fairness.

2.2.2 Background: Adversarial Learning

Adversarial learning is a popular method of training neural network-based models. Goodfellow et al. [2014] framed learning a deep generative model as a two-player game between a generator G and a discriminator D . Given a dataset X , the generator aims to fool the discriminator by generating convincing synthetic data, i.e., starting from random noise $z \sim p(z)$, $G(z)$ resembles X . Meanwhile, the discriminator aims to distinguish between real and synthetic data by assigning $D(G(z)) = 0$ and $D(X) = 1$. Learning proceeds by the max-min optimization of the joint objective

$$V(D, G) \triangleq \mathbb{E}_{p(X)}[\log(D(X))] + \mathbb{E}_{p(z)}[\log(1 - D(G(z)))],$$

where D and G seek to maximize and minimize this quantity, respectively.

2.2.3 Learning Adversarially Fair and Transferable Representations

We assume a generalized model (Figure 2.4), which seeks to learn a data representation Z capable of reconstructing the inputs X , classifying the target labels Y , and protecting the sensitive attribute A from an adversary. Either of the first two requirements can be omitted by setting hyperparameters to zero, so the model easily ports to strictly supervised or unsupervised settings as needed. This general formulation was originally proposed by Edwards and Storkey [2016]; below we address our specific choices of adversarial objectives and explore their fairness implications, which distinguish our work as more closely aligned to the goals of fair representation learning.

The dataset consists of tuples (X, A, Y) in \mathbb{R}^n , $\{0, 1\}$ and $\{0, 1\}$, respectively. The encoder $f : \mathbb{R}^n \rightarrow \mathbb{R}^m$ yields the representations Z . The encoder can also optionally receive A as input. The classifier and adversary¹ $g, h : \mathbb{R}^m \rightarrow \{0, 1\}$ each act on Z and attempt to predict Y and A , respectively. Optionally, a decoder $k : \mathbb{R}^m \times \{0, 1\} \rightarrow \mathbb{R}^n$ attempts to reconstruct the original data from the representation and the sensitive variable.

The adversary h seeks to maximize its objective $L_{Adv}(h(f(X, A)), A)$. We discuss a novel and theoretically motivated adversarial objective in Sections 2.2.3, whose exact terms are modified according to the fairness desideratum.

Meanwhile, the encoder, decoder, and classifier jointly seek to minimize classification loss and reconstruction error, and also minimize the adversary’s objective. Let L_C denote a suitable classifica-

¹In learning equalized odds or equal opportunity representations, the adversary $h : \mathbb{R}^m \times \{0, 1\} \rightarrow \{0, 1\}$ also takes the label Y as input.

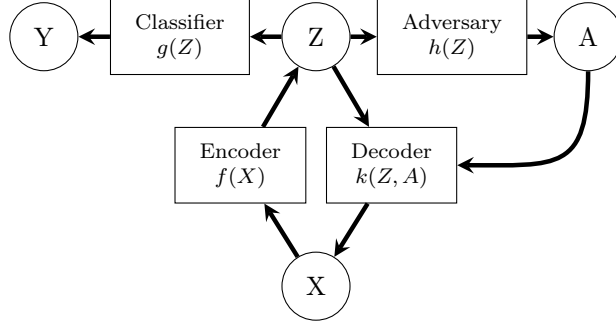


Figure 2.1: Model for learning adversarially fair representations. The variables are data X , latent representations Z , sensitive attributes A , and labels Y . The encoder f maps X (and possibly A - not shown) to Z , the decoder k reconstructs X from (Z, A) , the classifier g predicts Y from Z , and the adversary h predicts A from Z (and possibly Y - not shown).

tion loss (e.g., cross entropy, ℓ_1), and L_{Dec} denote a suitable reconstruction loss (e.g., ℓ_2). Then we train the generalized model according to the following min-max procedure:

$$\underset{f,g,k}{\text{minimize}} \underset{h}{\text{maximize}} \mathbb{E}_{X,Y,A} [L(f, g, h, k)], \quad (2.1)$$

with the combined objective expressed as

$$\begin{aligned} L(f, g, h, k) &= \alpha L_C(g(f(X, A)), Y) \\ &\quad + \beta L_{Dec}(k(f(X, A), A), X) \\ &\quad + \gamma L_{Adv}(h(f(X, A)), A) \end{aligned} \quad (2.2)$$

The hyperparameters α, β, γ respectively specify a desired balance between utility, reconstruction of the inputs, and fairness.

Due to the novel focus on fair transfer learning, we call our model Learned Adversarially Fair and Transferable Representations (LAFTR).

Learning Objective We realize f, g, h , and k as neural networks and alternate gradient descent and ascent steps to optimize their parameters according to (2.2). First the encoder-classifier-decoder group (f, g, k) takes a gradient step to minimize L while the adversary h is fixed, then h takes a step to maximize L with fixed (f, g, k) . Computing gradients necessitates relaxing the binary functions g and h , the details of which are discussed below.

For shorthand we denote the adversarial objective $L_{Adv}(h(f(X, A)), A)$ —whose functional form depends on the desired fairness criteria—as $L_{Adv}(h)$. For demographic parity, we take the average absolute difference on each sensitive group $\mathcal{D}_0, \mathcal{D}_1$:

$$L_{Adv}^{DP}(h) = 1 - \sum_{i \in \{0,1\}} \frac{1}{|\mathcal{D}_i|} \sum_{(x,a) \in \mathcal{D}_i} |h(f(x, a)) - a| \quad (2.3)$$

For equalized odds, we take the average absolute difference on each sensitive group-label combination $\mathcal{D}_0^0, \mathcal{D}_1^0, \mathcal{D}_0^1, \mathcal{D}_1^1$, where $\mathcal{D}_i^j = \{(x, y, a) \in \mathcal{D} | a = i, y = j\}$:

$$L_{Adv}^{EO}(h) = 2 - \sum_{(i,j) \in \{0,1\}^2} \frac{1}{|\mathcal{D}_i^j|} \sum_{(x,a) \in \mathcal{D}_i^j} |h(f(x, a)) - a| \quad (2.4)$$

To achieve equal opportunity, we need only sum terms corresponding to $Y = 0$.

Motivation For intuition on this approach and the upcoming theoretical section, we return to the *owner-vendor* framework previously discussed, with a data *owner* who sells representations to a (prediction) *vendor*. Suppose the data owner is concerned about the unfairness in the predictions made by vendors who use their data. Given that vendors are strategic actors with goals, the owner may wish to guard against two types of vendors:

- The *indifferent* vendor: this vendor is concerned with utility maximization, and doesn't care about the fairness or unfairness of their predictions.
- The *adversarial* vendor: this vendor will attempt to actively discriminate by the sensitive attribute.

In the adversarial model defined in Section 2.2.3, the encoder is what the data owner really wants; this yields the representations which will be sold to vendors. When the encoder is learned, the other two parts of the model ensure that the representations respond appropriately to each type of vendor: the classifier ensures utility by simulating an indifferent vendor with a prediction task, and the adversary ensures fairness by simulating an adversarial vendor with discriminatory goals. It is important to the data owner that the model's adversary be as strong as possible—if it is too weak, the owner will underestimate the unfairness enacted by the adversarial vendor.

However, there is another important reason why the model should have a strong adversary, which is key to our theoretical results. Intuitively, the degree of unfairness achieved by the adversarial vendor (who is optimizing for unfairness) will not be exceeded by the indifferent vendor. Beating a strong adversary h during training implies that downstream classifiers naively trained on the learned representation Z must also act fairly. Crucially, this fairness bound depends on the discriminative power of h ; this motivates our use of the representation Z as a direct input to h , because it yields a strictly more powerful h and thus tighter unfairness bound than adversarially training on the predictions and labels alone as in Zhang et al. [2018].

Theoretical Properties We now draw a connection between our choice of adversarial objective and several common metrics from the fair classification literature. We derive adversarial upper bounds on unfairness that can be used in adversarial training to achieve either demographic parity, equalized odds, or equal opportunity.

We are interested in quantitatively comparing two distributions corresponding to the learned group representations, so consider two distributions \mathcal{D}_0 and \mathcal{D}_1 over the same sample space $\Omega_{\mathcal{D}}$, as well as a binary test function $\mu : \Omega_{\mathcal{D}} \rightarrow \{0, 1\}$. μ is called a test since it can distinguish between samples from the two distributions according to the absolute difference in its expected value. We call this quantity the *test discrepancy* and express it as

$$d_{\mu}(\mathcal{D}_0, \mathcal{D}_1) \triangleq \left| \mathbb{E}_{x \sim \mathcal{D}_0} [\mu(x)] - \mathbb{E}_{x \sim \mathcal{D}_1} [\mu(x)] \right|. \quad (2.5)$$

The *statistical distance* (a.k.a. total variation distance) between distributions is defined as the maximum attainable test discrepancy [Cover and Thomas, 2012]:

$$\Delta^*(\mathcal{D}_0, \mathcal{D}_1) \triangleq \sup_{\mu} d_{\mu}(\mathcal{D}_0, \mathcal{D}_1). \quad (2.6)$$

When learning fair representations we are interested in the distribution of Z conditioned on a specific value of group membership $A \in \{0, 1\}$. As a shorthand we denote the distributions $p(Z|A = 0)$ and $p(Z|A = 1)$ as \mathcal{Z}_0 and \mathcal{Z}_1 , respectively.

Bounding Demographic Parity In supervised learning we seek a g that accurately predicts some label Y ; in fair supervised learning we also want to quantify g according to the fairness metrics discussed in Section 2.2.1. For example, the demographic parity distance is expressed as the absolute expected difference in classifier outcomes between the two groups:

$$\Delta_{DP}(g) \triangleq d_g(\mathcal{Z}_0, \mathcal{Z}_1) = |\mathbb{E}_{\mathcal{Z}_0}[g] - \mathbb{E}_{\mathcal{Z}_1}[g]|. \quad (2.7)$$

Note that $\Delta_{DP}(g) \leq \Delta^*(\mathcal{Z}_0, \mathcal{Z}_1)$, and also that $\Delta_{DP}(g) = 0$ if and only if $g(Z) \perp A$, i.e., demographic parity has been achieved.

Now consider an adversary $h : \Omega_{\mathcal{Z}} \rightarrow \{0, 1\}$ whose objective (negative loss) function² is expressed as

$$L_{Adv}^{DP}(h) \triangleq \mathbb{E}_{\mathcal{Z}_0}[1 - h] + \mathbb{E}_{\mathcal{Z}_1}[h] - 1. \quad (2.8)$$

Given samples from $\Omega_{\mathcal{Z}}$ the adversary seeks to correctly predict the value of A , and learns by maximizing $L_{Adv}^{DP}(h)$. Given an optimal adversary trained to maximize (2.8), the adversary’s loss will bound $\Delta_{DP}(g)$ from above for any function g learnable from Z . Thus a sufficiently powerful adversary h will expose through the value of its objective the demographic disparity of any classifier g . We will later use this to motivate learning fair representations via an encoder $f : \mathcal{X} \rightarrow \mathcal{Z}$ that simultaneously minimizes the task loss and minimizes the adversary objective.

Theorem. *Consider a classifier $g : \Omega_{\mathcal{Z}} \rightarrow \Omega_{\mathcal{Y}}$ and adversary $h : \Omega_{\mathcal{Z}} \rightarrow \Omega_{\mathcal{A}}$ as binary functions, i.e., $\Omega_{\mathcal{Y}} = \Omega_{\mathcal{A}} = \{0, 1\}$. Then $L_{Adv}^{DP}(h^*) \geq \Delta_{DP}(g)$: the demographic parity distance of g is bounded above by the optimal objective value of h .*

Proof. By definition $\Delta_{DP}(g) \geq 0$. Suppose without loss of generality (WLOG) that $\mathbb{E}_{\mathcal{Z}_0}[g] \geq \mathbb{E}_{\mathcal{Z}_1}[g]$, i.e., the classifier predicts the “positive” outcome more often for group A_0 in expectation. Then, an immediate corollary is $\mathbb{E}_{\mathcal{Z}_1}[1 - g] \geq \mathbb{E}_{\mathcal{Z}_0}[1 - g]$, and we can drop the absolute value in our expression of the disparate impact distance:

$$\Delta_{DP}(g) = \mathbb{E}_{\mathcal{Z}_0}[g] - \mathbb{E}_{\mathcal{Z}_1}[g] = \mathbb{E}_{\mathcal{Z}_0}[g] + \mathbb{E}_{\mathcal{Z}_1}[1 - g] - 1 \quad (2.9)$$

where the second equality is due to $\mathbb{E}_{\mathcal{Z}_1}[g] = 1 - \mathbb{E}_{\mathcal{Z}_1}[1 - g]$. Now consider an adversary that guesses the opposite of g , i.e., $h = 1 - g$. Then³, we have

$$\begin{aligned} L_{Adv}^{DP}(h) &= L_{Adv}^{DP}(1 - g) = \mathbb{E}_{\mathcal{Z}_0}[g] + \mathbb{E}_{\mathcal{Z}_1}[1 - g] - 1 \\ &= \Delta_{DP}(g) \end{aligned} \quad (2.10)$$

The optimal adversary h^* does at least as well as any arbitrary choice of h , therefore $L_{Adv}^{DP}(h^*) \geq L_{Adv}^{DP}(h) = \Delta_{DP}(g)$. \blacksquare

In Appendix A.1.1 we provide an analogous derivation for equalized odds [Hardt et al., 2016b].

²This is equivalent to the objective expressed by Equation 2.3 when the expectations are evaluated with finite samples.

³Before we assumed WLOG $\mathbb{E}_{\mathcal{Z}_0}[g] \geq \mathbb{E}_{\mathcal{Z}_1}[g]$. If instead $\mathbb{E}_{\mathcal{Z}_0}[g] < \mathbb{E}_{\mathcal{Z}_1}[g]$ then we simply choose $h = g$ instead to achieve the same result.

Additional points One interesting note is that in each proof, we provided an example of an adversary which was calculated only from the joint distribution of Y, A , and $\hat{Y} = g(Z)$ —we did not require direct access to Z —and this adversary achieved a loss exactly equal to the quantity in question (Δ_{DP} or Δ_{EO}). Therefore, if we only allow our adversary access to those outputs, our adversarial objective (assuming an optimal adversary), is equivalent to simply adding either Δ_{DP} or Δ_{EO} to our classification objective, similar to common regularization approaches [Bechavod and Ligett, 2017, Kamishima et al., 2012, Madras et al., 2017, Zafar et al., 2017]. Below we consider a stronger adversary, with direct access to the key intermediate learned representation Z . This allows for a potentially greater upper bound for the degree of unfairness, which in turn forces any classifier trained on Z to act fairly.

In our proofs we have considered the classifier g and adversary h as binary functions. In practice we want to learn these functions by gradient-based optimization, so we instead substitute their continuous relaxations $\tilde{g}, \tilde{h} : \Omega_Z \rightarrow [0, 1]$. By viewing the continuous output as parameterizing a Bernoulli distribution over outcomes we can follow the same steps in our earlier proofs to show that in both cases (demographic parity and equalized odds) $\mathbb{E}[L(\tilde{h}^*)] \geq \mathbb{E}[\Delta(\tilde{g})]$, where \tilde{h}^* and \tilde{g} are randomized binary classifiers parameterized by the outputs of \tilde{h}^* and \tilde{g} .

Comparison to Edwards and Storkey [2016] An alternative to optimizing the expectation of the randomized classifier \tilde{h} is to minimize its negative log likelihood (NLL - also known as cross entropy loss), given by

$$L(\tilde{h}) = -\mathbb{E}_{Z,A} \left[A \log \tilde{h}(Z) + (1 - A) \log(1 - \tilde{h}(Z)) \right]. \quad (2.11)$$

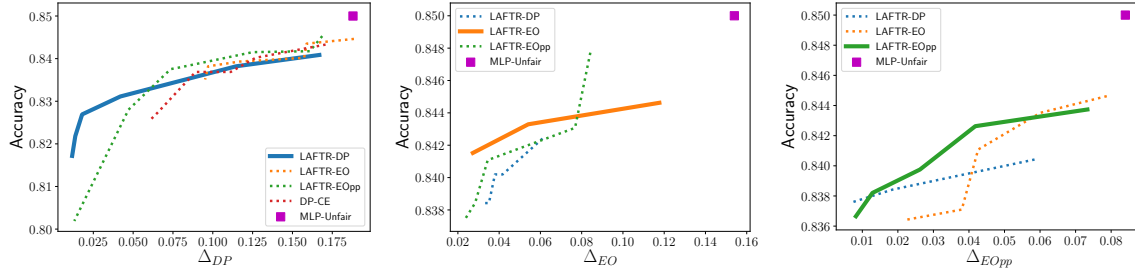
This is the formulation adopted by Ganin et al. [2016] and Edwards and Storkey [2016], which propose maximizing (2.11) as a proxy for computing the statistical distance⁴ $\Delta^*(\mathcal{Z}_0, \mathcal{Z}_1)$ during adversarial training.

The adversarial loss we adopt here instead of cross-entropy is group-normalized ℓ_1 , defined in Equations 2.3 and 2.4. The main problems with cross entropy loss in this setting arise from the fact that the adversarial objective should be calculating the test discrepancy. However, the cross entropy objective sometimes fails to do so, for example when the dataset is imbalanced. Furthermore, group normalized ℓ_1 corresponds to a more natural relaxation of the fairness metrics in question. It is important that the adversarial objective incentivizes the test discrepancy, as group-normalized ℓ_1 does; this encourages the adversary to get an objective value as close to Δ^* as possible, which is key for fairness. In practice, optimizing ℓ_1 loss with gradients can be difficult, so while we suggest it as a suitable theoretically-motivated continuous relaxation for our model (and present experimental results), there may be other suitable options beyond those considered in this work.

2.2.4 Experiments

Fair classification LAFTR seeks to learn an encoder yielding fair representations, i.e., the encoder’s outputs can be used by third parties with the assurance that their naively trained classifiers will be reasonably fair and accurate. Thus we evaluate the quality of the encoder according to the following training procedure, also described in pseudo-code by Algorithm 1. Using labels Y , sensitive attribute

⁴These papers discuss the bound on $\Delta_{DP}(g)$ in terms of the \mathcal{H} -divergence Blitzer et al. [2006], which is simply the statistical distance Δ^* up to a multiplicative constant.



(a) Tradeoff between accuracy and Δ_{DP} (b) Tradeoff between accuracy and Δ_{EO} (c) Tradeoff between accuracy and Δ_{EOpp}

Figure 2.2: Accuracy-fairness tradeoffs for various fairness metrics (Δ_{DP} , Δ_{EO} , Δ_{EOpp}), and LAFTR adversarial objectives (L_{Adv}^{DP} , L_{Adv}^{EO} , L_{Adv}^{EOpp}) on fair classification of the Adult dataset. Upper-left corner (high accuracy, low Δ) is preferable. Figure 2.2a also compares to a cross-entropy adversarial objective [Edwards and Storkey, 2016], denoted DP-CE. Curves are generated by sweeping a range of fairness coefficients γ , taking the median across 7 runs per γ , and computing the Pareto front. In each plot, the bolded line is the one we expect to perform the best. Magenta square is a baseline MLP with no fairness constraints. see Algorithm 1 and Appendix A.1.2.

ALGORITHM 1 Evaluation scheme for fair classification ($Y' = Y$) & transfer learning ($Y' \neq Y$).

Input: data $X \in \Omega_X$, sensitive attribute $A \in \Omega_A$, labels $Y, Y' \in \Omega_Y$, representation space Ω_Z .

Step 1: Learn an encoder $f : \Omega_X \rightarrow \Omega_Z$ using data X , task label Y , and sensitive attribute A .

Step 2: Freeze f .

Step 3: Learn a classifier (without fairness constraints) $g : \Omega_Z \rightarrow \Omega_Y$ on top of f , using data $f(X')$, task label Y' , and sensitive attribute A' .

Step 3: Evaluate the fairness and accuracy of the composed classifier $g \circ f : \Omega_X \rightarrow \Omega_Y$ on held out test data, for task Y' .

A , and data X , we train an encoder using the adversarial method outlined in Section 2.2.3, receiving both X and A as inputs. We then freeze the learned encoder; from now on we use it only to output representations Z . Then, using unseen data, we train a classifier on top of the frozen encoder. The classifier learns to predict Y from Z — note, this classifier is not trained to be fair. We can then evaluate the accuracy and fairness of this classifier on a test set to assess the quality of the learned representations.

During Step 1 of Algorithm 1, the learning algorithm is specified either as a baseline (e.g., unfair MLP) or as LAFTR, i.e., stochastic gradient-based optimization of (Equation 2.1) with one of the three adversarial objectives described in Section 2.2.3. When LAFTR is used in Step 1, all but the encoder f are discarded in Step 2. For all experiments we use cross entropy loss for the classifier (we observed training instability with other classifier losses). The classifier g in Step 3 is a feed-forward MLP trained with SGD. See Appendix A.1.2 for details.

We evaluate the performance of our model⁵ on fair classification on the UCI Adult dataset⁶, which contains over 40,000 rows of information describing adults from the 1994 US Census. We aimed to predict each person’s income category (either greater or less than 50K/year). We took the sensitive attribute to be gender, which was listed as Male or Female.

Figure 2.2 shows classification results on the Adult dataset. Each sub-figure shows the accuracy-fairness trade-off (for varying values of γ ; we set $\alpha = 1, \beta = 0$ for all classification experiments) evaluated according to one of the group fairness metrics: Δ_{DP} , Δ_{EO} , and Δ_{EOpp} . For each fairness

⁵See <https://github.com/VectorInstitute/lafr> for code.

⁶<https://archive.ics.uci.edu/ml/datasets/adult>

metric, we show the trade-off curves for LAFTR trained under three adversarial objectives: L_{Adv}^{DP} , L_{Adv}^{EO} , and L_{Adv}^{EOpp} . We observe, especially in the most important regiment for fairness (small Δ), that the adversarial objective we propose for a particular fairness metric tends to achieve the best trade-off. Furthermore, in Figure 2.2a, we compare our proposed adversarial objective for demographic parity with the one proposed in [Edwards and Storkey, 2016], finding a similar result.

For low values of un-fairness, i.e., minimal violations of the respective fairness criteria, the LAFTR model trained to optimize the target criteria obtains the highest test accuracy. While the improvements are somewhat uneven for other regions of fairness-accuracy space (which we attribute to instability of adversarial training), this demonstrates the potential of our proposed objectives. However, the fairness of our model’s learned representations are not limited to the task it is trained on. We now turn to experiments which demonstrate the utility of our model in learning fair representations for a variety of tasks.

Transfer Learning In this section, we show the promise of our model for *fair transfer learning*. As far as we know, beyond a brief introduction in Zemel et al. [2013], we provide the first in-depth experimental results on this task, which is pertinent to the common situation where the data owner and vendor are separate entities.

We examine the Heritage Health dataset⁷, which comprises insurance claims and physician records relating to the health and hospitalization of over 60,000 patients. We predict the Charlson Index, a comorbidity indicator that estimates the risk of patient death in the next several years. We binarize the (non negative) Charlson Index as zero/nonzero. We took the sensitive variable as binarized age (thresholded at 70 years old). This dataset contains information on sex, age, lab test, prescription, and claim details.

The task is as follows: using data X , sensitive attribute A , and labels Y , learn an encoding function f such that given unseen X' , the representations produced by $f(X', A)$ can be used to learn a fair predictor for new task labels Y' , even if the new predictor is being learned by a vendor who is indifferent or adversarial to fairness. This is an intuitively desirable condition: if the data owner can guarantee that predictors learned from their representations will be fair, then there is no need to impose fairness restrictions on vendors, or to rely on their goodwill.

The original task is to predict Charlson index Y fairly with respect to age A . The transfer tasks relate to the various primary condition group (PCG) labels, each of which indicates a patient’s insurance claim corresponding to a specific medical condition. PCG labels $\{Y'\}$ were held out during LAFTR training but presumably correlate to varying degrees with the original label Y . The prediction task was binary: did a patient file an insurance claim for a given PCG label in this year? For various patients, this was true for zero, one, or many PCG labels. There were 46 different PCG labels in the dataset; we considered only used the 10 most common—whose positive base rates ranged from 9-60%—as transfer tasks.

Our experimental procedure was as follows. To learn representations that transfer fairly, we used the same model as described above, but set our reconstruction coefficient $\beta = 1$. Without this, the adversary will stamp out any information not relevant to the label from the representation, which will hurt transferability. We can optionally set our classification coefficient α to 0, which worked better in practice. Note that although the classifier g is no longer involved when $\alpha = 0$, the target

⁷<https://www.kaggle.com/c/hhp>

task labels are still relevant for either equalized odds or equal opportunity transfer fairness.

We split our test set ($\sim 20,000$ examples) into transfer-train, -validation, and -test sets. We trained LAFTR ($\alpha = 0, \beta = 1$, ℓ_2 loss for the decoder) on the full training set, and then only kept the encoder. In the results reported here, we trained using the equalized odds adversarial objective described in Section 2.2.3; similar results were obtained with the other adversarial objectives. Then, we created a feed-forward model which consisted of our frozen, adversarially-learned encoder followed by an MLP with one hidden layer, with a loss function of cross entropy with no fairness modifications. Then, $\forall i \in 1 \dots 10$, we trained this feed-forward model on PCG label i (using the transfer-train and -validation) sets, and tested it on the transfer-test set. This procedure is described in Algorithm 1, with Y' taking 10 values in turn, and Y remaining constant ($Y \neq Y'$).

We trained four models to test our method against. The first was an MLP predicting the PCG label directly from the data (Target-Unfair), with no separate representation learning involved and no fairness criteria in the objective—this provides an effective upper bound for classification accuracy. The others all involved learning separate representations on the original task, and freezing the encoder as previously described; the internal representations of MLPs have been shown to contain useful information Hinton and Salakhutdinov [2006]. These (and LAFTR) can be seen as the values of REPRLEARN in Alg. 1. In two models, we learned the original Y using an MLP (one regularized for fairness [Bechavod and Ligett, 2017], one not; Transfer-Fair and -Unfair, respectively) and trained for the transfer task on its internal representations. As a third baseline, we trained an adversarial model similar to the one proposed in Zhang et al. [2018], where the adversary has access only to the classifier output $\hat{Y} = g(Z)$ and the ground truth label (Transfer-Y-Adv), to investigate the utility of our adversary having access to the underlying representation, rather than just the joint classification statistics (Y, A, \hat{Y}).

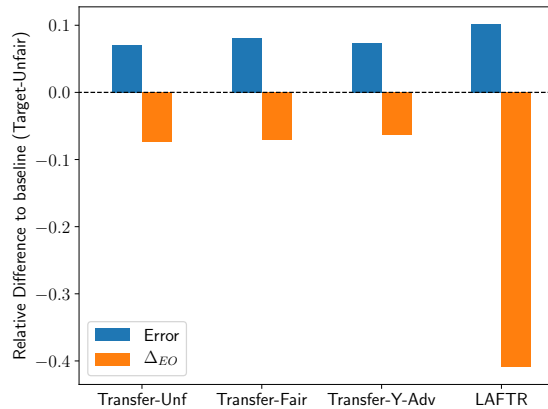


Figure 2.3: Fair transfer learning on Health dataset. Displaying average across 10 transfer tasks of relative difference in error and Δ_{EO} unfairness (the lower the better for both metrics), as compared to a baseline unfair model learned directly from the data. -0.10 means a 10% decrease. Transfer-Unf and -Fair are MLP’s with and without fairness restrictions respectively, Transfer-Y-Adv is an adversarial model with access to the classifier output rather than the underlying representations, and LAFTR is our model trained with the adversarial equalized odds objective.

We report our results in Figure 2.3 and Table 2.1. In Figure 2.3, we show the relative change from the high-accuracy baseline learned directly from the data for both classification error and Δ_{EO} .

LAFTR shows a clear improvement in fairness; it improves Δ_{EO} on average from the non-transfer baseline, and the relative difference is an average of $\sim 20\%$, which is much larger than other baselines. We also see that LAFTR’s loss in accuracy is only marginally worse than other models.

Table 2.1: Results from Figure 2.3 broken out by task. Δ_{EO} for each of the 10 transfer tasks is shown, which entails identifying a primary condition code that refers to a particular medical condition. Most fair on each task is bolded. All model names are abbreviated from Figure 2.3; “TarUnf” is a baseline, unfair predictor learned directly from the target data without a fairness objective.

TRA. TASK	TARUNF	TRAUNF	TRAFAIR	TRAY-AF	LAFTR
MSC2A3	0.362	0.370	0.381	0.378	0.281
METAB3	0.510	0.579	0.436	0.478	0.439
ARTHSPIN	0.280	0.323	0.373	0.337	0.188
NEUMENT	0.419	0.419	0.332	0.450	0.199
RESPR4	0.181	0.160	0.223	0.091	0.051
MISCHRT	0.217	0.213	0.171	0.206	0.095
SKNAUT	0.324	0.125	0.205	0.315	0.155
GIBLEED	0.189	0.176	0.141	0.187	0.110
INFEC4	0.106	0.042	0.026	0.012	0.044
TRAUMA	0.020	0.028	0.032	0.032	0.019

A fairly-regularized MLP (“Transfer-Fair”) does not actually produce fair representations during transfer; on average it yields similar fairness results to transferring representations learned without fairness constraints. Another observation is that the output-only adversarial model (“Transfer Y-Adv”) produces similar transfer results to the regularized MLP. This shows the practical gain of using an adversary that can observe the representations. Since transfer fairness varied much more than accuracy, we break out the results of Fig. 2.3 in Table 2.1, showing the fairness outcome of each of the 10 separate transfer tasks. We note that LAFTR provides the fairest predictions on 7 of the 10 tasks, often by a wide margin, and is never too far behind the fairest model for each task. The unfair model TraUnf achieved the best fairness on one task. We suspect this is due to some of these tasks being relatively easy to solve without relying on the sensitive attribute by proxy. Since the equalized odds metric is better aligned with accuracy than demographic parity [Hardt et al., 2016b], high accuracy classifiers can sometimes achieve good Δ_{EO} if they do not rely on the sensitive attribute by proxy. Because the data owner has no knowledge of the downstream task, however, our results suggest that using LAFTR is safer than using the raw inputs; LAFTR is relatively fair even when TraUnf is the most fair, whereas TraUnf is dramatically less fair than LAFTR on several tasks.

Table 2.2: Transfer fairness, other metrics. Models are as defined in Figure 2.3. MMD is calculated with a Gaussian RBF kernel ($\sigma = 1$). AdvAcc is the accuracy of a separate MLP trained on the representations to predict the sensitive attribute; due to data imbalance an adversary predicting 0 on each case obtains accuracy of approximately 0.74.

MODEL	MMD	ADVACC
TRANSFER-UNFAIR	1.1×10^{-2}	0.787
TRANSFER-FAIR	1.4×10^{-3}	0.784
TRANSFER-Y-ADV ($\beta = 1$)	3.4×10^{-5}	0.787
TRANSFER-Y-ADV ($\beta = 0$)	1.1×10^{-3}	0.786
LAFTR	2.7×10^{-5}	0.761

We provide coarser metrics of fairness for our representations in Table 2.2. We give two metrics:

maximum mean discrepancy (MMD) [Gretton et al., 2007], which is a general measure of distributional distance; and adversarial accuracy (if an adversary is given these representations, how well can it learn to predict the sensitive attribute?). In both metrics, our representations are more fair than the baselines. We give two versions of the “Transfer-Y-Adv” adversarial model ($\beta = 0, 1$); note that it has much better MMD when the reconstruction term is added, but that this does not improve its adversarial accuracy, indicating that our model is doing something more sophisticated than simply matching moments of distributions.

2.3 Flexible Fairness: Disentanglement Priors for Subgroup-fair Prediction

The previous Section emphasized transferability as a key property of fair representations, which provides a type of *flexibility* in terms of downstream tasks. However, this approach is *inflexible* with respect to sensitive attributes: while a single learned representation can adapt to the prediction of different task labels y , the single sensitive attribute a for *all* tasks must be specified at train time. Mis-specified or overly constraining train-time sensitive attributes could negatively affect performance on downstream prediction tasks. Can we instead learn a *flexibly fair* representation that can be *adapted*, at test time, to be fair to a variety of protected groups and their intersections? That is the focus of this Section.

A flexibly fair representation should satisfy two criteria. Firstly, the structure of the latent code should facilitate *simple* adaptation, allowing a practitioner to easily adapt the representation to a variety of fair classification settings, where each task may have a different task label y and sensitive attributes a . Secondly, the adaptations should be *compositional*: the representations can be made fair with respect to conjunctions of sensitive attributes, to guard against performance disparities between demographic *subgroups* (e.g., a classifier that is fair to women but not Black women over the age of 60). This type of subgroup unfairness has been observed in commercial machine learning systems [Buolamwini and Gebru, 2018a].

Towards these goals, we draw inspiration from the disentangled representation literature, where the goal is for each dimension of the representation (also called the “latent code”) to correspond to no more than one semantic factor of variation in the data (for example, independent visual features like object shape and position) [Higgins et al., 2017, Locatello et al., 2018]. Our method uses multiple sensitive attribute labels at train time to induce a disentangled structure in the learned representation, which allows us to easily eliminate their influence at test time. Importantly, at test time our method does not require access to the sensitive attributes, which can be difficult to collect in practice due to legal restrictions [DCCA, 1983, Elliot et al., 2008]. The trained representation permits simple and composable modifications at test time that eliminate the influence of sensitive attributes, enabling a wide variety of downstream tasks.

2.3.1 Background: Variational Autoencoders

The vanilla Variational Autoencoder (VAE) [Kingma and Welling, 2014] is typically implemented with an isotropic Gaussian prior $p(z) = \mathcal{N}(0, I)$. The objective to be maximized is the Evidence Lower Bound (a.k.a., the ELBO),

$$L_{\text{VAE}}(p, q) = \mathbb{E}_{q(z|x)} [\log p(x|z)] - D_{KL}[q(z|x)||p(z)],$$

which bounds the data log likelihood $\log p(x)$ from below for any choice of q . The encoder and decoder are often implemented as Gaussians

$$\begin{aligned} q(z|x) &= \mathcal{N}(z|\mu_q(x), \Sigma_q(x)) \\ p(x|z) &= \mathcal{N}(x|\mu_p(z), \Sigma_p(z)) \end{aligned}$$

whose distributional parameters are the outputs of neural networks $\mu_q(\cdot)$, $\Sigma_q(\cdot)$, $\mu_p(\cdot)$, $\Sigma_p(\cdot)$, with the Σ typically exhibiting diagonal structure. For modeling binary-valued pixels, a Bernoulli decoder $p(x|z) = \text{Bernoulli}(x|\theta_p(z))$ can be used. The goal is to maximize L_{VAE} —which is made differentiable by re-parameterizing samples from $q(z|x)$ —w.r.t. the network parameters.

β -VAE Higgins et al. [2017] modify the VAE objective:

$$L_{\beta\text{VAE}}(p, q) = \mathbb{E}_{q(z|x)} [\log p(x|z)] - \beta D_{KL} [q(z|x)||p(z)].$$

The hyperparameter β allows the practitioner to encourage the variational distribution $q(z|x)$ to reduce its KL-divergence to the isotropic Gaussian prior $p(z)$. With $\beta > 1$ this objective is a valid lower bound on the data likelihood. This gives greater control over the model’s adherence to the prior. Because the prior factorizes per dimension $p(z) = \prod_j p(z_j)$, Higgins et al. [2017] argue that increasing β yields “disentangled” latent codes in the encoder distribution $q(z|x)$. Broadly speaking, each dimension of a properly disentangled latent code should capture no more than one semantically meaningful factor of variation in the data. This allows the factors to be manipulated in isolation by altering the per-dimension values of the latent code. Disentangled autoencoders are often evaluated by their sample quality in the data domain, but we instead emphasize the role of the encoder as a representation learner to be evaluated on downstream fair classification tasks.

FactorVAE and β -TCVAE Kim and Mnih [2018] propose a different variant of the VAE objective:

$$L_{\text{FactorVAE}}(p, q) = L_{\text{VAE}}(p, q) - \gamma D_{KL}(q(z)||\prod_j q(z_j)).$$

The main idea is to encourage factorization of the aggregate posterior $q(z) = \mathbb{E}_{p_{\text{data}}(x)} [q(z|x)]$ so that z_i correlates with z_j if and only if $i = j$. The authors propose a simple trick to generate samples from the aggregate posterior $q(z)$ and its marginals $\{q(z_j)\}$ using shuffled minibatch indices, then approximate the $D_{KL}(q(z)||\prod_j q(z_j))$ term using the cross entropy loss of a classifier that distinguishes between the two sets of samples, which yields a mini-max optimization.

Chen et al. [2018] show that the $D_{KL}(q(z)||\prod_j q(z_j))$ term above—a.k.a. the “total correlation” of the latent code—can be naturally derived by decomposing the expected KL divergence from the

variational posterior to prior:

$$\begin{aligned} \mathbb{E}_{p^{\text{data}}(x)}[D_{KL}(q(z|x)||p(z))] = & \\ & D_{KL}(q(z|x)p^{\text{data}}(x)||q(z)p^{\text{data}}(x)) \\ & + D_{KL}(q(z)||\prod_j q(z_j)) \\ & + \sum_j D_{KL}[q(z_j)||p(z_j)]. \end{aligned}$$

They then augment the decomposed ELBO to arrive at the same objective as Kim and Mnih [2018], but optimize using a biased estimate of the marginal probabilities $q(z_j)$ rather than with the adversarial bound on the KL between aggregate posterior and its marginals.

2.3.2 Flexibly Fair VAE

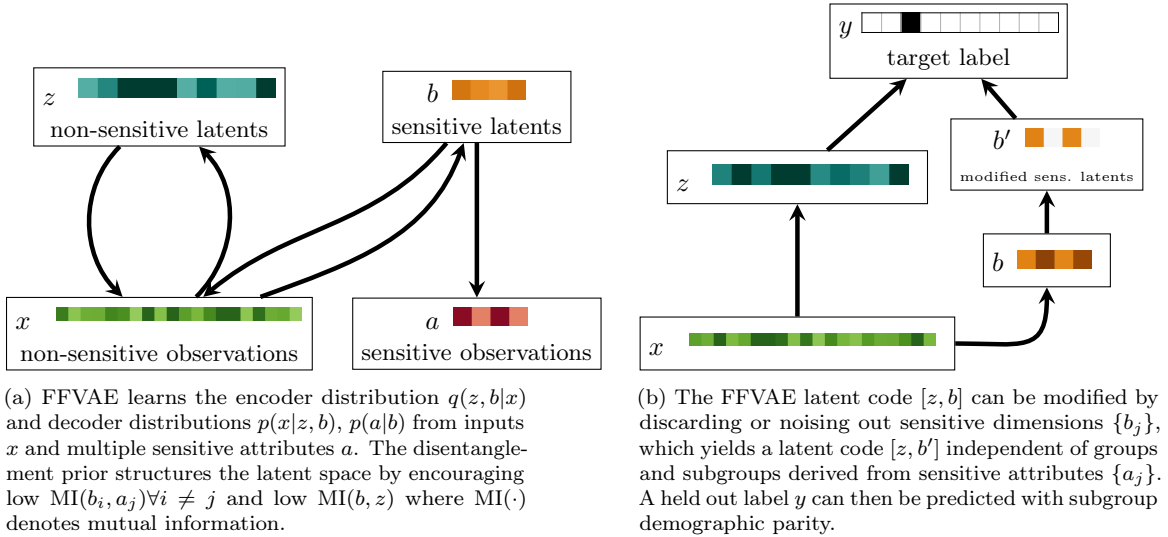


Figure 2.4: Data flow at train time (2.4a) and test time (2.4b) for our model, Flexibly Fair VAE (FFVAE).

We want to learn fair representations that—beyond being useful for predicting many test-time task labels y —can be adapted *simply* and *compositionally* for a variety of sensitive attributes settings a after training. We call this property *flexible fairness*. Our approach to this problem involves inducing structure in the latent code that allows for easy manipulation. Specifically, we isolate information about each sensitive attribute to a specific subspace, while ensuring that the latent space factorizes these subspaces independently.

Notation We employ the following notation:

- $x \in \mathcal{X}$: a vector of non-sensitive attributes, for example, the pixel values in an image or row of features in a tabular dataset;
- $a \in \{0, 1\}^{N_a}$: a vector of binary sensitive attributes;
- $z \in \mathbb{R}^{N_z}$: non-sensitive subspace of the latent code;

- $b \in \mathbb{R}^{N_b}$: sensitive subspace of the latent code⁸.

For example, we can express the VAE objective in this notation as

$$L_{\text{VAE}}(p, q) = \mathbb{E}_{q(z, b|x, a)} [\log p(x, a|z, b)] - D_{KL} [q(z, b|x, a) || p(z, b)].$$

In learning a flexibly fair representations $[z, b] = f([x, a])$, we aim to satisfy two general properties: *disentanglement* and *predictiveness*. We say that $[z, b]$ is *disentangled* if its aggregate posterior factorizes as $q(z, b) = q(z) \prod_j q(b_j)$ and is *predictive* if each b_i has high mutual information with the corresponding a_i . Note that under the disentanglement criteria the dimensions of z are free to co-vary together, but must be independent from all sensitive subspaces b_j . We have also specified factorization of the latent space in terms of the aggregate posterior $q(z, b) = \mathbb{E}_{p^{\text{data}}(x)} [q(z, b|x)]$, to match the global independence criteria of group fairness.

Desiderata We can formally express our desiderata as follows:

- $z \perp b_j \forall j$ (disentanglement of the non-sensitive and sensitive latent dimensions);
- $b_i \perp b_j \forall i \neq j$ (disentanglement of the various different sensitive dimensions);
- $\text{MI}(a_j, b_j)$ is large $\forall j$ (predictiveness of each sensitive dimension);

where $\text{MI}(u, v) = \mathbb{E}_{p(u, v)} \log \frac{p(u, v)}{p(u)p(v)}$ represents the mutual information between random vectors u and v . We note that these desiderata differ in two ways from the standard disentanglement criteria. The predictiveness requirements are stronger: they allow for the injection of external information into the latent representation, requiring the model to structure its latent code to align with that external information. However, the disentanglement requirement is less restrictive since it allows for correlations between the dimensions of z . Since those are the non-sensitive dimensions, we are not interested in manipulating those at test time, and so we have no need for constraining them.

If we satisfy these criteria, then it is possible to achieve demographic parity with respect to some a_i by simply removing the dimension b_i from the learned representation i.e. use instead $[z, b] \setminus b_i$. We can alternatively replace b_i with independent noise. This adaptation procedure is simple and compositional: if we wish to achieve fairness with respect to a conjunction of binary attributes⁹ $a_i \wedge a_j \wedge a_k$, we can simply use the representation $[z, b] \setminus \{b_i, b_j, b_k\}$.

By comparison, while FactorVAE may disentangle dimensions of the aggregate posterior— $q(z) = \prod_j q(z_j)$ —it does not automatically satisfy flexible fairness, since the representations are not predictive, and cannot necessarily be easily modified along the attributes of interest.

Distributions We propose a variation to the VAE which encourages our desiderata, building on methods for disentanglement and encouraging predictiveness. Firstly, we assume assume a variational posterior that factorizes across z and b :

$$q(z, b|x) = q(z|x)q(b|x). \tag{2.12}$$

⁸In our experiments we used $N_b = N_a$ (same number of sensitive attributes as sensitive latent dimensions) to model binary sensitive attributes. But categorical or continuous sensitive attributes can also be accommodated.

⁹ \wedge and \vee represent logical *and* and *or* operations, respectively.

The parameters of these distributions are implemented as neural network outputs, with the encoder network yielding a tuple of parameters for each input: $(\mu_q(x), \Sigma_q(x), \theta_q(x)) = \text{Encoder}(x)$. We then specify $q(z|x) = \mathcal{N}(z|\mu_q(x), \Sigma_q(x))$ and $q(b|x) = \delta(\theta_q(x))$ (i.e., b is non-stochastic)¹⁰.

Secondly, we model reconstruction of x and prediction of a separately using a factorized decoder:

$$p(x, a|z, b) = p(x|z, b)p(a|b) \quad (2.13)$$

where $p(x|z, b)$ is the decoder distribution suitably chosen for the inputs x , and

$$p(a|b) = \prod_j \text{Bernoulli}(a_j|\sigma(b_j)) \quad (2.14)$$

is a factorized binary classifier that uses b_j as the logit for predicting a_j ($\sigma(\cdot)$ represents the sigmoid function). Note that the $p(a|b)$ factor of the decoder requires no extra parameters.

Finally, we specify a factorized prior $p(z, b) = p(z)p(b)$ with $p(z)$ as a standard Gaussian and $p(b)$ as Uniform.

Learning Objective Using the encoder and decoder as defined above, we present our final objective:

$$\begin{aligned} L_{\text{FFVAE}}(p, q) = & \mathbb{E}_{q(z, b|x)}[\log p(x|z, b) + \alpha \log p(a|b)] \\ & - \gamma D_{KL}(q(z, b)||q(z) \prod_j q(b_j)) \\ & - D_{KL}[q(z, b|x)||p(z, b)]. \end{aligned} \quad (2.15)$$

It comprises the following four terms, respectively: a *reconstruction* term which rewards the model for successfully modeling non-sensitive observations; a *predictiveness* term which rewards the model for aligning the correct latent components with the sensitive attributes; a *disentanglement* term which rewards the model for decorrelating the latent dimensions of b from each other and z ; and a *dimension-wise KL* term which rewards the model for matching the prior in the latent variables. We call our model FFVAE for Flexibly Fair VAE (see Figure 2.4 for a schematic representation).

The hyperparameters α and γ control aspects relevant to flexible fairness of the representation. α controls the alignment of each a_j to its corresponding b_j (predictiveness), whereas γ controls the aggregate independence in the latent code (disentanglement).

The γ -weighted total correlation term is realized by training a binary adversary to approximate the log density ratio $\log \frac{q(z, b)}{q(z) \prod_j q(b_j)}$. The adversary attempts to classify between “true” samples from the aggregate posterior $q(z, b)$ and “fake” samples from the product of the marginals $q(z) \prod_j q(b_j)$ (see Appendix A.2 for further details). If a strong adversary can do no better than random chance, then the desired independence property has been achieved.

We note that our model requires the sensitive attributes a at training time but not at test time. This is advantageous, since often these attributes can be difficult to collect from users, due to practical and legal restrictions, particularly for sensitive information [DCCA, 1983, Elliot et al., 2008].

¹⁰We experimented with several distributions for modeling $b|x$ stochastically, but modeling this uncertainty did not help optimization or downstream evaluation in our experiments.

2.3.3 Experiments

Evaluation Criteria We evaluate the learned encoders with an “auditing” scheme on held-out data. The overall procedure is as follows:

1. **Split data** into a *training* set (for learning the encoder) and an *audit* set (for evaluating the encoder).
2. **Train** an encoder/representation using the training set.
3. **Audit** the learned encoder. Freeze the encoder weights and train an MLP to predict some task label given the (possibly modified) encoder outputs on the audit set.

To evaluate various properties of the encoder we conduct three types of auditing tasks—*fair classification*, *predictiveness*, and *disentanglement*—which vary in task label and representation modification. The *fair classification audit* [Madras et al., 2018] trains an MLP to predict y (held-out from encoder training) given $[z, b]$ with appropriate sensitive dimensions removed, and evaluates accuracy and Δ_{DP} on a test set. We repeat for a variety of demographic subgroups derived from the sensitive attributes. The *predictiveness audit* trains classifier C_i to predict sensitive attribute a_i from b_i alone. The *disentanglement audit* trains classifier $C_{\setminus i}$ to predict sensitive attribute a_i from the representation with b_i removed (e.g. $[z, b] \setminus b_i$). If C_i has low loss, our representation is predictive; if $C_{\setminus i}$ has high loss, it is disentangled.

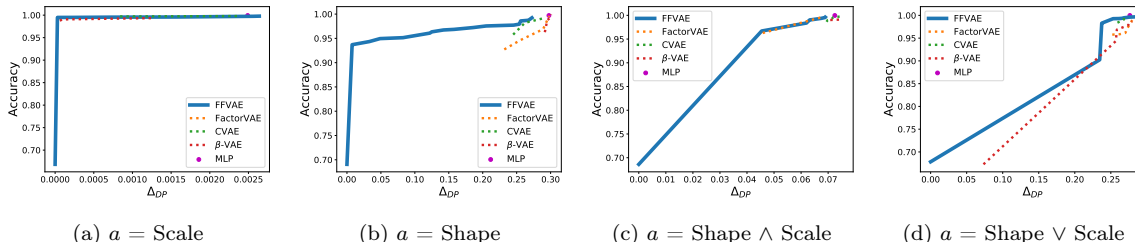


Figure 2.5: Fairness-accuracy tradeoff curves, DSpritesUnfair dataset. We sweep a range of hyperparameters for each model and report Pareto fronts. Optimal point is the top left hand corner — this represents perfect accuracy and fairness. MLP is a baseline classifier trained directly on the input data. For each model, encoder outputs are modified to remove information about a . $y = XPosition$ for each plot.

Synthetic Data

DSpritesUnfair Dataset The DSprites dataset¹¹ contains 64×64 -pixel images of white shapes against a black background, and was designed to evaluate whether learned representations have disentangled sources of variation. The original dataset has several categorical factors of variation—Scale, Orientation, XPosition, YPosition—that combine to create 700,000 unique images. We binarize the factors of variation to derive sensitive attributes and labels, so that many images now share any given attribute/label combination (See Appendix A.2.1 for details). In the original DSprites dataset, the factors of variation are sampled uniformly. However, in fairness problems, we are often concerned with correlations between attributes and the labels we are trying to predict (otherwise, achieving low Δ_{DP} is aligned with standard classification objectives). Hence, we sampled an “unfair” version of

¹¹<https://github.com/deepmind/dsprites-dataset>

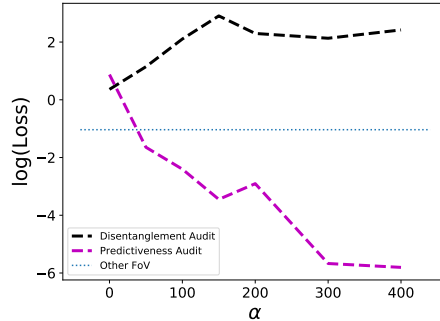


Figure 2.6: Black and pink dashed lines respectively show FFVAE disentanglement audit (the higher the better) and predictiveness audit (the lower the better) as a function of α . These audits use A_i =Shape (see text for details). The blue line is a reference value—the log loss of a classifier that predicts A_i from the other 5 DSprites factors of variation (FoV) alone, ignoring the image—representing the amount of information about A_i inherent in the data.

this data (DSpritesUnfair) with correlated factors of variation; in particular Shape and XPosition correlate positively. Then a non-trivial fair classification task would be, for instance, learning to predict shape without discriminating against inputs from the left side of the image.

Baselines To test the utility of our predictiveness prior, we compare our model to β -VAE (VAE with a coefficient $\beta \geq 1$ on the KL term) and FactorVAE, which have disentanglement priors but no predictiveness prior. We can also think of these as FFVAE with $\alpha = 0$. To test the utility of our disentanglement prior, we also compare against a version of our model with $\gamma = 0$, denoted CVAE. This is similar to the class-conditional VAE [Kingma et al., 2014], with sensitive attributes as labels — this model encourages predictiveness but no disentanglement.

Fair Classification We perform the fair classification audit using several group/subgroup definitions for models trained on DSpritesUnfair (see Appendix A.2.1 for training details), and report fairness-accuracy tradeoff curves in Fig. 2.5. In these experiments, we used Shape and Scale as our sensitive attributes during encoder training. We perform the fair classification audit by training an MLP to predict y = “XPosition”—which was not used in the representation learning phase—given the modified encoder outputs, and repeat for several sensitive groups and subgroups. We modify the encoder outputs as follows: When our sensitive attribute is a_i we remove the associated dimension b_i from $[z, b]$; when the attribute is a conjunction of a_i and a_j , we remove both b_i and b_j . For the baselines, we simply remove the latent dimension which is most correlated with a_i , or the two most correlated dimensions with the conjunction. We sweep a range of hyperparameters to produce the fairness-accuracy tradeoff curve for each model. In Fig. 2.5, we show the “Pareto front” of these models: points in $(\Delta_{DP}, \text{accuracy})$ -space for which no other point is better along both dimensions. The optimal result is the top left hand corner (perfect accuracy and $\Delta_{DP} = 0$).

Since we have a 2-D sensitive input space, we show results for four different sensitive attributes derived from these dimensions: $\{a = \text{“Shape”}, a = \text{“Scale”}, a = \text{“Shape”} \vee \text{“Scale”}, a = \text{“Shape”} \wedge \text{“Scale”}\}$. Recall that Shape and XPosition correlate in the DSpritesUnfair dataset. Therefore, for sensitive attributes that involve Shape, we expect to see an improvement in Δ_{DP} . For sensitive attributes that do not involve Shape, we expect that our method does not hurt performance at all — since the attributes are uncorrelated in the data, the optimal predictive solution also has $\Delta_{DP} = 0$.

When group membership a is uncorrelated with label y (Fig. 2.5a), all models achieve high

accuracy and low Δ_{DP} (a and y successfully disentangled). When a correlates with y by design (Fig. 2.5b), we see the clearest improvement of the FFVAE over the baselines, with an almost complete reduction in Δ_{DP} and very little accuracy loss. The baseline models are all unable to improve Δ_{DP} by more than about 0.05, indicating that they have not effectively disentangled the sensitive information from the label. In Figs. 2.5c and 2.5d, we examine conjunctions of sensitive attributes, assessing FFVAE’s ability to flexibly provide multi-attribute fair representations. Here FFVAE exceeds or matches the baselines accuracy-at-a-given- Δ_{DP} almost everywhere; by disentangling information from multiple sensitive attributes, FFVAE enables flexibly fair downstream classification.

Disentanglement and Predictiveness Fig. 2.6 shows the FFVAE disentanglement and predictiveness audits (see above for description of this procedure). This result aggregates audits across all FFVAE models trained in the setting from Figure 2.5b. The classifier loss is cross-entropy, which is a lower bound on the mutual information between the input and target of the classifier. We observe that increasing α helps both predictiveness and disentanglement in this scenario. In the disentanglement audit, larger α makes predicting the sensitive attribute from the modified representation (with b_i removed) more difficult. The horizontal dotted line shows the log loss of a classifier that predicts a_i from the other DSprites factors of variation (including labels not available to FFVAE); this baseline reflects the correlation inherent in the data. We see that when $\alpha = 0$ (i.e. FactorVAE), it is slightly more difficult than this baseline to predict the sensitive attribute. This is due to the disentanglement prior. However, increasing $\alpha > 0$ increases disentanglement benefits in FFVAE beyond what is present in FactorVAE. This shows that encouraging predictive structure can help disentanglement through isolating each attribute’s information in particular latent dimensions. Additionally, increasing α improves predictiveness, as expected from the objective formulation. We further evaluate the disentanglement properties of our model in Appendix A.2.2 using the Mutual Information Gap metric Chen et al. [2018].

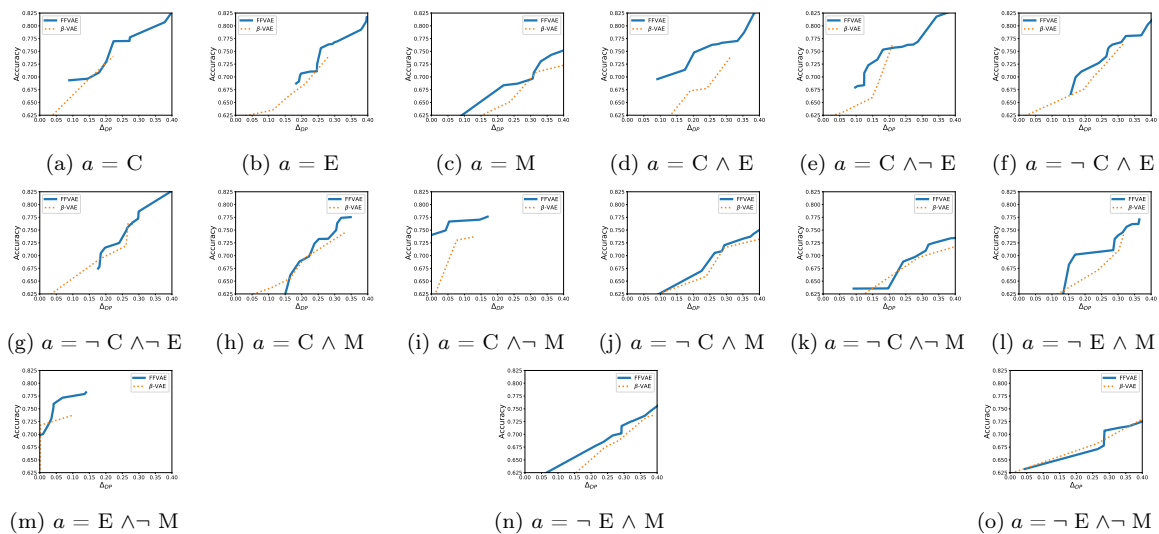


Figure 2.7: Celeb-A subgroup fair classification results. Sensitive attributes: Chubby (C), Eyeglasses (E), and Male (M). $y = \text{HeavyMakeup}$.

Celebrity Faces

Dataset The CelebA¹² dataset contains over 200,000 images of celebrity faces. Each image is associated with 40 human-labeled binary attributes (OvalFace, HeavyMakeup, etc.). We chose three attributes, Chubby, Eyeglasses, and Male as sensitive attributes¹³, and report fair classification results on 3 groups and 12 two-attribute-conjunction subgroups only (for brevity we omit three-attribute conjunctions). To our knowledge this is the first exploration of fair representation learning algorithms on the Celeb-A dataset. As in the previous sections we train the encoders on the train set, then evaluate performance of MLP classifiers trained on the encoded test set.

Fair Classification We follow the fair classification audit procedure described above, where the held-out label HeavyMakeup—which was not used at encoder train time—is predicted by an MLP from the encoder representations. When training the MLPs we take a fresh encoder sample for each minibatch (statically encoding the dataset with one encoder sample per image induced overfitting). We found that training the MLPs on encoder means (rather than samples) increased accuracy but at the cost of very unfavorable Δ_{DP} . We also found that FactorVAE-style adversarial training does not scale well to this high-dimensional problem, so we instead optimize Equation 2.15 using the biased estimator from Chen et al. [2018]. Figure 2.7 shows Pareto fronts that capture the fairness-accuracy tradeoff for FFVAE and β -VAE.

While neither method dominates in this challenging setting, FFVAE achieves a favorable fairness-accuracy tradeoff across many of subgroups. We believe that using sensitive attributes as side information gives FFVAE an advantage over β -VAE in predicting the held-out label. In some cases (e.g., $a = \neg E \wedge M$) FFVAE achieves better accuracy at all Δ_{DP} levels, while in others (e.g., $a = \neg C \wedge \neg E$), FFVAE did not find a low- Δ_{DP} solution. We believe Celeb-A—with its many high dimensional data and rich label correlations—is a useful test bed for subgroup fair machine learning algorithms, and we are encouraged by the reasonably robust performance of FFVAE in our experiments.

2.4 Related Work

Algorithmic fairness Interest in fair machine learning is burgeoning as researchers seek to define and mitigate unintended harm in automated decision making systems. Definitional works have been broadly concerned with *group fairness* or *individual fairness*. Dwork et al. [2012] discussed individual fairness within the owner-vendor framework we utilize. Zemel et al. [2013] encouraged elements of both group and individual fairness via a regularized objective. An intriguing body of recent work unifies the individual-group dichotomy by exploring fairness at the intersection of multiple group identities, and among small subgroups of individuals Hébert-Johnson et al. [2018], Kearns et al. [2017].

Calmon et al. [2017] and Hajian et al. [2015] explored fair machine learning by pre- and post-processing training datasets. McNamara et al. [2017] provides a framework where the data producer, user, and regulator have separate concerns, and discuss fairness properties of representations. Louizos et al. [2016a] give a method for learning fair representations with deep generative models by using maximum mean discrepancy [Gretton et al., 2007] to eliminate disparities between the two sensitive groups.

¹²<http://mmlab.ie.cuhk.edu.hk/projects/CelebA.html>

¹³We chose these attributes because they co-vary relatively weakly with each other (compared with other attribute triplets), but strongly with other attributes. Nevertheless the rich correlation structure amongst all attributes makes this a challenging fairness dataset; it is difficult to achieve high accuracy and low Δ_{DP} .

Adversarial training Adversarial training for deep generative modeling was popularized by Goodfellow et al. [2014] and applied to deep semi-supervised learning [Odena, 2016, Salimans et al., 2016] and segmentation [Luc et al., 2016], although similar concepts had previously been proposed for unsupervised and supervised learning [Gutmann and Hyvärinen, 2010, Schmidhuber, 1992]. Ganin et al. [2016] proposed adversarial representation learning for domain adaptation, which resembles fair representation learning in the sense that multiple distinct data distributions (e.g., demographic groups) must be expressively modeled by a single representation.

Edwards and Storkey [2016] made this connection explicit by proposing adversarially learning a classifier that achieves demographic parity. This work is the most closely related to LAFTR, although our choice of balanced ℓ_1 learning objective (rather than standard cross entropy loss) is more closely aligned to the goal of ensuring statistical parity in the learned representations. Recent work has explored the use of adversarial training to other notions of group fairness. Beutel et al. [2017] explored the particular fairness levels achieved by the algorithm from Edwards and Storkey [2016], and demonstrated that they can vary as a function of the demographic unbalance of the training data. In work concurrent to ours, Zhang et al. [2018] use an adversary which attempts to predict the sensitive variable solely based on the classifier output, to learn an equal opportunity fair classifier. Whereas they focus on fairness in classification outcomes, in our work we allow the adversary to work directly with the learned representation, which we show yields fair and transferable representations that in turn admit fair classification outcomes.

Disentanglement The search of independent latent components that explain observed data has long been a focus on the probabilistic modeling community Bach and Jordan [2002], Comon [1994], Hyvärinen and Oja [2000]. In light of the increased prevalence of neural networks models in many data domains, the machine learning community has renewed its interest in learned features that “disentangle” semantic factors of data variation. The introduction of the β -VAE [Higgins et al., 2017], as discussed in Section 2.3.1, motivated a number of subsequent studies that examine why adding additional weight on the KL-divergence of the ELBO encourages disentangled representations [Alemi et al., 2018, Burgess et al., 2017]. Chen et al. [2018], Kim and Mnih [2018] and Esmaili et al. [2019b] argue that decomposing the ELBO and penalizing the total correlation increases disentanglement in the latent representations. Locatello et al. [2018] conduct extensive experiments comparing existing unsupervised disentanglement methods and metrics. They conclude pessimistically that learning disentangled representations requires inductive biases and possibly additional supervision, but identify fair machine learning as a potential application where additional supervision is available by way of sensitive attributes.

Compositional representations FFVAE provides multi-attribute fair representation learning, which we accomplish by using sensitive attributes as labels to induce a factorized structure in the aggregate latent code. Bose and Hamilton [2018] proposed a compositional fair representation of graph-structured data. Kingma et al. [2014] previously incorporated (partially-observed) label information into the VAE framework to perform semi-supervised classification. Several recent VAE variants have incorporated label information into latent variable learning for image synthesis Klys et al. [2018] and single-attribute fair representation learning Botros and Tomczak [2018], Moyer et al. [2018], Song et al. [2019].

2.5 Discussion

This Chapter presented some approaches for mitigating algorithmic discrimination by learning a data representation that serves as a bottleneck, promoting group parity in downstream learning processes that consume the representation. This approach has found considerable purchase within the research community: firms have implemented fair representation learning in their products and open-source software [Bellamy et al., 2018, Beutel et al., 2019], while researchers have extended or analyzed the adversarial approach proposed in this Chapter (discussed concurrently by other research groups Beutel et al. [2017], Zhang et al. [2018]) in a number of directions [Adel et al., 2019, Agarwal et al., 2021, Moyer et al., 2018, Quadrianto et al., 2019, Samadi et al., 2018, Song et al., 2019, Zhao and Gordon, 2022]. We orient our discussion here towards articulating known limitations of the representation learning approach, which we feel is especially important given that the goal of fair ML is to ensure that emerging technologies confer social equal benefits regardless of social position.

Fair representation learning has close ties to OOD-robustness [Farnadi et al., 2022] and causality [Dieng et al., 2022, Madras et al., 2019]. In fact, recent work [Makar and D’Amour, 2022, Makar et al., 2022] provides a causal interpretation for the group-normalized losses of per-group losses discussed in Section 2.2.3. From this view point, a dataset reflecting societal bias is thought of as resulting from a *confounding* process on the observations. Thus, fair learning amounts to using importance weights (i.e. normalizing group losses by their subpopulation size) to emulate training on unconfounded data, which provides robustness to distribution shift. Thus, when used in an anti-causal prediction setting [Schoelkopf et al., 2012], LAFTR apparently provides some implicit causal inference!

This also suggests fair representations may naturally deliver a degree of robustness to distribution shift, which is supported by our theory (Section 2.2.3) and experiments (Section 2.2.4). However, this natural OOD-robustness is somewhat limited, as fair representations are now known to be vulnerable to worst-case distribution shifts [Lechner and Ben-David, 2022, Lechner et al., 2021].¹⁴ In general, fair regularizers and metrics (like other differentiable aggregate quantities such as cross-entropy loss) can be manipulated adversarially [Aivodji et al., 2019, Ghosh et al., 2022, Shamsabadi et al., 2022, Solans et al., 2020]. These results provide a cautionary tale: fair representations should be deployed with extreme care, which could include a characterization of which distribution shifts are *likely* during deployment or a security audit to assess vulnerability to adversarial actions like data poisoning.

One obstacle to applying fair representation learning within contemporary workflows is the somewhat onerous reliance on demographic labels during training. More recent representation learning approaches eschew labeled supervision, instead “pre-training” a large network using unsupervised and self-supervised learning objectives over massive corpora of web-scraped data [Radford et al., 2021]. This pre-training process provides high-fidelity representations (sometimes called “foundation models”) that can be adapted for use in a variety of downstream prediction tasks. However, the reliance on web data for pre-training can induce harmful stereotypical associations in the learned representations Bianchi et al. [2023], Hundt et al. [2022].

Addressing representational biases in pre-trained representations remains an important open question; while the discussions in this Chapter focused on fairness in a (variational) autoencoder

¹⁴Such counterexamples can be quite “worst-case” relative to the data bias being addressed, and may be unrealistic. For example, if upon deployment there is a *reversal* of which groups are privileged in the sense that their data correlate with “positive” labels (like loan approval), then a “fair” representation learned on the original data may lose its fairness properties upon deployment.

representations, which are derived using a relatively simpler training paradigm, they may shed some light on how to proceed. The key to encouraging fairness with FFVAE (Section 2.3) was the use of *supervised* disentanglement priors, which cannot be readily implemented in the pre-training regime due to the scale of data required. Unfortunately, VAEs with unsupervised disentanglement priors can struggle to learn disentangled representations when trained on data with strong correlation patterns [Träuble et al., 2021]. This suggests that updating the learning objective during pre-training (without explicit supervision) is unlikely to mitigate representational bias. Perhaps representation bias in pre-trained models could be addressed after the pre-training process by using human feedback to inform a more targeted adaptation (along the lines of Bolukbasi et al. [2016], Santurkar et al. [2021a]). One important obstacle along this research direction is the lack of suitable measures of representation bias [Bommasani et al., 2021]. There is also a concern that despite adaptation methods providing a superficial improvement on representation fairness metrics, they could still admit performance disparities in downstream prediction [Gonen and Goldberg, 2019, Zhou et al., 2021].

On the positive side, the bottleneck advocated by fair representation learning could ultimately be beneficial for other types of model failures. This is especially relevant to the setting where models are severely “over-parameterized”, that is, the number of model parameters (perhaps greatly) exceeds the number of available data points. By definition, over-parameterized prediction problems are underspecified [D’Amour et al., 2020]. Despite this issue, neural networks tend to generalize well to *i.i.d.* test data [Bartlett et al., 2020, Frei et al., 2022], although they may generalize poorly for subpopulations that are underrepresented in the training data [Sagawa et al., 2020c, Wald et al., 2023]. In this regard, the bottleneck effect of fair representation learning could be doubly effective, mitigating not only predictive disparities in prediction but also underspecification. This is because (unlike when models are fine-tuned or trained from scratch), adapting smaller models (say, linear probes) on top of learned representation mitigates the over-parameterization issue by greatly reducing the number of parameters being optimized. Future work is needed to more completely characterize this issue.

Chapter 3

Leveraging Shortcut Learning to Learn Robust Features

3.1 Towards Out-of-distribution Generalization

The previous Chapter discussed the tendency of ML to exhibit disparate performance across demographic groups, even in spite of high aggregate accuracy. These group disparities in model performance can be interpreted in terms of the model’s sensitivity to *distribution shift*: after training the model on a convex mixture of (non-overlapping) subpopulations, group fairness metrics can be expressed in terms of model behavior on shifted distributions where only one mixture component is present.¹ In fact, many types of model failure beyond algorithmic discrimination can be framed in terms of a lack of robustness to distribution shift. That is precisely the purpose of this Chapter, where we will address the out-of-distribution (OOD) generalization problem more broadly.

The ML research community has demonstrated impressive predictive performance on controlled benchmarks with *i.i.d.* evaluation data [He et al., 2015, Rajpurkar et al., 2017]. However, distribution shift abounds in practical settings, and subsequently model performance can severely degrade during deployment, even to below-chance predictions [Geirhos et al., 2020a]. Tiny perturbations can derail classifiers, as shown by adversarial examples [Szegedy et al., 2014] and common image corruptions [Hendrycks and Dietterich, 2019]. Even new test sets collected from the same data acquisition pipeline induce distribution shifts that significantly harm performance [Engstrom et al., 2020, Recht et al., 2019].

3.1.1 The Role of Side Information in Learning Robust Features

Many approaches have been proposed to overcome the brittleness of supervised learning—e.g. Empirical Risk Minimization (ERM) [Vapnik, 1991]—in the face of distribution shifts. Robust optimization aims to achieve good performance on any distribution close to the training distribution [Duchi et al., 2021, Goodfellow et al., 2015a, Madry et al., 2018]. Invariant learning on the other hand tries to go one step further, to generalize to distributions potentially far away from the training distribution. Such methods pose OOD generalization in terms of learning “robust features” that are reliable in all domains of interest [Peters et al., 2016], a framing that we follow in this Chapter.

¹This specific type of distribution shift is called “subpopulation shift”.

Unfortunately, common invariant learning methods typically come at a serious disadvantage: they require datasets to be partitioned into multiple domains or environments.² Environment assignments should implicitly define variation the algorithm should become invariant or robust to, but often such environment labels are unavailable at training time, either because they are difficult to obtain or due to privacy limitations. In some cases, relevant side-information or metadata—human annotations, or device ID used to take a medical image, hospital or department ID, etc.—may be abundant, but it remains unclear how best to specify environments based on this information [Srivastava et al., 2020].

A similar issue arises in mitigating algorithmic unfairness, where sensitive attributes may be difficult to define in practice [Hanna et al., 2020], or their values may be impossible to collect. The focus of this Chapter is to overcome the difficulty of manual environment specification by developing a new method inspired by fairness approaches for unknown group memberships [Kim et al., 2019, Lahoti et al., 2020]. Our approach is precisely to leverage the tendency of ERM to prefer “shortcut” features [Beery et al., 2018b, Geirhos et al., 2020b] (also referred to as “spurious” features [Lopez-Paz, 2016, Pearl, 2009b, Sober, 2001]), which we show can be used to partition the training data into *inferred* environments suitable for use with standard invariant learning approaches.

3.2 Environment Inference for Invariant Learning

3.2.1 Background: Invariant Learning

Notation Let \mathcal{X} be the input space, \mathcal{E}^{obs} the set of training environments (a.k.a. “domains”), \mathcal{Y} the target space. Let $x, y, e \sim p^{obs}(x, y, e)$ be observational data, with $x \in \mathcal{X}$, $y \in \mathcal{Y}$, and $e \in \mathcal{E}^{obs}$. \mathcal{H} denotes a representation space, from which a classifier $w \circ \Phi$ (that maps to the logit space of \mathcal{Y} via a linear map w) can be applied. $\Phi : \mathcal{X} \rightarrow \mathcal{H}$ denotes the parameterized mapping or “model” that we optimize. We refer to $\Phi(x) \in \mathcal{H}$ as the “representation” of example x . $\hat{y} \in \mathcal{Y}$ denotes a hard prediction derived from the classifier by stochastic sampling or probability thresholding. $\ell : \mathcal{H} \times \mathcal{Y} \rightarrow \mathbb{R}$ denotes a scalar loss, which guides the learning.

The empirical risk minimization (ERM) solution is found by minimizing the global risk, expressed as the expected loss over the observational distribution:

$$C^{ERM}(\Phi) = \mathbb{E}_{p^{obs}(x,y,e)}[\ell(\Phi(x), y)]. \quad (3.1)$$

Representation Learning with Environment Labels Domain generalization is concerned with achieving low error rates on unseen test distributions $p(x, y|e_{test})$ for $e_{test} \notin \mathcal{E}^{obs}$. Domain adaption is a related problem where model parameters can be adapted at test time using unlabeled data. *Invariant Learning* approaches such as Invariant Risk Minimization (IRM) [Arjovsky et al., 2019] and Risk Extrapolation (REx) [Krueger et al., 2021] were proposed to overcome the limitations of adversarial domain-invariant representation learning [Zhao et al., 2019] by discovering invariant relationships between inputs and targets across domains. Invariance serves as a proxy for causality, as features representing “causes” of target labels rather than effects will generalize well under intervention. In IRM, a representation $\Phi(x)$ is learned that performs optimally within each environment—and is thus invariant to the choice of environment $e \in \mathcal{E}^{obs}$ —with the ultimate goal of generalizing to an unknown test dataset $p(x, y|e_{test})$. Because optimal classifiers under standard loss functions can be

²We use “domains”, “environments” and “groups”/“subgroups” interchangeably.

realized via a conditional label distribution ($f^*(x) = \mathbb{E}[y|x]$), an invariant representation $\Phi(x)$ must satisfy the following *Environment Invariance Constraint*:

$$\begin{aligned} \mathbb{E}[y|\Phi(x) = h, e_1] &= \mathbb{E}[y|\Phi(x) = h, e_2] \\ \forall h \in \mathcal{H} \quad \forall e_1, e_2 \in \mathcal{E}^{obs}. \end{aligned} \tag{EIC}$$

Intuitively, the representation $\Phi(x)$ encodes features of the input x that induce the same conditional distribution over labels across each environment. This is closely related to the notion of “group sufficiency” studied in the fairness literature [Liu et al., 2019].

Because trivial representations such as mapping all x onto the same value may satisfy environment invariance, other objectives must be introduced to encourage the predictive utility of Φ . Arjovsky et al. [2019] propose IRM as a way to satisfy (EIC) while achieving a good overall risk. As a practical instantiation, the authors introduce IRMv1, a regularized objective enforcing simultaneous optimality of the same classifier $w \circ \Phi$ in all environments;³ here w.l.o.g. $w = \bar{w}$ is a constant scalar multiplier of 1.0 for each output dimension. Denoting by $R^e = \mathbb{E}_{p^{obs}(x,y|e)}[\ell]$ the per-environment risk, the objective to be minimized is

$$C^{IRM}(\Phi) = \sum_{e \in \mathcal{E}^{obs}} R^e(\Phi) + \lambda \|\nabla_{\bar{w}} R^e(\bar{w} \circ \Phi)\|. \tag{IRMv1}$$

Robust Optimization Another approach at generalizing beyond the training distribution is robust optimization [Ben-Tal et al., 2009b], where one aims to minimize the worst-case loss for every subset of the training set, or other well-defined perturbation sets around the data [Duchi et al., 2021, Madry et al., 2018]. Rather than optimizing a notion of invariance, Distributionally Robust Optimization (DRO) [Duchi et al., 2021] seeks good performance for all nearby distributions by minimizing the worst-case loss: $\max_q \mathbb{E}_q[\ell]$ s.t. $D(q||p) < \epsilon$, where D denotes similarity between two distributions (e.g., χ^2 divergence) and ϵ is a hyperparameter. The objective can be computed as an expectation over p via per-example importance weights $\gamma_i = \frac{q(x_i, y_i)}{p(x_i, y_i)}$. GroupDRO operationalizes this principle by sharing importance weights across training examples, using environment labels to define relevant groups for this parameter sharing. This can be expressed as an expected risk under a worst-case distribution over group proportions:

$$C^{GroupDRO}(\Phi) = \max_g \mathbb{E}_{g(e)}[R^e(\Phi)]$$

This is a promising approach towards tackling distribution shift with deep nets [Sagawa et al., 2020a], and we show in our experiments how environment inference enables application of GroupDRO to improve over standard learning without requiring group labels.

Limitations of Invariant Learning While the use of invariant learning to tackle domain generalization is still relatively nascent, several known limitations merit discussion. IRM can provably find an invariant predictor that generalizes OOD, but only under restrictive assumptions, such as linearity of the data generative process and access to many environments [Arjovsky et al., 2019]. However, most benchmark datasets are in the non-linear regime; Rosenfeld et al. [2021] demonstrated

³ $w \circ \Phi$ yields a classification decision via linear weighting on the representation features.

that for some non-linear datasets, the IRMv1 penalty term induces multiple optima, not all of which yield invariant predictors. Nevertheless, IRM has found empirical success in some high dimensional non-linear classification tasks (e.g. CMNIST) using just a few environments [Arjovsky et al., 2019, Koh et al., 2021]. On the other hand, it was recently shown that, using careful and fair model selection strategies across a suite of image classification tasks, neither IRM nor other invariant learners consistently beat ERM in OOD generalization [Gulrajani and Lopez-Paz, 2021]. This last study underscores the importance of *model selection* in any domain generalization approach, which we discuss further below.

3.2.2 Invariance Without Environment Labels

In this Section we propose a novel invariant learning framework that does not require a priori domain/environment knowledge. This framework is useful in algorithmic fairness scenarios when demographic makeup is not directly observed; it is also applicable in standard machine learning settings when relevant environment information is either unavailable or not clearly identified. In both cases, a method that sorts training examples \mathcal{D} into environments that maximally separate the spurious features—i.e. inferring populations $\mathcal{D}_1 \cup \mathcal{D}_2 = \mathcal{D}$ —can facilitate effective invariant learning.

Environment Inference for Invariant Learning Our aim is to find environments that maximally violate the invariant learning principle. We can then evaluate the quality of these inferred environments by utilizing them in an invariant learning method. Our overall algorithm EILL is a two-stage process: (1) Environment Inference (EI): infer the environment assignments; and (2) Invariant Learning (IL): run invariant learning given these assignments.

The primary goal of invariant-learning is to find features that are domain-invariant, i.e. that reliably predict the true class regardless of the domain. The EI phase aims to identify domains that help uncover these features. This phase depends on a reference classifier $\tilde{\Phi}$; which maps inputs X to outputs Y , and defines a putative set of invariant features. This model could be found using ERM on $p^{obs}(x, y)$, for example. Environments are then derived that partition the mapping of the reference model which maximally violate the invariance principle, i.e., where for the reference classifier the same feature vector is associated with examples of different classes. While any of the aforementioned invariant learning objectives can be incorporated into the EI phase, the invariance principle or group-sufficiency—as expressed in (EIC)—is a natural fit, since it explicitly depends on learned feature representations Φ .

To realize an EI phase focused on the invariance principle, we utilize the IRM objective (IRMv1). We begin by noting that the per-environment risk R^e depends implicitly on the manual environment labels from the dataset. For a given environment e' , we denote $\mathbb{1}(e_i = e')$ as an indicator that example i is assigned to that environment, and re-express the per-environment risk as:

$$R^e(\Phi) = \frac{1}{\sum_{i'} \mathbb{1}(e_{i'} = e)} \sum_i \mathbb{1}(e_i = e) \ell(\Phi(x_i), y_i) \quad (3.2)$$

Now we relax this risk measure to search over the space of environment assignments. We replace the manual assignment indicator $\mathbb{1}(e_i = e')$, with a probability distribution $\mathbf{q}_i(e') := q(e'|x_i, y_i)$, representing a soft assignment of the i -th example to the e' -th environment. To *infer* environments, we optimize $q(e|x_i, y_i)$ so that it captures the worst-case environments for a fixed classifier Φ . This

corresponds to maximizing w.r.t. \mathbf{q} the following soft relaxation of the regularizer⁴ from C^{IRM} :

$$C^{EI}(\Phi, \mathbf{q}) = \|\nabla_{\tilde{w}} \tilde{R}^e(\tilde{w} \circ \Phi, \mathbf{q})\|, \quad (3.3)$$

$$\tilde{R}^e(\Phi, \mathbf{q}) = \frac{1}{N} \sum_i \mathbf{q}_i(e) \ell(\Phi(x_i), y_i) \quad (3.4)$$

where \tilde{R}^e represents a soft per-environment risk that can pass gradients to the environment assignments \mathbf{q} . See Algorithm 3 in Appendix B.1 for pseudocode. To summarize, EIIL involves the following sequential⁵ approach:

1. Input *reference model* $\tilde{\Phi}$;
2. Fix $\Phi \leftarrow \tilde{\Phi}$ and optimize the EI objective to infer environments: $\mathbf{q}^* = \operatorname{argmax}_{\mathbf{q}} C^{EI}(\tilde{\Phi}, \mathbf{q})$;
3. Fix $\tilde{\mathbf{q}} \leftarrow \mathbf{q}^*$ and optimize the IL objective to yield the new model: $\Phi^* = \operatorname{argmin}_{\Phi} C^{IL}(\Phi, \tilde{\mathbf{q}})$

In our experiments we consider binary environments and parameterize the \mathbf{q} as a vector of probabilities for each example in the training data.⁶ EIIL is applicable more broadly to any environment-based invariant learning objective through the choice of C^{IL} in Step 3. We present experiments using $C^{IL} \in \{C^{IRM}, C^{GroupDRO}\}$, and leave a more complete exploration to future work.

Analyzing the Inferred Environments To characterize the ability of EIIL to generalize to unseen test data, we now examine the inductive bias for generalization provided by the reference model $\tilde{\Phi}$. We state the main result here and defer the proofs to Appendix B.2. Consider a dataset with some feature(s) z which are spurious, and other(s) v which are valuable/invariant/causal w.r.t. the label y . Our proof considers binary features/labels and two environments, but the same argument extends to other cases. Our goal is to find a model Φ whose representation $\Phi(v, z)$ is invariant w.r.t. z and focuses solely on v .

Proposition 1. *Consider environments that differ in the degree to which the label y agrees with the spurious features z : $\mathbb{P}(\mathbb{1}(y = z)|e_1) \neq \mathbb{P}(\mathbb{1}(y = z)|e_2)$: then a reference model $\tilde{\Phi} = \Phi_{Spurious}$ that is invariant to valuable features v and solely focuses on spurious features z maximally violates the invariance principle (EIC). Likewise, consider the case with fixed representation Φ that focuses on the spurious features: then a choice of environments that maximally violates (EIC) is $e_1 = \{v, z, y | \mathbb{1}(y = z)\}$ and $e_2 = \{v, z, y | \mathbb{1}(y \neq z)\}$.*

If environments are split according to agreement of y and z , then the constraint from (EIC) is satisfied by a representation that ignores z : $\Phi(x) \perp z$. Unfortunately this requires a priori knowledge of either the spurious feature z or a reference model $\tilde{\Phi} = \Phi_{Spurious}$ that extracts it. When the sub-optimal solution $\Phi_{Spurious}$ is not a priori known, it will sometimes be recovered directly from

⁴We omit the average risk term as we are focused on maximally violating (EIC) regardless of the risk.

⁵We also tried jointly training Φ and \mathbf{q} using alternating updates, as in GAN training, but did not find empirical benefits. This formulation introduces optimization and conceptual difficulties, e.g. ensuring that invariances apply to all environments discovered throughout learning.

⁶Note that under this parameterization, when optimizing the inner loop with fixed Φ the number of parameters equals the number of data points (which is small relative to standard neural net training). We leave amortization of q to future work.

the training data; for example in CMNIST we find that Φ_{ERM} approximates Φ_{Color} . This allows EIIL to find environment partitions providing the starkest possible contrast for invariant learning.

Even if environment partitions are available, it may be possible to improve performance by inferring new partitions from scratch. It can be shown that the environments provided in the CMNIST dataset [Arjovsky et al., 2019] do not maximally violate (EIC) for a reference model $\tilde{\Phi} = \Phi_{Color}$, and are thus not maximally informative for learning to ignore color. Accordingly, EIIL improves test accuracy for IRM compared with the hand-crafted environments (Table 3.1).

If $\tilde{\Phi} = \Phi_{ERM}$ focuses on a mix of z and v , EIIL may still find environment partitions that enable effective invariant learning, as we find in the Waterbirds dataset, but they are not guaranteed to maximally violate (EIC).

Binned Environment Invariance We can derive a heuristic algorithm for EI that maximizes violations of the invariance principle by stratifying examples into discrete bins (i.e. confidence bins for 1-D representations), then sorting them into environments within each bin. This algorithm provides insight into both the EI task and the relationship between the IRMv1 regularizer and the invariance principle. We define bins in the space of the learned representation $\Phi(x)$, indexed by b ; s_{ib} indicates whether example i is in bin b . The intuition behind the algorithm is that a simple approach can separate the examples in a bin to achieve the maximal value of the (EIC).

The degree to which the environment assignments violate (EIC) can be expressed as follows, which can then be approximated in terms of the bins:

$$\begin{aligned} \Delta\text{EIC} &= (E[y|\Phi(x), e_1] - E[y|\Phi(x), e_2])^2 \\ &\approx \sum_b \left(\sum_i s_{ib} y_i \mathbf{q}_i(e = e_1) - \sum_i s_{ib} y_i \mathbf{q}_i(e = e_2) \right)^2 \end{aligned}$$

Inspection of this objective leads to a simple algorithm: assign all the $y = 1$ examples to one environment, and $y = -1$ examples to the other. This results in the expected values of y equal to ± 1 , which achieves the maximum possible value of ΔEIC per bin.⁷

This binning leads to an important insight into the relationship between the IRMv1 regularizer and (EIC). Despite the analysis in Arjovsky et al. [2019], this link is not completely clear [Kamath et al., 2021, Rosenfeld et al., 2021]. However, in the situation considered here, with binary classes, we can use this binning approach to show a tight link between the two objectives: finding an environment assignment that maximizes the violation of our softened IRMv1 regularizer (Equation 3.3) also maximizes the violation of the softened Environment Invariance Constraint (ΔEIC); see Appendix B.2.2 for the proof. This binning approach highlights the dependence on the reference model, as the bins are defined in its learned Φ space; the reference model also played a key role in the analysis above. We analyze it empirically in Section 3.3.3.

3.3 Experiments

We proceed by describing the remaining datasets under study in Section 3.3.1. We then present the main results measuring the ability of EIIL to handle distribution shift in Section 3.3.2, and offer a more detailed analysis of the EIIL solution and its dependence on the reference model in Section 3.3.3. See <https://github.com/ecreager/eiil> for code.

⁷For very confident reference models, where few confidence bins are populated, splitting based on y relates to partitioning the error cases. This splitting strategy is not the only possible solution, as multiple global optima exist.

Model selection Tuning hyperparameters when train and test distributions differ is a difficult open problem [Gulrajani and Lopez-Paz, 2021, Krueger et al., 2021]. Where possible, we reuse effective hyperparameters for IRM and GroupDRO found by previous authors. Because these works allowed limited validation samples for hyperparameter tuning (all baseline methods benefit fairly from this strategy), these results represent an optimistic view on the ability for invariant learning. As discussed above, the choice of reference classifier is of crucial importance when deploying EIIL; if worst-group performance can be measured on a validation set, this could be used to tune the hyperparameters of the reference model (i.e. model selection subsumes reference model selection). See Appendix B.4 for further discussion.

3.3.1 Datasets

CMNIST CMNIST is a noisy digit recognition task⁸ where color is a spurious feature that correlates with the label at train time but anti-correlates at test time, with the correlation strength at train time varying across environments [Arjovsky et al., 2019]. In particular, the two training environments have $Corr(color, label) \in \{0.8, 0.9\}$ while the test environment has $Corr(color, label) = 0.1$. Crucially, label noise is applied by flipping y with probability $\theta_y = 0.25$. This implies that shape (the invariant feature) is marginally less reliable than color in the training data, so ERM ignores shape to focus on color and suffers from below-chance test performance.

Waterbirds To evaluate whether EIIL can infer useful environments in a more challenging setting with high-dimensional images, we turn to the Waterbirds dataset [Sagawa et al., 2020a]. Waterbirds is a composite dataset that combines 4,795 bird images from the CUB dataset [Welinder et al., 2010] with background images from the Places dataset [Zhou et al., 2017]. It examines the proposition (which frequently motivates invariant learning approaches) that modern networks often learn spurious background features (e.g. green grass in pictures of cows) that are predictive of the label at train time but fail to generalize in new contexts [Beery et al., 2018a, Geirhos et al., 2020a]. The target labels are two classes of birds—“landbirds” and “waterbirds” respectively coming from dry or wet habitats—superimposed on land and water backgrounds. At training time, landbirds and waterbirds are most frequently paired with land and water backgrounds, respectively, but at test time the 4 subgroup combinations are uniformly sampled. To mitigate failure under distribution shift, a robust representation should learn primarily features of the bird itself, since these are invariant, rather than features of the background. Beyond the increase in dimensionality, this task differs from CMNIST in that the ERM solution does not fail catastrophically at test time, and in fact can achieve 97.3% average accuracy. However, because ERM optimizes average loss, it suffers in performance on the worst-case subgroup (waterbirds on land, which has only 56 training examples).

CivilComments-WILDS We apply EIIL to a large and challenging comment toxicity prediction task with important fairness implications [Borkan et al., 2019], where ERM performs poorly on comments associated with certain identity groups. We follow the procedure and data splits of Koh et al. [2021] to finetune DistilBERT embeddings [Sanh et al., 2019]. EIIL uses an ERM reference classifier and its inferred environments are fed to a GroupDRO invariant learner. Because the large training set ($N_{train} = 269,038$) increases the convergence time for gradient-based EI, we deploy the binning heuristic discussed in Section 3.2.2, which in this instance finds environments that

⁸MNIST digits are grouped into $\{0, 1, 2, 3, 4\}$ and $\{5, 6, 7, 8, 9\}$ so the CMNIST target label y is binary.

correspond to the error and non-error cases of the reference classifier. While ERM and EIIL do not have access to the sensitive group labels, we note that worst-group validation accuracy is used to tune hyperparameters for all methods. See Appendix B.4 for details. We also compare against a GroupDRO (oracle) learner that has access to group labels.

3.3.2 Results

Table 3.1: Accuracy (%) on CMNIST, a digit classification task where color is a spurious feature correlated with the label during training but anti-correlated at test time. EIIL exceeds test-time performance of IRM *without* knowledge of pre-specified environment labels, by instead finding worst-case environments using aggregated data and a reference classifier.

Method	Handcrafted Environments	Train	Test
ERM	✗	86.3 ± 0.1	13.8 ± 0.6
IRM	✓	71.1 ± 0.8	65.5 ± 2.3
EIIL	✗	73.7 ± 0.5	68.4 ± 2.7

CMNIST IRM was previously shown to learn an invariant representation on this dataset, allowing it to generalize relatively well to the held-out test set whereas ERM fails dramatically [Arjovsky et al., 2019]. It is worth noting that label noise makes the problem challenging, so even an oracle classifier can achieve at most 75% test accuracy on this binary classification task. To realize EIIL in our experiments, we discard the environment labels, and run the procedure described in Section 3.2.2 with ERM as the reference model and IRM as the invariant learner used in the final stage. We find that EIIL’s environment labels are very effective for invariant learning, ultimately *outperforming* standard IRM using the environment labels provided in the dataset (Table 3.1). This suggests that in this case the EIIL solution approaches the *maximally informative* set of environments discussed in Proposition 1.

Waterbirds Sagawa et al. [2020a] demonstrated that ERM suffers from poor worst-group performance on this dataset, and that GroupDRO can mitigate this performance gap if group labels are available. In this dataset, group labels should be considered as oracle information, meaning that the relevant baseline for EIIL is standard ERM. The main contribution of Sagawa et al. [2020a] was to show *how* deep nets can be optimized for the GroupDRO objective using their online algorithm that adaptively adjusts per-group importance weights. In our experiment, we combine this insight with our EIIL framework to show that distributionally robust neural nets can be realized without access to oracle information. We follow the same basic procedure as above,⁹ in this case using GroupDRO as the downstream invariant learner for which EIIL’s inferred labels will be used.

EIIL is significantly more robust than the ERM baseline (Table 3.2), raising worst-group test accuracy by 18% with only a 1% drop in average accuracy. In Figure 3.1 we plot the distribution of subgroups for each inferred environment, showing that the minority subgroups (landbirds on water and waterbirds on land) are mostly organized in the same inferred environment. This suggests the possibility of leveraging environment inference for interpretability to automatically discover a model’s performance discrepancies on subgroups, which we leave for future work.

⁹For this dataset, environment inference worked better with reference models that were not fully trained. We suspect this is because ERM focuses on the easy-to-compute features like background color early in training, precisely the type of bias EIIL can exploit to learn informative environments.

Table 3.2: Accuracy (%) on the Waterbirds dataset. EIIL strongly outperforms ERM on worst-group performance, approaching the performance of the GroupDRO algorithm proposed by Sagawa et al. [2020a], which requires oracle access to group labels. In this experiment we feed environments inferred by EIIL into a GroupDRO learner.

Method	Train (avg)	Test (avg)	Test (worst group)
ERM	100.0	97.3	60.3
EIIL	99.6	96.9	78.7
GroupDRO (oracle)	99.1	96.6	84.6

Table 3.3: EIIL improves worst-group accuracy in the CivilComments-WILDS toxicity prediction task, without access to group labels.

Method	Train (avg)	Test (avg)	Test (worst group)
ERM	96.0 \pm 1.5	92.0 \pm 0.4	61.6 \pm 1.3
EIIL	97.0 \pm 0.8	90.5 \pm 0.2	67.0 \pm 2.4
GroupDRO (oracle)	93.6 \pm 1.3	89.0 \pm 0.3	69.8 \pm 2.4

CivilComments-WILDS Without knowledge of which comments are associated with which groups, EIIL improves worst-group accuracy over ERM with only a modest cost in average accuracy, approaching the oracle GroupDRO solution (which requires group labels).

3.3.3 Influence of the Reference Model

As discussed in Section 3.2.2, the ability of EIIL to find useful environments—partitions yielding an invariant representation when used by an invariant learner—depends on its ability to exploit variation in the predictive distribution of a reference classifier. Here we study the influence of the reference classifier on the final EIIL solution. We return to the CMNIST dataset, which provides a controlled sampling setup where particular ERM solutions can be induced to serve as reference for EIIL.

EIIL was shown to outperform IRM *without access to environment labels* in the standard CMNIST dataset (Table 3.1), which has label noise of $\theta_y = 0.25$. Because $\text{Corr}(\text{color}, \text{label})$ is 0.85 (on average)

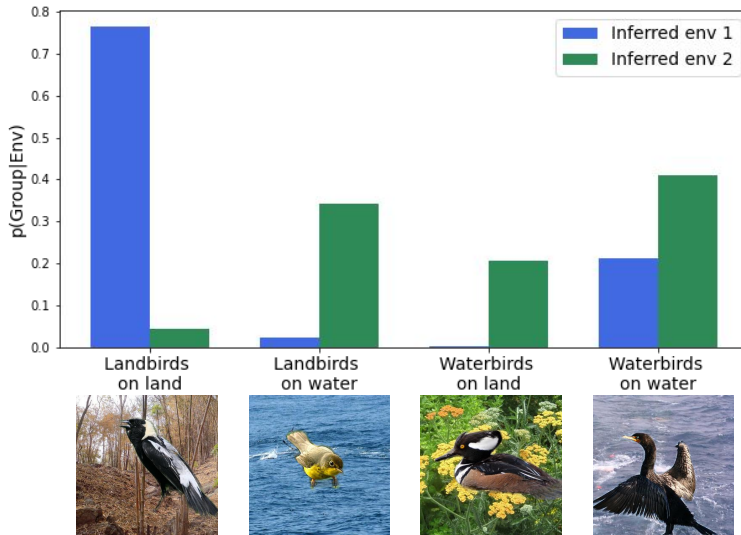


Figure 3.1: After using EIIL to directly infer two environments from the Waterbirds dataset, we examine the proportion of each subgroup (available in the original dataset but not used by EIIL) present in the inferred environment.

for the train set, this amount of label noise implies that color is the most predictive feature on aggregated training set (although its predictive power varies across environments). ERM, even with access to infinite data, will focus on color given this amount of label noise to achieve an average train accuracy of 85%. However we can implicitly control the ERM solution Φ_{ERM} by tuning θ_y , an insight that we use to study the dependence of EIIL on the reference model $\tilde{\Phi} = \Phi_{ERM}$.

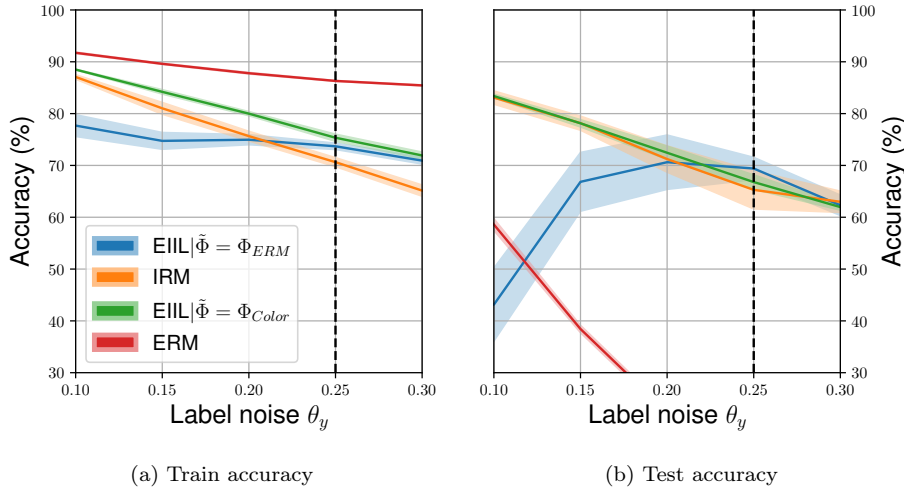


Figure 3.2: CMNIST with varying label noise θ_y . Under high label noise ($\theta_y > .2$), where the spurious feature color correlates to label *more* than shape on the train data, EIIL matches or exceeds the test performance of IRM *without relying on hand-crafted environments*. Under medium label noise ($.1 < \theta_y < .2$), EIIL is worse than IRM but better than ERM, the logical approach if environments are not available. Under low label noise ($\theta_y < .1$), where color is *less* predictive than shape at train time, ERM performs well and EIIL fails. The vertical dashed black line indicates the default setting of $\theta_y = 0.25$, which we report in Table 3.1.

Figure 3.2 shows the results of our study. We find that EIIL generalizes better than IRM with sufficiently high label noise $\theta_y > .2$, but generalizes poorly under low label noise. This is precisely because ERM learns the color feature under high label noise, and the shape feature under low label noise. We verify this conclusion by evaluating EIIL when $\tilde{\Phi} = \Phi_{Color}$, i.e. a hand-coded color-based predictor as reference, which does well across all settings of θ_y .

We saw in the Waterbirds experiment that it is not a strict requirement that ERM fail completely in order for EIIL to succeed. However, this controlled study highlights the importance of the reference model in the ability of EIIL to find environments that emphasize the right invariances, which leaves open the question of how to effectively choose a reference model for EIIL in general. One possible way forward is by using validation data that captures the *kind* of distribution shift we expect at test time, without exactly producing the test distribution, e.g. as in the WILDS benchmark [Koh et al., 2021]. In this case we could choose to run EIIL with a reference model that exhibits a large generalization gap between the training and validation distributions.

3.4 Related Work

Domain adaptation and generalization Beyond the methods discussed above, a variety of recent works have approached the domain generalization problem from the lens of learning invariances in the training data. Adversarial training is a popular approach for learning representations invariant [Ganin et al., 2016, Hoffman et al., 2018, Zhang et al., 2017] or conditionally invariant [Li et al.,

2018] to the environment. However, this approach has limitations in settings where distribution shift affects the marginal distribution over labels [Zhao et al., 2019].

Arjovsky et al. [2019] proposed IRM to mitigate the effect of test-time label shift, which was inspired by applications of causal inference to select invariant features [Peters et al., 2016]. Krueger et al. [2021] proposed the related Risk Extrapolation (REx) principle, which dictates a stronger preference to exactly equalize $R^e \forall e$ (e.g. by penalizing variance across e as in their practical algorithm V-REx), which is shown to improve generalization in several settings.¹⁰

Several large-scale benchmarks have been proposed to highlight difficult open problems in this field, including the use of real-world data [Koh et al., 2021], handling subpopulation shift [Santurkar et al., 2021b], and model selection [Gulrajani and Lopez-Paz, 2021].

Leveraging a reference classifier A number of methods have been proposed that improve performance by exploiting the mistakes of a pre-trained auxiliary model, as we do when inferring environments for the invariant learner using $\tilde{\Phi}$. Nam et al. [2020] jointly train a “biased” model f_B and a “debiased” model f_D , where the relative cross-entropy losses of f_B and f_D on each training example determine their importance weights in the overall training objective for f_D . Sohoni et al. [2020] infer a different set of “hidden subclasses” for each class label $y \in \mathcal{Y}$. Subclasses computed in this way are then used as group labels for training a GroupDRO model, so the overall two-step process corresponds to certain choices of EI and IL objectives.

Liu et al. [2021] and Dagaev et al. [2021] concurrently proposed to compute importance weights for the primary model using an ERM reference, which can be seen as a form of distributionally robust optimization where the worst-case distribution only updates once. Dagaev et al. [2021] use the confidence of the reference model to assign importance weights to each training example. Liu et al. [2021] split the training examples into two disjoint groups based on the errors of ERM, akin to our EI step, with the per-group importance weights treated as a hyperparameter for model selection (which requires a subgroup-labeled validation set). We note that the implementation of EIIL using binning, discussed in Section 3.2.2, can also realize an error splitting behavior. In this case, both methods use the same disjoint groups of training examples towards slightly different ends: we train an invariant learner, whereas Liu et al. [2021] train a cross-entropy classifier with fixed per-group importance weights.

Algorithmic fairness Our work draws inspiration from a rich body of work on learning fair classifiers in the absence of demographic labels [Hashimoto et al., 2018, Hébert-Johnson et al., 2018, Kearns et al., 2018, Kim et al., 2019, Lahoti et al., 2020]. Generally speaking, these works seek a model that performs well for group assignments that are the worst case according to some fairness criterion. Environment inference serves a similar purpose for our method, but with a slightly different motivation: rather than learn an fair model in an online way that provides favorable in-distribution predictions, we learn discrete data partitions as an intermediary step, which enables use of invariant learning methods to tackle distribution shift.

Adversarially Reweighted Learning (ARL) [Lahoti et al., 2020] is most closely related to ours, since they emphasize subpopulation shift as a key motivation. Whereas ARL uses a DRO objective that prioritizes stability in the loss space, we explore environment inference to encourage invariance

¹⁰Analogous to V-REx, Williamson and Menon [2019] adapt Conditional Variance at Risk (CVaR) [Rockafellar and Uryasev, 2002] to equalize risk across demographic groups.

in the learned representation space. We see these as complementary approaches that are each suited to different types of distribution shift.

When group labels are available for training, we can establish links between algorithmic fairness and related methods for invariant learning. Early approaches to learning fair representations [Edwards and Storkey, 2016, Louizos et al., 2016a, Madras et al., 2018, Zemel et al., 2013, Zhang et al., 2018] leveraged statistical independence regularizers from domain adaptation [Ben-David et al., 2010, Ganin et al., 2016, Long et al., 2018, Tzeng et al., 2017], noting that marginal or conditional independence from domain to prediction relates to the fairness notions of demographic parity $\hat{y} \perp e$ [Dwork et al., 2012] and equal opportunity $\hat{y} \perp e|y$ [Hardt et al., 2016b].

Recall that (EIC) involves an environment-specific conditional label expectation given a data representation $\mathbb{E}[y|\Phi(x) = h, e]$. Objects of this type have been closely studied in the fair machine learning literature, where e now denotes a “sensitive” attribute indicating membership in a protected demographic group (age, race, gender, etc.), and the vector representation $\Phi(x)$ is typically replaced by a scalar score¹¹ $S(x) \in \mathbb{R}$. Noting that $\sigma(S(x))$ represents the probability of the model prediction, $\mathbb{E}[y|S(x), e]$ can now be interpreted as a *calibration curve* that must be regulated according to some fairness constraint. Chouldechova [2017] showed that equalizing this calibration curve across groups is often incompatible with a common fairness constraint, demographic parity, while Liu et al. [2019] studied “group sufficiency” of classifiers with strongly convex losses, concluding that ERM naturally finds group sufficient solutions without fairness constraints.

3.5 Discussion

This Chapter presented EIIL, a framework that leverages a non-robust reference model to partition the training data, which can enable robust downstream learning. In general, learning to generalize OOD will require additional assumptions or inductive biases beyond what are typically used in supervised learning. Therefore, EIIL should be understood as a robust learning approach that uses a different inductive bias than standard Domain Generalization: rather than relying on human-specified side information (environment labels), EIIL assumes access to a reference model that is *not* robust under the distribution shifts of interest. In this sense, EIIL does not provide any free lunch, as the sensitivity of OOD performance to the reference model is a known issue (see Section 3.3.3). However, since EIIL was published as a conference paper, subsequent efforts have extended EIIL or otherwise addressed these limitations through complementary approaches.

Ahmed et al. [2021] demonstrated that EIIL can be extended to effectively handle “systematic” generalization [Bahdanau et al., 2019] on a semi-synthetic foreground/background task similar to the Waterbirds dataset that we study. To do so, they proposed a novel invariance regularizer for use in the IL stage, which is based on matching class-conditioned average predictive distributions across environments. We note that this is closely related to the equalized odds criterion commonly used in fair classification [Hardt et al., 2016b].

Mishra and Liu [2022] provide an insightful information-theoretic analysis of environment inference, where EI amounts to choosing a majority group (i.e. the inferred environment with the most examples) such that the reference representation $\Phi(x)$ has more information about the target label y within the majority group than it does in aggregate (in the original training distribution). They then formulate

¹¹For binary classification, score-based and representation-based approaches are closely related since scores are commonly implemented as (or can be interpreted as) as the linear mapping of a data representation: $S(x) = w \circ \Phi(x)$.

a procedure that improves the downstream invariant learner through a process of iterative repeated EIIL. Meanwhile, Zhang et al. [2022] showed that iteratively growing a set of invariant features (similar to repeated EIIL) is helpful in finding a good initialization for invariant learning. In early prototyping efforts, we tried a rudimentary version of repeated EIIL without the information theoretic interpretation, but found it to be unstable. The practical success of repeated EIIL demonstrated by Mishra and Liu [2022] suggests connections between environment-free invariant learning and boosting [Ben-David et al., 2001, Kalai et al., 2008, Kearns et al., 1992]. This connection is quite intuitive—boosting was a key inspiration for works on fair learning without demographic labels [Hébert-Johnson et al., 2018, Kearns et al., 2018], which in turn inspired EIIL—and could be further explored in the future.

All neural networks, even ones trained using unconstrained supervised learning (e.g. ERM), have internal representations. The arguments presented in this Chapter (like those in Chapter 2) follow the intuition that because ERM learns shortcuts, then using its internal representations could cause unintended downstream model failures, thus motivating more specialized representation learning algorithms. It is worth pausing to note that this position is not a universal consensus, especially in light of the fact that specialized representation learners often underperform relative to ERM on in-distribution data.¹²

One noteworthy countervailing argument is that that representation learning should be done by ERM or other unconstrained representation learners—e.g. self-supervised learners like CLIP [Radford et al., 2021]—then adapted for the task at hand using data from the target distribution [Kirichenko et al., 2022, Menon et al., 2021]. It would seem that while ERM predictions rely on shortcut features [Geirhos et al., 2020a], their internal representations contain more than just shortcut features [Menon et al., 2021]. Indeed, Eyre et al. [2022] found that even invariant representation learners like IRM [Arjovsky et al., 2019] can absorb shortcuts (in addition to robust features) into their internal representations, although these are typically projected out by the subsequent classification layer. Researchers will continue to study the properties of invariant and unconstrained representations. In the meantime, practitioners wondering whether one should be preferred over the other should consider whether labeled data can be acquired from the target domain, and also whether distribution shifts can be expected after model deployment.

¹²This is analogous to the fairness-accuracy tradeoffs discussed in Chapter 2

Chapter 4

Data Augmentation for Robust Reinforcement Learning

4.1 Contemporary RL Often Lacks Data Coverage

Chapters 2 and 3 provided variations on the theme of realizing robust prediction by addressing troublesome correlation patterns between observed inputs and targets in the training data. In this Chapter, we shift our focus from the static setting of supervised learning to *sequential decision making*, where our decision-making model is deployed in a dynamically changing world. In particular, we will follow the approach of Reinforcement Learning (RL) [Sutton and Barto, 2018] by requiring our decision-making model—hereafter referred to as the “agent”—to learn a mapping from observed states to pre-defined actions that maximizes a reward signal.

Let us formalize this setup using a Markov Decision Process (MDP), described by tuple $\langle \mathcal{S}, \mathcal{A}, P, R, \gamma \rangle$ consisting of the state space, action space, transition function, reward function, and discount factor, respectively [Puterman, 2014, Sutton and Barto, 2018]. We denote individual states and actions using lowercase $s \in \mathcal{S}$ and $a \in \mathcal{A}$, and variables using the uppercase S and A (e.g., $s \in \text{range}(S) \subseteq \mathcal{S}$). A policy $\pi : \mathcal{S} \times \mathcal{A} \rightarrow [0, 1]$ defines a probability distribution over the agent’s actions at each state, and an agent is typically tasked with learning a parameterized policy that maximizes the expected reward in the long run.

In order to act optimally in a given observed state s , it is thus necessary to reason about how candidate actions $a \in \mathcal{A}$ will affect rewards accrued in the distant future. For a given tuple (s, a) within the state-action space, the long-term prospects for a policy π are encapsulated by its value function

$$Q_\pi(s, a) = \mathbb{E}_{P, \pi}[R(s_t, s_a) + \gamma R(s_{t+1}, s_{a+1}) + \gamma^2 R(s_{t+2}, s_{a+2}) + \dots | s_t = s, a_t = a]. \quad (4.1)$$

The infinite summand in Equation 4.1 presents an apparent computational hurdle. One popular approach to resolving this issue is dynamic programming [Bellman, 1957, Kirk, 2004], which exploits the recursive structure in the summands. For example, the Bellman optimality condition provides a relation [Bellman, 1957] provides a relation between the value at the current state-action pair (s_t, a_t)

and its successor state s_{t+1} under the optimal policy π^* :

$$Q_{\pi^*}(s_t, a_t) = \mathbb{E}[r_t + \gamma \max_{a'} Q_{\pi^*}(s_{t+1}, a') | s_t, a_t].$$

The Q-learning algorithm [Watkins and Dayan, 1992] exploits this relation to derive a fixed-point update to an approximation of Q :

$$Q(s_t, a_t) \leftarrow Q(s_t, a_t) + \alpha[r_{t+1} + \gamma \max_{a'} Q(s_{t+1}, a') - Q(s_t, a_t)]$$

where α is a hyperparameter representing the step size. For appropriate settings of α , this approximation is known to converge to $Q_{\pi^*}(s, a)$, from which the optimal policy π^* can be derived [Watkins and Dayan, 1992].

At first glance this suggests an optimistic view on robust RL. Because the agent will converge to an optimal policy *regardless* of the training data distribution, it would seem that previously discussed concerns about fairness and shortcut learning—where models were seen to be highly sensitive to particularities in how training data is collected—simply do not apply in the RL setting. However, in practice, we find that RL algorithms are indeed sensitive to training data. This is because the available data typically do not satisfy the key assumptions underpinning classic convergence guarantees. In particular, with most dynamic programming algorithms, “all that is required for correct convergence is that all (state-action) pairs continue to be updated” [Sutton and Barto, 2018, Sec. 6.5]. In other words, the training data must have sufficient *coverage*: all vales of (s, a) must be visited with reasonable frequency. This is a tall order in real-world settings for two reasons: first, the state space grows exponentially in the number of observed features, of which there are many in contemporary tasks of interest; second, in safety critical applications like clinical health care and robotics, it may be unethical to deploy an exploratory policy (e.g. prescribing random treatments to patients) in order to realize this coverage condition [Brunke et al., 2021, Gottesman et al., 2019].

This Chapter addresses the data coverage issue in RL through the lens of data augmentation: by leveraging causal priors (typically specified by domain experts, although sometimes learned directly from data) we can improve the quantity and quality of available training data.

4.2 The Role of Data Augmentation in RL

Data augmentation has become a go-to tool in the arsenal of RL methods, especially in settings with large state spaces, or when using neural networks to approximate value functions during learning. Take for example Hindsight Experience Replay (HER) [Andrychowicz et al., 2017], which is designed for goal-conditioned RL, where the agent must learn to act optimally for any number of distinct goals $g \in \mathcal{G}$. Including the goal—perhaps a continuous vector indicating the target position where an object must be placed—as a special type of state in the MDP amplifies the size of the overall state-action space, and in fact Andrychowicz et al. [2017] show that many goal-conditioned continuous control tasks simply cannot be solved using this naive approach. To resolve this difficulty, they propose an application of *goal relabeling* [Kaelbling, 1993], which effectively reframes the observed data so far. For experiences where the agent fails to achieve the desired goal $g \in \mathcal{G}$, the experience is *relabelled* as a success under an alternate goal $g' \neq g$, where g' could indicate the coordinate where the object was dropped in reality (regardless of the agent’s original goal).

Learning to act from images presents an analogous coverage issue, as the number of pixels in

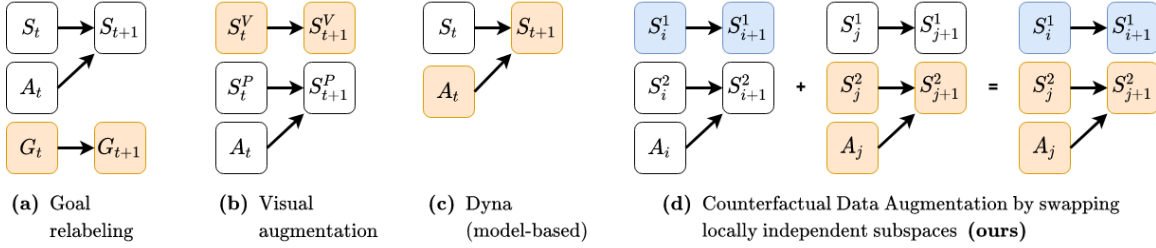


Figure 4.1: *Four instances of CoDA; orange nodes are relabeled, noise variables omitted for clarity. **First:** Goal relabeling [Kaelbling, 1993], including HER [Andrychowicz et al., 2017], augments transitions with counterfactual goals. **Second:** Visual feature augmentation [Andrychowicz et al., 2020, Laskin et al., 2020] uses domain knowledge to change visual features S_t^V (such as textures, lighting, and camera positions) that the designer knows do not impact the physical state S_t^P . **Third:** Dyna [Sutton, 1991], including MBPO [Janner et al., 2019], augments real states with new actions and resamples the next state using a learned dynamics model. **Fourth (ours):** Given two transitions that share local causal structures, we propose to swap connected components to form new transitions.*

images space is huge. In this case, training the agent on replicated observed experiences with superficial perturbations on the images (random crops, etc.) has been shown to improve the sample efficiency of RL [Kostrikov et al., 2020, Laskin et al., 2020].

RL methods are often categorized as being either “model-free” or “model-based”. Here the “model” in question is a learned dynamics model $P_\theta : \mathcal{S} \times \mathcal{A} \rightarrow \mathcal{S}$ trained to approximate the MDP’s true transition function P (which may be inaccessible to the agent). Model-free methods directly consume observed (s, a, s') data to learn values and policies. On the other hand, model-based methods like Dyna [Sutton, 1991] first fit $P_\theta : \mathcal{S} \times \mathcal{A} \rightarrow \mathcal{S}$ fit to the observed data (s, a, s') then add samples from it to the observed experience (thus augmenting the available data) during the learning process.

4.3 Amplifying the Experience Buffer Using Causal Priors

4.3.1 Why is Data Augmentation a Useful Heuristic in RL?

Data augmentation for RL is evidently effective, but why does it work? The key insight of this Chapter is that existing data augmentation methods can be interpreted as implicit counterfactual samplers. This involves formulating a causal graphical model [Pearl, 2009a] over single-step transition diagrams. We then observe that whenever this graph composes two or more *independent mechanisms*, then this independence justifies resampling one mechanism’s values to those consistent with the data distribution. For example, with HER [Andrychowicz et al., 2017] despite the policies being goal-conditioned, once the data is collected, the goals are independent of the other next-state dynamics (e.g. trajectories of objects) in the scene (See Fig. 4.1).

This Chapter formalizes and discusses a generic recipe for Counterfactual Data Augmentation (CoDA), and applies this recipe to improve RL in settings where the independent mechanisms correspond to objects in the underlying MDP.

4.3.2 An Opportunity to Augment: Local Independence of Objects

High-dimensional dynamical systems are often composed of simple subprocesses that affect one another through sparse interaction. If the subprocesses *never* interacted, an agent could realize significant gains in sample efficiency by globally factoring the dynamics and modeling each subprocess independently [Guestrin et al., 2003, Hallak et al., 2015]. In most cases, however, the subprocesses do *eventually* interact and so the prevailing approach is to model the entire process using a monolithic,

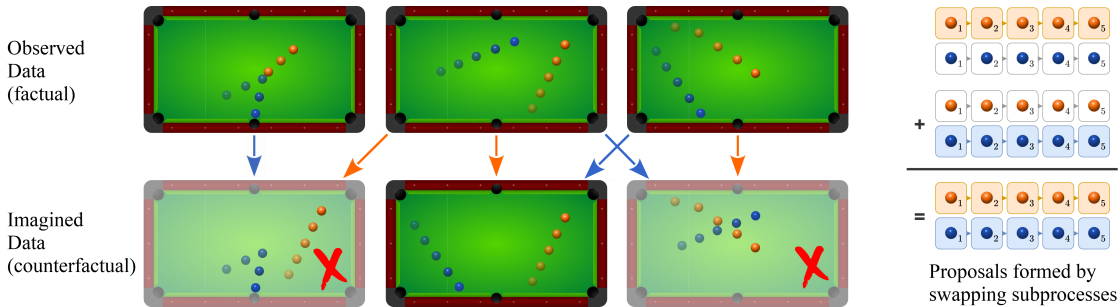


Figure 4.2: **Counterfactual Data Augmentation (CoDA)**. Given 3 factual samples, knowledge of the local causal structure lets us mix and match factored subprocesses to form counterfactual samples. The first proposal is rejected because one of its factual sources (the blue ball) is not locally factored. The third proposal is rejected because it is not itself factored. The second proposal is accepted, and can be used as additional training data for a reinforcement learning agent.

unfactored model. In this Section, we take advantage of the observation that *locally—during the time between their interactions—the subprocesses are causally independent*. By locally factoring dynamic processes in this way, we are able to capture the benefits of factorization even when their subprocesses interact on the global scale.

Consider a game of billiards, where each ball can be viewed as a separate physical subprocess. Predicting the opening break is difficult because all balls are mechanically coupled by their initial placement. Indeed, a dynamics model with dense coupling amongst balls may seem sensible when considering the expected outcomes over the course of the game, as each ball has a non-zero chance of colliding with the others. But at any given timestep, interactions between balls are usually sparse.

One way to take advantage of sparse interactions between otherwise disentangled entities is to use a structured state representation together with a graph neural network or other message passing transition model that captures the local interactions [Goyal et al., 2019, Kipf et al., 2019]. When it is tractable to do so, such architectures can be used to model the world dynamics directly, producing transferable, task-agnostic models. In many cases, however, the underlying processes are difficult to model precisely, and model-free [Laskin et al., 2020, Wang et al., 2019] or task-oriented model-based [Farahmand et al., 2017, Oh et al., 2017] approaches are less biased and exhibit superior performance. In this Section we argue that *knowledge of whether or not local interactions occur is useful in and of itself*, and can be used to generate causally-valid counterfactual data even in absence of a forward dynamics model. In fact, if two trajectories have the same local factorization in their transition dynamics, then under mild conditions we can produce new counterfactually plausible data using our proposed **Counterfactual Data Augmentation (CoDA)** technique, wherein factorized subspaces of observed trajectory pairs are swapped (Figure 4.2). This lets us sample from a counterfactual data distribution by stitching together subsamples from observed transitions. Since CoDA acts only on the agent’s training data, it is compatible with any agent architecture (including unfactored ones).

In the remainder of this Section, we formalize this data augmentation strategy and discuss how it can improve performance of model-free RL agents in locally factored tasks.

4.3.3 Background: Factored MDPs

The basic model for decision making in a controlled dynamic process is a Markov Decision Process (MDP), described by tuple $\langle \mathcal{S}, \mathcal{A}, P, R, \gamma \rangle$ consisting of the state space, action space, transition function, reward function, and discount factor, respectively [Puterman, 2014, Sutton and Barto, 2018]. Note that MDPs generalize uncontrolled Markov processes (set $A = \emptyset$), so that our work applies also

to sequential prediction. We denote individual states and actions using lowercase $s \in \mathcal{S}$ and $a \in \mathcal{A}$, and variables using the uppercase S and A (e.g., $s \in \text{range}(S) \subseteq \mathcal{S}$). A policy $\pi : \mathcal{S} \times \mathcal{A} \rightarrow [0, 1]$ defines a probability distribution over the agent’s actions at each state, and an agent is typically tasked with learning a parameterized policy π_θ that maximizes value $\mathbb{E}_{P, \pi} \sum_t \gamma^t R(s_t, a_t)$.

In most non-trivial cases, the state $s \in \mathcal{S}$ can be described as an object hierarchy together with global context. For instance, this decomposition will emerge naturally in any simulated process or game that is defined using a high-level programming language (e.g., the commonly used Atari [Bellemare et al., 2013] or Minecraft [Johnson et al., 2016] simulators). In this Chapter we consider MDPs with a single, known top-level decomposition of the state space $\mathcal{S} = \mathcal{S}^1 \oplus \mathcal{S}^2 \oplus \dots \oplus \mathcal{S}^n$ for fixed n , leaving extensions to hierarchical decomposition and multiple representations [Esmaili et al., 2019a, Higgins et al., 2018], dynamic factor count n [Zaheer et al., 2017], and (learned) latent representations [Burgess et al., 2019] to future work. The action space might be similarly decomposed: $\mathcal{A} = \mathcal{A}^1 \oplus \mathcal{A}^2 \oplus \dots \oplus \mathcal{A}^m$.

Given such state and action decompositions, we may model time slice $(t, t+1)$ using a structural causal model (SCM) $\mathcal{M}_t = \langle V_t, U_t, \mathcal{F} \rangle$ [Pearl, 2009a, Ch. 7] with directed acyclic graph (DAG) \mathcal{G} , where:

- $V_t = \{V_{t+1}^i\}_{i=0}^{2n+m} = \{S_t^1 \dots S_t^n, A_t^1 \dots A_t^m, S_{t+1}^1 \dots S_{t+1}^n\}$ are the nodes (variables) of \mathcal{G} .
- $U_t = \{U_{t+1}^i\}_{i=0}^{2n+m}$ is a set of noise variables, one for each V^i , determined by the initial state, past actions, and environment stochasticity. We assume that noise variables at time $t+1$ are independent from other noise variables: $U_{t+1}^i \perp U_{t+1}^j \forall i, j$. The instance $u = (u^1, u^2, \dots, u^{2n+m})$ of U_t denotes an individual realization of the noise variables.
- $\mathcal{F} = \{f^i\}_{i=0}^{2n+m}$ is a set of functions (“structural equations”) that map from $U_{t+1}^i \times \text{Pa}(V_{t+1}^i)$ to V_{t+1}^i , where $\text{Pa}(V_{t+1}^i) \subset V_t \setminus V_{t+1}^i$ are the parents of V_{t+1}^i in \mathcal{G} ; hence each f^i is associated with the set of incoming edges to node V_{t+1}^i in \mathcal{G} ; see, e.g., Figure 4.3 (center).

Note that while V_t , U_t , and \mathcal{M}_t are indexed by t (their distributions change over time), the structural equations $f^i \in \mathcal{F}$ and causal graph \mathcal{G} represent the global transition function P and apply at all times t . To reduce clutter, we drop the subscript t on V , U , and \mathcal{M} when no confusion can arise.

Critically, we require the set of edges in \mathcal{G} (and thus the number of inputs to each f^i) to be *structurally minimal* [Peters et al., 2017, Remark 6.6].

Assumption (Structural Minimality). $V^j \in \text{Pa}(V^i)$ if and only if there exists some $\{u^i, v^{-ij}\}$ with $u^i \in \text{range}(U^i)$, $v^{-ij} \in \text{range}(V \setminus \{V^i, V^j\})$ and pair (v_1^j, v_2^j) with $v_1^j, v_2^j \in \text{range}(V^j)$ such that $v_1^i = f^i(\{u^i, v^{-ij}, v_1^j\}) \neq f^i(\{u^i, v^{-ij}, v_2^j\}) = v_2^i$.

Intuitively, structural minimality says that V^j is a parent of V^i if and only if setting the value of V^j can have a nonzero *direct* effect¹ on the child V^i through the structural equation f^i . The structurally minimal representation is unique [Peters et al., 2017].

Given structural minimality, we can think of edges in \mathcal{G} as representing global causal dependence. The probability distribution of S_{t+1}^i is fully specified by its parents $\text{Pa}(S_{t+1}^i)$ together with its noise variable U_i ; that is, we have $P(S_{t+1}^i | S_t, A_t) = P(S_{t+1}^i | \text{Pa}(S_{t+1}^i))$ so that $S_{t+1}^i \perp V^j | \text{Pa}(S_{t+1}^i)$ for

¹Thus parentage does describe knock-on effects, e.g. V_1 on V_3 in the Markov chain $V_1 \rightarrow V_2 \rightarrow V_3$.

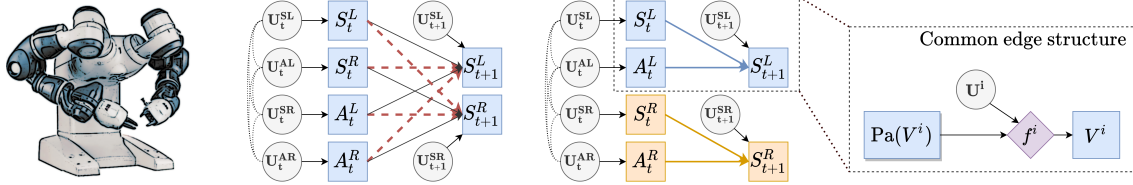


Figure 4.3: A two-armed robot (**left**) might be modeled as an MDP whose state and action spaces decompose into left and right subspaces: $\mathcal{S} = \mathcal{S}^L \oplus \mathcal{S}^R, \mathcal{A} = \mathcal{A}^L \oplus \mathcal{A}^R$. Because the arms can touch, the global causal model (**center left**) between time steps is fully connected, even though left-to-right and right-to-left connections (dashed red edges) are rarely active. By restricting our attention to the subspace of states in which left and right dynamics are independent we get a local causal model (**center right**) with two components that can be considered separately for training and inference.

all nodes $V^j \notin \text{Pa}(S_{t+1}^i)$. We call an MDP with this structure a *factored MDP* [Kearns and Koller, 1999]. When edges in \mathcal{G} are sparse, factored MDPs admit more efficient solutions than unfactored MDPs [Guestrin et al., 2003].

4.3.4 Local Causal Models (LCMs)

Limitations of Global Models Unfortunately, even if states and actions can be cleanly decomposed into several nodes, in most practical scenarios the DAG \mathcal{G} is fully connected (or nearly so): since the f^i apply globally, so too does structural minimality, and edge (S_k^i, S_{k+1}^j) at time k is present so long as there is a single instance—at any time t , no matter how unlikely—in which S_t^i influences S_{t+1}^j . In the words of Andrew Gelman, “*there are (almost) no true zeros*” [Gelman, 2011]. As a result, the factorized causal model \mathcal{M}_t , based on globally factorized dynamics, rarely offers an advantage over a simpler causal model that treats states and actions as monolithic entities (e.g., [Buesing et al., 2019]).

LCMs Our key insight is that for each pair of nodes (V_t^i, S_{t+1}^j) with $V_t^i \in \text{Pa}(S_{t+1}^j)$ in \mathcal{G} , there often exists a large subspace $\mathcal{L}^{(j \perp i)} \subset \mathcal{S} \times \mathcal{A}$ for which $S_{t+1}^j \perp\!\!\!\perp V_t^i \mid \text{Pa}(S_{t+1}^j) \setminus V_t^i, (s_t, a_t) \in \mathcal{L}^{(j \perp i)}$. For example, in case of a two-armed robot (Figure 4.3), there is a large subspace of states in which the two arms are too far apart to influence each other physically. Thus, if we restrict our attention to $(s_t, a_t) \in \mathcal{L}^{(j \perp i)}$, we can consider a *local* causal model $\mathcal{M}_t^{\mathcal{L}^{(j \perp i)}}$ whose local DAG $\mathcal{G}^{\mathcal{L}^{(j \perp i)}}$ is strictly sparser than the global DAG \mathcal{G} , as the structural minimality assumption applied to $\mathcal{G}^{\mathcal{L}^{(j \perp i)}}$ implies that there is no edge from V_t^i to S_{t+1}^j . More generally, for any subspace $\mathcal{L} \subseteq \mathcal{S} \times \mathcal{A}$, we can induce the Local Causal Model (LCM) $\mathcal{M}_t^{\mathcal{L}} = \langle V_t^{\mathcal{L}}, U_t^{\mathcal{L}}, \mathcal{F}^{\mathcal{L}} \rangle$ with DAG $\mathcal{G}^{\mathcal{L}}$ from the global model \mathcal{M}_t as:

- $V_t^{\mathcal{L}} = \{V_{t+1}^{\mathcal{L}, i}\}_{i=0}^{2n+m}$, where $P(V_{t+1}^{\mathcal{L}, i}) = P(V_{t+1}^i \mid (s_t, a_t) \in \mathcal{L})$.
- $U_t^{\mathcal{L}} = \{U_{t+1}^{\mathcal{L}, i}\}_{i=0}^{2n+m}$, where $P(U_{t+1}^{\mathcal{L}, i}) = P(U_{t+1}^i \mid (s_t, a_t) \in \mathcal{L})$.
- $\mathcal{F}^{\mathcal{L}} = \{f^{\mathcal{L}, i}\}_{i=0}^{2n+m}$, where $f^{\mathcal{L}, i} = f^i|_{\mathcal{L}}$ (f^i with range of input variables restricted to \mathcal{L}). Due to structural minimality, the signature of $f^{\mathcal{L}, i}$ may shrink (as the range of the relevant variables is now restricted to \mathcal{L}), and corresponding edges in \mathcal{G} will not be present in $\mathcal{G}^{\mathcal{L}}$.²

In case of the two-armed robot, conditioning on the arms being far apart simplifies the global DAG to a local DAG with two connected components (Figure 4.3). This can make counterfactual reasoning considerably more efficient: given a factual situation in which the robot’s arms are far apart, we can carry out separate counterfactual reasoning about each arm.

²As a trivial example, if f^i is a function of binary variable V^j , and $\mathcal{L} = \{(s, a) \mid V^j = 0\}$, then $f^{\mathcal{L}, i}$ is not a function of V^j (which is now a constant), and there is no longer an edge from V^j to V^i in $\mathcal{G}^{\mathcal{L}}$.

Leveraging LCMs To see the efficiency therein, consider a general case with global causal model \mathcal{M} . To answer the counterfactual question, “*what might the transition at time t have looked like if component S_t^i had value x instead of value y ?*”, we would ordinarily apply Pearl’s do-calculus to \mathcal{M} to obtain submodel $\mathcal{M}_{\text{do}(S_t^i=x)} = \langle V, U, \mathcal{F}_x \rangle$, where $\mathcal{F}_x = \mathcal{F} \setminus f^i \cup \{S_t^i = x\}$ and incoming edges to S_t^i are removed from $\mathcal{G}_{\text{do}(S_t^i=x)}$ [Pearl, 2009a]. The component distributions at time $t + 1$ can be computed by reevaluating each function f^j that depends on S_t^i . When S_t^i has many children (as is often the case in the global \mathcal{G}), this requires one to estimate outcomes for many structural equations $\{f^j | V^j \in \text{Children}(V_t^i)\}$. But if both the original value of S_t (with $S_t^i = y$) and its new value (with $S_t^i = x$) are in the set \mathcal{L} , the intervention is “within the bounds” of local model $\mathcal{M}^{\mathcal{L}}$ and we can instead work directly with local submodel $\mathcal{M}_{\text{do}(S_t^i=x)}^{\mathcal{L}}$ (defined accordingly). The validity of this follows from the definitions: since $f^{\mathcal{L},j} = f^j|_{\mathcal{L}}$ for all of S_t^i ’s children, the nodes V_t^k for $k \neq i$ at time t are held fixed, and the noise variables at time $t + 1$ are unaffected, the distribution at time $t + 1$ is the same under both models. When S_t^i has fewer children in $\mathcal{M}^{\mathcal{L}}$ than in \mathcal{M} , this reduces the number of structural equations that need to be considered.

4.3.5 A Generic Recipe for Counterfactual Data Augmentation

We hypothesize that local causal models will have several applications, and potentially lead to improved agent designs, algorithms, and interpretability. In this Section we focus on improving off-policy learning in RL by exploiting causal independence in local models for **Counterfactual Data Augmentation (CoDA)**. CoDA augments real data by making counterfactual modifications to a subset of the causal factors at time t , leaving the rest of the factors untouched. Following the logic outlined in the Subsection 4.3.3, this can be understood as manufacturing “fake” data samples using the counterfactual model $\mathcal{M}_{\text{do}(S_t^{i\dots j}=x)}^{\mathcal{L}}$, where we modify the causal factors $S_t^{i\dots j}$ and resample their children. While this is always possible using a model-based approach if we have good models of the structural equations, it is particularly nice when the causal mechanisms are independent, as we can do counterfactual reasoning directly by reusing subsamples from observed trajectories.

Definition. *The causal mechanisms represented by subgraphs $\mathcal{G}_i, \mathcal{G}_j \subset \mathcal{G}$ are **independent** when \mathcal{G}_i and \mathcal{G}_j are disconnected in \mathcal{G} .*

When \mathcal{G} is divisible into two (or more) connected components, we can think of each subgraph as an independent causal mechanism that can be reasoned about separately.

As briefly mentioned in Section 4.3.1, existing data augmentation techniques can be interpreted as specific instances of CoDA (Figure 4.1). For example, goal relabeling [Kaelbling, 1993], as used in Hindsight Experience Replay (HER) [Andrychowicz et al., 2017] and Q-learning for Reward Machines [Icarte et al., 2018], exploits the independence of the goal dynamics $G_t \mapsto G_{t+1}$ (identity map) and the next state dynamics $S_t \times A_t \mapsto S_{t+1}$ in order to relabel the goal variable G_t with a counterfactual goal. While the goal relabeling is done model-free, we typically assume knowledge of the goal-based reward mechanism $G_t \times S_t \times A_t \times S_{t+1} \mapsto R_{t+1}$ to relabel the reward, ultimately mixing model-free and model-based reasoning. Similarly, visual feature augmentation, as used in reinforcement learning from pixels [Kostrikov et al., 2020, Laskin et al., 2020] and sim-to-real transfer [Andrychowicz et al., 2020], exploits the independence of the physical dynamics $S_t^P \times A_t \mapsto S_{t+1}^P$ and visual feature dynamics $S_t^V \mapsto S_{t+1}^V$ such as textures and camera position, assumed to be static ($S_{t+1}^V = S_t^V$), to counterfactually augment visual features. Both goal relabeling and visual data augmentation rely on *global* independence relationships.

Algorithm 2 Mask-based Counterfactual Data Augmentation (CoDA)

function CODA(transition $\mathbf{t}1$, transition $\mathbf{t}2$): $\mathbf{s}1, \mathbf{a}1, \mathbf{s}1' \leftarrow \mathbf{t}1$ $\mathbf{s}2, \mathbf{a}2, \mathbf{s}2' \leftarrow \mathbf{t}2$ $\mathbf{m}1, \mathbf{m}2 \leftarrow \text{MASK}(\mathbf{s}1, \mathbf{a}1), \text{MASK}(\mathbf{s}2, \mathbf{a}2)$ $\mathbf{D}1 \leftarrow \text{COMPONENTS}(\mathbf{m}1)$ $\mathbf{D}2 \leftarrow \text{COMPONENTS}(\mathbf{m}2)$ $\mathbf{d} \leftarrow \text{random sample from } (\mathbf{D}1 \cap \mathbf{D}2)$ $\tilde{\mathbf{s}}, \tilde{\mathbf{a}}, \tilde{\mathbf{s}}' \leftarrow \text{copy}(\mathbf{s}1, \mathbf{a}1, \mathbf{s}1')$ $\tilde{\mathbf{s}}[\mathbf{d}], \tilde{\mathbf{a}}[\mathbf{d}], \tilde{\mathbf{s}}'[\mathbf{d}] \leftarrow \mathbf{s}2[\mathbf{d}], \mathbf{a}2[\mathbf{d}], \mathbf{s}2'[\mathbf{d}]$ $\tilde{\mathbf{D}} \leftarrow \text{COMPONENTS}(\text{MASK}(\tilde{\mathbf{s}}, \tilde{\mathbf{a}}))$ return $(\tilde{\mathbf{s}}, \tilde{\mathbf{a}}, \tilde{\mathbf{s}}')$ if $\mathbf{d} \in \tilde{\mathbf{D}}$ else \emptyset	function MASK(state \mathbf{s} , action \mathbf{a}): Returns $(n+m) \times (n)$ matrix indicating if the n next state components (columns) locally depend on the n state and m action components (rows). function COMPONENTS(mask \mathbf{m}): Using the mask as the adjacency matrix for $\mathcal{G}^{\mathcal{L}}$ (with dummy columns for next action), finds the set of connected components $C = \{C_j\}$, and returns the set of independent components $D = \{\mathcal{G}_i = \bigcup_k C_k^i \mid C^i \subset \text{powerset}(C)\}$.
--	--

We propose a novel form of data augmentation. In particular, we observe that whenever an environment transition is within the bounds of some local model $\mathcal{M}^{\mathcal{L}}$ whose graph $\mathcal{G}^{\mathcal{L}}$ has the locally independent causal mechanism \mathcal{G}_i as a disconnected subgraph (note: \mathcal{G}_i itself need not be connected), that transition contains an unbiased sample from \mathcal{G}_i . Thus, given two transitions in \mathcal{L} , we may mix and match the samples of \mathcal{G}_i to generate counterfactual data, so long as the resulting transitions are themselves in \mathcal{L} .

Remark 4.3.1. *How much data can we generate using our CoDA algorithm? If we have n independent samples from subspace \mathcal{L} whose graph $\mathcal{G}^{\mathcal{L}}$ has m connected components, we have n choices for each of the m components, for a total of n^m CoDA samples—an **exponential** increase in data! One might term this the “blessing of independent subspaces.”*

Remark 4.3.2. *Our discussion has been at the level of a single transition (time slice $(t, t+1)$), which is consistent with the form of data that RL agents typically consume. But we could also use CoDA to mix and match locally independent components over several time steps (see, e.g., Figure 4.2).*

Remark 4.3.3. *As is typical, counterfactual reasoning changes the data distribution. While off-policy agents are typically robust to distributional shift, future work might explore different ways to control or prioritize the counterfactual data distribution [Kumar et al., 2020a, Schaul et al., 2015b]. We note, however, that certain prioritization schemes may introduce selection bias [Hernán and Robins, 2020], effectively entangling otherwise independent causal mechanisms (e.g., HER’s “future” strategy [Andrychowicz et al., 2017] may introduce “hindsight bias” [Lanka and Wu, 2018, Schroecker and Isbell, 2020]).*

Remark 4.3.4. *The global independence relations relied upon by goal relabeling and image augmentation are incredibly general, as evidenced by their wide applicability. We posit that certain local independence relations are similarly general. For example, the physical independence of objects separated by space (the billiards balls of Figure 4.2, the two-armed robot of Figure 4.3, and the environments used in Section 4.3.6), and the independence between an agent’s actions and the truth of (but not belief about) certain facts the agent is ignorant of (e.g., an opponent’s true beliefs).*

Implementing CoDA We implement CoDA, as outlined above and visualized in Figure 4.1(d), as a function of two factual transitions and a mask function $M(s_t, a_t) : \mathcal{S} \times \mathcal{A} \rightarrow \{0, 1\}^{(n+m) \times n}$ that represents the adjacency matrix of the sparsest local causal graph $\mathcal{G}^{\mathcal{L}}$ such that \mathcal{L} is a neighborhood

of (s_t, a_t) .³ We apply M to each transition to obtain local masks \mathfrak{m}_1 and \mathfrak{m}_2 , compute their connected components, and swap independent components \mathcal{G}_i and \mathcal{G}_j (mutually disjoint and collectively exhaustive groups of connected components) between the transitions to produce a counterfactual proposal. We then apply M to the counterfactual $(\tilde{s}_t, \tilde{a}_t)$ to validate the proposal—if the counterfactual mask $\tilde{\mathfrak{m}}$ shares the same graph partitions as \mathfrak{m}_1 and \mathfrak{m}_2 , we accept the proposal as a CoDA sample. See Algorithm 2.

Note that masks \mathfrak{m}_1 , \mathfrak{m}_2 and $\tilde{\mathfrak{m}}$ correspond to different neighborhoods $\mathcal{L}_1, \mathcal{L}_2$ and $\tilde{\mathcal{L}}$, so it is not clear that we are “within the bounds” of any model $\mathcal{M}^{\mathcal{L}}$ as was required in Subsection 4.3.3 for valid counterfactual reasoning. To correct this discrepancy we use the following proposition and additionally require the causal mechanisms (subgraphs) for independent components \mathcal{G}_i and \mathcal{G}_j to share structural equations in each local neighborhood: $f^{\mathcal{L}_1, i} = f^{\mathcal{L}_2, i} = f^{\tilde{\mathcal{L}}, i}$ and $f^{\mathcal{L}_1, j} = f^{\mathcal{L}_2, j} = f^{\tilde{\mathcal{L}}, j}$.⁴ This makes our reasoning valid in the local subspace $\mathcal{L}^* = \mathcal{L}_1 \cup \mathcal{L}_2 \cup \tilde{\mathcal{L}}$. See Appendix C.1 for proof.

Proposition 2. *The causal mechanisms represented by $\mathcal{G}_i, \mathcal{G}_j \subset \mathcal{G}$ are independent in $\mathcal{G}^{\mathcal{L}_1 \cup \mathcal{L}_2}$ if and only if \mathcal{G}_i and \mathcal{G}_j are independent in both $\mathcal{G}^{\mathcal{L}_1}$ and $\mathcal{G}^{\mathcal{L}_2}$, and $f^{\mathcal{L}_1, i} = f^{\mathcal{L}_2, i}, f^{\mathcal{L}_1, j} = f^{\mathcal{L}_2, j}$.*

Since CoDA only modifies data within local subspaces, this biases the resulting replay buffer to have more factorized transitions. In our experiments below, we specify the ratio of observed-to-counterfactual data heuristically to control this selection bias, but find that off-policy agents are reasonably robust to large proportions of CoDA-sampled trajectories. We leave a full characterization of the selection bias in CoDA to future studies, noting that knowledge of graph topology was shown to be useful in mitigating selection bias for causal effect estimation [Bareinboim and Pearl, 2012, Bareinboim et al., 2014].

Inferring local factorization While the ground truth mask function M may be available in rare cases as part of a simulator, the general case either requires a domain expert to specify an approximate causal model (as in goal relabeling and visual data augmentation) or requires the agent to learn the local factorization from data. Given how common independence due to physical separation of objects is, the former option will often be available. In the latter case, we note that the same data could also be used to learn a forward model. Thus, there is an implicit assumption in the latter case that learning the local factorization is easier than modeling the dynamics. We think this assumption is rather mild, as an accurate forward dynamics model would subsume the factorization, and we provide some empirical evidence of its validity in Section 4.3.6.

Learning the local factorization is similar to conditional causal structure discovery [Peters et al., 2017, Runge et al., 2019, Spirtes et al., 2000], conditioned on neighborhood \mathcal{L} of (s_t, a_t) , except that the same structural equations must be applied globally (if the structural equations were conditioned on \mathcal{L} , Proposition 2 would fail). As there are many algorithms for general structure discovery [Runge et al., 2019, Spirtes et al., 2000], and the arrow of time simplifies the inquiry [Granger, 1969, Peters et al., 2017], there may be many ways to approach this problem. In the first of our two experiments we train a single-head set transformer architecture [Lee et al., 2018, Vaswani et al., 2017]. to do next-state prediction, then derive a locally conditioned network mask $M(s_t, a_t)$ as the product of the learned (input-specific) attention masks (see Appendix C.2.1 for details.) The second experiment uses

³If Jacobian $\partial P/\partial x$ exists at $x = (s_t, a_t)$, the ground truth $M(s_t, a_t)$ equals $|(\partial P/\partial x)^T| > 0$.

⁴To see why this is not trivially true, imagine there are two rooms, one of which is icy. In either room the ground conditions are locally independent of movement dynamics, but not so if we consider their union.

Table 4.1: **Batch RL** (10 seeds): Mean success (\pm standard error, estimated using 1000 bootstrap resamples) on **Pong** environment. CoDA with learned masking function more than doubles the effective data size, resulting in a 3x performance boost at smaller data sizes. Note that a 1r:5c Real:CoDA ratio performs slightly worse than a 1r:3c ratio due to distributional shift (Remark 4.3.3).

$ \mathcal{D} $ (1000s)	Real data 1r	MBPO 1r:1M	Ratio of Real:CoDA [:MBPO] data (ours)			
			1r:1c	1r:3c	1r:5c	1r:3c:1M
25	13.2 \pm 0.7	18.5 \pm 1.5	43.8 \pm 2.8	40.9 \pm 2.5	38.4 \pm 4.9	46.8 \pm 3.1
50	22.8 \pm 3.0	36.6 \pm 4.3	66.6 \pm 3.8	64.4 \pm 3.1	62.5 \pm 3.5	70.4 \pm 3.8
75	43.2 \pm 4.9	46.0 \pm 4.7	73.4 \pm 2.8	76.7 \pm 2.6	75.0 \pm 3.4	74.6 \pm 3.2
100	63.0 \pm 3.1	66.4 \pm 4.9	77.8 \pm 2.0	82.7 \pm 1.5	76.6 \pm 3.0	73.7 \pm 2.9
150	77.4 \pm 1.2	72.6 \pm 5.6	82.2 \pm 1.8	85.8 \pm 1.4	84.2 \pm 1.0	79.7 \pm 3.6
250	78.2 \pm 2.7	77.9 \pm 2.4	85.0 \pm 2.9	87.8 \pm 1.8	87.0 \pm 1.0	78.3 \pm 4.9

heuristic LCM that is specified by hand. We expect that CoDA will see an increase in performance an applicability alongside future improvements in (local) causal discovery in dynamic settings.

4.3.6 Experiments

Our experiments evaluate CoDA in the online, batch, and goal-conditioned settings, in each case finding that CoDA significantly improves agent performance as compared to non-CoDA baselines. Since CoDA only modifies an agent’s training data, we expect these improvements to extend to other off-policy task settings in which the state space can be accurately disentangled. Below we outline our experimental design and results, deferring specific details and additional results to Appendix C.2.

Batch RL A natural setting for CoDA is batch-constrained RL, where an agent has access to an existing transition-level dataset, but cannot collect more data via exploration [Fujimoto et al., 2018, Levine et al., 2020]. Another reason why CoDA is attractive in this setting is that there is no *a priori* reason to prefer the given batch data distribution to a counterfactual one. For this experiment we use a continuous control Pong environment based on RoboschoolPong [Klimov and Schulman, 2017]. The agent must hit the ball past the opponent, receiving reward of +1 when the ball is behind the opponent’s paddle, -1 when the ball is behind the agent’s paddle, and 0 otherwise. Since our transformer model performed poorly when used as a dynamics model, our Dyna baseline for batch RL adopts a state-of-the-art architecture [Janner et al., 2019] that employs a 7-model ensemble (MBPO). We collect datasets of up to 250,000 samples from an pre-trained policy with added noise. For each dataset, we train both mask and reward functions (and in case of MBPO, the dynamics model) on the provided data and use them to generate different amounts of counterfactual data. We also consider combining CoDA with MBPO, by first expanding the dataset with MBPO and then

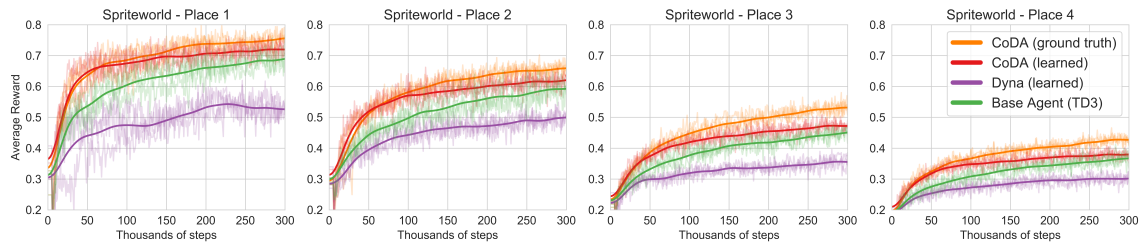
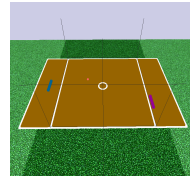


Figure 4.4: **Standard online RL** (3 seeds): CoDA with the ground truth mask always performs the best, validating our basic idea. CoDA with a pre-trained model also offers a significant early boost in sample efficiency and maintains its lead over the base TD3 agent throughout training. Using the same model to generate data directly (a la Dyna [Sutton, 1991]) performs poorly, suggesting significant model bias.

applying CoDA to the result. We train the same TD3 agent on the expanded datasets in batch mode for 500,000 optimization steps. The results in Table 4.1 show that with only 3 state factors (two paddles and ball), applying CoDA is approximately equivalent to doubling the amount of real data.

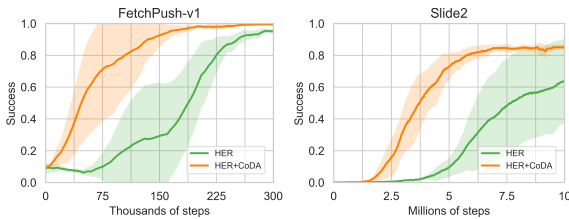
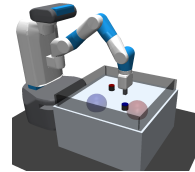


Fig. 4.5: **Goal-conditioned RL** (5 seeds): In **FetchPush** and the challenging **Slide2** environment, a HER agent whose dataset has been enlarged with CoDA approximately doubles the sample efficiency of the base HER agent.

Goal-conditioned RL As HER [Andrychowicz et al., 2017] is an instance of prioritized CoDA that greatly improves sample efficiency in sparse-reward tasks, can our unprioritized CoDA algorithm further improve HER agents? We use HER to relabel goals on real data only, relying on random CoDA-style goal relabeling for CoDA data. After finding that CoDA obtains state-of-the-art results in **FetchPush-v1** [Plappert et al., 2018], we show that CoDA also accelerates learning in a novel and significantly more challenging **Slide2** environment, where the agent must slide two pucks onto their targets (Figure 4.5). For this experiment, we specified a heuristic mask using domain knowledge (“objects are disentangled if more than 10cm apart”) that worked in both **FetchPush** and **Slide2** despite different dynamics.



4.4 Extending the Experience Buffer Using Dynamics Models that Generalize OOD

4.4.1 CoDA as an Implicit Generative Model

CoDA is a process of stitching together sub-trajectories of real experience to generate novel but plausible trajectories, thus amplifying the number of available training data. Stitching together data samples in this way is a form of implicit generative modeling that will interpolate the available training distribution. However, in more challenging settings there may be *zero* support in crucial subspaces of the state-action space. In this case, CoDA is unlikely to address the data coverage issue. This Section describes an extension to CoDA capable of *extrapolating* the training distribution. We do so modeling the transition dynamics explicitly using neural networks, then use object-centric causal priors to sample from a modified model with expanded support.

4.4.2 Motivating Model-based CoDA

Modern reinforcement learning (RL) algorithms have demonstrated remarkable success in several different domains such as games Mnih et al. [2015], Silver et al. [2017] and robotic manipulation Andrychowicz et al. [2020], Kalashnikov et al. [2018]. By repeatedly attempting a single task through trial-and-error, these algorithms can learn to collect useful experience and eventually solve the task of interest. However, designing agents that can generalize in *off-task* and *multi-task* settings remains an open and challenging research question. This is especially true in the offline and zero-shot settings, in which the training data might be unrelated to the target task, and may lack sufficient coverage over possible states.

One way to enable generalization in such cases is through structured representations of states, transition dynamics, or task spaces. These representations can be directly learned, sourced from known or learned abstractions over the state space, or derived from causal knowledge of the world. Symmetries present in such representations enable compositional generalization to new configurations of states or tasks, either by building the structure into the function approximator or algorithm [Goyal et al., 2019, Kipf et al., 2019, Nangue Tasse et al., 2020, Veerapaneni et al., 2020], or by using the structure for data augmentation [Andrychowicz et al., 2017, Laskin et al., 2020, Pitis et al., 2020c].

Here we extend past work on structure-driven data augmentation by using a locally factored model of the transition dynamics to generate counterfactual training distributions. This enables agents to generalize beyond the support of their original training distribution, including to novel tasks where learning the optimal policy requires access to states never seen in the experience buffer. Our key insight is that a learned dynamics model that accurately captures local causal structure (a “locally factored” dynamics model) will predictably exhibit good generalization performance outside the empirical training distribution. We propose Model-based Counterfactual Data Augmentation (MoCoDA), which generates an augmented state-action distribution where its locally factored dynamics model is likely to perform well, then applies its dynamics model to generate new transition data. By training the agent’s policy and value modules on this augmented dataset, they too learn to generalize well out-of-distribution.

4.4.3 Object-centric Models of Transition Dynamics

Sample Complexity of Training a Locally Factored Dynamics Model We now provide an original adaptation of an elementary result from model-based RL to the *locally* factored setting, to show that factorization can exponentially improve sample complexity. We note that several theoretical works have shown that the Factored MDP (FMDP) structure can be exploited to obtain similarly strong sample complexity bounds in the FMDP setting. Our goal here is not to improve upon these results, but to adapt a small part (model-based generalization) to the significantly more general locally factored setting and show that local factorization is enough for (1) *exponential gains in sample complexity* and (2) *out-of-distribution generalization* with respect to the empirical joint, to a set of states and actions that may be exponentially larger than the empirical set. Note that the following discussion applies to tabular RL, but we apply our method to continuous domains.

Notation. We work with finite state and action spaces ($|\mathcal{S}|, |\mathcal{A}| < \infty$) and assume that there are m local subspaces \mathcal{L} of size $|\mathcal{L}|$, such that $m|\mathcal{L}| = |\mathcal{S}||\mathcal{A}|$. For each subspace \mathcal{L} , we assume transitions factor into k causal mechanisms $\{P_i\}$, each with the same number of possible children, $|c_i|$, and the same number of possible parents, $|\text{Pa}_i|$. Note $m\Pi_i|c_i| = |\mathcal{S}|$ (child sets are mutually exclusive) but $m\Pi_i|\text{Pa}_i| \geq |\mathcal{S}||\mathcal{A}|$ (parent sets may overlap).

Theorem 1. *Let n be the number of empirical samples used to train the model of each local causal mechanism, $P_{i,\theta}^{\mathcal{L}}$ at each configuration of parents $\text{Pa}_i = x$. There exists constant c such that, if*

$$n \geq \frac{ck^2|c_i|\log(|\mathcal{S}||\mathcal{A}|/\delta)}{\epsilon^2},$$

then, with probability at least $1 - \delta$, we have:

$$\max_{(s,a)} \|P(s,a) - P_\theta(s,a)\|_1 \leq \epsilon.$$

Sketch of Proof. We apply a concentration inequality to bound the ℓ_1 error for fixed parents and extend this to a bound on the ℓ_1 error for a fixed (s, a) pair. The conclusion follows by a union bound across all states and actions. See Appendix C.3 for details. \square

To compare to full-state dynamics modeling, we can translate the sample complexity from the per-parent count n to a total count N . Recall $m\Pi_i|c_i| = |\mathcal{S}|$, so that $|c_i| = (|\mathcal{S}|/m)^{1/k}$, and $m\Pi_i|\text{Pa}_i| \geq |\mathcal{S}||\mathcal{A}|$. We assume a small constant overlap factor $v \geq 1$, so that $|\text{Pa}_i| = v(|\mathcal{S}||\mathcal{A}|/m)^{1/k}$. We need the total number of component visits to be $n|\text{Pa}_i|km$, for a total of $nv(|\mathcal{S}||\mathcal{A}|/m)^{1/k}m$ state-action visits, assuming that parent set visits are allocated evenly, and noting that each state-action visit provides k parent set visits. This gives:

Corollary 1. *To bound the error as above, we need to have*

$$N \geq \frac{cmk^2(|\mathcal{S}|^2|\mathcal{A}|/m^2)^{1/k} \log(|\mathcal{S}||\mathcal{A}|/\delta)}{\epsilon^2},$$

total train samples, where we have absorbed the overlap factor v into constant c .

Comparing this to the analogous bound for full-state model learning (Agarwal et al. [2019], Prop. 2.1):

$$N \geq \frac{c|\mathcal{S}|^2|\mathcal{A}| \log(|\mathcal{S}||\mathcal{A}|/\delta)}{\epsilon^2},$$

we see that we have gone from super-linear $O(|\mathcal{S}|^2|\mathcal{A}| \log(|\mathcal{S}||\mathcal{A}|))$ sample complexity in terms of $|\mathcal{S}||\mathcal{A}|$, to the exponentially smaller $O(mk^2(|\mathcal{S}|^2|\mathcal{A}|/m^2)^{1/k} \log(|\mathcal{S}||\mathcal{A}|))$.

This result implies that *for large enough $|\mathcal{S}||\mathcal{A}|$ our model must generalize to unseen states and actions*, since the number of samples needed (N) is exponentially smaller than the size of the state-action space ($|\mathcal{S}||\mathcal{A}|$). In contrast, if it did not, then sample complexity would be $\Omega(|\mathcal{S}||\mathcal{A}|)$.

Remark 4.4.1. *The global factorization property of FMDPs is a strict assumption that rarely holds in reality. Although local factorization is broadly applicable and significantly more realistic than the FMDP setting, it is not without cost. In FMDPs, we have a single subspace ($m = 1$). In the locally factored case, the number of subspaces m is likely to grow exponentially with the number of factors k , as there are exponentially many ways that k factors can interact. To be more precise, there are $k2^k$ possible bipartite graphs from k nodes to k nodes. Nevertheless, by comparing bases ($2 \ll |\mathcal{S}||\mathcal{A}|$), we see that we still obtain exponential gains in sample complexity from the locally factored approach.*

Training Value Functions and Policies for Out-of-Distribution Generalization In the previous subsection, we saw that a locally factored dynamics model provably generalizes outside of the empirical joint distribution. A natural question is whether such *local factorization can be leveraged to obtain similar results for value functions and policies?*

We will show that the answer is *yes*, but perhaps counter-intuitively, it is not achieved by directly training the value function and policy on the empirical distribution, as is the case for the dynamics model. The difference arises because learned value functions, and consequently learned policies, involve the long horizon prediction $\mathbb{E}_{P,\pi} \sum_{t=0}^{\infty} \gamma^t r(s_t, a_t)$, which may not benefit from the local sparsity of $\mathcal{G}^{\mathcal{L}}$. When compounded over time, sparse local structures can quickly produce an entangled long horizon structure (cf. the “butterfly effect”). Intuitively, even if several pool balls are

far apart and locally disentangled, future collisions are central to planning and the optimal policy depends on the relative positions of all balls. This applies even if rewards are factored (e.g., rewards in most pool variants) [Sodhani et al., 2022].

We note that, although temporal entanglement may be exponential in the branching factor of the unrolled causal graph, it’s possible for the long horizon structure to stay sparse (e.g., k independent factors that never interact, or long-horizon disentanglement between decision relevant and decision irrelevant variables [Huang et al., 2022]). It’s also possible that other regularities in the data will allow for good out-of-distribution generalization. Thus, we cannot claim that value functions and policies will never generalize well out-of-distribution (see Veerapaneni et al. [2020] for an example when they do). Nevertheless, we hypothesize that exponentially fast entanglement does occur in complex natural systems, making direct generalization of long horizon predictions difficult.

Out-of-distribution generalization of the policy and value function can be achieved, however, by leveraging the generalization properties of a locally factored dynamics model. We propose to do this by generating out-of-distribution states and actions (the “parent distribution”), and then applying our learned dynamics model to generate transitions that are used to train the policy and value function. We call this process Model-based Counterfactual Data Augmentation (MoCoDA).

4.4.4 Model-based CoDA Using Neural Networks

In the previous section, we discussed how locally factored dynamics model can generalize beyond the empirical dataset to provide accurate predictions on an augmented state-action distribution we call the “parent distribution”. We now seek to leverage this out-of-distribution generalization in the dynamics model to bootstrap the training of an RL agent. Our approach is to control the agent’s training distribution $P(s, a, s')$ via the locally factored dynamics $P_\phi(s'|s, a)$ and the parent distribution $P_\theta(s, a)$ (both trained using experience data). This allows us to sample *augmented* transitions (perhaps unseen in the experience data) for consumption by a downstream RL agent. We call this framework MoCoDA, and summarize it using the following three-step process:

- Step 1** Given known parent sets, generate appropriate parent distribution $P_\theta(s, a)$.
- Step 2** Apply a learned dynamics model $P_\phi(s'|s, a)$ to parent distribution to generate “augmented dataset” of transitions (s, a, s') .
- Step 3** Use augmented dataset $s, a, s' \sim P_\theta P_\phi$ (alongside experience data, if desired) to train an off-policy RL agent on the (perhaps novel) target task.

Figure 4.6 illustrates this framework in a block diagram. An instance of MoCoDA is realized by specific choices at each step. For example, the original CoDA method [Pitis et al., 2020c] is an instance of MoCoDA, which (1) generates the parent distribution by uniformly swapping non-overlapping parent sets, and (2) uses subsamples of empirical transitions as a locally factored dynamics model. CoDA works when local graphs have non-overlapping parent sets, but it does not allow for control over the parent distribution and does not work in cases where parent sets overlap. MoCoDA generalizes CoDA, alleviating these restrictions and allowing for significantly more design choices, discussed next.

4.4.5 Generating the Parent Distribution

What parent distribution (Step 1) should be used to generate the augmented dataset? We describe some options below, noting that our proposals (MOCODA, MOCODA-U, MOCODA-P) rely on knowledge of (possibly local) parent sets—i.e., they require the state to be decomposed into objects.

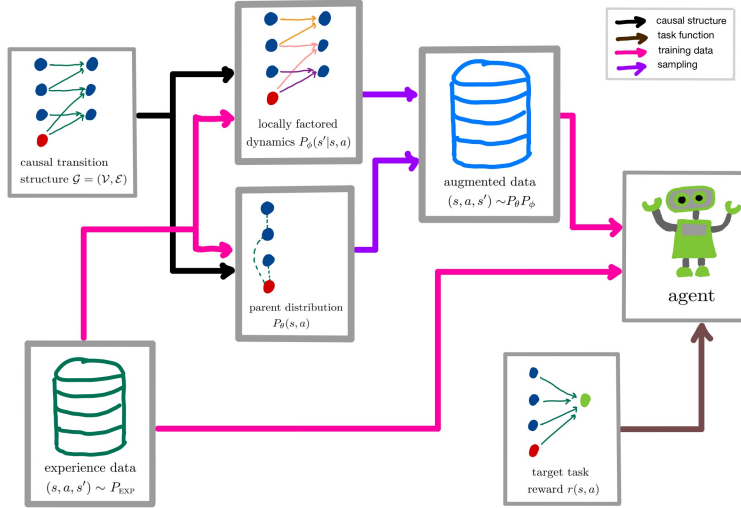


Figure 4.6: **Training an RL Agent with MoCoDA:** We use the empirical dataset to train parent distribution model, $P_\theta(s, a)$ and locally factored dynamics model $P_\phi(s'|s, a)$, both informed by the local structure. The dynamics model is applied to the parent distribution to produce augmented dataset $P_\theta P_\phi$. The augmented & empirical datasets are labeled with the target task reward, $r(s, a)$ and fed into the RL algorithm as training data.

Baseline Distributions. If we restrict ourselves to states and actions in the empirical dataset (**EMP**) or short-horizon rollouts that start in the empirical state-action distribution (**DYNA**), as is typical in Dyna-style approaches [Janner et al., 2019, Sutton and Barto, 2018], we limit ourselves to a small neighborhood of the empirical state-action distribution. This forgoes the opportunity to train our off-policy RL agent on out-of-distribution data that may be necessary for learning the target task.

Another option is to sample random state-actions from $\mathcal{S} \times \mathcal{A}$ (**RAND**). While this provides coverage of all state-actions relevant to the target task, there is no guarantee that our locally factorized model generalizes well in RAND. The proof of Theorem 1 shows that our model only generalizes well to a particular (s, a) if each component generalizes well on the configurations of each parent set in that (s, a) . In context of Theorem 1, this occurs only if the empirical data used to train our model contained at least n samples for each set of parents in (s, a) . This suggests focusing on data whose parent sets have sufficient support in the empirical dataset.

The MOCODA distribution. We do this by constraining the marginal distribution of each parent set (within local neighborhood \mathcal{L}) in the augmented distribution to match the corresponding marginal in the empirical dataset. As there are many such distributions, in absence of additional information, it is sensible to choose the one with maximum entropy [Jaynes, 1957]. We call this maximum entropy, marginal matching distribution the **MOCODA** augmented distribution. We propose an efficient way to generate the MOCODA distribution using a set of Gaussian Mixture Models, one for each parent set distribution. We sample parent sets one at a time, conditioning on any previous partial samples due to overlap between parent sets. This process is detailed in Appendix C.4.

Weaknesses of the MOCODA distribution. Although our locally factored dynamics model is likely to generalize well on MOCODA, there are a few reasons why training our RL agent on MOCODA in Step 3 may yield poor results. First, if there are empirical imbalances within parent sets (some parent configurations more common than others), these imbalances will appear in MOCODA.

Moreover, multiple such imbalances will compound exponentially, so that (s, a) tuples with rare parent combinations will be extremely rare in MOCODA, even if the model generalizes well to them. Second, $\text{Support}(\text{MOCODA})$ may be so large that it makes training the RL algorithm in Step 3 inefficient. Finally, the cost function used in RL algorithms is typically an expectation over the training distribution, and optimizing the agent in irrelevant areas of the state-action space may hurt performance. The above limitations suggest that rebalancing MOCODA might improve results.

MOCODA-U and MOCODA-P. To mitigate the first weakness of MOCODA we might skew MOCODA toward the uniform distribution over its support, $\mathcal{U}(\text{Support}(\text{MOCODA}))$. Although this is possible to implement using rejection sampling when k is small, exponential imbalance makes it impractical when k is large. A more efficient implementation reweights the GMM components used in our MOCODA sampler. We call this approach (regardless of implementation) **MOCODA-U**. To mitigate the second and third weaknesses of MOCODA, we need additional knowledge about the target task—e.g., domain knowledge or expert trajectories. We can use such information to define a prioritized parent distribution **MOCODA-P** with support in $\text{Support}(\text{MOCODA})$, which can also be obtained via rejection sampling (perhaps on MOCODA-U to also relieve the initial imbalance).

4.4.6 The Choice of Dynamics Model and RL Algorithm

Once we have a parent distribution, $P_\theta(s, a)$, we generate our augmented dataset by applying dynamics model $P_\phi(s' | s, a)$. The natural choice in light of the discussion in Section 4.4.3 is a locally factored model. This requires knowledge of the local factorization, which is more involved than the parent set knowledge used to generate the MOCODA distribution and its reweighted variants. We note, however, that a locally factored model may not be strictly necessary for MoCoDA, so long as the underlying dynamics are factored. Although unfactored models do not perform well in our experiments, we hypothesize that a good model with enough in-distribution data and the right regularization might learn to implicitly respect the local factorization. The choice of model architecture is not core to our work, and we leave exploration of this possibility to future work.

Masked Dynamics Model. In our experiments, we assume access to a mask function $M : \mathcal{S} \times \mathcal{A} \rightarrow \{0, 1\}^{(|\mathcal{S}|+|\mathcal{A}|) \times |\mathcal{S}|}$ (perhaps learned [Kipf et al., 2018, Pitis et al., 2020c]), which maps states and actions to the adjacency map of the local graph $\mathcal{G}^\mathcal{L}$. Given this mask function, we design a dynamics model P_ϕ that accepts $M(s, a)$ as an additional input and respects the causal relations in the mask (i.e., mutual information $I(X_t^i; X_{t+1}^j | (S_t, A_t) \setminus X_t^i) = 0$ if $M(s_t, a_t)_{ij} = 0$). There are many architectures that enforce this constraint. In our experiments we opt for a simple one, which first embeds each of the k parent sets: $f = [f_i(\text{Pa}_i)]_{i=1}^k$, and then computes the j -th child as a function of the sum of the masked embeddings, $g_j(M(s, a)_{\cdot, j} \cdot f)$. See Appendix C.4 for further implementation details.

The RL Algorithm. After generating an augmented dataset by applying our dynamics model to the augmented distribution, we label the data with our target task reward and use the result to train an RL agent. MoCoDA works with a wide range of algorithms, and the choice of algorithm will depend on the task setting. For example, our experiments are done in an offline setup, where the agent is given a buffer of empirical data, with no opportunity to explore. For this reason, it makes sense to use offline RL algorithms, as this setting has proven challenging for standard online algorithms [Levine et al., 2020].

Remark 4.4.2. *The rationales for (1) regularizing the policy toward the empirical distribution in*

offline RL algorithms, and (2) training on the MOCODA distribution, are compatible: in each case, we want to restrict ourselves to state-actions where our models generalize well. By using MOCODA we expand this set beyond the empirical distribution. Thus, when we apply offline RL algorithms in our experiments, we train their offline component (e.g., the action sampler in BCQ [Fujimoto et al., 2019] or the BC constraint in TD3-BC [Fujimoto and Gu, 2021]) on the expanded MOCODA training distribution.

4.4.7 Experiments

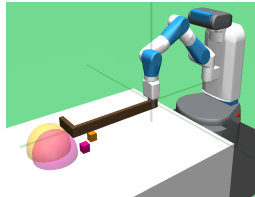
Hypotheses Our experiments are aimed at finding support for two critical hypotheses:

- H1** Dynamics models, especially ones sensitive to the local factorization, are able to generalize well in the MOCODA distribution.
- H2** This out-of-distribution generalization can be leveraged via data augmentation to train an RL agent to solve out-of-distribution tasks.

Note that support for **H2** provides implicit support for **H1**.

Domains We test MoCoDA on two continuous control domains. First is a simple, but controlled, 2D **Navigation** domain, where the agent must travel from one point in a square arena to another. States are 2D (x, y) coordinates and actions are 2D $(\Delta x, \Delta y)$ vectors. In most of the state space, the sub-actions Δx and Δy affect only their respective coordinate. In the top right quadrant, however, the Δx and Δy sub-actions each affect *both* x and y coordinates, so that the environment is locally factored. The agent has access to empirical training data consisting of left-to-right and bottom-to-top trajectories that are restricted to a \lrcorner shape of the state space (see the EMP distribution in Figure 4.7). We consider a target task where the agent must move from the bottom left to the top right. In this task there is sufficient empirical data to solve the task by following the \lrcorner shape of the data, but learning the optimal policy of going directly via the diagonal requires out-of-distribution generalization.

Second, we test MoCoDA in a challenging **HookSweep2** robotics domain based on Hook-Sweep [Kurenkov et al., 2020], in which a Fetch robot must use a long hook to sweep two boxes to one side of the table (either toward or away from the agent). The boxes are initialized near the center of the table, and the empirical data contains trajectories of the agent sweeping exactly one box to one side of the table, leaving the other in the center. The target task requires the agent to generalize to states that it has never seen before (both boxes together on one side of the table). This is particularly challenging because the setup is entirely offline (no exploration), where poor out-of-distribution generalization typically requires special offline RL algorithms that constrain the agent’s policy to the empirical distribution [Agarwal et al., 2020, Fujimoto and Gu, 2021, Kumar et al., 2020b, Levine et al., 2020].



Directly comparing model generalization error. In the 2D **Navigation** domain we have access to the ground truth dynamics, which allows us to directly compare generalization error on variety of distributions, visualized in Figure 4.7. We compare three different model architectures: unfactored, globally factored (assuming that the $(x, \Delta x)$ and $(y, \Delta y)$ causal mechanisms are independent everywhere, which is not true in the top right quadrant), and locally factored. The models are each trained on a empirical dataset of 35000 transitions for up to 600 epochs, which is

Table 4.2: **2D Navigation Dynamics Modeling Results:** Mean squared error \pm std. dev. over 5 seeds, scaled by $1e2$ for clarity (best model boldfaced). The locally factored model experienced less performance degradation out-of-distribution, and performed better on all distributions, except for the empirical distribution (EMP) itself.

Model Architecture	Generalization Error (MSE $\times 1e2$) (lower is better)				
	EMP	DYNA	RAND	MoCoDA	MoCoDA-U
Not Factored	0.14 \pm 0.04	2.41 \pm 0.29	4.4 \pm 0.31	0.95 \pm 0.06	1.29 \pm 0.15
Globally Factored	0.36 \pm 0.01	2.09 \pm 0.28	3.17 \pm 0.3	0.41 \pm 0.02	0.51 \pm 0.02
Locally Factored	0.23 \pm 0.1	1.47 \pm 0.27	2.03 \pm 0.19	0.33 \pm 0.11	0.46 \pm 0.11

Table 4.3: **2D Navigation Offline RL Results:** Average steps to completion \pm std. dev. over 5 seeds for various RL algorithms (best distribution in each row boldfaced), where average steps was computed over the last 50 training epochs. Training on MOCODA and MOCODA-U improved performance in all cases. Interestingly, even using RAND improves performance, indicating the importance of training on out-of-distribution data. Note that this is an offline RL task, and so SAC (an algorithm designed for online RL) is not expected to perform well.

RL Algorithm	Average Steps to Completion (lower is better)				
	EMP	RAND	MoCoDA	MoCoDA-U	CoDA [Pitis et al., 2020c]
SAC (online RL)	53.1 \pm 9.8	27.6 \pm 1.1	38.8 \pm 18.3	41.3 \pm 17.7	35.1 \pm 18.1
BCQ	58.5 \pm 10.1	31.7 \pm 2.4	22.8 \pm 0.4	24.8 \pm 4.2	25.0 \pm 0.4
CQL	45.8 \pm 4.0	27.6 \pm 1.3	22.8 \pm 0.2	22.7 \pm 0.3	23.6 \pm 0.5
TD3-BC	40.0 \pm 16.1	26.1 \pm 0.8	21.0 \pm 0.7	20.7 \pm 0.8	21.4 \pm 0.6

early stopped using a validation set of 5000 transitions. The results are shown in Table 4.2. We find strong support for **H1**: even given the simple dynamics of 2d Navigation, it is clear that the locally factored model is able to generalize better than a fully connected model, particularly on the MOCODA distribution, where performance degradation is minimal. We note that the DYNA distribution was formed by starting in EMP and doing 5-step rollouts with *random* actions. The random actions produce out-of-distribution data to which no model (not even the locally factored model) can generalize well to.

Solving out-of-distribution tasks. We apply the trained dynamics models to several

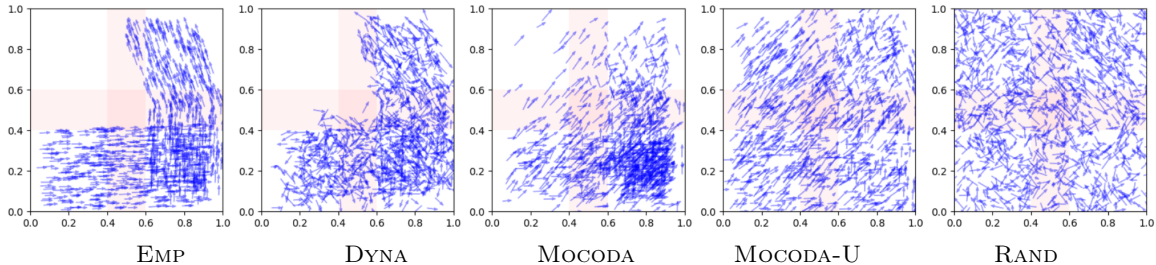


Figure 4.7: **2D Navigation Visualization.** (Best viewed with 2x zoom) Blue arrows represent transition samples as a vector from (x_t, y_t) to (x_{t+1}, y_{t+1}) . Shaded red areas mark the edges of the initial states of empirical trajectories and the center of the square. We see that 5-step rollouts (DYNA) do not fill in the center (needed for optimal policy), and fail to constrain actions to those that the model generalizes well on. For MOCODA, we see the effect of compounding dataset imbalance discussed in Subsection 4.4.5, which is resolved by MOCODA-U.

Figure 4.8: **HookSweep2 Visualization:** Stylized visualization of the distributions EMP (left), MOCODA (center), and MOCODA-P (right). Each figure can be understood as a top down view of the table, where a point is a plotted if the two blocks are close together on the table. The distribution EMP does not overlap with the green goal areas on the left and right, and so the agent is unable to learn. In the MOCODA distribution, the agent gets some success examples. In the MOCODA-P distribution, state-actions are reweighted so that the joint distribution of the two block positions is approximately uniform, leading to more evenly distributed coverage of the table.

Table 4.4: **HookSweep2 Offline RL Results:** Average success percentage (\pm std. dev. over 3 seeds), where the average was computed over the last 50 training epochs. SAC and CQL (omitted) were unsuccessful with all datasets. We see that MOCODA was necessary for learning, and that results improve drastically with MOCODA-P, which re-balances MOCODA toward a uniform distribution in the box coordinates (see Figure 4.8). Additionally, we show results from an ablation, which generates the MoCoDA datasets using a fully connected dynamics model. While this still achieves some success, it demonstrates that using a locally-factored model is important for OOD generalization. In this case the more OOD MoCoDA-P distribution does not help, suggesting that the fully connected model is failing to produce useful OOD transitions.

RLAlgorithm	Average Success Rate (higher is better)				
	EMP	MoCoDA	MoCoDA-P	MoCoDA (not factored)	MoCoDA-P (not factored)
BCQ	2.0 \pm 1.6	20.7 \pm 4.1	64.7 \pm 4.1	14.0 \pm 3.3	15.3 \pm 4.1
TD3-BC	0.7 \pm 0.9	38.7 \pm 7.5	84.0 \pm 2.8	29.3 \pm 3.8	26.0 \pm 1.6

base distributions and compare the performance of RL agents trained on each dataset. To ensure improvements are due to the augmented dataset and not agent architecture, we train several different algorithms, including: SAC [Haarnoja et al., 2018], BCQ [Fujimoto et al., 2019] (with DDPG [Lillicrap et al., 2015]), CQL [Kumar et al., 2020b] and TD3-BC [Fujimoto and Gu, 2021].

The results on 2D Navigation are shown in Table 4.3. We see that for all algorithms, the use of the MOCODA and MOCODA-U augmented datasets greatly improve the average step count, providing support for **H2** and suggesting that using these datasets allows the agents to learn to traverse the diagonal of the state space, even though it is out-of-distribution with respect to EMP. This is consistent with a qualitative assessment of the learned policies, which confirms that agents trained on the \perp -shaped EMP distribution learn a \perp -shaped policy, whereas agents trained on MOCODA and MOCODA-U learn the optimal (diagonal) policy.

The results on the more complex HookSweep2 environment, shown in Table 4.4, provide further support for **H2**. On this environment, only results for BCQ and TD3-BC are shown, as the other algorithms failed on all datasets. For HookSweep2 we used a prioritized MOCODA-P parent distribution, as follows: knowing that the target task involves placing two blocks, we applied rejection sampling to MOCODA to make the marginal distribution of the joint block positions approximately uniform over its support. The effect is to have good representation in all areas of the most important state features for the target task (the block positions). The visualization in Figure 4.8 makes clear why training on MOCODA or MOCODA-P was necessary in order to solve this task: the base EMP distribution simply does not have sufficient coverage of the goal space.

4.5 Related Work

Exploiting structure in MDPs Factored MDPs [Guestrin et al., 2003, Hallak et al., 2015, Weber et al., 2019] consider MDPs where state variables are only influenced by a fixed subset of “parent” variables at the previous timestep. The notion of “context specific independence” (CSI), which was used to compactly represent single factors of a Bayes net [Boutilier et al., 2013] or MDP [Boutilier et al., 1995] for efficient inference and model storage,⁵ is closely related to the local factorizations we study in this Section. CSI can be understood as going one step beyond CoDA, exploiting not only knowledge of the local factorization, but also the structural equations at play in the local factorization; CSI could be leveraged for model-based RL approaches where faithful models of factored dynamics can be realized. Object-oriented and relational approaches to RL and prediction [Diuk et al., 2008, Goyal et al., 2019, Kipf et al., 2019, Li et al., 2019, Zambaldi et al., 2018, Zhu et al., 2018] represent the dynamics as a set of interacting entities. Factored actions and policies have been used to formulate dimension-wise policy gradient baselines in standard and multi-agent settings [Foerster et al., 2018, Lowe et al., 2017, Wu et al., 2018].

Causality and RL A growing body of work applies causal reasoning the RL setting to improve sample efficiency, interpretability and learn better representations [Lu et al., 2018, Madumal et al., 2019, Rezende et al., 2020]. Particularly relevant is the work by Buesing et al. [2019], which improves sample efficiency by using a causal model to sample counterfactual trajectories, thereby reducing variance of off-policy gradient estimates in a guided policy search framework. These counterfactuals use coarse-grained representations at the trajectory level, while our approach uses factored representations within a single transition. Batch RL [Fujimoto et al., 2018, Levine et al., 2020, Mandel et al., 2014] and more generally off-policy RL [Munos et al., 2016, Watkins and Dayan, 1992] are counterfactual by nature, and are particularly important when it is costly or dangerous to obtain on-policy data [Thomas and Brunskill, 2016]. The use of counterfactual goals to accelerate learning goal-conditioned RL [Kaelbling, 1993, Plappert et al., 2018, Schaul et al., 2015a] is what inspired our local CoDA algorithm.

4.6 Discussion

This Chapter presented some promising initial results within the CoDA framework. Areas for future work include improved methods for learning LCM structure directly from data, which is closely related to causal structure discovery [Ke et al., 2020, Seitzer et al., 2021]. CoDA has so far only been applied to fully observed MDP where s informs the agent which objects are in the scene as well as the relevant state observations for each. Scaling up CoDA so that it can handle images would be a valuable extension, and some recent work on object-centric representation learning [Wu et al., 2023] could be helpful in this endeavor.

At the time of writing, commercial interest in generative models is waxing, mostly due to recent improvements to the fidelity of text and image sampling [Brown et al., 2020, Ho et al., 2020, Ouyang et al., 2022, Radford et al., 2021]. This Chapter provides a complementary view on the benefits of generative models. As discussed in Section 4.4.1 CoDA and MoCoDA are generative models (implicit and explicit, respectively) that function as an auxiliary module to help a different type of learning

⁵Note that these methods were proposed to efficiently encode conditional probability tables at the graph nodes, requiring that all variables considered be discrete; CoDA on the other hand works in continuous tasks.

algorithm (an RL agent, in this case). When turning our focus to other types of machine learning such as classification with fairness [Denton et al., 2019, Zhang and Sang, 2020] or explainability [Chang et al., 2019] requirements, we can likewise see the benefit of an indirect application of generative models. We expect methods like MoCoDA (which, unlike CoDA, relies on explicit generative modeling) to get better over time as high-quality generative models of RL environments become more widely available. Some preliminary success in applying diffusion models to augment RL datasets has already been realized [Yu et al., 2023].

The CoDA framework for causally-grounded data augmentation was developed for RL, but in other domains where data coverage is a concern—recommender systems, fair prediction, and robust learning, for example—CoDA could also be applied. Part of the reason for working in RL first is that the forward progression of time makes the question of causal discovery much easier. Prior work has shown the merit of using SCMs [Pearl, 2009a] to model causal processes in dynamic fairness settings [Creager et al., 2020]. However, there are some noteworthy objections to the use of causal graphs to model sociotechnical processes. Firstly, demographic group membership does not represent a truly manipulable variable, which calls into questions whether it is possible to meaningfully (statistically) reason about “interventions” on attributes like sex or race [Greiner and Rubin, 2011, Kohler-Hausmann, 2019]. Secondly, sociotechnical systems are incredibly sophisticated and nuanced. Computer scientists may be ill-equipped to model them at the whiteboard using simple graphs [Hu and Kohler-Hausmann, 2020, Kasirzadeh and Smart, 2021]. We remain optimistic about the potential to apply CoDA more broadly, but remind researchers that causal priors are typically untestable. We found in our experiments that CoDA was relatively insensitive to mis-specification of the LCM, but in high-stakes decision-making settings such observations may not hold.

Chapter 5

Conclusion

5.1 Summary: All Data are Imperfect Data

A favored mantra among statisticians is that “*all models are wrong (but some are useful)*” [Box, 1976, 1979]. This can be repeated periodically (or during times of scientific-spiritual turmoil!) as a helpful reminder that the modeler’s assumptions (made explicitly or otherwise) are inherited by any inferences made using the model. The less realistic the assumptions, the less bearing the resulting inferences have on reality. In other words, your mileage may vary.

We framed this thesis at the outset by describing ML as a process of turning data into computer programs (models). To continue along this theme, we will conclude by humbly offering an additional mantra: “*all data are imperfect (full stop)*”. While this is admittedly a weaker statement—“imperfections” being perhaps easier to recover from than “wrongness”, while “usefulness” is entirely left out of the equation—it is no less informative. It can help us to understand *why* ML models fail in unexpected ways: learning algorithms compound data imperfections by producing wrong models. The only perfect data are synthetic data. But this is the exception that proves the rule, as synthetic data are typically used to demonstrate proof-of-concept for a newly proposed method, and do not reflect what we expect to see in the real world. Yes, machine learning is a practice of data-driven—and thus, by definition, evidence-based—decision making. But we should not conclude that it provides a detached “view from nowhere” [D’ignazio and Klein, 2020, Haraway, 1988] from which *impartial* decisions can be automated. Rather, ML researchers and practitioners regularly make assumptions (explicitly or otherwise) about how data is generated and measured [Birhane et al., 2022, Paullada et al., 2021, Scheuerman et al., 2021], and these assumptions are inherited by any models trained on the data.

This new mantra also suggests that the aspiration of *Robust ML* is in fact a process rather than a destination. Not only are available training data imperfect, but so too are datasets used for evaluation. The process of building reliable models should be an adaptive one, where data imperfections are identified and addressed in perpetuity, with the overall effort keeping the wrongness of the downstream models in reasonable check (and hopefully shrinking over time).

This manuscript has discussed several approaches to addressing data imperfections, which may be of use in the process of robust machine learning. To some extent, detecting data imperfections may be possible to automate using machine learning (Chapter 3). However, useful auxiliary labels pertinent to model failure (Chapter 2) and human-specified prior knowledge (Chapter 4) are nevertheless key

components within this process.

5.2 What is Next?

In each of the preceding Chapters, the proposal of new methods to address data imperfections was punctuated by a brief discussion Section, which suggested some ideas for immediate extension of these ideas. For the remainder of this manuscript, we set aside short-term directions for future research and turn to the question of what lies further ahead. Our final discussion is thus more speculative, but it also provides a vantage with which to assess some broader dynamics within the field. We begin by outlining several contradictions characteristic of the contemporary state of ML research.

5.2.1 Some Contradictions Within Contemporary Machine Learning

New ML methods have developed at a staggering pace in recent years. And yet, it is difficult to identify a north star, or single unifying goal, guiding the research field towards a specific direction. How should we make sense of a scientific field that moves quickly, but with no apparent direction or purpose? In order to add some detail (and hopefully shed some light on the situation) let us begin by unpacking this initial paradox, and listing some follow-on contradictions within the field. Unlike the self-evident mantra discussed earlier, these observations act more like *koans*: self-refuting propositions that are nevertheless grounded in apparent truth. To be clear, it is extremely unlikely that these contradictions will be resolved by research activity alone. However, we hope that their recitation would serve as a murmur of background incoherence that drowns out the loudest and seemingly most urgent research questions—Which prompt to choose? How to string together APIs to “solve” benchmark tasks?—and allows us to formulate a more daring research agenda that will change the shape of the field in the long run.

- **Is this a scientific or engineering discipline?** Research concerning the social impacts of ML has recently been institutionalized, with teams devoted to “AI Ethics”, “Technology and Society”, and “Human Centered AI” proliferating in academic and corporate spheres.¹

When reflecting on the research output from these communities in the past five years, a strong argument can be made that the most impactful projects were those advocating for the adoption of systematic design protocols such as “datasheets” [Gebru et al., 2021] and “model cards” [Mitchell et al., 2019]. In other words, moving AI and ML research from a scientific endeavor to an engineering discipline is seen by many as an important step towards characterizing existing harms, and preventing future ones. Meanwhile, the pressure to commercialize emerging research can be felt most acutely in precisely those specific research subfields (e.g. adapting generative models for use as chatbots or text-to-image samplers) that are most technically challenging to characterize. Thus, we arrive at the following contradiction:

As we move to systematize our field, the object of our focus becomes more difficult to systematize.

- **Reproducibility crises** In spite of recent progress in ML research, individual results from the literature can be difficult to reproduce [Haibe-Kains et al., 2020, ?]. This could be interpreted as just one example of a broader crisis of reproducibility in the sciences. However, certain

¹Admittedly this is more of a re-organization than an institutionalization, given that these new teams typically constitute researchers with participatory some previous institutional credential (or new trainees). The failure to include stakeholders from outside institutions in the design of new technology is indeed a known and pressing issue [Abdurahman, 2019, Kulynych et al., 2020].

aspects of ML methodology exacerbate this tendency. The fast pace of the field intensifies the publish-or-perish mentality. Coupled with a benchmark culture that highly values empirical performance as a measure of scientific validity [Raji et al., 2021], this can create incentives for researchers to take shortcuts. For ML results to be legitimate, careful care must be taken to keep evaluation data out of the training process. Because ML is being applied broadly to a variety of scientific disciplines, a practical failure to adhere to these protocols can artificially inflate the numbers. To make matters worse, large firms have become less forthcoming in their recent technical notes and public papers, apparently due to a heightened sense of competition surrounding the emergent market for generative models. This makes models difficult to reproduce independently, and raises whether some of ML’s recent empirical successes—such as scoring highly on standardized testing primarily through language modeling—could be due to leakage of the test data into the training set [Narayanan and Kapoor, 2023]. Thus, we arrive at the following contradiction:

Machine learning’s crescendo of relevance in (economic and cultural) production is accompanied by a diminished capacity for (scientific) reproduction.

- **Double underspecification** Many prediction problems are underspecified in the sense that they admit a plurality of solutions of equal “quality” according to the training objective [D’Amour et al., 2020, Fisher et al., 2019] The learning algorithm, if trained to convergence, could choose any of these solutions; moreover, it is not obvious which one it *should* choose in light of the fact that they may have very different behaviors under distribution shift. This observation, coupled with legal and regulatory concerns surrounding deployment (e.g. algorithmic discrimination) have motivated research on how to learn models that satisfy additional requirements: we search for ML *with* fairness (or explainability, privacy, safety etc.) added on. One might hope that additional requirements would further constrain the solution space and mitigate the underspecification issue. However, these requirements are themselves often underspecified: what it means for an algorithm to be “fair” or “explainable” is fundamentally contested. We find ourselves in a sticky situation, attempting to solve learning problems that are *doubly underspecified*, both at the technical and conceptual level. Thus, we arrive at the following contradiction:

Resolving an underspecification in machine terms necessitates introducing an underspecification in human terms.

- **Organizing research subfields by adjectives.** Aside from the underspecification issue, there are many reasons to seek models that do *more* than just predict accurately. Indeed, many ML researchers are committed to working towards ensuring that emerging technologies are socially beneficial. We tend to organize these efforts by through the use of qualifying adjectives, organizing new ML subfields such as “Fair ML”, “Explainable ML”, and so on. This tendency is both productive and counterproductive. Organizing subfields by adjectives is an intuitive way to bring people together and catalyze research activity, and indeed tends to be the social norm across scientific and humanistic disciplines [Abbott, 2010, Whitley et al., 2000] The trade-off is that when we promote adjectives, we tend to demote verbs. This is especially important for ML research given the broad applicability of the methods we work on. What does it mean that big tent of “Fair ML” stretches over algorithms governing the legal allocation of resources (say,

lending) and also those encouraging group parity in facial recognition and law enforcement? What the algorithm *does* (in the real world) is paramount, and yet this is often reduced to a mere implementation detail barely worthy of discussion. Thus, we arrive at the following contradiction:

Organizing subfields by adjectives promotes research activity while simultaneously mystifying the actual uses of the resulting research artifacts.

- **“Scaling up”: power laws and the concentration of power.** Contemporary approaches for modeling text have benefited considerably by combining neural architectures that enable parallel training with the massive data source of web-scraped text [Brown et al., 2020]. Reaching state-of-the-art performance requires an ever-increasing number of model parameters and training data [Bender et al., 2021, Kaplan et al., 2020]. This has led to a steep barrier-to-entry in the research space: access to hardware and compute infrastructure now traces a dividing line between those who can train contemporary methods and those who cannot. This trend serves as a consolidation of power, with large firms standing to benefit the most [Luitse and Denkena, 2021]. However, open-source model sharing and adaptation has also thrived in this new training paradigm. This is because of the compute asymmetry inherent in the two stages of pre-training and fine-tuning. Once pre-training has been completed, model weights can be distributed just as freely on the web as their original training data. Unlike in the data owner/vendor paradigm of Chapter 2, where data representations served as an interface between firms, here the model weights are directly shared. Models can then be adapted during fine-tuning under a moderate compute and data budget. Thus, we arrive at the following contradiction:

“Scaling up” the learning process proliferates high-quality open-source generative models while simultaneously entrenching centralized power among firms.

- **The internet as a data source.** While the pre-training/fine-tuning recipe is currently the special du jour for ML practitioners (having been successfully applied to image and multi-modal domains [Radford et al., 2021]), there are reasons to believe that the web is a fundamentally limited data source in terms of quantity [Villalobos et al., 2022] and quality [Bender et al., 2021, Hanna and Park, 2020] of data. As more of the web is scraped as a data source, so too increases the likelihood of harmful content being used during training [Birhane and Prabhu, 2021] Furthermore, as firms race to deploy generative models in massive consumer markets, the text output sampled from these models will become a non-negligible portion of the text available on the web. Including today’s generative model output in tomorrow’s training data creates a new data-to-model-to-data circuit that is very poorly understood. Thus, we arrive at the following contradiction:

Freely accessible internet artifacts serve as “weak supervision” for powerful contemporary generative models, but may ultimately undercut their reliability in the long run.

- **Statics and dynamics.** To complement the data-to-model-to-data circuit, we can also take note of a model-to-data-to-model circuit completed when ML is embedded in a social context and induces a social response. People who interact with automated decision-making systems may alter their behavior, and perhaps even attempt to game the system towards their advantage[Hardt et al., 2016a]. This type of strategic behavior on part of the human

subjects could be realized when the model makes predictions during deployment, or perhaps even to create a strong training signal to anticipate the development of future models [Biggio et al., 2013, Demontis et al., 2019]. While the research community has begun to model these processes [Ensign et al., 2018, Perdomo et al., 2020], the presence of data feedback makes the learning considerably more challenging. Even approaches such as Reinforcement Learning that tackle feedback head-on typically require limiting assumptions such as Markovness and full observability, and even so are relatively sample inefficient. Thus, we arrive at the following contradiction:

Deploying ML in the real world induces feedback loops, which increases the difficulty of the learning process and undermines the credibility of deployed ML systems.

5.2.2 Open Research Questions

These contradictions need not be read with an air of hopelessness. Rather, studying the internal tensions within the field may lead us to some promising directions for long-term research that represent an important departure from conventional thinking of how data should be turned into computer programs. We draw this manuscript to a close with the following (non-exhaustive) list of open research questions worthy of further study:

- ↔ **Characterizing imperfect data.** ML methods have been remarkably influential across the academy. One notable cluster of activity is referred to as the “Digital Humanities”, where ML methods such as topic models [Blei, 2012] serve as crucial tools in the effort to extract new scholarly insights from the archives. In light of the sensitivities of ML to data imperfections discussed in this thesis, it is time to think more seriously about how to catalog and analyze our own data sources. There is a need to go beyond data sheets [Gebu et al., 2021] and thoroughly catalog data origins and known issues. Current practices around dataset curation within the ML field are also worthy of scrutiny [Paullada et al., 2021, Raji et al., 2021, Scheurman et al., 2021]. Fortunately, there is a flurry of ongoing effort in this area [Chang et al., 2023, Jo and Gebu, 2020, Mitchell et al., 2023, Siddiqui et al., 2022] demonstrating the potential promise of applying both ML and conventional archiving procedures towards these goals. Future work in this direction could also shed light on the question of what role synthetic data (e.g. sampled from language models) in ML.
- ↔ **Participatory priors.** Chapter 4 discussed how domain knowledge, in the form of causal priors [Pearl, 2009a], can help answer difficult computational questions with limited data. We also discussed some critiques of how causal inference is typically implemented, namely that these crucial and often untestable assumptions about social systems tend to be made by computer scientists working at a whiteboard. Given the importance causal priors in algorithm design, can we source them in a more participatory way? Recent work from Martin Jr et al. [2020] suggests a way forward, highlighting the role of collaborative causal theory formulation in “extending the ML abstraction boundary” to realize more inclusive and equitable development processes. They focus in particular on techniques from Community-based System Design (CBSD) [Hovmand and Hovmand, 2014] for collectively generating causal theories underlying ML systems, drawing on an established literature of participatory design that includes rigorous ways to model the social context in which a model is embedded. Perhaps causal inference can be synthesized

with CBSD to arrive at participatory models that provide rigorous causal inferences. This may unearth new technical problems: as mentioned above, feedback loops can be difficult to model from an ML perspective—we tend to roll them out, but in CBSD graphs this could involve unpacking tens of thousands of nodes—so it remains to be seen whether sourcing causal priors via community engagement would result in practically useful learning algorithms.

↔ **Collective action.** What is the role of community action in guiding the behavior of ML systems that are unaligned to community values? From the perspective of the model, all data subjects are *i.i.d.* and thus act independently. Of course, data subjects need not adhere to the model’s assumption about them. In settings where the model owner cannot be trusted to ensure socially beneficial properties such as fairness, data subjects may wish to take matters into their own hands by coordinating to change the overall data distribution. This type of collective action could empower data subjects to have a more democratic control over how machine learning systems function in their broader social context.

For example, *algorithmic recourse* considers what changes to an individual’s data profile will improve their future prospects following an adverse automated decision (say, a loan denial) [Karimi et al., 2022]. The typical framing for this problem assumes data subjects must each act alone and in their own self interests. However, in online settings—where the decision maker’s policy is updated over time—collective action can be a more effective strategy [Creager and Zemel, 2021]. Exploring the question of collective action more broadly—for example in recommender systems where myopic models can shape long-term user behavior [Carroll et al., 2022, Mladenov et al., 2020]—is a nascent research direction. Hardt et al. [2023] recently provided a general-purpose analytic framework that could prove helpful here; they also provide compelling theoretical results suggesting that, through coordination, small collectives can have an outsides influence on learned models.

↔ **Politics of refusal.** In theory, expressive models like deep neural networks can fit to any function given a sufficient number of examples [Hornik et al., 1989]. Meanwhile, in practice, datasets of increasing size and scope are being amassed [Bender et al., 2021, Kaplan et al., 2020]. Perhaps the most consequential research question, then, is what predictive models *should* we build using data [Barocas et al., 2020]. While policy advocates and organizers have frequently raised the alarm over dubious applications of data-driven prediction, computer science researchers have been quiet by comparison.

ML research tends to novel methodology above other possible contributions [Birhane et al., 2022, Sambasivan et al., 2021], although dataset contributions have recently been more widely accepted as well [Vanschoren and Yeung, 2021]. *Task definition* is an even more central topic that should be elevated as an equally important area for future contribution and contestation. Reorganizing research efforts accordingly is unlikely to produce a consensus, so methods to respectively adjudicate internal conflicts would be needed Mouffe [2013], Young et al. [2022].

Appendix A

Notes for Chapter 2

A.1 Notes on Section 2.2 (LAFTR)

A.1.1 Bounding Equalized Odds

We now turn our attention to equalized odds. First we extend our shorthand to denote $p(Z|A = a, Y = y)$ as \mathcal{Z}_a^y , the representation of group a conditioned on a specific label y . The equalized odds distance of classifier $g : \Omega_Z \rightarrow \{0, 1\}$ is

$$\begin{aligned} \Delta_{EO}(g) \triangleq & |\mathbb{E}_{\mathcal{Z}_0^0}[g] - \mathbb{E}_{\mathcal{Z}_1^0}[g]| \\ & + |\mathbb{E}_{\mathcal{Z}_0^1}[1 - g] - \mathbb{E}_{\mathcal{Z}_1^1}[1 - g]|, \end{aligned} \tag{A.1}$$

which comprises the absolute difference in false positive rates plus the absolute difference in false negative rates. $\Delta_{EO}(g) = 0$ means g satisfies equalized odds. Note that $\Delta_{EO}(g) \leq \Delta(\mathcal{Z}_0^0, \mathcal{Z}_1^0) + \Delta(\mathcal{Z}_0^1, \mathcal{Z}_1^1)$.

We can make a similar claim as above for equalized odds: given an optimal adversary trained on Z with the appropriate objective, if the adversary also receives the label Y , the adversary's loss will upper bound $\Delta_{EO}(g)$ for any function g learnable from Z .

Theorem. *Let the classifier $g : \Omega_Z \rightarrow \Omega_Y$ and the adversary $h : \Omega_Z \times \Omega_Y \rightarrow \Omega_Z$, as binary functions, i.e., $\Omega_Y = \Omega_A = \{0, 1\}$. Then $L_{Adv}^{EO}(h^*) \geq \Delta_{EO}(g)$: the equalized odds distance of g is bounded above by the optimal objective value of h .*

Proof. Let the adversary h 's objective be

$$\begin{aligned} L_{Adv}^{EO}(h) = & \mathbb{E}_{\mathcal{Z}_0^0}[1 - h] + \mathbb{E}_{\mathcal{Z}_1^0}[h] \\ & + \mathbb{E}_{\mathcal{Z}_0^1}[1 - h] + \mathbb{E}_{\mathcal{Z}_1^1}[h] - 2 \end{aligned} \tag{A.2}$$

By definition $\Delta_{EO}(g) \geq 0$. Let $|\mathbb{E}_{\mathcal{Z}_0^0}[g] - \mathbb{E}_{\mathcal{Z}_1^0}[g]| = \alpha \in [0, \Delta_{EO}(g)]$ and $|\mathbb{E}_{\mathcal{Z}_0^1}[1 - g] - \mathbb{E}_{\mathcal{Z}_1^1}[1 - g]| = \Delta_{EO}(g) - \alpha$. WLOG, suppose $\mathbb{E}_{\mathcal{Z}_0^0}[g] \geq \mathbb{E}_{\mathcal{Z}_1^0}[g]$ and $\mathbb{E}_{\mathcal{Z}_0^1}[1 - g] \geq \mathbb{E}_{\mathcal{Z}_1^1}[1 - g]$. Thus we can partition (A.1) as two expressions, which we write as

$$\begin{aligned} \mathbb{E}_{\mathcal{Z}_0^0}[g] + \mathbb{E}_{\mathcal{Z}_1^0}[1 - g] &= 1 + \alpha, \\ \mathbb{E}_{\mathcal{Z}_0^1}[1 - g] + \mathbb{E}_{\mathcal{Z}_1^1}[g] &= 1 + (\Delta_{EO}(g) - \alpha), \end{aligned} \tag{A.3}$$

which can be derived using the familiar identity $\mathbb{E}_p[\eta] = 1 - \mathbb{E}_p[1 - \eta]$ for binary functions.

Now, let us consider the following adversary h

$$h(z) = \begin{cases} g(z), & \text{if } y = 1 \\ 1 - g(z), & \text{if } y = 0 \end{cases}. \quad (\text{A.4})$$

Then the previous statements become

$$\begin{aligned} \mathbb{E}_{\mathcal{Z}_0^0}[1 - h] + \mathbb{E}_{\mathcal{Z}_1^0}[h] &= 1 + \alpha \\ \mathbb{E}_{\mathcal{Z}_0^1}[1 - h] + \mathbb{E}_{\mathcal{Z}_1^1}[h] &= 1 + (\Delta_{EO}(g) - \alpha) \end{aligned} \quad (\text{A.5})$$

Recalling our definition of $L_{Adv}^{EO}(h)$, this means that

$$\begin{aligned} L_{Adv}^{EO}(h) &= \mathbb{E}_{\mathcal{Z}_0^0}[1 - h] + \mathbb{E}_{\mathcal{Z}_1^0}[h] + \mathbb{E}_{\mathcal{Z}_0^1}[h] + \mathbb{E}_{\mathcal{Z}_1^1}[h] - 2 \\ &= 1 + \alpha + 1 + (\Delta_{EO}(g) - \alpha) - 2 = \Delta_{EO}(g) \end{aligned} \quad (\text{A.6})$$

That means that for the optimal adversary $h^* = \sup_h L_{Adv}^{EO}(h)$, we have $L_{Adv}^{EO}(h^*) \geq L_{Adv}^{EO}(h) = \Delta_{EO}$.

■

An adversarial bound for equal opportunity distance, defined as $\Delta_{EOpp}(g) \triangleq |\mathbb{E}_{\mathcal{Z}_0^0}[g] - \mathbb{E}_{\mathcal{Z}_1^0}[g]|$, can be derived similarly.

A.1.2 Experimental Details

We used single-hidden-layer neural networks for each of our encoder, classifier and adversary, with 20 hidden units for the Health dataset and 8 hidden units for the Adult dataset. We also used a latent space of dimension 20 for Health and 8 for Adult. We train with L_C and L_{Adv} as absolute error, as discussed in Section 2.2.3, as a more natural relaxation of the binary case for our theoretical results. Our networks used leaky rectified linear units and were trained with Adam [Kingma and Ba, 2015] with a learning rate of 0.001 and a minibatch size of 64, taking one step per minibatch for both the encoder-classifier and the discriminator. When training CLASSLEARN in Algorithm 1 from a learned representation we use a single hidden layer network with half the width of the representation layer, i.e., g. REPRLEARN (i.e., LAFTR) was trained for a total of 1000 epochs, and CLASSLEARN was trained for at most 1000 epochs with early stopping if the training loss failed to reduce after 20 consecutive epochs.

To get the fairness-accuracy tradeoff curves in Figure 2.2, we sweep across a range of fairness coefficients $\gamma \in [0.1, 4]$. To evaluate, we use a validation procedure. For each encoder training run, model checkpoints were made every 50 epochs; r classifiers are trained on each checkpoint (using r different random seeds), and epoch with lowest median error $+\Delta$ on validation set was chosen. We used $r = 7$. Then r more classifiers are trained on an unseen test set. The median statistics (taken across those r random seeds) are displayed.

For the transfer learning experiment, we used $\gamma = 1$ for models requiring a fair regularization coefficient.

A.2 Notes on Section 2.3 (FFVAE)

Discriminator approximation of total correlation

This section describes how density ratio estimation is implemented to train the FFVAE encoder. We follow the approach of Kim and Mnih [2018].

Generating Samples The binary classifier adversary seeks to discriminate between

- $[z, b] \sim q(z, b)$, “true” samples from the aggregate posterior; and
- $[z', b'] \sim q(z) \prod_j q(b_j)$, “fake” samples from the product of the marginal over z and the marginals over each b_j .

At train time, after splitting the latent code $[z^i, b^i]$ of the i -example along the dimensions of b as $[z^i, b_0^i \dots b_j^i]$, the minibatch index order for each subspace is then randomized, simulating samples from the product of the marginals; these dimension-shuffled samples retain the same marginal statistics as “real” (unshuffled) samples, but with joint statistics between the subspaces broken. The overall minibatch of encoder outputs contains twice as many examples as the original image minibatch, and comprises equal number of “real” and “fake” samples.

As we describe below, the encoder output minibatch is used as training data for the adversary, and the error is backpropagated to the encoder weights so the encoder can better fool the adversary. If a strong adversary can do no better than random chance, then the desired independence property has been achieved.

Discriminator Approximation Here we summarize the approximation of the

$$D_{KL}(q(z, b) || q(z) \prod_j q(b_j))$$

term from equation 2.15. Let $u \in \{0, 1\}$ be an indicator variable with $u = 1$ indicating $[z, b] \sim q(z, b)$ comes from a minibatch of “real” encoder distributions, while $u = 0$ indicating $[z', b'] \sim q(z) \prod_j q(b_j)$ is drawn from a “fake” minibatch of shuffled samples, i.e., is drawn from the product of the marginals of the aggregate posterior. The discriminator network outputs the probability that vector $[z, b]$ is a “real” sample, i.e., $d(u|z, b) = \text{Bernoulli}(u|\sigma(\theta_d(z, b)))$ where $\theta_d(z, b)$ is the discriminator and σ is the sigmoid function. If the discriminator is well-trained to distinguish between “real” and “fake” samples then we have

$$\begin{aligned} \log d(u = 1|z, b) - \log d(u = 0|z, b) &\approx \\ \log q(z, b) - \log q(z) \prod_j q(b_j). &\end{aligned} \tag{A.7}$$

We can substitute this into the KL divergence as

$$\begin{aligned}
D_{KL}(q(z, b) || q(z) \prod_j q(b_j)) &= \\
\mathbb{E}_{q(z, b)}[\log q(z, b) - \log q(z) \prod_j q(b_j)] &\approx \\
\mathbb{E}_{q(z, b)}[\log d(u = 1|z, b) - \log d(u = 0|z, b)]. & \tag{A.8}
\end{aligned}$$

Meanwhile the discriminator is trained by minimizing the standard cross entropy loss

$$\begin{aligned}
L_{\text{Disc}}(d) &= \mathbb{E}_{z, b \sim q(z, b)}[\log d(u = 1|z, b)] \\
&+ \mathbb{E}_{z', b' \sim q(z) \prod_j q(b_j)}[\log(1 - d(u = 0|z', b'))], \tag{A.9}
\end{aligned}$$

w.r.t. the parameters of $d(u|z, b)$. This ensures that the discriminator output $\theta_d(z, b)$ is a calibrated approximation of the log density $\log \frac{q(z, b)}{q(z) \prod_j q(b_j)}$.

$L_{\text{Disc}}(d)$ and $L_{\text{FFVAE}}(p, q)$ (Equation 2.15) are then optimized in a min-max fashion. In our experiments we found that single-step alternating updates using optimizers with the same settings sufficed for stable optimization.

A.2.1 Experimental Details

DSpritesUnfair data generation The original DSprites dataset has six ground truth factors of variation (FOV):

- Color: white
- Shape: square, ellipse, heart
- Scale: 6 values linearly spaced in $[0.5, 1]$
- Orientation: 40 values in $[0, 2\pi]$
- XPosition: 32 values in $[0, 1]$
- YPosition: 32 values in $[0, 1]$

In the original dataset the joint distribution over all FOV factorized; each FOV was considered independent. In our dataset, we instead sample such that the FOVs Shape and X-position correlate. We associate an index with each possible value of each attribute, and then sample a (Shape, X-position) pair with probability proportional to $(\frac{i_S}{n_S})^{q_S} + (\frac{i_X}{n_X})^{q_X}$, where i, n, q are the indices, total number of options, and a real number for each of Shape and X-position (S, X respectively). We use $q_S = 1, q_X = 3$. All other attributes are sampled uniformly, as in the standard version of DSprites.

We binarized the factors of variation by using the Boolean outputs of the following operations:

- Color ≥ 1
- Shape ≥ 1
- Scale ≥ 3
- Rotation ≥ 20

- XPosition ≥ 16
- YPosition ≥ 16

Training details All network parameters were optimized using the Adam [Kingma and Ba, 2015], with learning rate 0.001. Our encoders trained 3×10^5 iterations with minibatch size 64 (as in Kim and Mnih [2018]). Our MLP classifier has two hidden layers with 128 units each, and is trained with patience of 5 epochs on validation loss.

A.2.2 Mutual Information Gap

Evaluation Criteria Here we analyze the encoder mutual information in the synthetic setting of the DSpritesUnfair dataset, where we know the ground truth factors of variation. In Fig. A.1, we calculate the *Mutual Information Gap* (MIG) [Chen et al., 2018] of FFVAE across various hyperparameter settings. With J latent variables z_j and K factors of variation v_k , MIG is defined as

$$\frac{1}{K} \sum_{k=1}^K \frac{1}{H(v_k)} (MI(z_{j_k}; v_k) - \max_{j \neq j_k} MI(z_j; v_k)) \quad (\text{A.10})$$

where $j_k = \underset{j}{\operatorname{argmax}} MI(z_j; v_k)$, $MI(\cdot; \cdot)$ denotes mutual information, and K is the number of factors of variation. Note that we can only compute this metric in the synthetic setting where the ground truth factors of variation are known. MIG measures the difference between the latent variables which have the highest and second-highest MI with each factor of variation, rewarding models which allocate one latent variable to each factor of variation. We test our disentanglement by training our models on a biased version of DSprites, and testing on a balanced version (similar to the “skewed” data in Chen et al. [2018]). This allows us to separate out two sources of correlation — the correlation existing across the data, and the correlation in the model’s learned representation.

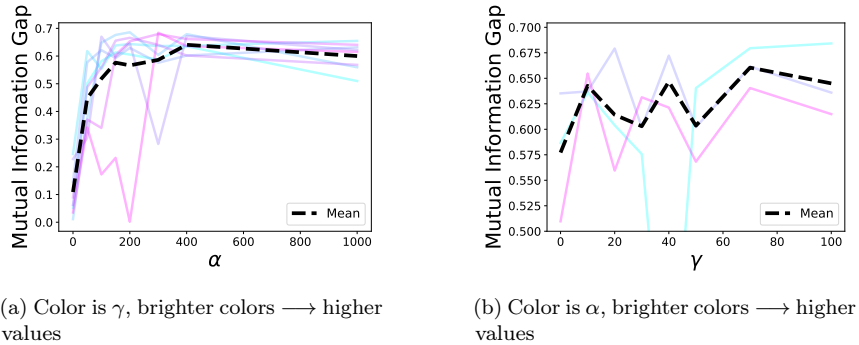


Figure A.1: Mutual Information Gap (MIG) for various (α, γ) settings of the FFVAE. In Fig. A.1a, each line is a different value of $\gamma \in [10, 20, 30, 40, 50, 70, 100]$, with brighter colors indicating larger values of γ . In Fig. A.1b, each line is a different value of $\alpha \in [300, 400, 1000]$, with brighter colors indicating larger values of α . Models trained on DspritesUnfair, MIG calculated on Dsprites. Higher MIG is better. Black dashed line indicates mean (with outliers excluded). $\alpha = 0$ is equivalent to the FactorVAE.

Results In Fig. A.1a, we show that MIG increases with α , providing more evidence that the supervised structure of the FFVAE can create disentanglement. This improvement holds across values of γ , except for some training instability for the highest values of γ . It is harder to assess the

relationship between γ and MIG, due to increased instability in training when γ is large and α is small. However, in Fig. A.1b, we look only at $\alpha \geq 300$, and note that in this range, MIG improves as γ increases. See Appendix A.2.2 for more details.

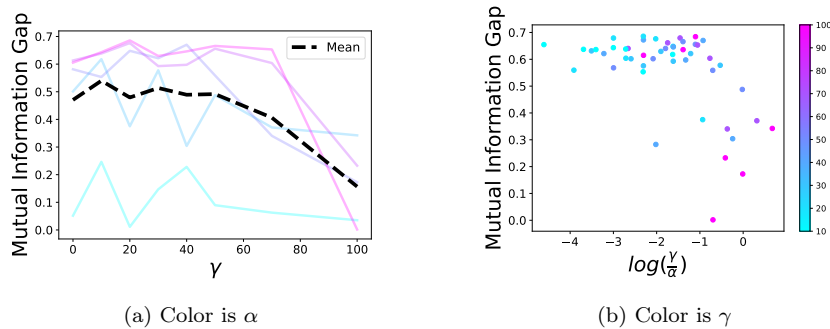


Figure A.2: Mutual Information Gap (MIG) for various (α, γ) settings of the FFVAE. In Fig. A.2a, each line is a different value of $\alpha \in [0, 50, 100, 150, 200]$, with brighter colors indicating larger values of α . In Fig. A.2b, all combinations with $\alpha, \gamma > 0$ are shown. Models trained on DspritesUnfair, MIG calculated on Dsprites. Higher MIG is better. Black dashed line indicates mean (outliers excluded). $\alpha = 0$ is equivalent to the FactorVAE.

In Fig. A.2a, we show that for low values of α , increasing γ leads to worse MIG, likely due to increased training instability. This is in contrast to Fig. A.1b, which suggests that for high enough α , increasing γ can improve MIG. This leads us to believe that α and γ have a complex relationship with respect to disentanglement and MIG.

To better understand the relationship between these two hyperparameters, we examine how MIG varies with the ratio $\frac{\gamma}{\alpha}$ in Fig. A.2b. We find that in general, a higher ratio yields lower MIG, but that the highest MIGs are around $\log \frac{\gamma}{\alpha} = -2$, with a slight tailing off for smaller ratios. This indicates there is a dependent relationship between the values of γ and α .

Discussion What does it mean for our model to demonstrate disentanglement on test data drawn from a new distribution? For interpretation, we can look to the causal inference literature, where one goal is to produce models that are robust to certain interventions in the data generating process [Rothenhäusler et al., 2018]. We can interpret Figure A.1 as evidence that our learned representations are (at least partially) invariant to *interventions* on a . This property relates to counterfactual fairness, which requires that models be robust with respect to counterfactuals along a [Kusner et al., 2017].

Appendix B

Notes for Chapter 3

B.1 Environment Inference Pseudocode

Algorithm 3 provides pseudocode for the environment inference procedure used in our experiments.

B.2 Proofs

B.2.1 Proof of Proposition 1

Consider a dataset with some feature(s) z which are spurious, and other(s) v which are valuable/causal w.r.t. the label y . This includes data generated by models where $v \rightarrow y \rightarrow z$, such that $P(y|v, z) = P(y|v)$. Assume further that the observations x are functions of both spurious and valuable features: $x := f(v, z)$. The aim of invariant learning is to form a classifier that predicts y from x that focuses solely on the causal features, i.e., is invariant to z and focuses solely on v .

Consider a classifier that produces a score $S(x)$ for example x . In the binary classification setting S is analogous to the model Φ , while the score $S(x)$ is analogous to the representation $\Phi(x)$. To quantify the degree to which the constraint in the Invariant Principle (EIC) holds, we introduce a

Algorithm 3 Pseudocode for environment inference (EI) with the invariance principle (realized via relaxed IRMv1 penalty) as the EI objective.

Input: Reference model Φ , dataset $\mathcal{D} = \{x_i, y_i\}$, loss ℓ , duration N_{steps}

Output: Worst case data splits $\mathcal{D}_1, \mathcal{D}_2$ for use with an invariant learner.

def $\tilde{R}^e(\Phi, \mathbf{q})$:

return $\frac{1}{N} \sum_i \mathbf{q}_i(e) \ell(\Phi(x_i), y_i)$

Equation 3.4

Randomly init. $\mathbf{q} \in [0, 1]^N$ environment posterior ($\mathbf{q}_i(e) := q(e|x_i, y_i)$) $n \in 1 \dots N_{steps}$

$SoftVari = \sum_{e \in \{1, 2\}} \|\nabla_{\bar{w}} \tilde{R}^e(\bar{w} \circ \Phi, \mathbf{q})\|$ Aggregate reference model variances across soft envs

$Loss = -1 \cdot SoftVari$ Maximize the EI objective by minimizing this loss

$\mathbf{q} \leftarrow OptimUpdate(\mathbf{q}, \nabla_{\mathbf{q}} Loss)$

$\hat{\mathbf{q}} \sim Bernoulli(\mathbf{q})$

sample splits

$\mathcal{D}_1 \leftarrow \{x_i, y_i | \hat{\mathbf{q}}_i = 1\}, \mathcal{D}_2 \leftarrow \{x_i, y_i | \hat{\mathbf{q}}_i = 0\}$

split data

return $\mathcal{D}_1, \mathcal{D}_2$

measure called the *group sufficiency gap*¹:

$$\Delta(S, e) = \mathbb{E}[\mathbb{E}[(y|S(x), e_1)] - \mathbb{E}[(y|S(x), e_2)]]$$

Now consider the notion of an environment: some setting in which the $x \rightarrow y$ relationship varies (based on spurious features). Assume a single binary spurious feature z . We restate Proposition 1 as follows:

Claim: If environments are defined based on the agreement of the spurious feature z and the label y , then a classifier that predicts based on z alone maximizes the group-sufficiency gap (and vice versa – if a classifier predicts y directly by predicting z , then defining two environments based on agreement of label and spurious feature— $e_1 = \{v, z, y|\mathbb{1}(y = z)\}$ and $e_2 = \{v, z, y|\mathbb{1}(y \neq z)\}$ —maximizes the gap).

We can show this by first noting that if the environment is based on spurious feature-label agreement, then with $e \in \{0, 1\}$ we have $e = \mathbb{1}(y = z)$. If the classifier predicts z , i.e. $S(x) = z$, then we have

$$\Delta(S, e) = \mathbb{E}[\mathbb{E}[y|z(x), \mathbb{1}(y = z)] - \mathbb{E}[y|z(x), \mathbb{1}(y \neq z)]]$$

For each instance of x either $z = 0$ or $z = 1$. Now we note that when $z = 1$ we have $\mathbb{E}(y|z, \mathbb{1}(y = z)) = 1$ and $\mathbb{E}(y|z, \mathbb{1}(y \neq z)) = 0$, while when $z = 0$ $\mathbb{E}(y|z, \mathbb{1}(y = z)) = 0$ and $\mathbb{E}(y|z, \mathbb{1}(y \neq z)) = 1$. Therefore for each example $|E(y|z(x), \mathbb{1}(y = z)) - E(y|z(x), \mathbb{1}(y \neq z))| = 1$, contributing to an overall $\Delta(S, e) = 1$, which is the maximum value for the sufficiency gap.

B.2.2 Analysis of the Binning Heuristic

Here we analyze the heuristic discussed in Section 3.2.2. We want to show that finding environment assignments in this way both maximizes the violation of the softened version of the regularizer (Equation 3.3), and also also maximally violates the invariance principle (EIC).

Because the invariance principle $\mathbb{E}[Y|\Phi(X), e] = \mathbb{E}[Y|\Phi(X), e'] \forall e, e'$ is difficult to quantify for continuous $\Phi(X)$, we consider a binned version of the representation, with b denoting the discrete index of the bin in representation space. Let $q_i \in [0, 1]$ denote the soft assignment of example i to environment 1, and $1 - q_i$ denote its converse, the assignment of example i to environment 2. Denote by $y_i \in \{0, 1\}$ the binary target for example i , and $\hat{y} \in [0, 1]$ as the model prediction on this example. Assume that ℓ represents a cross entropy or squared error loss so that $\nabla_w \ell(\hat{y}, y) = (\hat{y} - y)\Phi(x)$.

Consider the IRMv1 regularizer with soft assignment, expressed as

$$\begin{aligned} D(q) &= \sum_e \|\nabla_{w|w=1.0} \frac{1}{N_e} \sum_i q_i(e) \ell(w \circ \Phi(x_i), y_i)\|^2 \\ &= \sum_e \left\| \frac{1}{N_e} \sum_i q_i(e) (\hat{y}_i - y_i) \Phi(x_i) \right\|^2 \\ &= \left\| \frac{1}{\sum_i q_i} \sum_i q_i (\hat{y}_i - y_i) \Phi(x_i) \right\|^2 + \left\| \frac{1}{\sum_i (1 - q_i)} \sum_i (1 - q_i) (\hat{y}_i - y_i) \Phi(x_i) \right\|^2 \\ &= \left\| \frac{\sum_i q_i \hat{y}_i \Phi(x_i)}{\sum_{i'} q_{i'}} - \frac{\sum_i q_i y_i \Phi(x_i)}{\sum_{i'} q_{i'}} \right\|^2 + \left\| \frac{\sum_i (1 - q_i) \hat{y}_i \Phi(x_i)}{\sum_{i'} (1 - q_{i'})} - \frac{\sum_i (1 - q_i) y_i \Phi(x_i)}{\sum_{i'} (1 - q_{i'})} \right\|^2. \quad (\text{B.1}) \end{aligned}$$

Now consider that the space of $\Phi(X)$ is discretized into disjoint bins b over its support, using

¹This was previously used in a fairness setting by Liu et al. [2019] to measure differing calibration curves across groups.

$z_{i,b} \in \{0, 1\}$ to indicate whether example i falls into bin b according to its mapping $\Phi(x_i)$. Thus we have

$$D(q) = \sum_b \left(\left\| \frac{\sum_i z_{i,b} q_i \hat{y}_i \Phi(x_i)}{\sum_{i'} z_{i',b} q_{i'}} - \frac{\sum_i z_{i,b} q_i y_i \Phi(x_i)}{\sum_{i'} z_{i',b} q_{i'}} \right\|^2 + \left\| \frac{\sum_i z_{i,b} (1 - q_i) \hat{y}_i \Phi(x_i)}{\sum_{i'} z_{i',b} (1 - q_{i'})} - \frac{\sum_i z_{i,b} (1 - q_i) y_i \Phi(x_i)}{\sum_{i'} z_{i',b} (1 - q_{i'})} \right\|^2 \right) \quad (\text{B.2})$$

The important point is that within a bin, all examples have roughly the same $\Phi(x_i)$ value, and the same value for \hat{y}_i as well. So denoting $K_b^{(1)} := \frac{\sum_i z_{i,b} q_i \hat{y}_i \Phi(x_i)}{\sum_{i'} z_{i',b} q_{i'}}$ and $K_b^{(2)} := \frac{\sum_i z_{i,b} (1 - q_i) \hat{y}_i \Phi(x_i)}{\sum_{i'} z_{i',b} (1 - q_{i'})}$ as the relevant constant within-bin summations, we have the following objective to be maximized by EIIL:

$$D(q) = \sum_b \left(\left\| K_b^{(1)} - \frac{\sum_i z_{i,b} q_i y_i \Phi(x_i)}{\sum_{i'} z_{i',b} q_{i'}} \right\|^2 + \left\| K_b^{(2)} - \frac{\sum_i z_{i,b} (1 - q_i) y_i \Phi(x_i)}{\sum_{i'} z_{i',b} (1 - q_{i'})} \right\|^2 \right).$$

One way to maximize this is to assign all $y_i = 1$ values to environment 1 ($q_i = 1$ for these examples) and all $y_i = 0$ to the other environment ($q_i = 0$). We can show this is maximized by considering all of the examples except the i -th one have been assigned this way, and then that the loss is maximized by assigning the i -th example according to this rule.

Now we want to show that the same assignment maximally violates the invariance principle (showing that this soft EIIL solution provides maximal non-invariance). Intuitively within each bin the difference between $\mathbb{E}[y|e = 1]$ and $\mathbb{E}[y|e = 2]$ is maximized (within the bin) if one of these expected label distributions is 1 while the other is 0. This can be achieved by assigning all the $y_i = 1$ values to the first environment and the $y_i = 0$ values to the second.

Thus a global optimum for the relaxed version of EIIL (using the IRMv1 regularizer) also maximally violates the invariance principle.

B.3 Dataset Details

CMNIST This dataset was provided by Arjovsky et al. [2019]². The two training environments comprise 25,000 images each, with $\text{Corr}(\text{color}, \text{label}) = 0.8$ for the first training environment and $\text{Corr}(\text{color}, \text{label}) = 0.8$ for the second. A held-out test set with $\text{Corr}(\text{color}, \text{label}) = 0.1$ is used for evaluation. Label noise is applied by flipping the binary target y with probability $\theta_y = 0.25$, with color correlation applied w.r.t. the noisy label. Given that only two color channels are used, we follow Arjovsky et al. [2019] in downsampling the digit images to 14×14 pixels and 2 channels.

Waterbirds We follow the procedure outlined by Sagawa et al. [2020a] to reproduce the Waterbirds dataset. As noted by the authors, due to random seed differences our version of the dataset may differ slightly from the one originally used by the paper. The train/validation/test splits are of size 4,795/1,200/5,794. As noted in the Appendix of [Sagawa et al., 2020a], the validation and test distributions represent upweight the minority groups so that the number of examples coming from each habitat is equal (although there are still marginally more landbirds than waterbirds). For example on train set the subgroup sizes are 3,498/184/56/1,057 while on the test set the sizes are 467/466/133/133.

²<https://github.com/facebookresearch/InvariantRiskMinimization>

CivilComments-WILDS We use the train/validation/test splits from Koh et al. [2021]; we refer the interested reader the Appendix of their paper for a detailed description of this version of the dataset, including how it differs from the original dataset [Borkan et al., 2019].

B.4 Experimental Details

Model selection Krueger et al. [2021] discussed the pitfalls of achieving good test performance on CMNIST by using test data to tune hyperparameters. Because our primary interest is in the properties of the inferred environment rather than the final test performance, we sidestep this issue in the Synthetic Regression and CMNIST experiments by using the default parameters of IRM without further tuning.

We refer the interested reader to Gulrajani and Lopez-Paz [2021] for an extensive discussion of possible model selection strategies. They also provide a large empirical study showing that ERM is difficult baseline to beat when all methods are put on equal footing w.r.t. model selection.

In our case, we use the most relaxed model selection method proposed by Gulrajani and Lopez-Paz [2021], which amounts to allowing each method a 20 test evaluations using hyperparameter chosen at random from a reasonable range, with the best hyperparameter setting selected for each method. While none of the methods is given an unfair advantage in the search over hyperparameters, the basic model selection premise does not translate to real-world applications, since information about the test-time distribution is required to select hyperparameters. Thus these results can be understood as being overly optimistic for each method, although the relative ordering between the methods can still be compared.

Training times Because EIIL requires a pre-trained reference model and optimization of the EI objective, overall training time is longer than standard invariant learning. It depends primarily on the number of steps used to train the reference model and number of steps used in EI optimization. The extra training time incurred is manageable and varies from dataset to dataset.

In CMNIST, we train the ERM reference model for 1,000 steps, which is the same duration as the downstream invariant learner that eventually uses the inferred environments. In this setting the 10,000 steps required to optimize the EI objective is actually more than used for representation learning. The overall EIIL train time is 6.6 minutes to run 10 restarts on a NVIDIA Tesla P100, compared with 2.18 minutes for ERM and 2.20 minutes for IRM.

However, as the problem size scales, the relative overhead cost of EIIL becomes progressively discounted. On Waterbirds, training GroupDRO takes 4.716 hours on a NVIDIA Tesla P100. Our reference model trains for 1 epoch, so taking this into account along with the 20,000 steps of EI optimization, EIIL runs at 4.737 hours. This is a relative increase of 0.4%.

Batch environment inference As mentioned in Chapter 3, we aggregate logits for the entire training set and optimize the EI objective using the entire training batches. This can be done by cycling through the train set once in minibatches, computing logits per minibatch, and aggregating the logits only (discarding network activations) prior to EI. We leave minibatched environment inference and amortization of the soft environment assignments to future work.

Experimental infrastructure Our experiments were run on a cluster of NVIDIA Tesla P100 machines.

CMNIST IRM is trained on the two training environments and tested on a holdout environment constructed from 10,000 test images in the same way as the training environments, where color is predictive of the noisy label 10% of the time. So using color as a feature to predict the label will lead to an accuracy of roughly 10% on the test environment, while it yields 80% and 90% accuracy respectively on the training environments.

To evaluate EIIL we remove the environment identifier from the training set and thus have one training set comprised of 50,000 images from both original training environments. We then train an MLP with binary cross-entropy loss on the training environments, freeze its weights and use the obtained model to learn environment splits that maximally violate the IRM penalty. When optimizing the inner loop of EIIL, we use Adam with learning rate 0.001 for 10,000 steps with full data batches used to compute gradients.

The obtained environment partitions are then used to train a new model from scratch with IRM. Following Arjovsky et al. [2019], we allow the representation to train for several hundred annealing steps before applying the IRMv1 penalty.

We used the default architecture—an MLP with two hidden layers of 390 neurons—and hyperparameter values³—learning rate, weight decay, and penalty strength—from [Arjovsky et al., 2019]. We do not use minibatches as the entire dataset fits into memory.

Waterbirds Following Sagawa et al. [2020a], we use the default `torchvision` ResNet50 models, using the pre-trained weights as the initial model parameters, and train without any data augmentation using the For GroupDRO and ERM, we use hyperparameters reported by the authors⁴, and note that the authors make use of the validation set (whose distribution contains less group imbalance than the training data), to select hyperparameters in their experiments (all methods benefit equally from this strategy). We train for 300 epochs without any early stopping (to avoid any further influence from the validation data). For EIIL, we optimize the EI objective of EIIL with learning rate 0.01 for 20,000 steps using the Adam optimizer, and use GroupDRO (using the same hyperparameters as the GroupDRO baseline) as the invariant learner. An ERM model trained for 1 epoch was used as the reference model. We also tried using reference modeled trained for longer, but found that EIIL did not perform as well in this case. We hypothesize that this is because the reference ERM model focuses on background features early in training, leading to stark performance discrepancies across subgroups, which in turn provides a strong learning signal for EIIL to infer effective environments. While subgroup disparities are present for more well-trained models, the learning signal in the EI phase will weaken.

CivilComments-WILDS Following [Koh et al., 2021], we finetune DistilBERT embeddings [Sanh et al., 2019] using the default HuggingFace implementation and default weights [Wolf et al., 2019]. EIIL uses an ERM reference classifier and its inferred environments are fed to a GroupDRO invariant learner. During prototyping the EI step, we noticed that the binning heuristic described in Section 3.2.2 consistently split the training examples into environments according to the error cases of the reference classifier. Because error splitting is even simpler to implement than confidence binning, we used this heuristic for the EI step; we believe this is a promising approach for scaling EI to large

³https://github.com/facebookresearch/InvariantRiskMinimization/blob/master/code/colored_mnist/reproduce_paper_results.sh

⁴<https://worksheets.codalab.org/worksheets/0x621811fe446b49bb818293bae2ef88c0>

datasets, and note its equivalence to the first stage of the method independently proposed by Liu et al. [2021], which is published concurrently to ours. We experimented with gradient-based EI on this dataset, but did not find any improvement over the (faster) heuristic EI.

On this dataset, we treat reference model selection as part of the overall model selection process, meaning that the hyperparameters of the ERM reference model are treated as a subset of the overall hyperparameters tuned during model selection. Specifically we used a grid search to tune the reference model learning rate (1e-5, 1e-4), optimizer type (Adam, SGD) and scheduler (linear, plateau), and gradient norm clamping (off, clamped at 1.0), as well as the invariant learner (GroupDRO) learning rate (1e-5, 1e-4). Moreover, we allow all methods to evaluate worst-group validation accuracy to tune these hyperparameters; such validation data will not be available in most settings, so this result can be seen as an optimistic view of the performance of all methods, including EIIL. We train all methods (including the reference model) for 5 epochs, with the best epoch chosen according to validation performance. Interestingly, the reference model chosen in this way was a constant classifier, so the overall EIIL solution is equivalent to GroupDRO using the class label as the environment label.

The oracle GroupDRO method trains on two environments, with one containing comments where *any* of the 8 sensitive groups was mentioned, and other environment containing the remaining comments. We experimented with allowing the oracle method access to more fine-grained environment labels by evaluating all 2^8 combinations of binary group labels, but did not find any significant performance boost (consistent with observations from Koh et al. [2021]).

B.5 Additional Empirical Results

B.5.1 ColorMNIST

Table B.1: Additional baselines for the CMNIST experiment reported in Table 3.1. The mean and standard deviation of accuracy across ten runs ($\theta_y = 0.25$) are reported. See text for description of the baseline methods.

	Train accs	Test accs
Grayscale (oracle)	75.3 ± 0.1	72.6 ± 0.6
IRM (oracle envs)	71.1 ± 0.8	65.5 ± 2.3
ERM	86.3 ± 0.1	13.8 ± 0.6
EIIL	73.7 ± 0.5	68.4 ± 2.7
Binned EI heuristic	73.9 ± 0.5	69.0 ± 1.5
Φ_{Color}	85.0 ± 0.1	10.1 ± 0.2
EIIL $\tilde{\Phi} = \Phi_{Color}$	75.9 ± 0.4	68.0 ± 1.2
ARL	88.9 ± 0.2	20.7 ± 0.9
GEORGE	84.6 ± 0.3	12.8 ± 2.0
LFF; $\mathcal{L}_{bias} = \text{GCE}_{q \rightarrow 0}$	96.6 ± 1.3	30.6 ± 1.0
LFF; $\mathcal{L}_{bias} = \text{GCE}_{q=0.7}$	15.0 ± 0.1	90.0 ± 0.3

Table B.1 expands on the results from Table 3.1 by adding the following baselines that do not require environment labels:

- Grayscale: a classifier that removes color via pre-processing, which represents an oracle solution
- EIIL| $\tilde{\Phi} = \Phi_{ERM}$ (reported as EIIL in Table 3.1)
- Binned EI heuristic: the binning heuristic for environment inference described in Section 3.2.2.

- Φ_{Color} : a hard-coded classifier that predicts *only* based on the digit color
- $EIIL|\tilde{\Phi} = \Phi_{Color}$: EIIL using color-based classifier (rather than Φ_{ERM}) as reference.
- GEORGE [Sohoni et al., 2020]: This two-stage method seeks to learn the “hidden subclasses” by fitting a latent cluster model to the (per-class) distribution of logits of a reference model. The inferred hidden subclasses are fed to a GroupDRO learner, so this approach can be seen as an instance of EIIL under particular choices of (unsupervised) EI and (robust optimization) IL objectives.
- ARL [Lahoti et al., 2020]: A variant of DRO that uses an adversary/auxiliary model to learn worst-case per-example importance weights. Unlike with EIIL, the auxiliary model and main model are trained jointly.
- LFF [Nam et al., 2020] jointly trains a “biased” model f_B and “debiased” model f_D . f_B is similar to our ERM reference model, but is trained with $GCE_q(p(x; \theta), y) = \frac{1-p_y(x; \theta)^q}{q}$ with hyperparameter $q \in (0, 1]$,⁵ and its per-example losses determine importance weights for f_D .

When expanding this study we find that, unlike EIIL, the new baselines fail to find an invariant classifier that predicts based on shape rather than color. Given that GEORGE does a type of unsupervised EI, it is perhaps surprising that it cannot uncover optimal environments for use with its GroupDRO learner. We hypothesize that this is due to assumption of the relevant latent environment labels being “hidden subclasses”, meaning that all examples in an optimal environment must share the same class label value. In the CMNIST dataset, this assumption does not hold due to label noise.

We find that, on this dataset, LFF is very sensitive to the hyperparameter q , which shapes the GCE loss of f_B . Interestingly, using the default value of $q = 0.7$, LFF performs optimally on the test set, but this is *not* because the method has learned an invariant classifier based on the digit shape. The below-chance train set performance reveals that LFF has learned an *anti-color* classifier, exactly the opposite of what ERM does. When q approaches zero (GCE approaches standard cross entropy), LFF fails to generalize to the OOD test distribution.

Finally, we found that because the reference classifier predicts with high confidence on the training set, there are only two populated bins in practice. Consequentially, the binned EI heuristic is equivalent to splitting errors into one environment and correct predictions into the other.

⁵as $q \rightarrow 0$ GCE becomes standard cross entropy

Appendix C

Notes for Chapter 4

C.1 Proof of Proposition 1

Lemma 1. *If $V^j \in \text{Pa}^{\mathcal{L}}(V^i)$ in DAG $\mathcal{G}^{\mathcal{L}}$ of (local) causal model $\mathcal{M}^{\mathcal{L}}$, and $\mathcal{L} \subset \mathcal{X}$, then $V^j \in \text{Pa}^{\mathcal{X}}(V^i)$ in DAG $\mathcal{G}^{\mathcal{X}}$ corresponding to causal model $\mathcal{M}^{\mathcal{X}}$.*

Proof. By minimality, there exist $\{u^i, v^{-j}, v_1^j\}$ and $\{u^i, v^{-j}, v_2^j\}$ with $v^{-j} \in \text{Pa}^{\mathcal{L}}(V^i) \setminus V^j$ for which $f^i(\{u^i, v^{-j}, v_1^j\}) \neq f^i(\{u^i, v^{-j}, v_2^j\})$. Expand $\{v^{-j}, v_1^j\}$ and $\{v^{-j}, v_2^j\}$ to $(s_1, a_1), (s_2, a_2) \in \mathcal{L}$ (with any values of other components). But $\mathcal{L} \subset \mathcal{X}$, so $(s_1, a_1), (s_2, a_2) \in \mathcal{X}$ and it follows from minimality in \mathcal{X} that $V^j \in \text{Pa}^{\mathcal{X}}(V^i)$. \square

Corollary 2. *If $\mathcal{L} \subset \mathcal{X}$, $\mathcal{G}^{\mathcal{L}}$ is sparser (has fewer edges) than $\mathcal{G}^{\mathcal{X}}$.*

Proposition 1. *The causal mechanisms represented by $\mathcal{G}_i, \mathcal{G}_j \subset \mathcal{G}$ are independent in $\mathcal{G}^{\mathcal{L}_1 \cup \mathcal{L}_2}$ if and only if \mathcal{G}_i and \mathcal{G}_j are independent in both $\mathcal{G}^{\mathcal{L}_1}$ and $\mathcal{G}^{\mathcal{L}_2}$, and $f^{\mathcal{L}_1, i} = f^{\mathcal{L}_2, i}, f^{\mathcal{L}_1, j} = f^{\mathcal{L}_2, j}$.*

Proof. (\Rightarrow) If \mathcal{G}_i and \mathcal{G}_j are independent in $\mathcal{G}^{\mathcal{L}_1 \cup \mathcal{L}_2}$, independence in $\mathcal{G}^{\mathcal{L}_1}$ and $\mathcal{G}^{\mathcal{L}_2}$ follows from Corollary 2. That $f^{\mathcal{L}_1, i} = f^{\mathcal{L}_2, i}$ (and $f^{\mathcal{L}_1, j} = f^{\mathcal{L}_2, j}$), on their shared domain, follows since each is a restriction of the same function $f^{\mathcal{L}_1 \cup \mathcal{L}_2, i}$ (or $f^{\mathcal{L}_1 \cup \mathcal{L}_2, j}$).

(\Leftarrow) Suppose \mathcal{G}_i and \mathcal{G}_j are independent in $\mathcal{G}^{\mathcal{L}_1}$ and $\mathcal{G}^{\mathcal{L}_2}$ but not $\mathcal{G}^{\mathcal{L}_1 \cup \mathcal{L}_2}$. By the definition of independence applied to $\mathcal{G}^{\mathcal{L}_1 \cup \mathcal{L}_2}$, we have that, without loss of generality, there is a $V_i \in \mathcal{G}_i, V_j \in \mathcal{G}_j$ with $V_j \in \text{Pa}^{\mathcal{L}_1 \cup \mathcal{L}_2}(V_i)$. Then, from the definition of minimality, it follows that there exist $(s_1, a_1), (s_2, a_2) \in \mathcal{L}_1 \cup \mathcal{L}_2$ that differ only in the value of V_j , and $u_i \in \text{range}(U_i)$ for which $f^i(s_1, a_1, u_i) \neq f^i(s_2, a_2, u_i)$.

Clearly, if (s_1, a_1) and (s_2, a_2) are both in \mathcal{L}_1 (or \mathcal{L}_2), there will be an edge from V_j to V_i in $\mathcal{G}^{\mathcal{L}_1}$ (or $\mathcal{G}^{\mathcal{L}_2}$) and the claim follows by contradiction. Thus, the only interesting case is when, without loss of generality, $(s_1, a_1) \in \mathcal{L}_1$ and $(s_2, a_2) \in \mathcal{L}_2$. The key observation is that (s_1, a_1) and (s_2, a_2) differ only in the value of node $V_j \notin \mathcal{G}_i$: since \mathcal{G}_i is an independent causal mechanism in both $\mathcal{G}^{\mathcal{L}_1}$ and $\mathcal{G}^{\mathcal{L}_2}$ and the parents of V_i take on the same values in each, we have that $f^i(s_1, a_1, u_i) = f^{i, \mathcal{L}_1}(s_1, a_1, u_i) = f^{i, \mathcal{L}_2}(s_2, a_2, u_i) = f^i(s_2, a_2, u_i)$ and the claim follows by contradiction. \square

C.2 Additional Experiment Details

This section provides training details for the experiments discussed in Section 4.3.6 as well as some additional results. Code is available at <https://github.com/spitis/mr1> Pitis et al. [2020a].

C.2.1 Batch RL

Here we detail the procedure used in the Batch RL experiments in the Pong environment.

Implementation Our experiment first builds the agent’s dataset (consisting of real data, dyna data and/or CoDA data), then instantiates a TD3 agent by filling its replay buffer with the dataset. The replay buffer is always expanded to include the entire enlarged dataset (for the 5x CoDA ratio at 250,000 data size this means the buffer has 1.5E6 experiences). The agent is run for 500,000 optimization steps.

Hyperparameters We used similar hyperparameters to the original TD3 codebase, with the following differences:

- We use a discount factor of $\gamma = 0.98$ instead of 0.99.
- Since Pong is a sparse reward task with $\gamma = 0.98$, we clip critic targets to $(-50, 50)$.
- We use networks of size (128, 128) instead of (256, 256).
- We use a batch size of 1000.

Environment We base our Pong environment on RoboSchoolPong-v1 Klimov and Schulman [2017]. The original environment allowed the ball to teleport back to the center after one of the players scored, offered a small dense reward signal for hitting the ball, and included a stray “timeout” feature in the agent’s state representation. We fix the environment so that the ball does not teleport, and instead have the episode reset every 150 steps, and also 10 steps after either player scores. The environment is treated as continuous and never returns a done signal that is not also accompanied by a `TimeLimit.truncated` indicator Brockman et al. [2016]. We change the reward to be strictly sparse, with reward of ± 1 given when the ball is behind one of the players’ paddles. Finally, we drop the stray “timeout” feature, so that the state space is 12-dimensional, where each set of 4 dimensions is the x-position, y-position, x-velocity, and y-velocity of the corresponding object (2 paddles and one ball).

The opponent in the environment uses a small pre-trained policy that was included in the original environment Klimov and Schulman [2017] (the effectiveness of this policy was unaffected by the removal of the timeout feature). To collect the batch dataset, we use the same policy as an “expert” policy, but replace 50% of its actions by random actions.

Training the CoDA model Without access to a ground truth mask, we needed to train a masking function ?? to identify local disentanglement. We also forewent the ground truth reward, instead training our own reward classifier. In each case we used the batch dataset given, and so we trained different models for each random seed. For our masking model, we stacked two single-head transformer blocks (without positional encodings) and used the product of their attention masks as the mask. Each block consists of query Q , key K , and value V networks that each have 3-layers of 256 neurons each, with the attention computed as usual Lee et al. [2018], Vaswani et al. [2017]. The transformer is trained to minimize the L2 error of the next state prediction given the current state and action as inputs. The input is disentangled, and so has shape `(batch_size, num_components,`

`num_features`). In each row (component representation) of each sample, features corresponding to other components are set to zero. The transformer is trained for 2000 steps with a batch size of 256, Adam optimizer Kingma and Ba [2015] with learning rate of $3e-4$ and weight decay of $1e-5$. For our reward function we use a fully-connected neural network with 1 hidden layer of 128 units. The reward network accepts an (s, a, s') tuple as input (not disentangled) and outputs a softmax over the possible reward values of $[-1, 0, 1]$. It is trained for 2000 steps with a batch size of 512, Adam optimizer Kingma and Ba [2015] with learning rate of $1e-3$ and weight decay of $1e-4$. All hyperparameters were rather arbitrary (we used the default setting, or in case it did not work, the first setting that gave reasonable results, as was determined by inspection). To ensure that our model and reward functions are trained appropriately (i.e., do not diverge) for each seed, we confirm that the average loss of the CoDA model is below 0.005 at the training and that the average loss of the reward model is below 0.1, which values were found by inspection of a prototype run. These conditions were met by all seeds.

When used to produce masks, we chose a threshold of $\tau = 0.02$ by inspection, which seemed to produce reasonable results. A more principled approach would do cross-validation on the available data.

Tested configurations Table 4.1 reports a subset of our tested configurations. We report our results in full below. We considered the following configurations:

1. **Real data only.**
2. **CoDA + real data:** after training the CoDA model, we expand the base dataset by either 2, 3, 4 or 6 times.
3. **Dyna (using CoDA model):** after training the CoDA model, we use it as a forward dynamics model instead of for CoDA; we use 1-step rollouts with random actions from random states in the given dataset to expand the dataset by 2x. We also tried with 5-step rollouts, but found that this further hurt performance (not shown). Note that Dyna results use only 5 seeds.
4. **Dyna (using MBPO model):** as the CoDA model exhibits significant model bias when used as a forward dynamics model, we replicate the state-of-the-art model-based architecture used by MBPO Janner et al. [2019] and use it as a forward dynamics model for Dyna; we experimented with 1-step and 5-step rollouts with random actions from random states in the given dataset to expand the dataset by 2x. This time we found that the 5-step rollouts do better, which we attribute to the lower model bias together with the ability to create a more diverse dataset (1-step not shown). The MBPO model is described below. We use the same reward model as CoDA to relabel rewards for the MBPO model, which only predicts next state.
5. **MBPO + CoDA:** as MBPO improved performance over the baseline (real data only) at lower dataset sizes, we considered using MBPO together with CoDA. We use the base dataset to train the MBPO, CoDA, and reward models, as described above. We then use the MBPO model to expand the base dataset by 2x, as described above. We then use the CoDA model to expand *the expanded dataset* by 3x the original dataset size. Thus the final dataset is 5x as large as the original dataset (1 real : 1 MBPO : 3 CoDA).

All configurations alter only the training dataset, and the same agent architecture/hyperparameters (reported above) are used in each case.

MBPO model Since using the CoDA model for Dyna harms rather than helps, we consider using a stronger, state-of-the-art model-based approach. In particular, we adopt the model used by Model-Based Policy Optimization Janner et al. [2019]. This model consists of a size 7 ensemble of neural networks, each with 4 layers of 200 neurons. We use ReLU activations, Adam optimizer Kingma and Ba [2015] with weight decay of $5e-5$, and have each network output a the mean and (log) diagonal covariance of a multi-variate Gaussian. We train the networks with a maximum likelihood loss. To sample from the model, we choose an ensemble member uniformly at random and sample from its output distribution, as in Janner et al. [2019].

C.2.2 Goal-conditioned RL

Here we detail the procedure used in the Goal-conditioned RL experiments on the `Fetchpush-v1` and `Slide2` environments.

Hyperparameters For `Fetchpush-v1` we use the default hyperparameters from the codebase (see Pitis et al. [2020b] for details on how they were selected), which outperform the original HER agents of Andrychowicz et al. [2017], Plappert et al. [2018] and follow-up works. We do not tune the CoDA agent (but see additional CoDA hyperparameters below). They are as follows:

- Off-policy algorithm: DDPG Lillicrap et al. [2015]
- Hindsight relabeling strategy: `futureactual_2_2` Pitis et al. [2019], using exclusively `future` Andrychowicz et al. [2017] relabeling for the first 25,000 steps
- Optimizer: Adam Kingma and Ba [2015] with default hyperparameters
- Batch size: 2000
- Optimization frequency: 1 optimization step every 2 environment steps after the 5000th environment step
- Target network updates: update every 10 optimization steps with a Polyak averaging coefficient of 0.05
- Discount factor: 0.98
- Action l2 regularization: 0.01
- Networks: 3x512 layer-normalized Ba et al. [2016] hidden layers with ReLU activations
- Target clipping: (-50, 0)
- Action noise: 0.1 Gaussian noise
- Epsilon exploration Plappert et al. [2018]: 0.2, with an initial 100% exploration period of 10,000 steps
- Observation normalization: yes

- Buffer size: 1M

On `Slide2` we tried to tune the baseline hyperparameters somewhat, but note that this is a fairly long experiment (10M timesteps) and so only a few settings were tested due to constraints. In particular, we considered the following modifications:

- Expanding the replay buffer to 2M (effective)
- Reducing the batch size to 1000 (effective)* (used for results)
- Using the `future_4` strategy (agent fails to learn in 10M steps)
- Reducing optimization step frequency to 1 step every 4 environment steps (about the same performance)

We tried similar adjustments to our CoDA agent, but found the default hyperparameters (used for results) performed well. We found that the CoDA agent outperforms the base HER agent on all tested settings.

For CoDA, we used the following additional hyperparameters:

- CoDA buffer size: 3M
- Make CoDA data every: 250 environment steps
- Number of source pairs from replay buffer used to make CoDA data: 2000
- Number of CoDA samples per source pair: 2
- Maximum ratio of CoDA:Real data to train on: 3:1

Environment On `FetchPush-v1` the standard state features include the relative position of the object and gripper, which entangles the two. While this could be dealt with by dynamic relabeling (as used for HER’s reward), we simply drop the corresponding features from the state.

`Slide2` has two pucks that slide on a table and bounce off of a solid railing. Observations are 40-dimensional (including the 6-dimensional goal), and actions are 4-dimensional. Initial positions and goal positions are sampled randomly on the table. During training, the agent gets a sparse reward of 0 (otherwise -1) if *both* pucks are within 5cm of their ordered target. At test time we count success as having both pucks within 7.5cm of the target on the last step of the episode. Episodes last 75 steps and there is no done signal (this is intended as a continuous task).

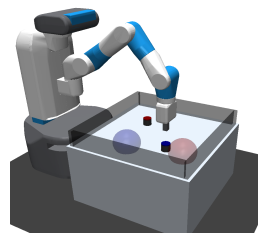


Figure C.1: The `Slide2` environment.

CoDA Heuristic For these experiments we use a hand-coded heuristic designed with domain knowledge. In particular, we assert that the action is always entangled with the gripper, and that gripper/action and objects (pucks or blocks) are disentangled whenever they are more than 10cm apart. This encodes independence due to physical separation, which we hypothesize is a very generally heuristic that humans implicitly rely on all the time. The pucks have a radius of 2.5cm and height of 4cm, and the blocks are 5cm x 5cm x 5cm, so this heuristic is quite generous / suboptimal. Despite being suboptimal, it demonstrates the ease with which domain knowledge can be injected via the CoDA mask: we need only a high precision (low false positive rate) heuristic—the recall is not as important. It is likely that an agent could learn a better mask that also takes into account velocity.

Results plot The plot shows mean ± 1 standard deviation of the smoothed data over 5 seeds.

C.3 Proof of Theorem 1

The dynamics model assumed is a maximum-likelihood, count-based model that has separate parameters for each causal mechanism, $P_{i,\theta}^{\mathcal{L}}$, in each local neighborhood. That is, for a given configuration of the parents $\text{Pa}_i = x$ in $P_{i,\theta}^{\mathcal{L}}$, we define count parameter θ_{ij} for the j -th possible child, c_{ij} , so that $P_{i,\theta}^{\mathcal{L}}(c_{ij} | x) = \theta_{ij} / \sum_{k=1}^{|c_i|} \theta_k$.

We use the following two lemmas (see source material for proof):

Lemma 2 (Proposition A.8 of Agarwal et al. [2019]). *Let z be a discrete random variable that takes values in $\{1, \dots, d\}$, distributed according to q . We write q as a vector where $\vec{q} = [Pr(z = j)]_{j=1}^d$. Assume we have n i.i.d. samples, and that our empirical estimate of \vec{q} is $[\hat{q}]_j = \sum_{i=1}^n \mathbf{1}[z_i = j] / n$. We have that $\forall \epsilon > 0$:*

$$Pr(\|\hat{q} - \vec{q}\|_2 \geq 1/\sqrt{n} + \epsilon) \leq e^{-n\epsilon^2}$$

which implies that:

$$Pr(\|\hat{q} - \vec{q}\|_1 \geq \sqrt{d}(1/\sqrt{n} + \epsilon)) \leq e^{-n\epsilon^2}$$

Lemma 3 (Corollary 1 of Strehl [2007]). *If for all states and actions, each model $P_{i,\theta}$ of P_i is ϵ/k close to the ground truth in terms of the ℓ_1 norm: $\|P_i(s, a) - P_{i,\theta}(s, a)\|_1 < \epsilon/k$, then the aggregate transition model P_θ is ϵ close to the ground truth transition model: $\|P(s, a) - P_\theta(s, a)\|_1 < \epsilon$.*

Theorem 1. *Let n be the number of empirical samples used to train the model of each local causal mechanism $P_{i,\theta}^{\mathcal{L}}$ at each configuration of parents $\text{Pa}_i = x$. There exists positive constant c such that, if*

$$n \geq \frac{ck^2 |c_i| \log(|\mathcal{S}||\mathcal{A}|/\delta)}{\epsilon^2},$$

then, with probability at least $1 - \delta$, we have:

$$\max_{(s,a)} \|P(s, a) - P_\theta(s, a)\|_1 \leq \epsilon.$$

Proof. Applying Lemma 2, we have that for fixed parents $\text{Pa}_i = x$, wp. at least $1 - \delta$,

$$\|P_i(x) - P_{i,\theta}(x)\|_1 \leq c \sqrt{\frac{|c_i| \log(1/\delta)}{n}},$$

where n is the number of independent samples used to train $P_{i,\theta}$ and c is a positive constant. Now consider a fixed (s, a) , consisting of k parent sets. Applying Lemma 3 we have that, wp. at least $1 - \delta$,

$$\|P(s, a) - P_\theta(s, a)\|_1 \leq ck \sqrt{\frac{|c_i| \log(1/\delta)}{n}}.$$

We apply the union bound across all states and actions to get that wp. at least $1 - \delta$,

$$\max_{(s,a)} \|P(s, a) - P_\theta(s, a)\|_1 \leq ck \sqrt{\frac{|c_i| \log(|\mathcal{S}||\mathcal{A}|/\delta)}{n}}.$$

The result follows by rearranging for n and relabeling c . \square

To compare to full-state dynamics modeling, we can translate the sample complexity from the per-parent count n to a total count N . Recall $m\Pi_i|c_i| = |\mathcal{S}|$, so that $|c_i| = (|\mathcal{S}|/m)^{1/k}$, and $m\Pi_i|\text{Pa}_i| \geq |\mathcal{S}||\mathcal{A}|$. We assume a small constant overlap factor $v \geq 1$, so that $|\text{Pa}_i| = v(|\mathcal{S}||\mathcal{A}|/m)^{1/k}$. We need the total number of component visits to be $n|\text{Pa}_i|km$, for a total of $nv(|\mathcal{S}||\mathcal{A}|/m)^{1/k}m$ state-action visits, assuming that parent set visits are allocated evenly, and noting that each state-action visit provides k parent set visits. This gives:

Corollary 1. *To bound the error as above, we need to have*

$$N \geq \frac{cmk^2(|\mathcal{S}|^2|\mathcal{A}|/m^2)^{1/k} \log(|\mathcal{S}||\mathcal{A}|/\delta)}{\epsilon^2},$$

total train samples, where we have absorbed the overlap factor v into constant c .

To extend this and adapt other results to our setting, we could now apply the Simulation Lemma Agarwal et al. [2019] to bound the value difference given the model error, or alternatively, develop the theory in the direction of Strehl [2007] and related work. However, we believe the core insights are already contained in Theorem 1 and Corollary 1.

C.4 Implementation Details

Code is available at <https://github.com/spitis/mocoda> (using <https://github.com/spitis/mrl> for RL algorithms). There are numerous components involved that each have several different settings that were mostly just taken “as-is” or picked as reasonable defaults (e.g., using a layer size of 512 in most neural networks, or having 5 components in the MDN, or the specific implementation of rejection sampling for Mocoda-U). The best documentation for specific details is the code itself. As such, the implementation details below cover the broad strokes so that a reader might understand the general pipeline, and we refer the reader to the provided code for precise details.

C.4.1 Causal Transition Structure and Parent Set Definitions

We implement the local causal model as a mask function M that maps (state, action) tuples to an adjacency matrix of the causal structure. For example, in 2d Navigation, the mask function was implemented as follows:

```
def Mask2dNavigation(input_tensor):
    """
    accepts B x num_sa_features, and returns B x num_parents x num_children
    """

    # base local mask
    mask = torch.tensor(
        [[1, 0],
         [0, 1],
         [1, 0],
         [0, 1]]).to(input_tensor.device)
```

```

# change local mask in top right quadrant
mask = mask[None].repeat((input_tensor.shape[0], 1, 1))
mask[torch.logical_and(input_tensor[:,0] > 0.5, input_tensor[:, 1] > 0.5)] = 1

return mask

```

As an example, the causal graph for the base local mask, which applies for most of the state space is shown in the figure C.2. We used the base local graph to select the parent sets, in this case, $(x, \Delta x)$ and $(y, \Delta y)$.

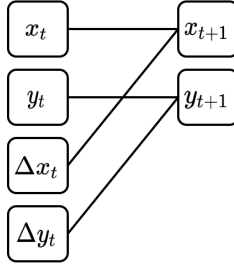


Figure C.2: Causal graph for local mask

C.4.2 Parent Distribution

To sample the parent distribution in Step 1 of MoCoDA, we use the Gaussian Mixture Model (GMM) based approach described in the main text. The advantage of this approach is that we can easily do conditional sampling in case of overlapping parent sets. For a given local subset \mathcal{L} , we fit a separate GMM to the marginal of each parent set, as it appears in the empirical distribution for \mathcal{L} . To generate a new sample, we optionally shuffle the GMMs, and then sample from one GMM at a time, conditioning on any already generated features. This process eliminates any spurious correlations between features that are not part of the same parent set, and thus results in the maximum-entropy, marginal matching distribution.

In cases of multiple local neighborhoods, $\mathcal{L}_1, \mathcal{L}_2, \dots$, one should respect the boundaries of the current local subset \mathcal{L} during both training *and* generation. If a sample generated with the GMM for \mathcal{L} falls outside of \mathcal{L} , that sample should be rejected, as the local causal structure is no longer valid, and the generalization guarantee for the locally factored model no longer holds.

As the local factorization in our experiments is quite simple, we did not stratify the GMM generator, and instead used a single GMM generator for the sparsest local causal structure. In the case of 2d Navigation this did not generate any data that was out-of-distribution for the locally factored model components (as the agent’s policy was consistent in all local neighborhoods). In the case of HookSweep2, there was a bit of locally out-of-distribution data in the local subspace in which there is a block collision; however, most of this data is unreachable as it involves overlapping blocks, and we obtained strong results even with this shortcut.

C.4.3 Dynamics Models

Our experiments used three different dynamics models. In each case, we used an ensemble of 5 base models, described below. The base models output a Gaussian mean and variance for each output variable and are trained independently via a negative log likelihood loss. All models are trained using Adam Optimizer Kingma and Ba [2015].

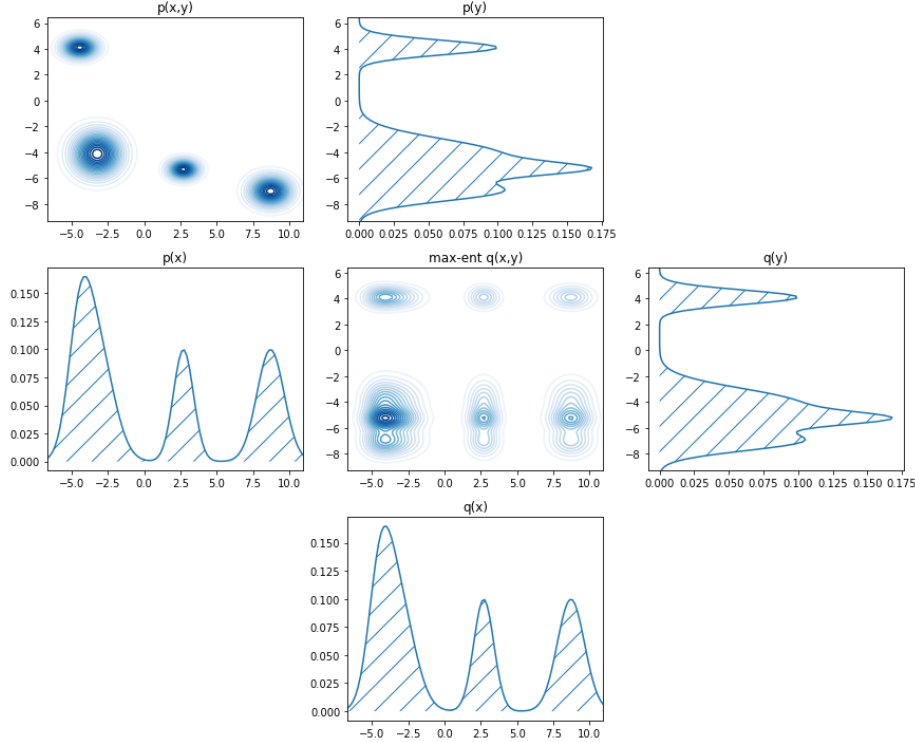


Figure C.3: Hypothetical 2D illustration of the GMM-based parent set sampler. It is assumed that there are two non-overlapping parent sets $\{x\}$ and $\{y\}$, but that x and y exhibit dependence in the empirical data. We fit a GMM to each marginal $P(x)$ and $P(y)$ and sample from them independently to get $Q(x, y)$, which has the same marginal distributions (so that the components in a locally factored dynamics model will generalize), but eliminates the spurious dependence in the empirical data.

1. **Unfactored:** The base model is a fully connected neural network with ReLU activations (MLP).
2. **Globally Factored:** The base model has one MLP for each causal mechanism in the sparsest local graph. For both 2d Navigation and HookSweep2 the sparsest local graph has two components, so the base global model is composed of two MLPs.
3. **Locally factored:** The base model is designed as follows. For each child node, c_i , there is a separately parameterized single MLP that is preceded by a “Masked Composer” module. The Masked Composer applies a single layer MLP (linear transform followed by ReLU) to each root node, r_i (each parent set has several nodes), to obtain embeddings $\varepsilon_i(r_i)$. The i -th column of the mask is used to zero out the corresponding embeddings which are then summed, $\sum_i M_{ij}\varepsilon_i(r_i)$, and the result is passed as an input to the MLP.

This architecture works (and enforces local factorization), but is likely poor, because it does not take advantage of potentially useful shared representations between parent nodes across children (since there is a separately parameterized Masked Composer for each child). A better architecture would likely use a single parameterization for a single, possibly deeper Masked Composer. As this is not the focus of our contribution, we stuck with simple model, as it “just worked” for purposes of our experiments.

C.4.4 Training Data for the RL Algorithm

This varied by experiment, and is described in the next Section. Notably, we divided the standard deviation returned by our dynamics models by a factor of three when generating data to avoid data that was too far out of distribution.

C.4.5 Reinforcement Learning Algorithms

We use Modular RL Pitis et al. [2020a], adding three offline RL Levine et al. [2020] algorithms: BCQ [Fujimoto et al., 2019], CQL [Kumar et al., 2020b] & TD3-BC [Fujimoto and Gu, 2021].

The BCQ implementation uses DDPG Lillicrap et al. [2015]. For the generative model we use a Mixture Density Network (MDN) Bishop [1994] with 5 components, that produces 20 action samples at each call (both during test rollouts and when creating critic targets). The MDN was trained for 1000 batches with batch size of 2000. We did not use a perturbation model.

The CQL implementation uses SAC Haarnoja et al. [2018]. Rewards in our environments are sparse, and so value targets can be accurately clipped between two values (depends on the discount factor). CQL balances two losses: a penalty for Q-values of some non-behavioral distribution/policy (we use a random policy), and a bonus for the Q-values behavioral actions. We use an L1 penalty toward the lower end of the value target clipping range, and an L1 bonus toward the higher end of the value target clipping range. We then multiply that by a minimum Q coefficient, as in the original CQL implementation.

The TD3-BC implementation follows Fujimoto and Gu [2021].

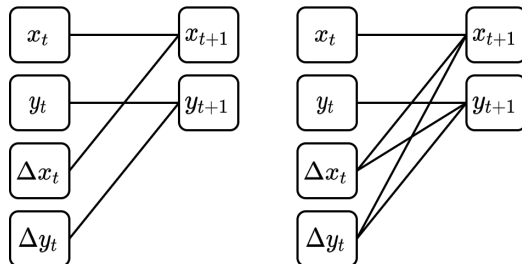
C.5 Experimental Details

C.5.1 2D Navigation

In this environment, the agent must travel from one point in a square arena to another. States are 2D (x, y) coordinates and actions are 2D $(\Delta x, \Delta y)$ vectors.

```
observation_space = spaces.Box(np.zeros((2,)), np.ones((2,)), dtype=np.float32)
action_space = spaces.Box(-np.ones((2,)), np.ones((2,)), dtype=np.float32)
```

Episodes run for up to 70 steps. Rewards are sparse, with a -1 reward everywhere except the goal, where reward is 0. In most of the state space, the sub-actions Δx and Δy affect only their respective coordinate. In the top right quadrant, however, the Δx and Δy sub-actions each affect *both* x and y coordinates, so that the environment is locally factored. The two causal graphs are as follows:



The graph on the right applies only in the top-right quadrant; otherwise the graph on the left applies. The graph on the left has non-overlapping parent sets $(x, \Delta x)$ and $(y, \Delta y)$. The graph on the right has overlapping parent sets $(x, \Delta x, \Delta y)$ and $(y, \Delta x, \Delta y)$.

The agent has access to an empirical dataset consisting of left-to-right & bottom-to-top trajectories (20,000 transitions of each type):

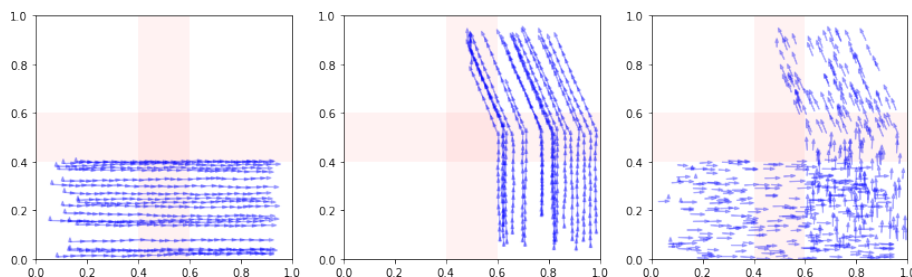


Figure C.4: **Left/Middle:** Random samples of the two types of trajectories the agent has access to. **Right:** Random sample of transitions from this empirical dataset.

We consider a target task where the agent must move from the bottom left to the top right. In this task there is sufficient empirical data to solve the task by following the \perp shape of the data, but learning the optimal policy of going directly via the diagonal requires out-of-distribution generalization.

For 2d Navigation, we generated the MOCODA distribution by fitting a GMM generator as described in the previous Section. Each GMM (one for each parent set) had 32 components, and was fit using expectation maximization. To obtain MOCODA-U, we implemented rejection sampling by using a KDE density estimator as follows:

```
def prune_to_uniform(proposals, target_size=12000.):
    from sklearn.neighbors import KernelDensity
    sample = proposals[-10000:]

    fmap = lambda s: s[:, :2]
    K = KernelDensity(bandwidth=0.05)
    K.fit(fmap(sample))
    scores = K.score_samples(fmap(proposals))
    scores = np.maximum(scores, np.log(0.01))
    scores = (1. / np.exp(scores))
    scores = scores / scores.mean() * (target_size / len(proposals))

    return proposals[np.random.uniform(size=scores.shape) < scores]
```

The dynamics models each had 2 layers of 256 neurons and were trained with a batch size of 512

and learning rate of $1e-4$. Hyperparameters were not tuned once a working setting was found. Of the 40K empirical samples, 35K were used for training, and 5000 for validation. The models were trained for 600 epochs, with early stopping used in the last 50 epochs to find a locally optimal stopping point.

Augmented datasets of 200K samples were generated. In each case except EMP, 40K were the original empirical dataset (thus 160K new samples were generated by applying the dynamics model to samples from the augmented distribution). In case of EMP, the 40K original samples were simply repeated 5 times to get a size 200K dataset. The locally factored network was used to generate the augmented datasets.

These augmented distributions were then used to train the downstream RL agents. The agent algorithms used a discount factor of 0.98, a target cutoff range of $(-50, 0)$, batch size of 500, and used 2 layers of 512 neurons in both actor and critic networks. The agents were trained for 25K batches (for a total of 62.5 passes over the dataset).

For 2D Navigation we ran 5 seeds, which all yielded similar results. For each seed we trained new parent set samplers and generated new augmented datasets.

C.5.2 HookSweep2

HookSweep2 is a challenging robotics domain based on Hook-Sweep [Kurenkov et al., 2020], in which a Fetch robot must use a long hook to sweep two boxes to one side of the table (either toward or away from the agent). States, excluding the goal, are 16 dimensional continuous vectors. Goals are 6 dimensions. The agents all concatenate the goal to the state, and so operate on 22 dimensional states. The action space is a 4 dimensional continuous vector.

The environment contains two boxes that are initialized near the center of the table.

The empirical data contains 1M transitions from trajectories of an expert agent sweeping exactly one box to one side of the table, leaving the other in the center. The target task requires the agent to sweep *both* boxes together to one side of the table. This is particularly challenging because the setup is entirely offline (no exploration), where poor out-of-distribution generalization typically requires special offline RL algorithms that constrain the agent’s policy to the empirical distribution [Agarwal et al., 2020, Fujimoto and Gu, 2021, Kumar et al., 2020b, Levine et al., 2020].

Episodes run for 75 steps. Rewards are dense, but structured similarly to a sparse reward, with a base reward of -1 everywhere except the goal and a reward of 0 at the goal. Additional small rewards are given if the agent keeps the hook near the table (this was required to obtain natural movements from the trained expert agent).

In this environment, *we did not have the ground truth causal graph*, and so a heuristic was used. The heuristic (wrongly) assumes that the agent/hook *always* causes each of the next object position (hook and objects are always entangled), even though this is only true when the hook and the objects are touching. The heuristic considers the two boxes to be separate whenever they are further than 5cm from each other. Here is the implementation of the heuristic:

```
def MaskHookSweep2(input_tensor):

    # base local mask for when boxes are far apart
    mask = torch.tensor(
        [[1, 1, 1],
         [1, 1, 0],
         [1, 0, 1],
         [1, 1, 1]]
```

```

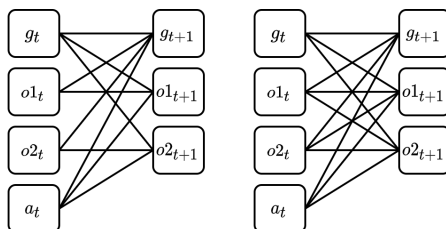
    ).to(input_tensor.device)
    mask = mask[None].repeat((input_tensor.shape[0], 1, 1))

    # change local mask when boxes are close to each other
    mask[torch.sum(torch.abs(input_tensor[:,01X:01X+2] - \
        input_tensor[:,02X:02X+2]), axis=1) < 0.05] = 1

    return mask

```

where the state-action components are (gripper, box1, box2, action). This heuristic returns the following two causal graphs (note that goals are not part of the dynamics, and are separately labeled using random goal samples from the environment):



The parent sets are $(g, o1, a)$ and $(g, o2, a)$ for the first graph, and $(g, o1, o2, a)$ in the second graph.

For `HookSweep2`, the generation of the MOCODA distribution is identical to how it was generated in `2d Navigation` (see previous subsection). To obtain MOCODA-P, we implemented rejection sampling as follows:

```

def prune_to_uniform2(proposals, target_size=12000., smaller=True):
    proposals = proposals[np.linalg.norm(proposals[:,01X:01X+2] - proposals[:,02X:02X+2], axis=-1) < 0.3]
    sample = proposals[-5000:]

    fmap = lambda s: s[:,[01X,01X+1,02X,02X+1]]
    K = KernelDensity(bandwidth=0.05)
    K.fit(fmap(sample))
    scores = K.score_samples(fmap(proposals))
    scores = np.maximum(scores, np.log(0.05))
    scores = (1. / np.exp(scores))
    if np.minimum(scores, 1).sum() > 10000:
        while np.minimum(scores, 1).sum() > 10000:
            scores = scores * 0.99
        else:
            while np.minimum(scores, 1).sum() < 10000:
                scores = scores / 0.99

    return proposals[np.random.uniform(size=scores.shape) < scores]

```

The key difference to the `2d Navigation` is the definition of the `fmap` function, which defines the feature map under which the density is computed for rejection sampling.

The dynamics models for `HookSweep2` each had 2 layers of 512 neurons and were trained with a batch size of 512 and learning rate of $2e-4$. Hyperparameters were not tuned once a working setting was found (learning rate was increased to make training slightly faster). Of 1M empirical samples, 5000 were used for validation. The models were trained for 4000 epochs, where each epoch involved 40K random samples, with early stopping used in the last 50 epochs to find a locally optimal stopping point.

Augmented datasets of 5M samples were generated. In each case except EMP, 1M were the original empirical dataset (thus 4M new samples were generated). In the case of EMP, the 1M original samplers were simply repeated 5 times to get the full augmented dataset. The locally factored network was used to generate the augmented datasets.

These augmented distributions were then used to train the downstream RL agents. The agent algorithms were the same as for 2d *Navigation*, except that they used 3 layers of 512 neurons in both actor and critic networks. The agents were trained for 1M steps with batch size 500 (for a total of 100 passes over the dataset).

C.6 MoCoDA sampling pseudocode

Algorithm 4 shows the pseudocode for MoCoDA sampling for a FMDP, where the causal structure of the transition dynamics is assumed known. For simplicity of exposition we describe the case where each “factor” in the factorized dynamics is modeled using an MLP, which corresponds to the “Globally Factored” model architecture referred to in Table 4.2. Realizing the “Locally Factored” architecture is simply a matter of replacing $\text{MLP}(\cdot)$ in the pseudocode with $(\text{MLP} \circ \text{MaskedComposer})(\cdot)$ described in Section C.4.3.

Implementing MoCoDA sampling for a Local Causal Model rather than an FMDP is also a straightforward extension. The dynamics modeling is the same (but for the dynamics being conditioned on \mathcal{L}). The parent sampling procedure is described in C.4.2.

Algorithm 4 MoCoDA for FMDPs, assuming hand-specified dynamics factorization

```

1: function GENERATEMOCODADATA(N):
2:   Input: observed transition dataset  $(s, a, s') \in \mathcal{D}$ 
3:   Input: causal structure of transition dynamics  $\mathcal{G} := \{(i, \text{Pa}(i)) \forall i \in N_s\}$  a.k.a. “parent sets”
4:     NOTE:  $\text{Pa}(i)$  is shorthand for  $\{j : s_j \in \text{CausalParent}(s'_i)\}$ 
5:     NOTE:  $\text{Pa}(i) \subset [N_s + N_a]$  can index into states or actions
6:    $\mathcal{D}_{tr}, \mathcal{D}_{va} = \text{train\_val\_split}(\mathcal{D})$  ▷ Split data
7:    $\theta := \text{TRAINGMMPARENTSMODEL}(\mathcal{D}_{tr}, \mathcal{D}_{va}, \mathcal{G})$  ▷ train GMM parent distribution  $P_\theta(s, a)$ 
8:    $\phi := \text{TRAINFACTOREDYNAMICS}(\mathcal{D}_{tr}, \mathcal{D}_{va}, \mathcal{G})$  ▷ train factored dynamics model  $P_\phi(s'|s, a)$ 
9:   return SAMPLEAUGMENTEDDATASET(N,  $\theta$ ,  $\phi$ ,  $\mathcal{G}$ )

10: function TRAINGMMPARENTSMODEL( $\mathcal{D}_{tr}, \mathcal{D}_{va}, \mathcal{G}$ ):
11:   for  $(i, \text{Pa}(i)) \in \mathcal{G}$  : do ▷ iterate over parent sets for each child
12:      $\{\mu_{\text{Pa}(i)}^k, \Sigma_{\text{Pa}(i)}^k, \gamma_{\text{Pa}(i)}^k\} = \text{init\_gmm\_params}(N_k)$  ▷ NOTE: only for this parent set
13:      $\mathcal{D}_{\text{Pa}(i)}^{tr}(s, a) := \{(s[\text{Pa}(i)], a[\text{Pa}(i)\%N_s]) \forall (s, a, s') \in \mathcal{D}^{tr}\}$ 
14:      $\mathcal{D}_{\text{Pa}(i)}^{va}(s, a) := \{(s[\text{Pa}(i)], a[\text{Pa}(i)\%N_s]) \forall (s, a, s') \in \mathcal{D}^{va}\}$  ▷ subsample relevant dims
15:     while not_converged(GMM( $\cdot$ ;  $\mu_{\text{Pa}(i)}^k, \Sigma_{\text{Pa}(i)}^k, \gamma_{\text{Pa}(i)}^k$ ),  $\mathcal{D}_{\text{Pa}(i)}^{va}(s, a)$ ) do
16:        $\{\mu_{\text{Pa}(i)}^k, \Sigma_{\text{Pa}(i)}^k, \gamma_{\text{Pa}(i)}^k\} \leftarrow \text{update\_gmm\_params}(\{\mu_{\text{Pa}(i)}^k, \Sigma_{\text{Pa}(i)}^k, \gamma_{\text{Pa}(i)}^k\}, \mathcal{D}_{\text{Pa}(i)}^{tr}(s, a))$ 
17:      $\theta.\text{append}(\{\mu_{\text{Pa}(i)}^k, \Sigma_{\text{Pa}(i)}^k, \gamma_{\text{Pa}(i)}^k\})$ 
18:   return  $\theta$ 

19: function TRAINFACTOREDYNAMICS( $\mathcal{D}_{tr}, \mathcal{D}_{va}, \mathcal{G}$ ):
20:   for  $(i, \text{Pa}(i)) \in \mathcal{G}$  : do ▷ iterate over parent sets for each child
21:      $\phi_i = \text{init\_mlp\_params}()$  ▷ NOTE: only for this parent set
22:      $\mathcal{D}_{\text{Pa}(i)}^{tr}(s, a, s') := \{(s[\text{Pa}(i)], a[\text{Pa}(i)\%N_s], s'[i]) \forall (s, a, s') \in \mathcal{D}^{tr}\}$ 
23:      $\mathcal{D}_{\text{Pa}(i)}^{va}(s, a, s') := \{(s[\text{Pa}(i)], a[\text{Pa}(i)\%N_s], s'[i]) \forall (s, a, s') \in \mathcal{D}^{va}\}$  ▷ subsample relevant dims
24:     while not_converged(MLP( $\cdot$ ;  $\phi_i$ ),  $\mathcal{D}_{\text{Pa}(i)}^{va}(s, a, s')$ ) do
25:        $\phi_i \leftarrow \text{update\_mlp\_params}(\phi_i, \mathcal{D}_{\text{Pa}(i)}^{tr}(s, a, s'))$ 
26:   return  $\phi$ 

27: function SAMPLEAUGMENTEDDATA(N,  $\theta$ ,  $\phi$ ,  $\mathcal{G}$ )
28:   for  $\_ \in \text{range}(N)$ : do
29:     ▷ sample parent data, i.e.  $(\tilde{s}, \tilde{a})$ : sequentially sample the parent set GMMs, conditioning
30:     ▷ each GMM on previous samples to handle any overlap between parent sets
31:      $\mathcal{AS} := \{\}$  ▷ define an “already sampled” set to track any parent set overlap
32:      $\tilde{s} := []$ ;  $\tilde{a} := []$ 
33:     for  $i \in \text{range}(N_s)$ : do
34:       if  $\text{Pa}(i) \cap \mathcal{AS} = \emptyset$  : then ▷ no vars in this parent set already sampled
35:          $(\tilde{s}_{\text{Pa}(i)}, \tilde{a}_{\text{Pa}(i)}) \sim \text{GMM}(\cdot; \mu_{\text{Pa}(i)}^k, \Sigma_{\text{Pa}(i)}^k, \gamma_{\text{Pa}(i)}^k)$ 
36:          $\tilde{s}.\text{extend}(\tilde{s}_{\text{Pa}(i)})$ 
37:          $\tilde{a}.\text{extend}(\tilde{a}_{\text{Pa}(i)})$ 
38:       else ▷ some vars in this parent set already sampled and must be conditioned on
39:         condition this GMM already-sampled vars, then sample remaining vars
40:          $(\tilde{s}_{\text{Pa}(i) \setminus \mathcal{AS}}, \tilde{a}_{\text{Pa}(i) \setminus \mathcal{AS}}) \sim \text{GMM}(\cdot | \mathcal{AS}; \mu_{\text{Pa}(i)}^k, \Sigma_{\text{Pa}(i)}^k, \gamma_{\text{Pa}(i)}^k)$ 
41:         NOTE: this sampling is easily realized by conditioning each Gaussian component
42:         and updating mixture components in proportion to density of already-sampled vars
43:          $\tilde{s}.\text{extend}(\tilde{s}_{\text{Pa}(i) \setminus \mathcal{AS}})$ 
44:          $\tilde{a}.\text{extend}(\tilde{a}_{\text{Pa}(i) \setminus \mathcal{AS}})$ 
45:        $\mathcal{AS} \leftarrow \mathcal{AS} \cup \text{Pa}(i)$ 
46:     ▷ sample next states, i.e.  $\tilde{s}' | (\tilde{s}, \tilde{a})$ : sequentially sample each “factor” in the factorized dynamics
47:      $\tilde{s}' := []$ 
48:     for  $i \in \text{range}(N_s)$ : do
49:        $\tilde{s}'_i \sim \text{MLP}(\cdot | \tilde{s}, \tilde{a}; \phi_i)$ 
50:      $\tilde{s}'.\text{append}(\tilde{s}'_i)$ 
51:     ▷ assemble transition
52:      $\tilde{s} = \text{array}(\tilde{s}); \tilde{a} = \text{array}(\tilde{a}); \tilde{s}' = \text{array}(\tilde{s}')$ 
53:      $\tilde{\mathcal{D}}.\text{append}((\tilde{s}, \tilde{a}, \tilde{s}'))$ 
54:   return  $\tilde{\mathcal{D}}$ 

```

Bibliography

- Andrew Abbott. *Chaos of disciplines*. University of Chicago Press, 2010.
- J Khadijah Abdurahman. Fat* be wilin', 2019.
- Tameem Adel, Isabel Valera, Zoubin Ghahramani, and Adrian Weller. One-network adversarial fairness. In *Proceedings of the AAAI Conference on Artificial Intelligence*, volume 33, pages 2412–2420, 2019.
- Alekh Agarwal, Nan Jiang, Sham M Kakade, and Wen Sun. Reinforcement learning: Theory and algorithms. *CS Dept., UW Seattle, Seattle, WA, USA, Tech. Rep*, 2019.
- Chirag Agarwal, Himabindu Lakkaraju, and Marinka Zitnik. Towards a unified framework for fair and stable graph representation learning. In *Uncertainty in Artificial Intelligence*, pages 2114–2124. PMLR, 2021.
- Rishabh Agarwal, Dale Schuurmans, and Mohammad Norouzi. An optimistic perspective on offline reinforcement learning. In *International Conference on Machine Learning*, pages 104–114. PMLR, 2020.
- Faruk Ahmed, Yoshua Bengio, Harm van Seijen, and Aaron Courville. Systematic generalisation with group invariant predictions. In *International Conference on Learning Representations*, 2021.
- Ulrich Aivodji, Hiromi Arai, Olivier Fortineau, Sébastien Gambs, Satoshi Hara, and Alain Tapp. Fairwashing: the risk of rationalization. In *Proceedings of the 36th International Conference on Machine Learning*, pages 161–170. PMLR, May 2019. ISSN: 2640-3498.
- Alexander Alemi, Ben Poole, Ian Fischer, Joshua Dillon, Rif A Saurous, and Kevin Murphy. Fixing a broken elbo. In *International Conference on Machine Learning*, pages 159–168, 2018.
- Marcin Andrychowicz, Filip Wolski, Alex Ray, Jonas Schneider, Rachel Fong, Peter Welinder, Bob McGrew, Josh Tobin, OpenAI Pieter Abbeel, and Wojciech Zaremba. Hindsight experience replay. In *Advances in neural information processing systems*, pages 5048–5058, 2017.
- OpenAI: Marcin Andrychowicz, Bowen Baker, Maciek Chociej, Rafal Jozefowicz, Bob McGrew, Jakub Pachocki, Arthur Petron, Matthias Plappert, Glenn Powell, Alex Ray, et al. Learning dexterous in-hand manipulation. *The International Journal of Robotics Research*, 39(1):3–20, 2020.
- Martin Arjovsky, Léon Bottou, Ishaan Gulrajani, and David Lopez-Paz. Invariant risk minimization. *arXiv preprint arXiv:1907.02893*, 2019.

- Jimmy Lei Ba, Jamie Ryan Kiros, and Geoffrey E Hinton. Layer normalization. *arXiv preprint arXiv:1607.06450*, 2016.
- Francis R Bach and Michael I Jordan. Kernel independent component analysis. *Journal of machine learning research*, 3(Jul):1–48, 2002.
- Dzmitry Bahdanau, Shikhar Murty, Michael Noukhovitch, Thien Huu Nguyen, Harm de Vries, and Aaron Courville. Systematic generalization: what is required and can it be learned? In *International Conference of Machine Learning*, 2019.
- Elias Bareinboim and Judea Pearl. Controlling selection bias in causal inference. In *Artificial Intelligence and Statistics*, pages 100–108, 2012.
- Elias Bareinboim, Jin Tian, and Judea Pearl. Recovering from selection bias in causal and statistical inference. In *AAAI*, pages 2410–2416. Citeseer, 2014.
- Solon Barocas and Andrew D Selbst. Big data’s disparate impact. *Calif. L. Rev.*, 104:671, 2016a.
- Solon Barocas and Andrew D. Selbst. Big Data’s Disparate Impact. *California Law Review*, 104(3): 671–732, 2016b. Publisher: California Law Review, Inc.
- Solon Barocas, Kate Crawford, Aaron Shapiro, and Hanna Wallach. The problem with bias: Allocative versus representational harms in machine learning. In *9th Annual conference of the special interest group for computing, information and society*, 2017.
- Solon Barocas, Asia J. Biega, Benjamin Fish, Jędrzej Niklas, and Luke Stark. When not to design, build, or deploy. In *Proceedings of the 2020 Conference on Fairness, Accountability, and Transparency*, pages 695–695, Barcelona Spain, January 2020. ACM.
- Peter L. Bartlett, Philip M. Long, Gábor Lugosi, and Alexander Tsigler. Benign overfitting in linear regression. *Proceedings of the National Academy of Sciences*, 117(48):30063–30070, December 2020.
- Yahav Bechavod and Katrina Ligett. Learning fair classifiers: A regularization-inspired approach. *arXiv preprint arXiv:1707.00044*, 2017.
- Stafford Beer. What is cybernetics? *Kybernetes*, 31(2):209–219, January 2002. Publisher: MCB UP Ltd.
- Sara Beery, Grant Van Horn, and Pietro Perona. Recognition in terra incognita. In *Proceedings of the European Conference on Computer Vision*, pages 456–473, 2018a.
- Sara Beery, Grant Van Horn, and Pietro Perona. Recognition in Terra Incognita. In Vittorio Ferrari, Martial Hebert, Cristian Sminchisescu, and Yair Weiss, editors, *Computer Vision – ECCV 2018*, volume 11220, pages 472–489. Springer International Publishing, Cham, 2018b. Series Title: Lecture Notes in Computer Science.
- Rachel K. E. Bellamy, Kuntal Dey, Michael Hind, Samuel C. Hoffman, Stephanie Houde, Kalapriya Kannan, Pranay Lohia, Jacquelyn Martino, Sameep Mehta, Aleksandra Mojsilovic, Seema Nagar, Karthikeyan Natesan Ramamurthy, John Richards, Diptikalyan Saha, Prasanna Sattigeri, Moninder Singh, Kush R. Varshney, and Yunfeng Zhang. AI Fairness 360: An Extensible Toolkit for Detecting, Understanding, and Mitigating Unwanted Algorithmic Bias, October 2018. arXiv:1810.01943 [cs].

- Marc G Bellemare, Yavar Naddaf, Joel Veness, and Michael Bowling. The arcade learning environment: An evaluation platform for general agents. *Journal of Artificial Intelligence Research*, 47:253–279, 2013.
- Richard E Bellman. *Dynamic programming*. Princeton university press, 1957.
- Shai Ben-David, Philip M. Long, and Yishay Mansour. Agnostic Boosting. In G. Goos, J. Hartmanis, J. Van Leeuwen, David Helmbold, and Bob Williamson, editors, *Computational Learning Theory*, volume 2111, pages 507–516. Springer Berlin Heidelberg, Berlin, Heidelberg, 2001. Series Title: Lecture Notes in Computer Science.
- Shai Ben-David, John Blitzer, Koby Crammer, Alex Kulesza, Fernando Pereira, and Jennifer Wortman Vaughan. A theory of learning from different domains. *Machine Learning*, 79(1-2):151–175, 2010.
- A. Ben-Tal, Laurent El Ghaoui, and A. S. Nemirovskii. *Robust optimization*. Princeton series in applied mathematics. Princeton University Press, Princeton, 2009a. OCLC: ocn318672208.
- Aharon Ben-Tal, Laurent El Ghaoui, and Arkadi Nemirovski. *Robust Optimization*, volume 28. Princeton University Press, 2009b.
- Emily M. Bender, Timnit Gebru, Angelina McMillan-Major, and Shmargaret Shmitchell. On the Dangers of Stochastic Parrots: Can Language Models Be Too Big? In *Proceedings of the 2021 ACM Conference on Fairness, Accountability, and Transparency*, pages 610–623, Virtual Event Canada, March 2021. ACM.
- Yoshua Bengio, Aaron Courville, and Pascal Vincent. Representation learning: A review and new perspectives. *IEEE transactions on pattern analysis and machine intelligence*, 35(8):1798–1828, 2013a.
- Yoshua Bengio, Aaron Courville, and Pascal Vincent. Representation Learning: A Review and New Perspectives. *IEEE Transactions on Pattern Analysis and Machine Intelligence*, 35(8):1798–1828, August 2013b. Conference Name: IEEE Transactions on Pattern Analysis and Machine Intelligence.
- Alex Beutel, Jilin Chen, Zhe Zhao, and Ed H Chi. Data decisions and theoretical implications when adversarially learning fair representations. In *4th Workshop on Fairness, Accountability, and Transparency in Machine Learning (FAT/ML 2017)*, 2017.
- Alex Beutel, Jilin Chen, Tulsee Doshi, Hai Qian, Allison Woodruff, Christine Luu, Pierre Kreitmann, Jonathan Bischof, and Ed H. Chi. Putting Fairness Principles into Practice: Challenges, Metrics, and Improvements. In *Proceedings of the 2019 AAAI/ACM Conference on AI, Ethics, and Society*, pages 453–459, Honolulu HI USA, January 2019. ACM.
- Federico Bianchi, Pratyusha Kalluri, Esin Durmus, Faisal Ladhak, Myra Cheng, Debora Nozza, Tatsunori Hashimoto, Dan Jurafsky, James Zou, and Aylin Caliskan. Easily Accessible Text-to-Image Generation Amplifies Demographic Stereotypes at Large Scale. In *2023 ACM Conference on Fairness, Accountability, and Transparency*. arXiv, June 2023. arXiv:2211.03759 [cs].
- Battista Biggio, Blaine Nelson, and Pavel Laskov. Poisoning Attacks against Support Vector Machines, March 2013. arXiv:1206.6389 [cs, stat].

- Reuben Binns. Fairness in machine learning: Lessons from political philosophy. In *Conference on fairness, accountability and transparency*, pages 149–159. PMLR, 2018.
- Abeba Birhane and Vinay Uday Prabhu. Large image datasets: A pyrrhic win for computer vision? In *2021 IEEE Winter Conference on Applications of Computer Vision (WACV)*, pages 1536–1546. IEEE, 2021.
- Abeba Birhane, Pratyusha Kalluri, Dallas Card, William Agnew, Ravit Dotan, and Michelle Bao. The values encoded in machine learning research. In *2022 ACM Conference on Fairness, Accountability, and Transparency*, pages 173–184, 2022.
- Christopher M Bishop. Mixture density networks. 1994.
- Gilles Blanchard, Gyemin Lee, and Clayton Scott. Generalizing from Several Related Classification Tasks to a New Unlabeled Sample. In *Advances in Neural Information Processing Systems*, volume 24. Curran Associates, Inc., 2011.
- David M Blei. Topic modeling and digital humanities. *Journal of Digital Humanities*, 2(1):8–11, 2012.
- John Blitzer, Ryan McDonald, and Fernando Pereira. Domain adaptation with structural correspondence learning. In *Proceedings of the 2006 conference on empirical methods in natural language processing*, pages 120–128. Association for Computational Linguistics, 2006.
- Su Lin Blodgett and Brendan O’Connor. Racial disparity in natural language processing: A case study of social media african-american english. *arXiv preprint arXiv:1707.00061*, 2017.
- Tolga Bolukbasi, Kai-Wei Chang, James Y Zou, Venkatesh Saligrama, and Adam T Kalai. Man is to computer programmer as woman is to homemaker? debiasing word embeddings. In *Advances in Neural Information Processing Systems*, pages 4349–4357, 2016.
- Rishi Bommasani, Drew A Hudson, Ehsan Adeli, Russ Altman, Simran Arora, Sydney von Arx, Michael S Bernstein, Jeannette Bohg, Antoine Bosselut, Emma Brunskill, et al. On the opportunities and risks of foundation models. *arXiv preprint arXiv:2108.07258*, 2021.
- Daniel Borkan, Lucas Dixon, Jeffrey Sorensen, Nithum Thain, and Lucy Vasserman. Nuanced metrics for measuring unintended bias with real data for text classification. In *Companion proceedings of the 2019 world wide web conference*, pages 491–500, 2019.
- Avishek Joey Bose and William L. Hamilton. Compositional fairness constraints for graph embeddings. *Relational Representation Learning Workshop, Neural Information Processing Systems 2018*, 2018.
- Philip Botros and Jakub M Tomczak. Hierarchical vampprior variational fair auto-encoder. In *ICML 2018 Workshop on Theoretical Foundations and Applications of Deep Generative Models*, 2018.
- Craig Boutilier, Richard Dearden, Moises Goldszmidt, et al. Exploiting structure in policy construction. In *IJCAI*, volume 14, pages 1104–1113, 1995.
- Craig Boutilier, Nir Friedman, Moises Goldszmidt, and Daphne Koller. Context-specific independence in bayesian networks. *arXiv preprint arXiv:1302.3562*, 2013.

- George EP Box. Science and statistics. *Journal of the American Statistical Association*, 71(356): 791–799, 1976.
- G.E.P. Box. Robustness in the Strategy of Scientific Model Building. In *Robustness in Statistics*, pages 201–236. Elsevier, 1979.
- Greg Brockman, Vicki Cheung, Ludwig Pettersson, Jonas Schneider, John Schulman, Jie Tang, and Wojciech Zaremba. Openai gym. *arXiv preprint arXiv:1606.01540*, 2016.
- Tom B. Brown, Benjamin Mann, Nick Ryder, Melanie Subbiah, Jared Kaplan, Prafulla Dhariwal, Arvind Neelakantan, Pranav Shyam, Girish Sastry, Amanda Askell, Sandhini Agarwal, Ariel Herbert-Voss, Gretchen Krueger, Tom Henighan, Rewon Child, Aditya Ramesh, Daniel M. Ziegler, Jeffrey Wu, Clemens Winter, Christopher Hesse, Mark Chen, Eric Sigler, Mateusz Litwin, Scott Gray, Benjamin Chess, Jack Clark, Christopher Berner, Sam McCandlish, Alec Radford, Ilya Sutskever, and Dario Amodei. Language Models are Few-Shot Learners, July 2020. arXiv:2005.14165 [cs].
- Lukas Brunke, Melissa Greeff, Adam W. Hall, Zhaocong Yuan, Siqi Zhou, Jacopo Panerati, and Angela P. Schoellig. Safe Learning in Robotics: From Learning-Based Control to Safe Reinforcement Learning, December 2021. arXiv:2108.06266 [cs, eess].
- Lars Buesing, Theophane Weber, Yori Zwols, Sebastien Racaniere, Arthur Guez, Jean-Baptiste Lespiau, and Nicolas Heess. Woulda, coulda, shoulda: Counterfactually-guided policy search. *International Conference on Learning Representations*, 2019.
- Joy Buolamwini and Timnit Gebru. Gender shades: Intersectional accuracy disparities in commercial gender classification. In *Conference on Fairness, Accountability and Transparency*, pages 77–91, 2018a.
- Joy Buolamwini and Timnit Gebru. Gender Shades: Intersectional Accuracy Disparities in Commercial Gender Classification. In *Proceedings of the 1st Conference on Fairness, Accountability and Transparency*, pages 77–91. PMLR, January 2018b. ISSN: 2640-3498.
- Christopher P Burgess, Irina Higgins, Arka Pal, Loic Matthey, Nick Watters, Guillaume Desjardins, and Alexander Lerchner. Understanding disentangling in β -VAE. In *2017 NIPS Workshop on Learning Disentangled Representations*, 2017.
- Christopher P Burgess, Loic Matthey, Nicholas Watters, Rishabh Kabra, Irina Higgins, Matt Botvinick, and Alexander Lerchner. Monet: Unsupervised scene decomposition and representation. *arXiv preprint arXiv:1901.11390*, 2019.
- Toon Calders and Sicco Verwer. Three naive bayes approaches for discrimination-free classification. *Data Mining and Knowledge Discovery*, 21(2):277–292, 2010.
- Flavio Calmon, Dennis Wei, Bhanukiran Vinzamuri, Karthikeyan Natesan Ramamurthy, and Kush R Varshney. Optimized pre-processing for discrimination prevention. In *Advances in Neural Information Processing Systems*, pages 3992–4001, 2017.

- Micah D Carroll, Anca Dragan, Stuart Russell, and Dylan Hadfield-Menell. Estimating and penalizing induced preference shifts in recommender systems. In *International Conference on Machine Learning*, pages 2686–2708. PMLR, 2022.
- Chun-Hao Chang, Elliot Creager, Anna Goldenberg, and David Duvenaud. Explaining Image Classifiers by Counterfactual Generation, February 2019. arXiv:1807.08024 [cs].
- Kent K Chang, Mackenzie Cramer, Sandeep Soni, and David Bamman. Speak, memory: An archaeology of books known to chatgpt/gpt-4. *arXiv preprint arXiv:2305.00118*, 2023.
- Tian Qi Chen, Xuechen Li, Roger B Grosse, and David K Duvenaud. Isolating sources of disentanglement in variational autoencoders. In *Advances in Neural Information Processing Systems*, pages 2610–2620, 2018.
- Alexandra Chouldechova. Fair prediction with disparate impact: A study of bias in recidivism prediction instruments. *Big data*, 5(2):153–163, 2017.
- Pierre Comon. Independent component analysis, a new concept? *Signal processing*, 36(3):287–314, 1994.
- Thomas M Cover and Joy A Thomas. *Elements of information theory*. John Wiley & Sons, 2012.
- Elliot Creager and Richard Zemel. Online algorithmic recourse by collective action. In *ICML Workshop on Algorithmic Recourse*, 2021.
- Elliot Creager, David Madras, Joern-Henrik Jacobsen, Marissa Weis, Kevin Swersky, Toniann Pitassi, and Richard Zemel. Flexibly Fair Representation Learning by Disentanglement. In *Proceedings of the 36th International Conference on Machine Learning*, pages 1436–1445. PMLR, May 2019. ISSN: 2640-3498.
- Elliot Creager, David Madras, Toniann Pitassi, and Richard Zemel. Causal Modeling for Fairness In Dynamical Systems. In *Proceedings of the 37th International Conference on Machine Learning*, pages 2185–2195. PMLR, November 2020. ISSN: 2640-3498.
- Elliot Creager, Joern-Henrik Jacobsen, and Richard Zemel. Environment Inference for Invariant Learning. In *Proceedings of the 38th International Conference on Machine Learning*, pages 2189–2200. PMLR, July 2021. ISSN: 2640-3498.
- Nikolay Dagaev, Brett D Roads, Xiaoliang Luo, Daniel N Barry, Kaustubh R Patil, and Bradley C Love. A too-good-to-be-true prior to reduce shortcut reliance. *arXiv preprint arXiv:2102.06406*, 2021.
- Alexander D’Amour, Katherine Heller, Dan Moldovan, Ben Adlam, Babak Alipanahi, Alex Beutel, Christina Chen, Jonathan Deaton, Jacob Eisenstein, Matthew D. Hoffman, Farhad Hormozdiari, Neil Houlsby, Shaobo Hou, Ghassen Jerfel, Alan Karthikesalingam, Mario Lucic, Yian Ma, Cory McLean, Diana Mincu, Akinori Mitani, Andrea Montanari, Zachary Nado, Vivek Natarajan, Christopher Nielson, Thomas F. Osborne, Rajiv Raman, Kim Ramasamy, Rory Sayres, Jessica Schrouff, Martin Seneviratne, Shannon Sequeira, Harini Suresh, Victor Veitch, Max Vladymyrov, Xuezhi Wang, Kellie Webster, Steve Yadlowsky, Taedong Yun, Xiaohua Zhai, and D. Sculley.

- Underspecification Presents Challenges for Credibility in Modern Machine Learning, November 2020. arXiv:2011.03395 [cs, stat].
- DCCA. Division of consumer and community affairs. 2011-07. 12 cfr supplement i to part 202 - official staff interpretations. https://www.law.cornell.edu/cfr/text/12/appendix-Supplement_I_to_part_202, 1983.
- Alex J. DeGrave, Joseph D. Janizek, and Su-In Lee. AI for radiographic COVID-19 detection selects shortcuts over signal. *Nature Machine Intelligence*, 3(7):610–619, July 2021.
- Ambra Demontis, Marco Melis, Maura Pintor, Matthew Jagielski, Battista Biggio, Alina Oprea, Cristina Nita-Rotaru, and Fabio Roli. Why Do Adversarial Attacks Transfer? Explaining Transferability of Evasion and Poisoning Attacks, June 2019. arXiv:1809.02861 [cs, stat].
- Emily Denton, Ben Hutchinson, Margaret Mitchell, Timnit Gebru, and Andrew Zaldivar. Image Counterfactual Sensitivity Analysis for Detecting Unintended Bias. In *CVPR 2019 Workshop on Fairness Accountability Transparency and Ethics in Computer Vision*. arXiv, 2019. arXiv:1906.06439 [cs, stat].
- Jacob Devlin, Ming-Wei Chang, Kenton Lee, and Kristina Toutanova. Bert: Pre-training of deep bidirectional transformers for language understanding. *arXiv preprint arXiv:1810.04805*, 2018.
- Awa Dieng, Jessica Schrouff, Matt Kusner, Golnoosh Farnadi, and Fernando Diaz. Algorithmic fairness through the lens of causality and interpretability. In *NeurIPS Workshop, 2022*.
- Catherine D’ignazio and Lauren F Klein. *Data feminism*. MIT press, 2020.
- Carlos Diuk, Andre Cohen, and Michael L Littman. An object-oriented representation for efficient reinforcement learning. In *Proceedings of the 25th international conference on Machine learning*, pages 240–247, 2008.
- John C Duchi, Peter W Glynn, and Hongseok Namkoong. Statistics of robust optimization: A generalized empirical likelihood approach. *Mathematics of Operations Research*, 2021.
- Cynthia Dwork, Moritz Hardt, Toniann Pitassi, Omer Reingold, and Rich Zemel. Fairness Through Awareness, November 2011. arXiv:1104.3913 [cs].
- Cynthia Dwork, Moritz Hardt, Toniann Pitassi, Omer Reingold, and Richard Zemel. Fairness through awareness. In *Proceedings of the 3rd innovations in theoretical computer science conference*, pages 214–226. ACM, 2012.
- Harrison Edwards and Amos Storkey. Censoring representations with an adversary. In *International Conference on Learning Representations*, 2016.
- Marc N. Elliot, Allen Fremont, Peter A Morrison, Philip Pantoja, and Nicole Lurie. A New Method for Estimating Race/Ethnicity and Associated Disparities Where Administrative Records Lack Self-Reported Race/Ethnicity. *Health Services Research*, 2008.
- Logan Engstrom, Andrew Ilyas, Shibani Santurkar, Dimitris Tsipras, Jacob Steinhardt, and Aleksander Madry. Identifying statistical bias in dataset replication. In *International Conference on Machine Learning*, 2020.

- Danielle Ensign, Sorelle A Friedler, Scott Neville, Carlos Scheidegger, and Suresh Venkatasubramanian. Runaway feedback loops in predictive policing. In *Conference on fairness, accountability and transparency*, pages 160–171. PMLR, 2018.
- Babak Esmaeili, Hao Wu, Sarthak Jain, Alican Bozkurt, N Siddharth, Brooks Paige, Dana H Brooks, Jennifer Dy, and Jan-Willem Meent. Structured disentangled representations. In *The 22nd International Conference on Artificial Intelligence and Statistics*, pages 2525–2534, 2019a.
- Babak Esmaeili, Hao Wu, Sarthak Jain, Alican Bozkurt, N Siddharth, Brooks Paige, Dana H. Brooks, Jennifer Dy, and Jan-Willem van de Meent. Structured disentangled representations. In *The 22nd International Conference on Artificial Intelligence and Statistics*, 2019b.
- Virginia Eubanks. *Automating inequality: How high-tech tools profile, police, and punish the poor*. St. Martin’s Press, 2018.
- Benjamin Eyre, Richard Zemel, and Elliot Creager. Towards Environment-Invariant Representation Learning for Robust Task Transfer. In *ICML Workshop on Spurious Correlations, Invariance, and Stability*, page 8, 2022.
- Amir-massoud Farahmand, Andre Barreto, and Daniel Nikovski. Value-aware loss function for model-based reinforcement learning. In *Artificial Intelligence and Statistics*, pages 1486–1494, 2017.
- Golnoosh Farnadi, Q. Vera Liao, and Elliot Creager. Algorithmic fairness: at the intersections. In *NeurIPS Tutorial*, 2022.
- Aaron Fisher, Cynthia Rudin, and Francesca Dominici. All models are wrong, but many are useful: Learning a variable’s importance by studying an entire class of prediction models simultaneously. *J. Mach. Learn. Res.*, 20(177):1–81, 2019.
- Jakob N Foerster, Gregory Farquhar, Triantafyllos Afouras, Nantas Nardelli, and Shimon Whiteson. Counterfactual multi-agent policy gradients. In *Thirty-second AAAI conference on artificial intelligence*, 2018.
- Spencer Frei, Niladri S. Chatterji, and Peter L. Bartlett. Benign Overfitting without Linearity: Neural Network Classifiers Trained by Gradient Descent for Noisy Linear Data, September 2022. arXiv:2202.05928 [cs, math, stat].
- Scott Fujimoto and Shixiang Shane Gu. A minimalist approach to offline reinforcement learning. *Advances in Neural Information Processing Systems*, 34, 2021.
- Scott Fujimoto, David Meger, and Doina Precup. Off-policy deep reinforcement learning without exploration. *arXiv preprint arXiv:1812.02900*, 2018.
- Scott Fujimoto, David Meger, and Doina Precup. Off-policy deep reinforcement learning without exploration. In *International Conference on Machine Learning*, pages 2052–2062. PMLR, 2019.
- Yaroslav Ganin, Evgeniya Ustinova, Hana Ajakan, Pascal Germain, Hugo Larochelle, François Laviolette, Mario Marchand, and Victor Lempitsky. Domain-adversarial training of neural networks. *The Journal of Machine Learning Research*, 17(1):2096–2030, 2016.

- Timnit Gebru, Jamie Morgenstern, Briana Vecchione, Jennifer Wortman Vaughan, Hanna Wallach, Hal Daumé Ii, and Kate Crawford. Datasheets for datasets. *Communications of the ACM*, 64(12): 86–92, 2021.
- Robert Geirhos, Jörn-Henrik Jacobsen, Claudio Michaelis, Richard Zemel, Wieland Brendel, Matthias Bethge, and Felix A Wichmann. Shortcut learning in deep neural networks. *Nature Machine Intelligence*, 2(11):665–673, 2020a.
- Robert Geirhos, Jörn-Henrik Jacobsen, Claudio Michaelis, Richard Zemel, Wieland Brendel, Matthias Bethge, and Felix A. Wichmann. Shortcut Learning in Deep Neural Networks. *Nature Machine Intelligence*, 2(11):665–673, November 2020b. arXiv:2004.07780 [cs, q-bio].
- Andrew Gelman. Causality and statistical learning, 2011.
- Avijit Ghosh, Matthew Jagielski, and Christo Wilson. Subverting Fair Image Search with Generative Adversarial Perturbations. In *2022 ACM Conference on Fairness, Accountability, and Transparency*, pages 637–650, Seoul Republic of Korea, June 2022. ACM.
- Sharad Goel, Ravi Shroff, Jennifer Skeem, and Christopher Slobogin. The accuracy, equity, and jurisprudence of criminal risk assessment. In *Research handbook on big data law*, pages 9–28. Edward Elgar Publishing, 2021.
- Hila Gonen and Yoav Goldberg. Lipstick on a pig: Debiasing methods cover up systematic gender biases in word embeddings but do not remove them. *arXiv preprint arXiv:1903.03862*, 2019.
- Ian Goodfellow, Jean Pouget-Abadie, Mehdi Mirza, Bing Xu, David Warde-Farley, Sherjil Ozair, Aaron Courville, and Yoshua Bengio. Generative adversarial nets. In *Advances in neural information processing systems*, pages 2672–2680, 2014.
- Ian J Goodfellow, Jonathon Shlens, and Christian Szegedy. Explaining and harnessing adversarial examples. In *International Conference on Learning Representations*, 2015a.
- Ian J. Goodfellow, Jonathon Shlens, and Christian Szegedy. Explaining and Harnessing Adversarial Examples, March 2015b. arXiv:1412.6572 [cs, stat].
- Omer Gottesman, Fredrik Johansson, Matthieu Komorowski, Aldo Faisal, David Sontag, Finale Doshi-Velez, and Leo Anthony Celi. Guidelines for reinforcement learning in healthcare. *Nature Medicine*, 25(1):16–18, 2019.
- Anirudh Goyal, Alex Lamb, Jordan Hoffmann, Shagun Sodhani, Sergey Levine, Yoshua Bengio, and Bernhard Schölkopf. Recurrent independent mechanisms. *arXiv preprint arXiv:1909.10893*, 2019.
- Clive WJ Granger. Investigating causal relations by econometric models and cross-spectral methods. *Econometrica: journal of the Econometric Society*, pages 424–438, 1969.
- D. James Greiner and Donald B. Rubin. Causal Effects of Perceived Immutable Characteristics. *The Review of Economics and Statistics*, 93(3):775–785, 2011. Publisher: The MIT Press.
- Arthur Gretton, Karsten Borgwardt, Malte Rasch, Bernhard Schölkopf, and Alex J Smola. A kernel method for the two-sample-problem. In *Advances in neural information processing systems*, pages 513–520, 2007.

- Carlos Guestrin, Daphne Koller, Ronald Parr, and Shobha Venkataraman. Efficient solution algorithms for factored mdps. *Journal of Artificial Intelligence Research*, 19:399–468, 2003.
- Ishaan Gulrajani and David Lopez-Paz. In search of lost domain generalization. In *International Conference on Learning Representations*, 2021.
- Michael Gutmann and Aapo Hyvärinen. Noise-contrastive estimation: A new estimation principle for unnormalized statistical models. In *Proceedings of the Thirteenth International Conference on Artificial Intelligence and Statistics*, pages 297–304, 2010.
- Tuomas Haarnoja, Aurick Zhou, Pieter Abbeel, and Sergey Levine. Soft actor-critic: Off-policy maximum entropy deep reinforcement learning with a stochastic actor. In *International conference on machine learning*, pages 1861–1870. PMLR, 2018.
- Benjamin Haibe-Kains, George Alexandru Adam, Ahmed Hosny, Farnoosh Khodakarami, Massive Analysis Quality Control (MAQC) Society Board of Directors Shraddha Thakkar 35 Kusko Rebecca 36 Sansone Susanna-Assunta 37 Tong Weida 35 Wolfinger Russ D. 38 Mason Christopher E. 39 Jones Wendell 40 Dopazo Joaquin 41 Furlanello Cesare 42, Levi Waldron, Bo Wang, Chris McIntosh, Anna Goldenberg, Anshul Kundaje, et al. Transparency and reproducibility in artificial intelligence. *Nature*, 586(7829):E14–E16, 2020.
- Sara Hajian, Josep Domingo-Ferrer, Anna Monreale, Dino Pedreschi, and Fosca Giannotti. Discrimination-and privacy-aware patterns. *Data Mining and Knowledge Discovery*, 29(6):1733–1782, 2015.
- Assaf Hallak, François Schnitzler, Timothy Mann, and Shie Mannor. Off-policy model-based learning under unknown factored dynamics. In *International Conference on Machine Learning*, pages 711–719, 2015.
- Foad Hamidi, Morgan Klaus Scheuerman, and Stacy M. Branham. Gender Recognition or Gender Reductionism?: The Social Implications of Embedded Gender Recognition Systems. In *Proceedings of the 2018 CHI Conference on Human Factors in Computing Systems*, pages 1–13, Montreal QC Canada, April 2018. ACM.
- Alex Hanna and Tina M Park. Against scale: Provocations and resistances to scale thinking. *arXiv preprint arXiv:2010.08850*, 2020.
- Alex Hanna, Emily Denton, Andrew Smart, and Jamila Smith-Loud. Towards a critical race methodology in algorithmic fairness. In *Proceedings of the 2020 conference on Fairness, Accountability, and Transparency*, pages 501–512, 2020.
- Donna Haraway. Situated knowledges: The science question in feminism and the privilege of partial perspective. *Feminist studies*, 14(3):575–599, 1988.
- Moritz Hardt, Nimrod Megiddo, Christos Papadimitriou, and Mary Wootters. Strategic classification. In *Proceedings of the 2016 ACM conference on innovations in theoretical computer science*, pages 111–122, 2016a.
- Moritz Hardt, Eric Price, Nati Srebro, et al. Equality of opportunity in supervised learning. In *Advances in Neural Information Processing Systems (NIPS 2016)*, 2016b.

- Moritz Hardt, Eric Mazumdar, Celestine Mendler-Dünner, and Tijana Zrnic. Algorithmic collective action in machine learning. *arXiv preprint arXiv:2302.04262*, 2023.
- Tatsunori B Hashimoto, Megha Srivastava, Hongseok Namkoong, and Percy Liang. Fairness without demographics in repeated loss minimization. In *International Conference on Machine Learning*, 2018.
- Kaiming He, Xiangyu Zhang, Shaoqing Ren, and Jian Sun. Delving Deep into Rectifiers: Surpassing Human-Level Performance on ImageNet Classification. In *2015 IEEE International Conference on Computer Vision (ICCV)*, pages 1026–1034, Santiago, Chile, December 2015. IEEE.
- Ursula Hébert-Johnson, Michael P Kim, Omer Reingold, and Guy N Rothblum. Calibration for the (computationally-identifiable) masses. In *International Conference on Machine Learning*, 2018.
- Dan Hendrycks and Thomas Dietterich. Benchmarking neural network robustness to common corruptions and perturbations. In *International Conference on Learning Representations*, 2019.
- MA Hernán and JM Robins. Causal inference: What if. *Boca Raton: Chapman & Hill/CRC*, 2020.
- Irina Higgins, Loic Matthey, Arka Pal, Christopher Burgess, Xavier Glorot, Matthew Botvinick, Shakir Mohamed, and Alexander Lerchner. In *International Conference on Learning Representations*, 2017.
- Irina Higgins, Nicolas Sonnerat, Loic Matthey, Arka Pal, Christopher P Burgess, Matko Bošnjak, Murray Shanahan, Matthew Botvinick, Demis Hassabis, and Alexander Lerchner. SCAN: Learning hierarchical compositional visual concepts. In *International Conference on Learning Representations*, 2018.
- Geoffrey E Hinton and Ruslan R Salakhutdinov. Reducing the dimensionality of data with neural networks. *science*, 313(5786):504–507, 2006.
- Jonathan Ho, Ajay Jain, and Pieter Abbeel. Denoising Diffusion Probabilistic Models, December 2020. arXiv:2006.11239 [cs, stat].
- Judy Hoffman, Eric Tzeng, Taesung Park, Jun-Yan Zhu, Phillip Isola, Kate Saenko, Alexei Efros, and Trevor Darrell. Cycada: Cycle-consistent adversarial domain adaptation. In *International Conference on Machine Learning*, pages 1989–1998, 2018.
- Kurt Hornik, Maxwell Stinchcombe, and Halbert White. Multilayer feedforward networks are universal approximators. *Neural Networks*, 2(5):359–366, January 1989.
- Peter S Hovmand and Peter S Hovmand. *Group model building and community-based system dynamics process*. Springer, 2014.
- Lily Hu and Issa Kohler-Hausmann. What’s Sex Got To Do With Fair Machine Learning? In *Proceedings of the 2020 Conference on Fairness, Accountability, and Transparency*, pages 513–513, January 2020. arXiv:2006.01770 [cs].
- Biwei Huang, Chaochao Lu, Liu Leqi, José Miguel Hernández-Lobato, Clark Glymour, Bernhard Schölkopf, and Kun Zhang. Action-sufficient state representation learning for control with structural constraints. In *International Conference on Machine Learning*, pages 9260–9279. PMLR, 2022.

- Minyoung Huh, Pulkit Agrawal, and Alexei A Efros. What makes imagenet good for transfer learning? *arXiv preprint arXiv:1608.08614*, 2016.
- Andrew Hundt, William Agnew, Vicky Zeng, Severin Kacianka, and Matthew Gombolay. Robots Enact Malignant Stereotypes. In *2022 ACM Conference on Fairness, Accountability, and Transparency*, pages 743–756, June 2022. arXiv:2207.11569 [cs].
- Ben Hutchinson and Margaret Mitchell. 50 years of test (un) fairness: Lessons for machine learning. In *Proceedings of the Conference on Fairness, Accountability, and Transparency*, pages 49–58. ACM, 2019.
- Ben Hutchinson, Vinodkumar Prabhakaran, Emily Denton, Kellie Webster, Yu Zhong, and Stephen Denuyl. Social biases in NLP models as barriers for persons with disabilities. In *Proceedings of the 58th Annual Meeting of the Association for Computational Linguistics*, pages 5491–5501, Online, July 2020. Association for Computational Linguistics.
- Aapo Hyvärinen and Erkki Oja. Independent component analysis: algorithms and applications. *Neural networks*, 13(4-5):411–430, 2000.
- Rodrigo Toro Icarte, Toryn Klassen, Richard Valenzano, and Sheila McIlraith. Using reward machines for high-level task specification and decomposition in reinforcement learning. In *International Conference on Machine Learning*, pages 2107–2116, 2018.
- Michael Janner, Justin Fu, Marvin Zhang, and Sergey Levine. When to trust your model: Model-based policy optimization. In *Advances in Neural Information Processing Systems*, pages 12498–12509, 2019.
- Edwin T Jaynes. Information theory and statistical mechanics. *Physical review*, 106(4):620, 1957.
- Eun Seo Jo and Timnit Gebru. Lessons from archives: Strategies for collecting sociocultural data in machine learning. In *Proceedings of the 2020 conference on fairness, accountability, and transparency*, pages 306–316, 2020.
- Matthew Johnson, Katja Hofmann, Tim Hutton, and David Bignell. The malmo platform for artificial intelligence experimentation. In *IJCAI*, pages 4246–4247, 2016.
- Leslie Pack Kaelbling. Learning to achieve goals. In *IJCAI*, pages 1094–1099. Citeseer, 1993.
- Adam Tauman Kalai, Yishay Mansour, and Elad Verbin. On agnostic boosting and parity learning. In *Proceedings of the fortieth annual ACM symposium on Theory of computing*, pages 629–638, Victoria British Columbia Canada, May 2008. ACM.
- Dmitry Kalashnikov, Alex Irpan, Peter Pastor, Julian Ibarz, Alexander Herzog, Eric Jang, Deirdre Quillen, Ethan Holly, Mrinal Kalakrishnan, Vincent Vanhoucke, et al. Scalable deep reinforcement learning for vision-based robotic manipulation. In *Conference on Robot Learning*, pages 651–673. PMLR, 2018.
- Pritish Kamath, Akilesh Tangella, Danica J Sutherland, and Nathan Srebro. Does invariant risk minimization capture invariance? In *International Conference on Artificial Intelligence and Statistics*, 2021.

- Faisal Kamiran and Toon Calders. Classifying without discriminating. In *Control and Communication 2009 2nd International Conference on Computer*, pages 1–6, February 2009.
- Toshihiro Kamishima, Shotaro Akaho, and Jun Sakuma. Fairness-aware learning through regularization approach. In *2011 IEEE 11th International Conference on Data Mining Workshops*, pages 643–650. IEEE, 2011.
- Toshihiro Kamishima, Shotaro Akaho, Hideki Asoh, and Jun Sakuma. Fairness-aware classifier with prejudice remover regularizer. In *Joint European Conference on Machine Learning and Knowledge Discovery in Databases*, pages 35–50. Springer, 2012.
- Jared Kaplan, Sam McCandlish, Tom Henighan, Tom B. Brown, Benjamin Chess, Rewon Child, Scott Gray, Alec Radford, Jeffrey Wu, and Dario Amodei. Scaling Laws for Neural Language Models, January 2020. arXiv:2001.08361 [cs, stat].
- Amir-Hossein Karimi, Gilles Barthe, Bernhard Schölkopf, and Isabel Valera. A survey of algorithmic recourse: contrastive explanations and consequential recommendations. *ACM Computing Surveys*, 55(5):1–29, 2022.
- Atoosa Kasirzadeh and Andrew Smart. The Use and Misuse of Counterfactuals in Ethical Machine Learning. In *Proceedings of the 2021 ACM Conference on Fairness, Accountability, and Transparency*, pages 228–236, Virtual Event Canada, March 2021. ACM.
- Nan Rosemary Ke, Olexa Bilaniuk, Anirudh Goyal, Stefan Bauer, Hugo Larochelle, Bernhard Schölkopf, Michael C. Mozer, Chris Pal, and Yoshua Bengio. Learning Neural Causal Models from Unknown Interventions, August 2020. arXiv:1910.01075 [cs, stat].
- Michael Kearns and Daphne Koller. Efficient reinforcement learning in factored mdps. In *IJCAI*, volume 16, pages 740–747, 1999.
- Michael Kearns, Seth Neel, Aaron Roth, and Zhiwei Steven Wu. Preventing fairness gerrymandering: Auditing and learning for subgroup fairness. *arXiv preprint arXiv:1711.05144*, 2017.
- Michael Kearns, Seth Neel, Aaron Roth, and Zhiwei Steven Wu. Preventing fairness gerrymandering: Auditing and learning for subgroup fairness. In *International Conference on Machine Learning*, pages 2564–2572, 2018.
- Michael J. Kearns, Robert E. Schapire, and Linda M. Sellie. Toward efficient agnostic learning. In *Proceedings of the fifth annual workshop on Computational learning theory*, pages 341–352, Pittsburgh Pennsylvania USA, July 1992. ACM.
- Hyunjik Kim and Andriy Mnih. Disentangling by factorising. *arXiv preprint arXiv:1802.05983*, 2018.
- Michael P Kim, Amirata Ghorbani, and James Zou. Multiaccuracy: Black-box post-processing for fairness in classification. In *Proceedings of the 2019 AAAI/ACM Conference on AI, Ethics, and Society*, pages 247–254, 2019.
- Diederik Kingma and Jimmy Ba. Adam: A method for stochastic optimization. In *International Conference on Learning Representations*, 2015.

- Diederik P Kingma and Max Welling. Auto-encoding variational bayes. In *International Conference on Learning Representations*, 2014.
- Durk P Kingma, Shakir Mohamed, Danilo Jimenez Rezende, and Max Welling. Semi-supervised learning with deep generative models. In *Advances in neural information processing systems*, pages 3581–3589, 2014.
- Thomas Kipf, Ethan Fetaya, Kuan-Chieh Wang, Max Welling, and Richard Zemel. Neural relational inference for interacting systems. In *International Conference on Machine Learning*, pages 2688–2697. PMLR, 2018.
- Thomas Kipf, Elise van der Pol, and Max Welling. Contrastive learning of structured world models. *arXiv preprint arXiv:1911.12247*, 2019.
- Polina Kirichenko, Pavel Izmailov, and Andrew Gordon Wilson. Last Layer Re-Training is Sufficient for Robustness to Spurious Correlations, April 2022. arXiv:2204.02937 [cs, stat].
- Donald E Kirk. *Optimal control theory: an introduction*. Courier Corporation, 2004.
- Jon Kleinberg, Sendhil Mullainathan, and Manish Raghavan. Inherent trade-offs in the fair determination of risk scores. *arXiv preprint arXiv:1609.05807*, 2016.
- Jon Kleinberg, Jens Ludwig, Sendhil Mullainathan, and Cass R Sunstein. Discrimination in the age of algorithms. *Journal of Legal Analysis*, 10:113–174, 2018.
- Oleg Klimov and John Schulman. Roboschool, 2017.
- Jack Klys, Jake Snell, and Richard Zemel. Learning latent subspaces in variational autoencoders. In *Advances in Neural Information Processing Systems*, pages 6443–6453, 2018.
- Pang Wei Koh, Shiori Sagawa, Henrik Marklund, Sang Michael Xie, Marvin Zhang, Akshay Balsubramani, Weihua Hu, Michihiro Yasunaga, Richard Lanus Phillips, Sara Beery, et al. WILDS: A benchmark of in-the-wild distribution shifts. In *International Conference on Machine Learning*, 2021.
- Issa Kohler-Hausmann. Eddie Murphy and the Dangers of Counterfactual Causal Thinking About Detecting Racial Discrimination. *Northwestern University Law Review*, page 66, 2019.
- Ilya Kostrikov, Denis Yarats, and Rob Fergus. Image augmentation is all you need: Regularizing deep reinforcement learning from pixels. *arXiv preprint arXiv:2004.13649*, 2020.
- Alex Krizhevsky, Ilya Sutskever, and Geoffrey E Hinton. ImageNet Classification with Deep Convolutional Neural Networks. In *Advances in Neural Information Processing Systems*, volume 25. Curran Associates, Inc., 2012.
- David Krueger, Ethan Caballero, Joern-Henrik Jacobsen, Amy Zhang, Jonathan Binas, Remi Le Priol, and Aaron Courville. Out-of-distribution generalization via risk extrapolation (REx). In *International Conference on Machine Learning*, 2021.

- Bogdan Kulynych, David Madras, Smitha Milli, Inioluwa Deborah Raji, Angela Zhou, and Richard Zemel. Participatory approaches to machine learning. In *International Conference on Machine Learning Workshop*, 2020.
- Aviral Kumar, Abhishek Gupta, and Sergey Levine. Discor: Corrective feedback in reinforcement learning via distribution correction. *arXiv preprint arXiv:2003.07305*, 2020a.
- Aviral Kumar, Aurick Zhou, George Tucker, and Sergey Levine. Conservative q-learning for offline reinforcement learning. *Advances in Neural Information Processing Systems*, 33:1179–1191, 2020b.
- Andrey Kurenkov, Ajay Mandlekar, Roberto Martin-Martin, Silvio Savarese, and Animesh Garg. Ac-teach: A bayesian actor-critic method for policy learning with an ensemble of suboptimal teachers. In *Conference on Robot Learning*, pages 717–734. PMLR, 2020.
- Matt J Kusner, Joshua Loftus, Chris Russell, and Ricardo Silva. Counterfactual fairness. In *Advances in Neural Information Processing Systems*, pages 4066–4076, 2017.
- Preethi Lahoti, Alex Beutel, Jilin Chen, Kang Lee, Flavien Prost, Nithum Thain, Xuezhi Wang, and Ed H Chi. Fairness without demographics through adversarially reweighted learning. In *Neural Information Processing Systems*, 2020.
- Sameera Lanka and Tianfu Wu. Archer: Aggressive rewards to counter bias in hindsight experience replay. *arXiv preprint arXiv:1809.02070*, 2018.
- Michael Laskin, Kimin Lee, Adam Stooke, Lerrel Pinto, Pieter Abbeel, and Aravind Srinivas. Reinforcement learning with augmented data. *arXiv preprint arXiv:2004.14990*, 2020.
- Tosca Lechner and Shai Ben-David. Inherent Limitations of Multi-Task Fair Representations. In *Proceedings of The 1st Conference on Lifelong Learning Agents*, pages 583–603. PMLR, November 2022. ISSN: 2640-3498.
- Tosca Lechner, Shai Ben-David, Sushant Agarwal, and Nivasini Ananthakrishnan. Impossibility results for fair representations, July 2021. arXiv:2107.03483 [cs, stat].
- Juho Lee, Yoonho Lee, Jungtaek Kim, Adam R Kosioerek, Seungjin Choi, and Yee Whye Teh. Set transformer: A framework for attention-based permutation-invariant neural networks. *arXiv preprint arXiv:1810.00825*, 2018.
- Sergey Levine, Aviral Kumar, George Tucker, and Justin Fu. Offline reinforcement learning: Tutorial, review, and perspectives on open problems. *arXiv preprint arXiv:2005.01643*, 2020.
- Richard Li, Allan Jabri, Trevor Darrell, and Pulkit Agrawal. Towards practical multi-object manipulation using relational reinforcement learning. *arXiv preprint arXiv:1912.11032*, 2019.
- Ya Li, Xinmei Tian, Mingming Gong, Yajing Liu, Tongliang Liu, Kun Zhang, and Dacheng Tao. Deep domain generalization via conditional invariant adversarial networks. In *Proceedings of the European Conference on Computer Vision*, pages 624–639, 2018.
- Timothy P Lillicrap, Jonathan J Hunt, Alexander Pritzel, Nicolas Heess, Tom Erez, Yuval Tassa, David Silver, and Daan Wierstra. Continuous control with deep reinforcement learning. *arXiv preprint arXiv:1509.02971*, 2015.

- Evan Liu, Behzad Haghgoo, Annie Chen, Aditi Raghunathan, Pang Wei Koh, Shiori Sagawa, Percy Liang, and Chelsea Finn. Just train twice: Improving group robustness without training group information. In *International Conference on Machine Learning*, 2021.
- Lydia T Liu, Max Simchowitz, and Moritz Hardt. The implicit fairness criterion of unconstrained learning. In *International Conference on Machine Learning*, 2019.
- Francesco Locatello, Stefan Bauer, Mario Lucic, Sylvain Gelly, Bernhard Schölkopf, and Olivier Bachem. Challenging common assumptions in the unsupervised learning of disentangled representations. *arXiv preprint arXiv:1811.12359*, 2018.
- Mingsheng Long, Zhangjie Cao, Jianmin Wang, and Michael I Jordan. Conditional adversarial domain adaptation. In *Advances in Neural Information Processing Systems*, pages 1640–1650, 2018.
- David Lopez-Paz. From Dependence to Causation, July 2016. arXiv:1607.03300 [stat] version: 1.
- Christos Louizos, Kevin Swersky, Yujia Li, Max Welling, and Richard Zemel. The variational fair autoencoder. 2016a.
- Christos Louizos, Kevin Swersky, Yujia Li, Max Welling, and Richard Zemel. The Variational Fair Autoencoder. In *International Conference on Representation Learning*, April 2016b. arXiv:1511.00830 [cs, stat].
- Ryan Lowe, Yi Wu, Aviv Tamar, Jean Harb, OpenAI Pieter Abbeel, and Igor Mordatch. Multi-agent actor-critic for mixed cooperative-competitive environments. In *Advances in neural information processing systems*, pages 6379–6390, 2017.
- Chaochao Lu, Bernhard Schölkopf, and José Miguel Hernández-Lobato. Deconfounding reinforcement learning in observational settings. *arXiv preprint arXiv:1812.10576*, 2018.
- Pauline Luc, Camille Couprie, Soumith Chintala, and Jakob Verbeek. Semantic segmentation using adversarial networks. In *NIPS Workshop on Adversarial Training*, 2016.
- Dieuwertje Luitse and Wiebke Denkena. The great Transformer: Examining the role of large language models in the political economy of AI. *Big Data & Society*, 8(2):205395172110477, July 2021.
- Chris J Maddison, Aja Huang, Ilya Sutskever, and David Silver. Move evaluation in go using deep convolutional neural networks. *arXiv preprint arXiv:1412.6564*, 2014.
- David Madras, Toniann Pitassi, and Richard Zemel. Predict responsibly: Increasing fairness by learning to defer. *arXiv preprint arXiv:1711.06664*, 2017.
- David Madras, Elliot Creager, Toniann Pitassi, and Richard Zemel. Learning adversarially fair and transferable representations. In *International Conference on Machine Learning (ICML 2018)*, 2018.
- David Madras, Elliot Creager, Toniann Pitassi, and Richard Zemel. Fairness Through Causal Awareness: Learning Latent-Variable Models for Biased Data. In *ACM FAT* Conference*. arXiv, 2019. arXiv:1809.02519 [cs, stat].

- Aleksander Madry, Aleksandar Makelov, Ludwig Schmidt, Dimitris Tsipras, and Adrian Vladu. Towards deep learning models resistant to adversarial attacks. In *International Conference on Learning Representations*, 2018.
- Aleksander Madry, Aleksandar Makelov, Ludwig Schmidt, Dimitris Tsipras, and Adrian Vladu. Towards Deep Learning Models Resistant to Adversarial Attacks, September 2019. arXiv:1706.06083 [cs, stat].
- Prashan Madumal, Tim Miller, Liz Sonenberg, and Frank Vetere. Explainable reinforcement learning through a causal lens. *arXiv preprint arXiv:1905.10958*, 2019.
- Maggie Makar and Alexander D’Amour. Fairness and robustness in anti-causal prediction, September 2022. arXiv:2209.09423 [cs, stat].
- Maggie Makar, Ben Packer, Dan Moldovan, Davis Blalock, Yoni Halpern, and Alexander D’Amour. Causally motivated shortcut removal using auxiliary labels. In *Proceedings of The 25th International Conference on Artificial Intelligence and Statistics*, pages 739–766. PMLR, May 2022. ISSN: 2640-3498.
- Travis Mandel, Yun-En Liu, Sergey Levine, Emma Brunskill, and Zoran Popovic. Offline policy evaluation across representations with applications to educational games. In *AAMAS*, pages 1077–1084, 2014.
- Donald Martin Jr, Vinodkumar Prabhakaran, Jill Kuhlberg, Andrew Smart, and William S Isaac. Extending the machine learning abstraction boundary: A complex systems approach to incorporate societal context. *arXiv preprint arXiv:2006.09663*, 2020.
- Sandra G Mayson. Bias in, bias out. *The Yale Law Journal*, 128(8):2218–2300, 2019.
- Daniel McNamara, Cheng Soon Ong, and Robert C Williamson. Provably fair representations. *arXiv preprint arXiv:1710.04394*, 2017.
- Aditya Krishna Menon, Sadeep Jayasumana, Ankit Singh Rawat, Himanshu Jain, Andreas Veit, and Sanjiv Kumar. LONG-TAIL LEARNING VIA LOGIT ADJUSTMENT. page 24, 2021.
- Aayush Mishra and Anqi Liu. Repeated Environment Inference for Invariant Learning, August 2022. arXiv:2207.12876 [cs] version: 2.
- Margaret Mitchell, Simone Wu, Andrew Zaldivar, Parker Barnes, Lucy Vasserman, Ben Hutchinson, Elena Spitzer, Inioluwa Deborah Raji, and Timnit Gebru. Model cards for model reporting. In *Proceedings of the conference on fairness, accountability, and transparency*, pages 220–229, 2019.
- Margaret Mitchell, Alexandra Sasha Luccioni, Nathan Lambert, Marissa Gerchick, Angelina McMillan-Major, Ezinwanne Ozoani, Nazneen Rajani, Tristan Thrush, Yacine Jernite, and Douwe Kiela. Measuring Data, February 2023. arXiv:2212.05129 [cs].
- Martin Mladenov, Elliot Creager, Omer Ben-Porat, Kevin Swersky, Richard Zemel, and Craig Boutilier. Optimizing long-term social welfare in recommender systems: A constrained matching approach. In *ICML*, 2020.

- Volodymyr Mnih, Koray Kavukcuoglu, David Silver, Andrei A Rusu, Joel Veness, Marc G Bellemare, Alex Graves, Martin Riedmiller, Andreas K Fidjeland, Georg Ostrovski, et al. Human-level control through deep reinforcement learning. *nature*, 518(7540):529–533, 2015.
- Chantal Mouffe. *Agonistics: Thinking the world politically*. Verso Books, 2013.
- Daniel Moyer, Shuyang Gao, Rob Brekelmans, Aram Galstyan, and Greg Ver Steeg. Invariant representations without adversarial training. In *Advances in Neural Information Processing Systems (NeurIPS 2018)*, 2018.
- Krikamol Muandet, David Balduzzi, and Bernhard Schölkopf. Domain generalization via invariant feature representation. In *International conference on machine learning*, pages 10–18. PMLR, 2013.
- Rémi Munos, Tom Stepleton, Anna Harutyunyan, and Marc Bellemare. Safe and efficient off-policy reinforcement learning. In *Advances in Neural Information Processing Systems*, pages 1054–1062, 2016.
- Junhyun Nam, Hyuntak Cha, Sungsoo Ahn, Jaeho Lee, and Jinwoo Shin. Learning from failure: Training debiased classifier from biased classifier. In *Neural Information Processing Systems 2020*, 2020.
- Geraud Nangue Tasse, Steven James, and Benjamin Rosman. A boolean task algebra for reinforcement learning. *Advances in Neural Information Processing Systems*, 33:9497–9507, 2020.
- Arvind Narayanan and Sayash Kapoor. Gpt-4 and professional benchmarks: the wrong answer to the wrong question, 2023.
- Safiya Umoja Noble. Algorithms of oppression. In *Algorithms of oppression*. New York University Press, 2018.
- Ziad Obermeyer, Brian Powers, Christine Vogeli, and Sendhil Mullainathan. Dissecting racial bias in an algorithm used to manage the health of populations. *Science*, 366(6464):447–453, 2019.
- Augustus Odena. Semi-supervised learning with generative adversarial networks. *arXiv preprint arXiv:1606.01583*, 2016.
- Junhyuk Oh, Satinder Singh, and Honglak Lee. Value prediction network. In *Advances in Neural Information Processing Systems*, pages 6118–6128, 2017.
- Long Ouyang, Jeff Wu, Xu Jiang, Diogo Almeida, Carroll L Wainwright, Pamela Mishkin, Chong Zhang, Sandhini Agarwal, Katarina Slama, Alex Ray, John Schulman, Jacob Hilton, Fraser Kelton, Luke Miller, Maddie Simens, Amanda Askell, Peter Welinder, Paul Christiano, Jan Leike, and Ryan Lowe. Training language models to follow instructions with human feedback. In *Advances in Neural Information Processing Systems*, 2022.
- Vishal M Patel, Raghuraman Gopalan, Ruonan Li, and Rama Chellappa. Visual domain adaptation: A survey of recent advances. *IEEE signal processing magazine*, 32(3):53–69, 2015.
- Amandalynne Paullada, Inioluwa Deborah Raji, Emily M. Bender, Emily Denton, and Alex Hanna. Data and its (dis)contents: A survey of dataset development and use in machine learning research. *Patterns*, 2(11):100336, November 2021. arXiv:2012.05345 [cs].

- Judea Pearl. Causal inference in statistics: An overview. *Statistics surveys*, 3:96–146, 2009a.
- Judea Pearl. Causal inference in statistics: An overview. *Statistics Surveys*, 3(none), January 2009b.
- Dino Pedreshi, Salvatore Ruggieri, and Franco Turini. Discrimination-aware data mining. In *Proceedings of the 14th ACM SIGKDD international conference on Knowledge discovery and data mining*, pages 560–568, Las Vegas Nevada USA, August 2008. ACM.
- Juan Perdomo, Tijana Zrnic, Celestine Mendler-Düner, and Moritz Hardt. Performative prediction. In *International Conference on Machine Learning*, pages 7599–7609. PMLR, 2020.
- Jonas Peters, Peter Bühlmann, and Nicolai Meinshausen. Causal inference by using invariant prediction: identification and confidence intervals. *Journal of the Royal Statistical Society: Series B (Statistical Methodology)*, 78(5):947–1012, 2016.
- Jonas Peters, Dominik Janzing, and Bernhard Schölkopf. *Elements of causal inference: foundations and learning algorithms*. MIT press, 2017.
- Silviu Pitis, Harris Chan, and Jimmy Ba. Protoge: Prototype goal encodings for multi-goal reinforcement learning. *The 4th Multidisciplinary Conference on Reinforcement Learning and Decision Making (RLDM2019)*, 2019.
- Silviu Pitis, Harris Chan, and Stephen Zhao. mrl: modular rl. <https://github.com/spitis/mrl>, 2020a.
- Silviu Pitis, Harris Chan, Stephen Zhao, Bradly Stadie, and Jimmy Ba. Maximum entropy gain exploration for long horizon multi-goal reinforcement learning. In *Proceedings of the Thirty-seventh International Conference on Machine Learning*, 2020b.
- Silviu Pitis, Elliot Creager, and Animesh Garg. Counterfactual data augmentation using locally factored dynamics. *Advances in Neural Information Processing Systems*, 33:3976–3990, 2020c.
- Silviu Pitis, Elliot Creager, Ajay Mandlekar, and Animesh Garg. MoCoDA: Model-based Counterfactual Data Augmentation, October 2022. arXiv:2210.11287 [cs].
- Matthias Plappert, Marcin Andrychowicz, Alex Ray, Bob McGrew, Bowen Baker, Glenn Powell, Jonas Schneider, Josh Tobin, Maciek Chociej, Peter Welinder, et al. Multi-goal reinforcement learning: Challenging robotics environments and request for research. *arXiv preprint arXiv:1802.09464*, 2018.
- Geoff Pleiss, Manish Raghavan, Felix Wu, Jon Kleinberg, and Kilian Q Weinberger. On fairness and calibration. In *Advances in Neural Information Processing Systems*, pages 5684–5693, 2017.
- Martin L Puterman. *Markov decision processes: discrete stochastic dynamic programming*. John Wiley & Sons, 2014.
- Novi Quadrianto, Viktoriia Sharmanska, and Oliver Thomas. Discovering fair representations in the data domain. In *Proceedings of the IEEE/CVF Conference on Computer Vision and Pattern Recognition*, pages 8227–8236, 2019.

- Alec Radford, Jeffrey Wu, Rewon Child, David Luan, Dario Amodei, and Ilya Sutskever. Language Models are Unsupervised Multitask Learners, 2019.
- Alec Radford, Jong Wook Kim, Chris Hallacy, Aditya Ramesh, Gabriel Goh, Sandhini Agarwal, Girish Sastry, Amanda Askell, Pamela Mishkin, Jack Clark, Gretchen Krueger, and Ilya Sutskever. Learning Transferable Visual Models From Natural Language Supervision, February 2021. arXiv:2103.00020 [cs].
- Inioluwa Deborah Raji, Emily M. Bender, Amandalynne Paullada, Emily Denton, and Alex Hanna. AI and the Everything in the Whole Wide World Benchmark, November 2021. arXiv:2111.15366 [cs].
- Pranav Rajpurkar, Jeremy Irvin, Kaylie Zhu, Brandon Yang, Hershel Mehta, Tony Duan, Daisy Ding, Aarti Bagul, Curtis Langlotz, Katie Shpanskaya, Matthew P. Lungren, and Andrew Y. Ng. CheXNet: Radiologist-Level Pneumonia Detection on Chest X-Rays with Deep Learning, December 2017. arXiv:1711.05225 [cs, stat].
- Benjamin Recht, Rebecca Roelofs, Ludwig Schmidt, and Vaishaal Shankar. Do imagenet classifiers generalize to imagenet? In *International Conference on Machine Learning*, pages 5389–5400. PMLR, 2019.
- Danilo J Rezende, Ivo Danihelka, George Papamakarios, Nan Rosemary Ke, Ray Jiang, Theophane Weber, Karol Gregor, Hamza Merzic, Fabio Viola, Jane Wang, et al. Causally correct partial models for reinforcement learning. *arXiv preprint arXiv:2002.02836*, 2020.
- R Tyrrell Rockafellar and Stanislav Uryasev. Conditional value-at-risk for general loss distributions. *Journal of Banking & Finance*, 26(7):1443–1471, 2002.
- Elan Rosenfeld, Pradeep Ravikumar, and Andrej Risteski. The risks of invariant risk minimization. In *International Conference on Learning Representations*, 2021.
- Dominik Rothenhäusler, Nicolai Meinshausen, Peter Bühlmann, and Jonas Peters. Anchor regression: heterogeneous data meets causality. *arXiv preprint arXiv:1801.06229*, 2018.
- Peter J Rousseeuw. Tutorial to robust statistics. *Journal of chemometrics*, 5(1):1–20, 1991.
- Donald B Rubin. Causal inference using potential outcomes: Design, modeling, decisions. *Journal of the American Statistical Association*, 100(469):322–331, 2005.
- Jakob Runge, Sebastian Bathiany, Erik Bollt, Gustau Camps-Valls, Dim Coumou, Ethan Deyle, Clark Glymour, Marlene Kretschmer, Miguel D Mahecha, Jordi Muñoz-Marí, et al. Inferring causation from time series in earth system sciences. *Nature communications*, 10(1):1–13, 2019.
- Shiori Sagawa, Pang Wei Koh, Tatsunori B Hashimoto, and Percy Liang. Distributionally robust neural networks for group shifts: On the importance of regularization for worst-case generalization. In *International Conference on Learning Representations*, 2020a.
- Shiori Sagawa, Pang Wei Koh, Tatsunori B. Hashimoto, and Percy Liang. Distributionally Robust Neural Networks for Group Shifts: On the Importance of Regularization for Worst-Case Generalization, April 2020b. arXiv:1911.08731 [cs, stat] version: 2.

- Shiori Sagawa, Aditi Raghunathan, Pang Wei Koh, and Percy Liang. An Investigation of Why Overparameterization Exacerbates Spurious Correlations. In *Proceedings of the 37th International Conference on Machine Learning*, pages 8346–8356. PMLR, November 2020c. ISSN: 2640-3498.
- Tim Salimans, Ian Goodfellow, Wojciech Zaremba, Vicki Cheung, Alec Radford, and Xi Chen. Improved techniques for training gans. In *Advances in Neural Information Processing Systems*, pages 2234–2242, 2016.
- Samira Samadi, Uthaipon Tantipongpipat, Jamie H Morgenstern, Mohit Singh, and Santosh Vempala. The price of fair pca: One extra dimension. In *Advances in Neural Information Processing Systems*, pages 10976–10987, 2018.
- Nithya Sambasivan, Shivani Kapania, Hannah Highfill, Diana Akrong, Praveen Paritosh, and Lora M Aroyo. “everyone wants to do the model work, not the data work”: Data cascades in high-stakes ai. In *proceedings of the 2021 CHI Conference on Human Factors in Computing Systems*, pages 1–15, 2021.
- Victor Sanh, Lysandre Debut, Julien Chaumond, and Thomas Wolf. Distilbert, a distilled version of bert: smaller, faster, cheaper and lighter. In *The 5th Workshop on Energy Efficient Machine Learning and Cognitive Computing*, 2019.
- Shibani Santurkar, Dimitris Tsipras, Mahalaxmi Elango, David Bau, Antonio Torralba, and Aleksander Madry. Editing a classifier by rewriting its prediction rules. *Advances in Neural Information Processing Systems*, 34:23359–23373, 2021a.
- Shibani Santurkar, Dimitris Tsipras, and Aleksander Madry. Breeds: Benchmarks for subpopulation shift. In *International Conference on Learning Representations*, 2021b.
- Tom Schaul, Daniel Horgan, Karol Gregor, and David Silver. Universal value function approximators. In *International conference on machine learning*, pages 1312–1320, 2015a.
- Tom Schaul, John Quan, Ioannis Antonoglou, and David Silver. Prioritized experience replay. *arXiv preprint arXiv:1511.05952*, 2015b.
- Morgan Klaus Scheuerman, Alex Hanna, and Emily Denton. Do Datasets Have Politics? Disciplinary Values in Computer Vision Dataset Development. *Proceedings of the ACM on Human-Computer Interaction*, 5(CSCW2):1–37, October 2021.
- Jürgen Schmidhuber. Learning factorial codes by predictability minimization. *Neural Computation*, 4(6):863–879, 1992.
- Bernhard Schoelkopf, Dominik Janzing, Jonas Peters, Eleni Sgouritsa, Kun Zhang, and Joris Mooij. On Causal and Anticausal Learning, June 2012. arXiv:1206.6471 [cs, stat].
- Yannick Schroecker and Charles Isbell. Universal value density estimation for imitation learning and goal-conditioned reinforcement learning. *arXiv preprint arXiv:2002.06473*, 2020.
- Maximilian Seitzer, Bernhard Schölkopf, and Georg Martius. Causal Influence Detection for Improving Efficiency in Reinforcement Learning. In *Advances in Neural Information Processing Systems*, volume 34, pages 22905–22918. Curran Associates, Inc., 2021.

- Ali Shahin Shamsabadi, Mohammad Yaghini, and Natalie Dullerud. Washing The Unwashable : On The (Im)possibility of Fairwashing Detection. In *Advances in Neural Information Processing Systems*, 2022.
- Shoaib Ahmed Siddiqui, Nitarshan Rajkumar, Tegan Maharaj, David Krueger, and Sara Hooker. Metadata Archaeology: Unearthing Data Subsets by Leveraging Training Dynamics, September 2022. arXiv:2209.10015 [cs].
- David Silver, Julian Schrittwieser, Karen Simonyan, Ioannis Antonoglou, Aja Huang, Arthur Guez, Thomas Hubert, Lucas Baker, Matthew Lai, Adrian Bolton, et al. Mastering the game of go without human knowledge. *nature*, 550(7676):354–359, 2017.
- Leanne Betasamosake Simpson. *As we have always done: Indigenous freedom through radical resistance*. U of Minnesota Press, 2017.
- Elliott Sober. Venetian Sea Levels, British Bread Prices, and the Principle of the Common Cause. *The British Journal for the Philosophy of Science*, 52(2):331–346, June 2001.
- Shagun Sodhani, Sergey Levine, and Amy Zhang. Improving generalization with approximate factored value functions. In *ICLR Workshop on the Elements of Reasoning: Objects, Structure and Causality*, 2022.
- Nimit S Sohoni, Jared A Dunnmon, Geoffrey Angus, Albert Gu, and Christopher Ré. No subclass left behind: Fine-grained robustness in coarse-grained classification problems. In *Neural Information Processing Systems 2020*, 2020.
- David Solans, Battista Biggio, and Carlos Castillo. Poisoning Attacks on Algorithmic Fairness, June 2020. arXiv:2004.07401 [cs, stat].
- Jiaming Song, Pratyusha Kalluri, Aditya Grover, Shengjia Zhao, and Stefano Ermon. Learning controllable fair representations. In *The 22nd International Conference on Artificial Intelligence and Statistics*, 2019.
- Peter Spirtes, Clark N Glymour, Richard Scheines, and David Heckerman. *Causation, prediction, and search*. MIT press, 2000.
- Megha Srivastava, Tatsunori Hashimoto, and Percy Liang. Robustness to spurious correlations via human annotations. In *International Conference on Machine Learning*, pages 9109–9119. PMLR, 2020.
- Alexander L Strehl. Model-based reinforcement learning in factored-state mdps. In *2007 IEEE International Symposium on Approximate Dynamic Programming and Reinforcement Learning*, pages 103–110. IEEE, 2007.
- Richard S Sutton. Dyna, an integrated architecture for learning, planning, and reacting. *ACM Sigart Bulletin*, 2(4):160–163, 1991.
- Richard S Sutton and Andrew G Barto. *Reinforcement learning: An introduction*. MIT press, 2018.

- Christian Szegedy, Wojciech Zaremba, Ilya Sutskever, Joan Bruna, Dumitru Erhan, Ian Goodfellow, and Rob Fergus. Intriguing properties of neural networks. In *International Conference on Learning Representations*, 2014.
- Philip Thomas and Emma Brunskill. Data-efficient off-policy policy evaluation for reinforcement learning. In *International Conference on Machine Learning*, pages 2139–2148, 2016.
- Nenad Tomasev, Kevin R. McKee, Jackie Kay, and Shakir Mohamed. Fairness for unobserved characteristics: Insights from technological impacts on queer communities. In *Proceedings of the 2021 AAAI/ACM Conference on AI, Ethics, and Society*, AIES '21, page 254–265, New York, NY, USA, 2021. Association for Computing Machinery.
- Frederik Träuble, Elliot Creager, Niki Kilbertus, Francesco Locatello, Andrea Dittadi, Anirudh Goyal, Bernhard Schölkopf, and Stefan Bauer. On Disentangled Representations Learned from Correlated Data. In *Proceedings of the 38th International Conference on Machine Learning*, pages 10401–10412. PMLR, July 2021. ISSN: 2640-3498.
- Eric Tzeng, Judy Hoffman, Kate Saenko, and Trevor Darrell. Adversarial discriminative domain adaptation. In *Proceedings of the IEEE conference on Computer Vision and Pattern Recognition*, pages 7167–7176, 2017.
- Joaquin Vanschoren and Serena Yeung. Announcing the neurips 2021 datasets and benchmarks track, 2021.
- V. Vapnik. Principles of Risk Minimization for Learning Theory. In *Advances in Neural Information Processing Systems*, volume 4. Morgan-Kaufmann, 1991.
- Ashish Vaswani, Noam Shazeer, Niki Parmar, Jakob Uszkoreit, Llion Jones, Aidan N Gomez, Lukasz Kaiser, and Illia Polosukhin. Attention is all you need. In *Advances in neural information processing systems*, pages 5998–6008, 2017.
- Rishi Veerapaneni, John D Co-Reyes, Michael Chang, Michael Janner, Chelsea Finn, Jiajun Wu, Joshua Tenenbaum, and Sergey Levine. Entity abstraction in visual model-based reinforcement learning. In *Conference on Robot Learning*, pages 1439–1456. PMLR, 2020.
- Pablo Villalobos, Jaime Sevilla, Lennart Heim, Tamay Besiroglu, Marius Hobbhahn, and Anson Ho. Will we run out of data? An analysis of the limits of scaling datasets in Machine Learning, October 2022. arXiv:2211.04325 [cs].
- Pascal Vincent, Hugo Larochelle, Yoshua Bengio, and Pierre-Antoine Manzagol. Extracting and composing robust features with denoising autoencoders. In *Proceedings of the 25th international conference on Machine learning*, pages 1096–1103. ACM, 2008.
- Yoav Wald, Gal Yona, Uri Shalit, and Yair Carmon. MALIGN OVERFITTING: INTERPOLATION CAN PROBABLY PRECLUDE INVARIANCE. 2023.
- Tingwu Wang, Xuchan Bao, Ignasi Clavera, Jerrick Hoang, Yeming Wen, Eric Langlois, Shunshi Zhang, Guodong Zhang, Pieter Abbeel, and Jimmy Ba. Benchmarking model-based reinforcement learning. *arXiv preprint arXiv:1907.02057*, 2019.

- Christopher JCH Watkins and Peter Dayan. Q-learning. *Machine learning*, 8(3-4):279–292, 1992.
- Théophane Weber, Nicolas Heess, Lars Buesing, and David Silver. Credit assignment techniques in stochastic computation graphs. *arXiv preprint arXiv:1901.01761*, 2019.
- P. Welinder, S. Branson, T. Mita, C. Wah, F. Schroff, S. Belongie, and P. Perona. Caltech-UCSD Birds 200. Technical Report CNS-TR-2010-001, California Institute of Technology, 2010.
- Richard Whitley et al. *The intellectual and social organization of the sciences*. Oxford University Press on Demand, 2000.
- Robert C Williamson and Aditya Krishna Menon. Fairness risk measures. In *International Conference on Machine Learning*, 2019.
- Thomas Wolf, Lysandre Debut, Victor Sanh, Julien Chaumond, Clement Delangue, Anthony Moi, Pierric Cistac, Tim Rault, Rémi Louf, Morgan Funtowicz, et al. Huggingface’s transformers: State-of-the-art natural language processing. *arXiv preprint arXiv:1910.03771*, 2019.
- Cathy Wu, Aravind Rajeswaran, Yan Duan, Vikash Kumar, Alexandre M Bayen, Sham Kakade, Igor Mordatch, and Pieter Abbeel. Variance reduction for policy gradient with action-dependent factorized baselines. *arXiv preprint arXiv:1803.07246*, 2018.
- Ziyi Wu, Nikita Dvornik, Klaus Greff, Thomas Kipf, and Animesh Garg. SlotFormer: Unsupervised Visual Dynamics Simulation with Object-Centric Models, January 2023. arXiv:2210.05861 [cs].
- Meg Young, Michael Katell, and PM Krafft. Confronting power and corporate capture at the facct conference. In *2022 ACM Conference on Fairness, Accountability, and Transparency*, pages 1375–1386, 2022.
- Tianhe Yu, Ted Xiao, Austin Stone, Jonathan Tompson, Anthony Brohan, Su Wang, Jaspier Singh, Clayton Tan, Dee M, Jodilyn Peralta, Brian Ichter, Karol Hausman, and Fei Xia. Scaling Robot Learning with Semantically Imagined Experience, February 2023. arXiv:2302.11550 [cs].
- Muhammad Bilal Zafar, Isabel Valera, Manuel Gomez Rodriguez, and Krishna P Gummadi. Fairness beyond disparate treatment & disparate impact: Learning classification without disparate mistreatment. In *Proceedings of the 26th International Conference on World Wide Web*, pages 1171–1180. International World Wide Web Conferences Steering Committee, 2017.
- Manzil Zaheer, Satwik Kottur, Siamak Ravanbakhsh, Barnabas Poczos, Russ R Salakhutdinov, and Alexander J Smola. Deep sets. In *Advances in neural information processing systems*, pages 3391–3401, 2017.
- Vinicius Zambaldi, David Raposo, Adam Santoro, Victor Bapst, Yujia Li, Igor Babuschkin, Karl Tuyls, David Reichert, Timothy Lillicrap, Edward Lockhart, et al. Relational deep reinforcement learning. *arXiv preprint arXiv:1806.01830*, 2018.
- Rich Zemel, Yu Wu, Kevin Swersky, Toni Pitassi, and Cynthia Dwork. Learning fair representations. In *International Conference on Machine Learning (ICML 2013)*, 2013.

- Brian Hu Zhang, Blake Lemoine, and Margaret Mitchell. Mitigating unwanted biases with adversarial learning. In *Proceedings of the 2018 AAAI/ACM Conference on AI, Ethics, and Society*, pages 335–340. ACM, 2018.
- Jianyu Zhang, David Lopez-Paz, and Leon Bottou. Rich Feature Construction for the Optimization-Generalization Dilemma. In *Proceedings of the 39th International Conference on Machine Learning*, pages 26397–26411. PMLR, June 2022. ISSN: 2640-3498.
- Yi Zhang and Jitao Sang. Towards Accuracy-Fairness Paradox: Adversarial Example-based Data Augmentation for Visual Debiasing. In *Proceedings of the 28th ACM International Conference on Multimedia*, pages 4346–4354, Seattle WA USA, October 2020. ACM.
- Yuan Zhang, Regina Barzilay, and Tommi Jaakkola. Aspect-augmented adversarial networks for domain adaptation. *Transactions of the Association for Computational Linguistics*, 5:515–528, 2017.
- Han Zhao and Geoffrey J Gordon. Inherent tradeoffs in learning fair representations. *Journal of Machine Learning Research*, 23:1–26, 2022.
- Han Zhao, Remi Tachet Des Combes, Kun Zhang, and Geoffrey Gordon. On learning invariant representations for domain adaptation. In *International Conference on Machine Learning*, pages 7523–7532. PMLR, 2019.
- Bolei Zhou, Agata Lapedriza, Aditya Khosla, Aude Oliva, and Antonio Torralba. Places: A 10 million image database for scene recognition. *IEEE Transactions on Pattern Analysis and Machine Intelligence*, 40(6):1452–1464, 2017.
- Xuhui Zhou, Maarten Sap, Swabha Swayamdipta, Yejin Choi, and Noah Smith. Challenges in automated debiasing for toxic language detection. In *Proceedings of the 16th Conference of the European Chapter of the Association for Computational Linguistics: Main Volume*, pages 3143–3155. Association for Computational Linguistics, April 2021.
- Guangxiang Zhu, Zhiao Huang, and Chongjie Zhang. Object-oriented dynamics predictor. In *Advances in Neural Information Processing Systems*, pages 9804–9815, 2018.